A STUDY OF CONVENTIONAL AND UNCONVENTIONAL FLANGED PIPE JOINT STYLES USING NON LINEAR FINITE ELEMENT ANALYSIS TECHNIQUES

A thesis submitted in fulfilment of the degree of Master of Philosophy in Mechanics of Materials.

by

David J. Power

UNIVERSITY OF STRATHCLYDE,
Department of Mechanical Engineering.

August 1997

Declaration of Author's Rights

Abstract

The Department of Mechanical Engineering has conducted numerous studies in the area of pressurised systems including pressure vessels, methods of support, local loading and other studies of pressure system components. The investigation in this area has been continued with this study of conventional and unconventional flanged pipe joints.

A finite element comparison of three flanged joint styles that were subject to an internal pressure load is presented. The three styles commonly used in industry are the ANSI B16.5, the Desflex, and the Verax Compact Flanged (VCF) joint. The comparison was conducted using the $1500^{\#}$ and $2500^{\#}$ pressure classes and three nominal bore sizes of four, eight and twelve inches.

An investigation into the fundamental joint characteristics of joint strength and sealing ability was carried out using three-dimensional general surface contact elements between the contacting surfaces and a bi-linear kinematic material model within the flanged joint components.

The results of the study demonstrate the advantages of the VCF joint over the Desflex and conventional ANSI flanged joints in the $1500^{\#}$ pressure class. The VCF joint demonstrated very little yielding of the hub and less yielding of the flange ring due to the bolt loading. In contrast, the ANSI flanged joint yielded significantly in both of these areas whilst the Desflex joint yielded less than the ANSI flanged joint around the hub. The Desflex joint also yielded heavily at the outside edge of the flange ring. All of the $2500^{\#}$ class joints that were examined demonstrated very little yielding.

The VCF joint exhibited contact over a large portion of the flange faces, while the ANSI and Desflex flanged joints relied on a large contact pressure being exerted over small contact areas.

The use of a nonlinear material model demonstrated a significantly more accurate stress distribution through the flanged joints. The geometric nonlinearities associated with the use of the contact elements greatly increased the solution times of the models. This was most evident when the two contacting surfaces were not flat and parallel and of high strength. As this was the case with both the ANSI and Desflex flanged joints, their solution times were approximately 12 and 50-70 CPU hours respectively.

Acknowledgements

The author wishes to thank Mr. David Nash for his supervision, advice and direction throughout this project.

Gratitude is also given to Mr. Ching Wan of Shell (UK) Exploration and Production, Lowestoft, for the financial support of this work and for his comments based upon practical experience with flanged pipe joints.

Thanks should also be given to Mr. Luigi Cordani, support engineer, of IDAC Ltd., for his constantly available advice about the ANSYS finite element program and contact analysis in particular.

The author also thanks Mr. Jan Webjörn of Verax, Sweden for his provision of both background information and details of the Verax compact flanged joint. Acknowledgement should also be given to Destec Engineering Ltd, Lincoln for providing geometric details of their Desflex flanged joint.

Table of Contents

Table of Figures

Table of Tables

Nomenclature

The parameters listed below denote the variable used within the finite element models. The values of these variables are listed in Appendix I.

bd	bolt diameter
fd	flange ring diameter
fh	flange ring height
gcringod	gasket centring ring outside diameter
gid	gasket inside diameter
gsringid	gasket seal ring inside diameter
gsringht	gasket seal ring height
gsringod	gasket seal ring outside diameter
gth	gasket centring ring height
hubang	hub angle
hubht	hub height
i	element node
j	element node
jh	joint height
k	element node
l	element node
m	element node
n	element node
nbolts	number of bolts
o	element node
p	element node
$P_{internal}$	Internal Pressure
P_{axial}	Axial or end-cap loading
pcd	pitch circle diameter
pid	pipe inside diameter
pod	pipe outside diameter
pt	pipe wall thickness

r	radius of hub/flange ring connection
sh	shoulder height
sod	shoulder outside diameter
x	global x-axis
x_e	x-axis of element co-ordinate system
y	global y-axis
y_e	y-axis of element co-ordinate system
z	global z-axis

1. Introduction

1.1. Background

From years of experience of the offshore gas installations, Shell (UK) has found that the traditional gasketed ANSI flanged joint has several points of weakness which can cause problems in service: flange rotation, leakage, heavy maintenance requirements and weight. As the bolts of the flanged joint are pretensioned, the flange ring deflects around the centre of rotation between the gasket and the outer edge of the shoulder as shown in the Figure 1 below:

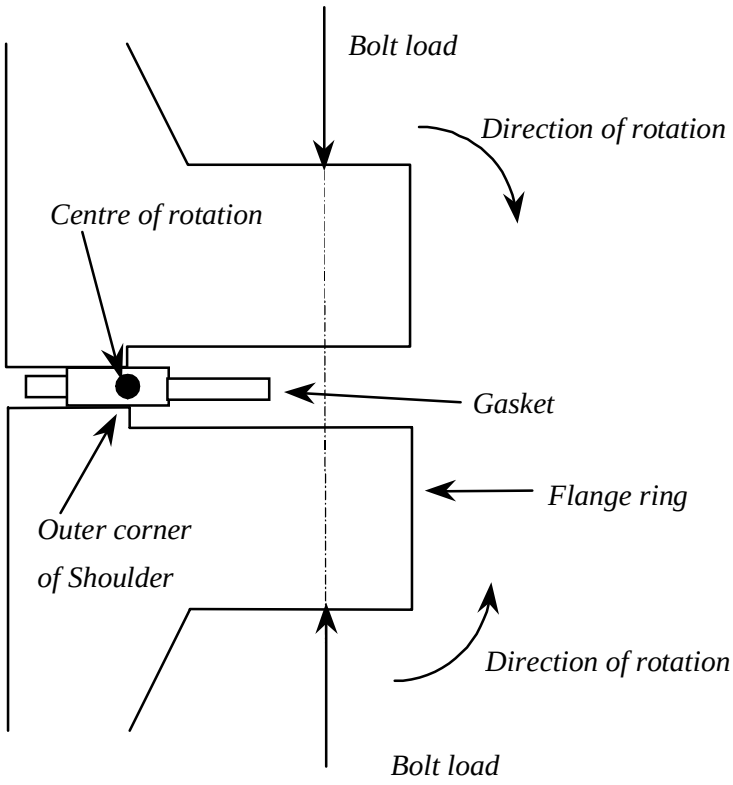

Figure 1: Rotation of ANSI Style Flanged Joint

As the flange ring rotates against the constraining pipework or vessel, the ring begins to deform under the increasing bolt load. This factor alone reduces the reusability of the ANSI flanged joint. In addition, as the joint rotates around the corner of the shoulder (as indicated in Figure 1), the area over which a seal exists, between the flange shoulder and the gasket is reduced significantly and thus the possibility of leakage increases. It is common practice throughout the oil and gas industry that the quickest method of stopping a leak from an ANSI flanged joint is to further tighten the bolts until the leak

has stopped. This procedure can damage or perhaps crush the gasket resulting in further maintenance being required to replace the gasket. The ANSI flanged joint requires substantial raw material to make, and consequently, the joint is heavy. In some applications, i.e. offshore oil platforms, where total system weight is of great importance, expensive materials are required for these joints to maximise the strength of the ANSI joint without increasing the weight of the joint.

If an alternative joint to the traditional ANSI flanged joint, were available, one which was of greater strength, had better sealing ability and was lighter and less expensive, then offshore industries in particular could reduce their costs significantly.

1.2. Problem Statement

Upon discussion with a major gas supplier, and having examined the relevant literature, several practical alternatives to the ANSI flanged joint required consideration. These comprised of the VCF joint from Verax, Sweden and the Desflex flanged joint from Destec Ltd., Lincoln (UK).

The technical benefits and drawbacks of the joint styles, can be demonstrated by comparing the two main flanged joint characteristics:

- Joint strength under working pressure and,
- Sealing ability.

The comparative study was to be conducted using the finite element method for a combination of flange sizes and pressure ratings. The flanged joints of four, eight and twelve inch nominal bore were to be examined for both the $1500^{\#}$ class and $2500^{\#}$ class, these represent common flange sizes and pressure classes where problems had previously occurred.

The dimensions for the ANSI B16.5 flanged joint and gasket were obtained from British Standards 1560 Section 3.1:1989 and 3381:1989 respectively.

The ANSYS finite element program version 5.3 was used throughout the study.

2. Literature Survey

In order to become familiar with the background, operational behaviour and problems associated with flanged joints, a comprehensive literature survey was conducted. From this survey, a concise summary of all of the most relevant works to date was compiled and has been presented in this chapter.

2.1. Flanged Joints with Gaskets

2.1.1.1. [Waters and Taylor [1]]

Waters and Taylor (1927) developed the first analysis of the flanged joint in 1927, using flat plate and elastically supported beam theory. From this, Waters *et al.* [2] (1937) developed the theoretical method for analysing the stresses in taper hubbed flanged joints which is commonly known as the 'Taylor Forge' method. This method forms the basis of the design methods found in international pressure vessel codes such as BS5500 and ASME VIII. This method of analysis divided the flanged joint into three components, the cylinder, the taper hub and the flange. The authors assumed that the mean diameter of each component was equal to the inside diameter of the cylinder (i.e. the pipework or the pressure vessel) as shown in Figure 2 below. This assumption was from shell theory.

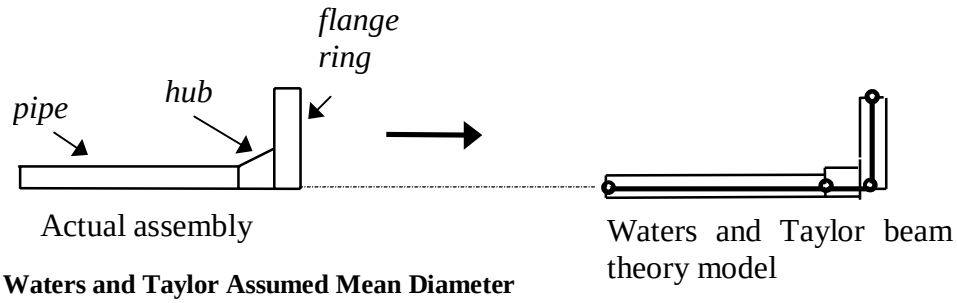

Figure 2: Waters and Taylor Assumed Mean Diameter

Waters used the principle of superposition to combine the results from each component to obtain an overall solution. Their analysis was conducted for standard cases of an applied internal load (i.e. pressure) and a moment about the ring (i.e. applied bolt load). In this work, the authors did not compare their results to any experimental work nor gave any discussion, nor drew any conclusions.

2.1.1.2. [Almen [3]]

Almen (1944) determined a relationship between the preload applied to a bolt and the fatigue life of the bolt. Almen found that the change in load, i.e. difference between the preload and the applied load, was related to the life of the bolt. He conducted experiments on several groups of around 16 bolts and applied a different preload to each group. A known alternating external load was then applied to the bolts and the fatigue life measured. Before the fatigue tests were undertaken, incremental stress-strain measurements were made during the application of an external load. From these measurements, Almen certified that the bolted members were flexible and that the bolt load was increased by the elastic recovery of the bolted members. Having repeated these experiments using a stiffer, less flexible, material he was able to make comparisons and noted that the effect of the cyclic load on the bolt was increased as the flexibility of the bolted members (i.e. the flanges) was increased. Almen also found that the effect of the cyclic load on the bolt decreased as the bolt flexibility increased.

He commented on the use of gaskets between the bolted members and stated that they should remain as stiff as possible but still function as a seal. In conclusion, Almen commented that it was much better to tighten a bolt beyond the yield point than to risk the bolt not being tight enough. He stated that this was not a recommendation for general practice but only in the case where circumstances prevented no better solution.

This conclusion, however, does not consider the downtime required for maintenance to correct any excess leakage from a permanently deformed flange.

2.1.1.3. [Murray and Stewart [4]]

Extending the work of Taylor-Forge, Murray and Stewart (1961) investigated the behaviour of large taper hub flanges by removing one of the major simplifications of the Taylor Forge method. They tested their theoretical analysis by comparing the results to their own experimental work on a flange 15 feet in diameter. The authors analysed the flanged joint by dividing it into three separate components (i.e. pipe cylinder, taper hub and flange) and then combined their results by satisfying compatibility and equilibrium conditions. The major assumption made by Murray and Stewart was that all three components of the flanged joint have the same mean diameter as the cylinder section (i.e. the pressure vessel or pipework) as shown in

Figure 3 below:

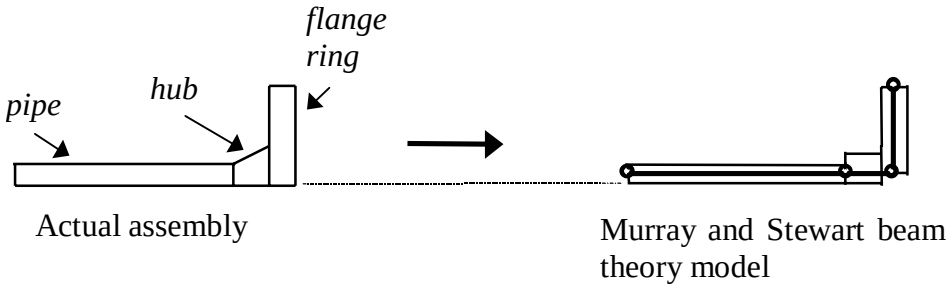

Figure 3: Murray and Stewart Assumed Mean Diameter.

Murray and Stewart found that this method gave higher stress results than that of the Taylor Forge method that was found to consistently underestimate the maximum stresses for all flange sizes. They also found that the Taylor Forge method was only slightly inaccurate when the flange size is small but the margin of error became considerable for flanges larger than 5 feet in diameter.

2.1.1.4. [Keer et al. [5]]

Several years later, Keer *et al* (1972) derived a solution to the elastostatic problem of receding contact between an infinite layer and a base containing a hole. A solution was found for both plane and axisymmetric problems. Keer set-up the plane problem using a mathematical technique known as 'Papkovich-Neuber' potentials. After applying the boundary conditions, the authors found that a Fourier transform and a multiplier evolved. Solving this resulted in a Fredholm integral equation of the second kind, which could be treated as an eigenvalue problem.

From this solution they noted that the contact area and contact pressure depend only on one single parameter, this a function of the elastic constants. They also found that for an identical material, the stress fields are completely independent of the elastic constants, which is in agreement with previous results.

Keer set up the axisymmetric problem in the same way as the plane problem, and used the same general method to find the solution. The authors then solved both problems numerically and drew several conclusions. It was noted that the stresses were proportional to the applied loads and that the extent of contact was independent of the magnitude of loading. For the axisymmetrical problem, the same results had been found as for the plane problem, except that these results had not been predicted by any previous work.

2.1.1.5.[Thomson [6]]

Thomson (1988) developed a new simpler method for the calculation of stresses in taper hubbed flanges. The model is shown in Figure 4 below:

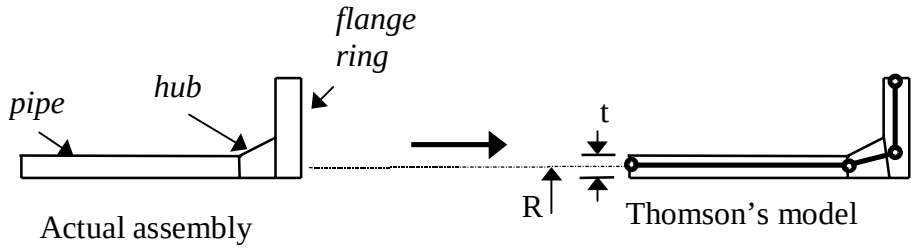

Figure 4: Thomson's Model.

The method uses the minimum total potential energy theorem and is applied to suitable selected displacement fields that satisfy the kinematic boundary conditions. From these fields the total potential energy function is found. Thomson states that a finite shell with length $3\sqrt{Rt}$ (as shown in Figure 4) or greater will act in the same way as an infinite shell and so this should be the minimum shell length as shown in Figure 4.

The open end of the shell is fixed in the longitudinal direction, but is free to move in the radial direction. At the flange end, the shell displacements were made equal to the flange displacements by determining a trigonometric series as though the end was free and then calculating the flange displacements from the end values.

Thomson separated the loading into two discrete cases: the bending moment due to bolt tightening, and the internal pressure. These cases were then combined by superposition. The total potential energy of the system was found by summing all of the strain energy components and subtracting the potential energy of the applied loads. The result of this was then differentiated to find the minimum total potential energy.

Thomson compared the results of his work to that produced by the Taylor Forge and Murray and Stewart methods. His method was found to compare well with that of Murray and Stewart but not with the Taylor Forge method. He also found that the reason for this was an assumption in the Taylor Forge method that does not allowing the flange to rotate. Thomson found that good comparison with Murray and Stewart was shown for both radial displacements and longitudinal stress levels for both the bending moment and internal pressure cases.

2.1.1.6. [Sawa *et al.* [7]]

The work of Sawa *et al.* (1991) complemented the work of Thompson by concentrating on the contributions of the gasket to the joint characteristics. Sawa conducted both a theoretical analysis and experimental study in order to determine the effects of the stiffness and the thickness of metallic gaskets on the contact stresses and effective gasket sealing width. They used axisymmetrical three-dimensional theory of elasticity as the basis for their theoretical analysis. They also examined the stresses produced in the hub region, the load factor and the maximum stresses in the bolts. The problem was simplified by considering the whole joint as a single structure. The flanges and the raised face gasket were replaced with finite hollow cylinders and the problem was then considered to be an elastic contact problem. Sawa *et al.* assumed that the shearing forces on the contact surfaces between the hollow cylinders were negligible. They then used superposition of the initial clamping analysis and the internal pressure analysis to obtain their final model. For the experimental work, several strain gauges were attached to the hub, some in line with bolt and others at mid pitch between bolts. The shanks of the bolts were also strain-gauged. A known clamping force was applied and then a known internal pressure was supplied using an oil pressure pump. The experiments were carried out using two different gasket materials; namely, steel and aluminium. The numerical calculations showed that the effective gasket seating width increased as the thickness of the gaskets increased. The authors noted that this result deviated from the ASME codes assumption in that the gasket effective width is stated in the codes to remain constant.

Upon applying the internal pressure to the joint, they observed leakage from the gasket. From the analytical model, the leakage assumed to have happened when 98% of the gasket effective seating had separated.

When Sawa examined the stress values around the hub it was noted that they were much higher when the aluminium gasket was used. The hub stresses were also noted to increase with an increase in the gasket thickness. The authors noted throughout that there was good agreement between the analytical and experimental results.

2.1.1.7. [Laviolette *et al.* [8]]

Following this, Laviolette *et al.* (1996) determined the behaviour of a bolted joint (with a gasket) under the influence of an external bending moment. This was done using analytical, finite element and experimental methods.

The two-dimensional finite element model consisted of a length of pipe with a flanged joint located a set distance from the middle of the pipe. The pipe was fixed at one end and a vertical force was applied a set distance from the fixed end. The experimental set-up was geometrically similar as that for the finite element model. Special foil sensors were used to measure the contact stresses around the gasket during the application and relaxation of the bending moment. The authors defined the circumferential variation of the applied load as a seven term Fourier expansion. Young's modulus for the gasket material was estimated from the stress-strain curve and shell elements were used throughout the model. Laviolette noted that for the second and third applications of the bending moment good agreement was found between the finite element and experimental results. This was not the case for the first application of the bending moment due to the non-linearity of the gasket material behaviour. It was noticed from the results that the average of the finite element results was very similar to three of the four transducer results. The results from the fourth transducer gave a compressive stress 50% higher than expected from the finite element results. The authors noticed large discrepancies between the experimental and FEM results at the upper and lower extremities of the gasket with the experimental results indicating much higher gasket stresses. No explanation was given for this observation although the authors concluded that the uncertainty and non-linearity of the gasket material introduced significant errors relative to the finite element results.

2.1.1.8. [Price and Chanana [9]]

Price and Chanana (1996) discuss the need for change in the use of the traditional flanged joint. They criticise ASME standards which contain values from the 1940's which are claimed to be suspect. It was also stated that the ASME codes do not address the problems of leakage resulting from the flexibility and movement of the flanges. Price and Chanana mentioned that the flanges are rated on a basis of the level of allowable stress that the flange can endure and that this condition is not related to the ability of the flanged joint to withstand leaks. The factors associated with leakage are claimed to be lower rigidity of the flanges, larger diameter flanges, stiffer gaskets and lower bolt tightening stresses.

The authors commented on the lack of a suitable replacement for the now unpopular compressed asbestos fibre gasket, although they mention that the spirally wound expanded (or flaked) graphite filled gasket could be suitable in some cases. This graphite gasket is not a suitable replacement in every case. This is because the

maximum permitted surface stress of a graphite gasket is 40% less than that of the compressed asbestos fibre gasket. As a proposed solution to the problem of leakage the authors emphasised the availability, and increasing use of welded joints as a suitable alternative to the flanged joint. They questioned the need for the flanged joint in certain types of pipelines and suggested that the overall costs of the welded joint, including initial purchase, maintenance, and operation to be less. They also noted that the possibility of a welded joint being the cause of a major leak (if any) was very rare and that the cost to the company, in terms of downtime, of any leak of this type continues to increase.

2.1.2. Summary Points:

- Increasing the elasticity of the bolts, or decreasing the elasticity of the flanges, decreases the stresses produced by cyclic loading. [3]
- The Taylor Forge method, which assumes that the diameter of each component of the flanged joint is equal to the inner diameter of the pipework, is inaccurate for flanges larger than 5 feet in diameter. [4]
- The contact area between flange faces is independent of the loading level, but the stresses are proportional to the applied loads. [5]
- The effective gasket seating width and level of hub stress both increase with increasing gasket thickness. [7]
- Factors leading to increased probability of leakage are lower rigidity of the flanges, large flange diameter, stiff gaskets and lower bolt tightening stresses. [9]

2.2. Flanged Joints without Gaskets

2.2.1.1. [Webjörn [10]]

Webjörn (1967) outlined the basic principles underlying a new design of flange assembly. He specifies several principles that should be employed when designing flanges. These principles include the replacement of gaskets with O-rings or equivalent; the flanges should be as strong as the associated pipework and should only be of the weld-neck type. International pipe dimensions should be used as a basis for design, and concepts like design pressure; maximum allowable stress and the safety factor should be revised. He emphasises the use of higher quality, or treated (i.e. quenched and tempered) materials for

bolts especially when such materials are sometimes available for little extra cost. Webjörn also states that elastic bolts and stiff flanges should be used so that the flanges absorb the majority of the workload and not the bolts.

The new design also uses several smaller diameter bolts rather than fewer larger bolts. The flange thickness is recommended to be at least four times the nominal diameter of the bolts. This design also requires that the bolts be tightened to above 80% of their guaranteed minimum yield strength preferably using the "angle-of-turn" method that the author describes.

Webjörn commented on that the use of large safety factors is costly, as compared with implementation of modern inspection techniques. He concludes by listing the experimental work that has been completed on the compact flange design. This work included the case of cyclic loading of the internal pressure and testing the flange strength during bending. Webjörn mentioned the ongoing design of a compact flange with a metallic seal.

2.2.1.2. [Schneider [11]]

Schneider (1968) gives a solution for the problem of flanges with flat faces in metal-to-metal contact using beam theory. He states that although this analysis does not apply to flanged joints with hubs, an extension to his presented work would allow this to become possible.

Schneider treated the flange ring as a series of discrete radial beams with forces being applied at the flange/shell junction, the bolt circle and the bearing circle. This section of the flange ring is then modified into an equivalent beam for simplicity. He found excellent agreement between results from this simplification and the original flange shape.

In order to determine the distribution of the contact for the equivalent beam, he conducted experiments using strain gauges and several small metal beams, applying loads similar to those applied in the analysis. The distribution of the contact pressure was thus found. The tests were then repeated with unsymmetrical beams and the same contact pressure distribution was found. Equations for the rest of the body, i.e. the shell /flange connection and the flange contact with the bolt circle, were given and it was noted that the effects of the bolt holes had been ignored. The effect of the bolt holes on the flexural behaviour could be included by a minor change in the solution. Schneider

then suggests a possible method for applying his approach to the design of a flanged connection and emphasises that this type of design work is normally by trial and error.
In conclusion, it was noted that pretensioning of the bolts does not induce significant stresses in the flange and increases the fatigue life of the bolts. He also concluded that pretensioning of the bolts reduces flange separation and gasket extrusion and subsequent leakage. The highest stresses in flat flanged joints occur in the bolts and in the flange at the bolt circle as well as the shell/flange connection.

2.2.1.3. [Waters and Schneider [12]]

Waters and Schneider (1969) extended the work of Schneider to make the analysis applicable to axisymmetric non-identical flanges that may incorporate an O-ring. They demonstrate the same beam analogy method as before using the same simplifying principles and then continue by describing two alternative methods of determining the operating bolt load. They concluded that prestressing the bolts reduces the levels of significant stress and flange separation as well as increasing the fatigue life of the bolts. It was also noted that if the bolts were prestressed in a joint with a gasket, then leakage and the possibility of a gasket blow-out increased.

2.2.1.4. [Meck [13]]

Meck (1969) used the theory of elasticity as a basis for his derivation of a formula to determine the maximum spacing between bolt for the complete sealing of flat flanges in metal-to-metal contact. He stated that if the bolts supply a positive pressure to the flanges then separation occurs if a negative pressure exists between any two bolts. The problem was simplified to that of an infinite two-dimensional strip along which distributed loads are applied at regular intervals. A Fourier series represented the load distribution and the author assumed that the force exerted by the bolt on the flange is sinusoidal in nature. It is also assumed that the minimum pressure occurs midway between two bolts and, so long as the pressure at this point is non-negative, then no separation exists.
Meck then solved the equations for the maximum permissible bolt spacing and derived several equations for the different ratios between the maximum and minimum pressures (q_{max} and q_{min}) existing in the area between two bolts as shown in Figure 5. He noted that the graphs of these equations are parabolic and terminate when the spacing between the bolts (s) equals the bolt head diameter (d).

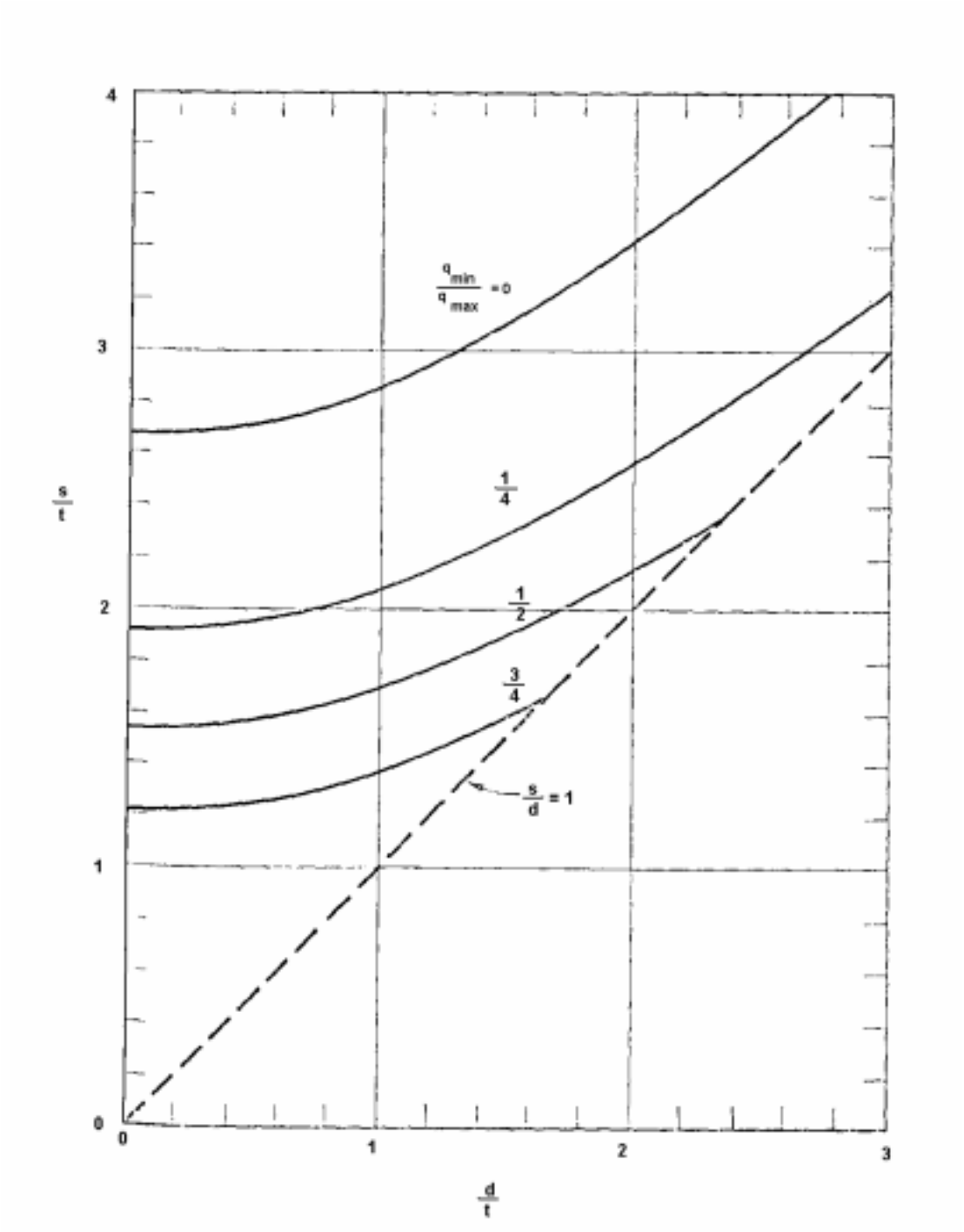

Figure 5: Bolt Spacing Curves – After Meck

2.2.1.5. [Pindera and Sze [14]]

Pindera and Sze (1972) concentrated on experimental methods to determine the influence of the bolt (including washers) on the flanged joint without a gasket. The authors made

three experimental models, a bolted model made from steel, pressurised to 300psi using oil, a boltless model made from epoxy resin, representing the mathematical model commonly used. The boltless model was pressurised to 15psi (equivalent to 855psi in the bolted model). The boltless model assembly force was 10% of the allowable working load. The third model was a flange model made from Plexiglas which representing flanges which are not connected to shells.

Pindera and Sze used several different bolt loads including 50 and 100% of the allowable bolt loads and modified the results for their plastic models for steel using the model law. They found from their results that the boltless and bolted models produced qualitatively identical results. Both models demonstrated that any variation in the bolt working forces were insignificant when the bolt assembly force is above a certain level which depends on the internal working pressure.

When the authors examined the results of the flange model, they noticed that the bolt working forces and the interface contact forces increase with increasing bolt tensile stiffness. It was also noted that when the bolt assembly force increases, the interface contact area approaches that of the bolt hole circle. In conclusion, the authors stated that the bolt tensile stiffness and the bolt preload are both major design parameters. The authors also concluded that if the bolt preload and tensile stiffness were increased, the flange deformation and bolt working forces decrease.

2.2.1.6. [Gould and Mikic [15]]

Gould and Mikic took this work further by determining the pressure distribution and contact areas surrounding bolted joints using finite element methods and two forms of experiment. Their finite element models covered the general case of two plates of different thickness and to the special case where the plates are of the same thickness.

They used small elements in the areas where high stress gradients were expected and large elements were the stress was expected to be approximately constant.

Gould and Mikic stated that if the frictional forces were sufficient to prevent sliding, then the finite element model would be identical to the physical model.

The experiments were conducted using four different plate thicknesses. The first method to determine the contact area between the plates while bolted together was to rotate one plate relative to the other by $\pm 5°$. This action caused polishing of the surfaces that came into contact. This area was measured using an optical comparator. The

second method involved the electrolytic plating of one side of one of the plates firstly using copper and secondly using silver with its radioactive isotope. The plates were then bolted together and rotated under load for 5° relative to each other. X-ray film was then placed on the contaminated plates and a 5lb load was applied. The film was then developed.

For all of the models tested, Gould and Mikic found that the contact areas between the plates was considerably smaller than shown by theoretical studies previously published. They also found that the experimental and finite element methods compared very well. The discrepancy between this work and previous work was due to an earlier simplification that the two plates could be modelled as a single plate.

2.2.1.7. [Thompson *et al.* [16]]

Thompson *et al.* (1976) also investigated the size of the contact region surrounding each bolt connection on the circumference of the flange. Experimental and two-dimensional finite element methods were used. It was assumed that circular plates, compressed together by a single loaded bolt could model the bolted flanges. A range of loading disk diameters and bolt hole diameters was tested and over 200 experiments were carried out. The physical experiments were carried out using plates made from glass, Plexiglas and several other plastics. It was noted that these materials followed the standard modelling laws of linear elasticity or viscoelasticity. As a result of this, and since the Poisson's ratio of steel is greater than that of glass and less than that of the plastics, the authors believed that equivalent results could be obtained for steel plates by interpolation. The contact areas were determined by reflecting light across the plates and noting the interference pattern on the separate surfaces.

The finite element model was based on the results from the experiments that indicated a working relationship between the loading disk diameter and the diameter of the contact region. Nine-noded elements were used within the contact region while five-noded elements were used in the outer regions where bending stresses were believed to dominate. Thompson assumed that the element boundary displacements would be linear which allowed the midside nodes to be disregarded. The surface nodes within the contact region were constrained in vertical direction but were allowed to move horizontally. All other surface nodes were unconstrained.

They noted that the size of the contact zone varied with the applied load up to the point where any roughness or waviness of the surfaces could be neglected. It was also noted that there were significant differences between the experiments and the finite element model unless the contact zone was stabilised with respect to imperfections, i.e. localised plastic deformation removed any roughness. From the results of both approaches it was observed that the bolt hole size had no influence on the size of the contact region. The authors observed a relationship between the size of the contact region and the plate thickness and the loading disk diameter. An empirical formula was derived which predicts the contact region in non-dimensional form within a 3% margin of uncertainty. Thompson found the stress distribution to be almost linear when the difference between the diameters of the bolt hole and the loaded region is less than half the total thickness of the plates. They concluded that the stress distribution could be assumed to be conical in shape around the centre of the bolt hole. Thompson stated that only the stresses near the perimeter of the loading disk were radially distributed while the remaining stresses were transmitted directly through the plates. The bolt hole could then be simulated by removing some of the stresses that would have been directly distributed through the plates. They noted that outside a region of radial distance equal to one flange thickness beyond the contact zone, the deformation state can be found using simple plate theory. Inside this region a three dimensional deformation state exists. When applying these results to existing pipe flanges the authors stated that if the bolt spacing is less that 1.5 times the diameter of the contact region then the contact regions around individual bolts will interact and elongate in the direction of the bolt circle. It was also stated that this interaction would not change the magnitude of the stress levels significantly.

2.2.1.8. [Webjörn and Schneider [17]]

Webjörn and Schneider (1980) complemented their theoretical work by conducting their own experiments on a pressure vessel comprising of a pair of compact flanges. The flange face had a small positive taper angle thus creating contact at the inside of the flange first. The bolts were strain gauged and preloaded to 80% of their minimum yield stress. The vessel was pressurised with water, first to the working pressure and then to the specified proof pressure (1.3 times the working pressure). Due to an operating error, the pressure was then allowed to increase to 2.25 times the working pressure. Results were recorded throughout all of the tests with separation gauges fitted to the interior of

the vessel and strain gauges fitted to the hubs of the flanges. The tests were repeated for a bolt preload of half the design value. The authors noted that at the working pressure the vessel showed no signs of separation at the bore. This was not the case at the proof pressure. It was also noted that the operating bolt load was slightly lower that the design preload value. At the highest pressure it was observed that although separation had occurred, the vessel did not leak and the bolt loads were only increased by 6%. They also found that the separation distance was only 0.0015mm and that an O-ring could have easily sealed this gap without extruding. For the test cases at half the design bolt loads the authors noted that the proof pressure caused an increase in the bolt load of only 5%. Webjörn and Schneider stated in general that the operating bolt loads were similar to the preload values for pressures below that required for separation of the flanges.

It was noted that until the outer diameter flange edges were closed, then the joint acted like a pair of conventional raised face flanges with no contact beyond the bolt circle. In conclusion they stated that cyclic pressure could not cause damage to an O-ring at the working pressure, as there is no separation at the bore. It was also concluded that the fatigue life of the bolts was significantly increased as the preload and working load of the bolts were very similar. From the results of the hub stresses calculated. Webjörn and Schneider noted that the stresses could be minimised by controlling the amount of taper in the hub, but this would also affect the separation pressure.

2.2.1.9. [Webjörn [18]]

This experimental study was continued by thermal study of the compact flanged joint. Webjörn (1983) conducted experiments and developed a simple two dimensional finite element analysis in order to determine the effects of severe thermal shock through compact flanges compared with conventional flanges. The flanged joint used fitted 88.9x3.2 mm pipe. He found great difficulty in drilling a precision hole for the thermocouples and so used several recognisable locations. Temperature calculations were conducted in time steps and correlated with actual readings. The flanges were connected to a short length of pipe and attached, using a ball valve, to a fire hydrant containing water at 5°C. The outside surfaces of the flanges were heated to 250°C using several radiant-heating elements. A recording device was used to record the thermocouple readings. The two-dimensional finite element model was built using an equivalent mass equal to the proportion associated

with each bolt. He devised a method of calculating the isotherms through the bolt. This was done by assuming that the temperature at the nodes of the grid was equal to the mean temperature of a surrounding cylinder. The input data was then adapted to agree with a similar model and by iteration a constant of thermal conductivity was calculated. A second model of a section of the flange was made and, using the previous constant of thermal conductivity and a heat transfer coefficient that suited the experimental results, the isotherms were determined. Webjörn found that the heat transfer coefficient was unstable and was recalculated for different time intervals. He found a good agreement between the final model and the experimental results. From the results, Webjörn noted that the compact flange was less sensitive to thermal shock than the equivalent conventional flange. It was also noted that only one third of the bolt preload of the compact flange would have been lost due to the thermal shock whilst the conventional flange would have lost all preload. Webjorn stated that the temperature difference between the bolt and the flange could be kept to a minimum under these test circumstances if surfaces were smooth and perpendicular and the bolt had a high initial preload.

2.2.1.10. [Junker and Wallace [19]]

Junker and Wallace (1984) re-examined the theoretical assumptions made in the classical analysis of bolted joints. This assumes that the joints behave linearly and that the transfer of loading between the clamped parts does not vary over a broad range of bolt clamping loads. The authors demonstrated the effects of eccentricity and how it affects the sensitivity of the joint to bolt clamping loads. It could be concluded that the bolt should be more flexible in comparison to the other clamped parts or alleviate eccentricity effects. They suggested the use of reduced shank diameter bolts as the slope of the bolt load-deformation curve is reduced leading to an increased joint fatigue strength. Junker and Wallace also reached the conclusion that the fatigue strength of the bolts could be improved by using high-grade heat-treated fasteners with asymmetrical thread profiles and lead correction. It was stated that this alteration would increase the fatigue strength of the bolts by around 100%. In the classical bolted joint analysis the authors noted that preload was shown to have only a minor effect on the fatigue strength of the joint.

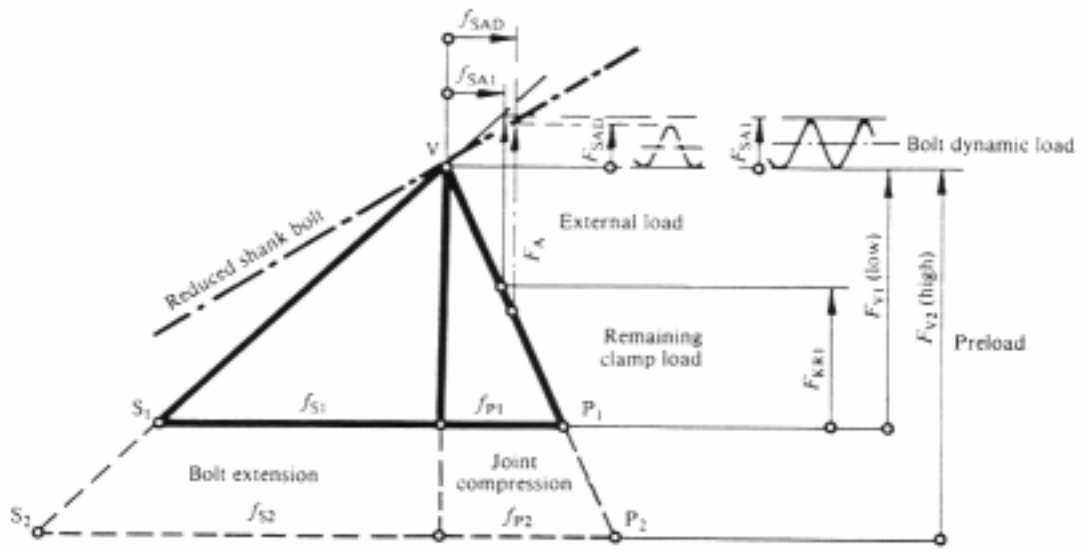

Figure 6: Classic Bolted Joint Diagram

Junker and Wallace introduced a more comprehensive bolted joint diagram, which included the effects of eccentricity that occurs in almost every joint.

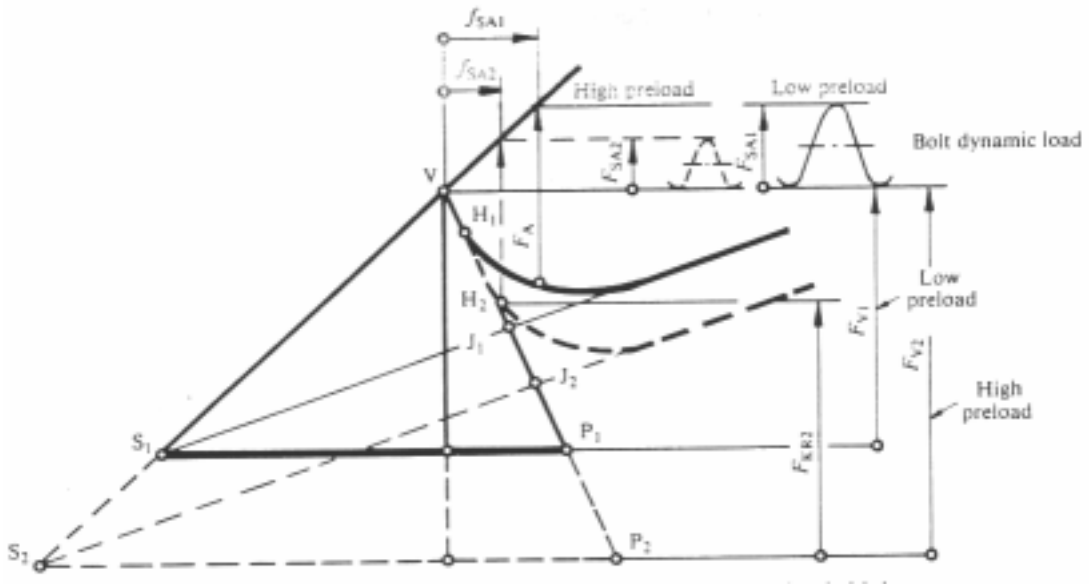

Figure 7: Modified Bolt Diagram - Including The Effects of Eccentricity After Junker and Wallace

The classical analysis did not include the effects of the three axes that exist in eccentric joints. These axes take into account the way in which the joint opens (from one side), it takes into account the effects of preload in a more accurate way and demonstrates the increasing proportion of the external load that the bolt is subjected to as the external load increases. In this new bolted joint model it is demonstrated that the effects on bolt resilience is minor compared to the effects of preload. They stated that it is preferable to

use a full shank bolt with a higher preload than using a reduced shank bolt with a lower preload. Experiments were conducted by the authors using a fatigue testing machine and the effects of static and dynamic loading were determined for several levels of preload. The results of these experiments showed that at the lower preload level of 50% bolt yield, the joint 'opened' at a low level of external loading. At the higher preload that was equal to 100% bolt yield stress, the joint fatigue strength was increased by 100%. Junker and Wallace summarised the relationship between applied torque and preload. It was noted that an indirect relationship exists because of the existence of friction. Over 500 tightening tests were conducted and the results were statistically averaged. It was shown that the mean under-head friction varies between 48% and 23% depending upon material and finish quality. From the results it was also determined that increasing the accuracy of the tightening torque from $\pm$10% to $\pm$3% improves the preload accuracy by around 2%. They also detailed the 'angle control' method of tightening that has been in use since 1948. The main disadvantages of this method are that the reusability of the bolts is limited, the method is not universally applicable, especially if the bolt has very few extra threads or, if the material is not ductile. The method also requires extensive time be spent determining the starting torque from which the angle is to be measured. The 'joint control or yield control' method of tightening as described by Junker and Wallace is conducted by continually calculating the rate of change of the measured torque and rotation. A snug torque is found at the start of the linear slope between the bolt torque and the rotation angle. When the gradient of this slope reduces at a certain rate the tightening device is shut off. The authors stated that this method controlled the preload to $\pm$6%.

2.2.1.11. [Lewis *et al.* [20]]

Lewis *et al.* (1987) started their study of gasket-free flanges by describing a method to determine the size of the initial gaps that exist between the flat faces of metal-to-metal flanged joints under a no-load condition. The bolt spacing in the experiments conducted by the authors was greater than that specified as the maximum for complete sealing by Meck.

In their experiments, the authors measured the leakage rate of a variety of joints at several low pressures and extrapolated the results to a zero pressure condition to obtain an initial leakage rate. From this, they found the initial gap size using incompressible fluid flow theory. Lewis used pressure tappings to find the shape of the gaps and found three

different shapes of initial gap. Six different flange sizes were examined including a flange that had a small negative face taper angle. Positive and negative taper angles are shown in Figure 8 below:

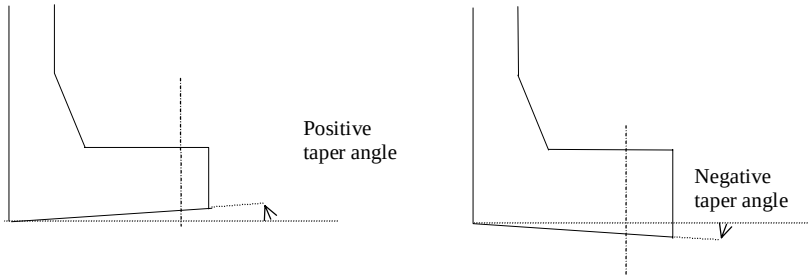

Figure 8: Positive and Negative Taper Angles.

The flanges under test were sealed off using flat end plates positioned away from the test flange. Air was used as the working fluid and supplied through a regulated supply and into the other end of the casing. The authors used a rotameter to measure the inlet air flow and a water manometer to measure the internal pressure. Lewis found that if laminar viscous flow was assumed then the linearity of the results demonstrated that load-induced deflections were insignificant. They also found that on one model, where an 'as cast' face finish had first been used, machining the flange faces resulted in an order of magnitude reduction in the initial leakage rate. The first model was made from Araldite and demonstrated a small increase in the leakage rate when the bolt strain was reduced. The steel flanges that subsequently were tested showed different changes in the leakage rate when the bolt strain was changed. The authors reported that one of the steel flanges showed a steady increase in the leakage rate with an increase in bolt strain, whilst a second steel flange (with the negative face taper angle) showed a small initial reduction in the leakage rate, but this reduced as the bolt strain was further increased. The third steel model showed no change in the initial leakage rate with increasing bolt strain. Using the third steel model, Lewis found that by rotating the flanges relative to each other large changes in the leakage rate could be achieved. The leakage rate varied from a 60% increase to a 30% decrease from the original results depending on the angle of rotation. Lewis took their investigation a further step by conducting a finite element study to find the variation in flange contact. From this, the authors found good agreement with the previously published works of Meck, who stated that the contact area would be only slightly greater than the bolt head area. The authors concluded from the experimental work that a very small

positive face taper angle made the initial leakage rate very sensitive to bolt load, but a very small negative taper angle made the initial leakage rate of a joint insensitive to axial load.

2.2.1.12. [Fessler *et al.* [21]]

This work was continued by other authors who studied the effects of an applied load. Fessler *et al.* (1988) used three different flange shapes in this study. The first flange contained a flat face but had a 'step' hub. The second flange contained a small negative face taper angle, and the third flange was of the same design as the second but had a normal flat face. It was assumed that the fluid would display isentropic flow conditions through the small gaps. The authors used air as the working fluid and sealed the flanges under test by the use of O-rings and endplates in a separate joint. A rotating flowmeter was again used to measure the inlet air flow and pressure transducers measured the internal pressure of the test section.

Fessler used concrete cylinders of known volume inside the test sections to reduce the total volume of compressed air inside the test section. The flanges were tapped for pressure readings at five points, each midway between two bolts. No axial tension was applied to the second and third flange pairs (which were made from steel) but the testing of the first flange was slightly different. The first flange, cast from Araldite, was tested in the same way as before, with a range of internal pressures but it was also tested with the application of a range of axial loads. The pressure tappings on this flange were the same as the other two flanges. A total of twelve flange pairs were tested. From experimental results, it was consistently noticed by the Fessler that there was trend of decreasing leakage with increasing bolt load. They also noted that leakage increases linearly with axial joint force, but it was suggested that this result may be associated with the high stiffness of the steel bolts. Fessler concluded that their fluid flow assumption gives good results at low pressures but underestimates the leakage as the internal/external pressure ratio increases. They then extended their study by conducting a linear-elastic finite element study of the load-induced deflections of the flanges. Fessler studied the three loading cases of internal pressure and axial tension. As a result of the finite element work the authors found that the assumed passage shape of rectangular at the inlet and sinusoidal at the outlet was very close to the true shape of the gap. The flow rate and pressure distribution where then calculated by a specially written computer program. The program was based on the classic case of laminar viscous flow between two flat plates. The gap was given an equivalent

rectangular width for use in the program. It was also noted by Fessler that the program could not be used when the momentum term dominated the viscous term or when the flow velocity approached the sonic velocity, i.e. the flow neared choking conditions. The authors concluded that when a small positive taper angle (i.e. contact on the inside surface first) was machined onto the faces of the flanges, then the passage becomes convergent and can reduce the leakage significantly when compared to the flange with a small negative taper angle. It was also noted that the leakage through the bolt threads of flanged joints with a negative taper could become significant if the axial load to initial bolt load ratio exceeds 0.2.

2.2.1.13. [Hyde *et al.* [22]]

The work of Fessler was extended by Hyde who studied the effects of bolting and loss of contact in gasket-free joints. Hyde *et al.*(1988) used both finite element analysis and experimental methods to determine the contact regions between flat-faced flanges (without gaskets) for several different operating conditions. The two flanges had different face angles; one set has nominally flat faces and the other has a small negative taper angle such that the outside edge of the flanges touched first.

Hyde strain-gauged four diametrically opposite bolts in order to measure the strains that were exerted on the bolt. Strain measurements were taken during the torquing operation as well as during the tests. The casings were then pressurised with air and the axial tension on the joint was the same as the pressure on the end plates. The joint with the small taper angle exhibited less leakage than the joint that had nominally flat faces and consequently a higher internal pressure was achieved. The authors recorded the strain measurements at regular intervals up to the highest internal pressure and then repeated the experiments for a higher bolt load. The authors noted that significant errors existed due to thread friction and the inaccuracy of the torque wrench. Hyde noted that when an axial load and internal pressure were applied, a general pattern of bolt strain was consistently followed. The gradient of the strain measurements taken from the inside of the bolt started with a negative slope and then inflected to an increasingly positive slope. The outside strain measurements started with a zero gradient and slowly changed to a small negative gradient demonstrating a compressive strain. The authors also noted that the position of the

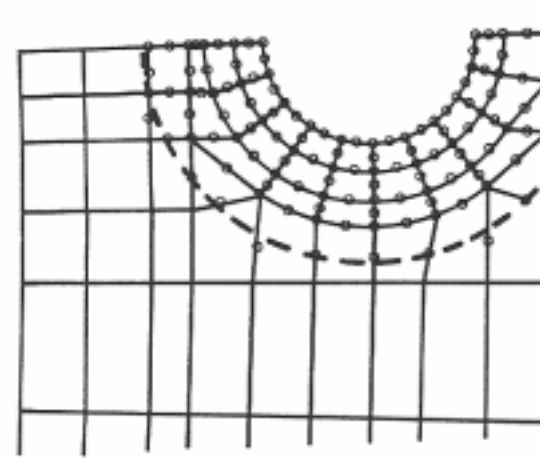

Figure 9: Full Contact Boundary Condition

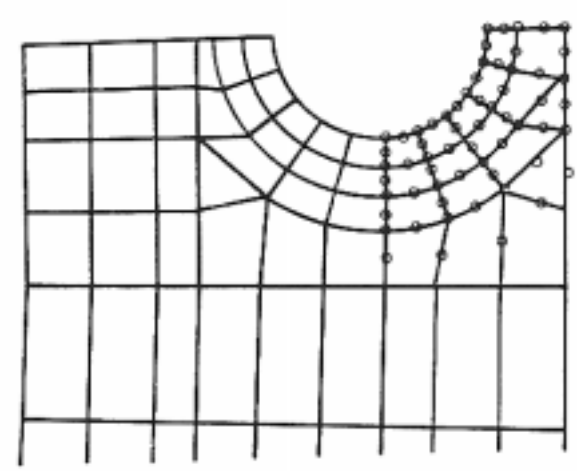

Figure 10: Half Contact Boundary Condition.

asymptotes differed for the two joints: the asymptotes for the joint with the negative taper angle occurred at a smaller bolt force ratio (axial bolt force/ initial bolt force) that those for the nominally flat faced joint.

Hyde also conducted a three dimensional finite element analysis in order to determine the bolt stresses, flange deflections and contact areas. This model was of the flat faced flanged joint with three different contact conditions: full contact, half contact and 'outside' contact, as shown in Figures 9-11 on this page.

The small circles in Figures 9-11 demonstrate assumed contact between the flange faces. From the results produced by this model, Hyde noted that the effects of axial loading predominate over those caused by internal pressure, and conclude that this dominance increases as the contact area decreases. For the full contact area condition (Figure 9), the finite element and experimental bolt stresses were in good agreement. When examining the effects that the load conditions had on the gap sizes, the authors noted that all applied loading conditions increased the size of the gap at the inside of the flange. When axial load and radial pressure were

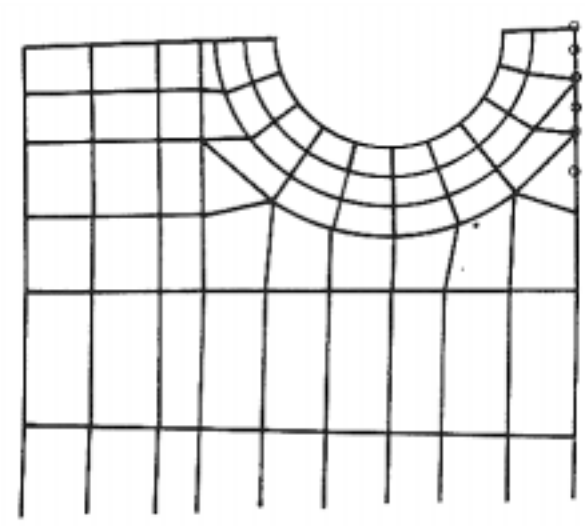

Figure 11: Outside Contact Boundary Condition.

applied they observed a decrease in the size of the gap.

2.2.1.14. [Webjörn [23]]

Webjörn (1989) continued his study by summarising the theory behind the compact flange design. The operation of the compact flange was demonstrated by the use of Rotscher diagrams, to show the preloading and operation stages and the load effects that these stages have on the bolts. He then stated the stress in the bolts caused by a dynamic external load could be reduced to almost zero by preloading the correctly designed bolt properly. The author then set out several principles for this type of flange design. It was stated that the bolts should be slender and elastic, but the flanges should be rigid and solid with no gaskets. Thick hard washers should be used throughout, nuts should conform to ISO 898/1 and that the joint should only be assembled by a trained mechanic familiar with the background theory. Webjörn also stated that the joint should always be designed to be stronger that its' associated pipework. He compared the operation of the compact flange to the conventional flange and illustrated the different centres of rotation of the two types of flanged joint. Webjörn also emphasised the need for proper training and qualifications for mechanics who assemble and preload flanges joints. He stated that the preloading operation was of premium importance and that a minimum of 80% of the guaranteed yield strength should be applied. The use of hydraulic tensioners is recommended by the author for the larger sizes of bolts, but the tensioners must be of good quality and the threads of both the nut and bolt must allow a "sloppy" fit when no load is applied. He concluded by demonstrating that the compact flange has consistently lower stress levels at the hub/flange connection and the areas under the bolt heads when compared with the conventional flange.

2.2.1.15. [Cao and Bell [24]]

Cao and Bell also studied the problem of the flanged joint. Cao and Bell (1993) simplified the joint, which consisted of a flange, hub and tube, and removed the hub and any gasket in order for the authors to conduct an elastic analysis of an axial force exerted on a circular flange joint. The resistive forces of the bolts are assumed to be uniformly distributed around the flange at a distance equal to the bolt circle. The authors considered two models, one that assumes the flange thickness to be negligible, the second, more common, model takes into account the flange thickness and transfers the radial force to the middle of the

flange thickness and includes the additional bending moment caused by this transfer. They solved both models for the interactive force and bending moment that acts between the flange and tube. They state the relating equation between the two models. From previous work, the authors stated that the maximum bending and hoop moments occur at either the inner or outer edge of the tube/flange connection. Cao and Bell calculated these moments at both surfaces for a single tensile force, a single bending moment and thereafter superimposed these effects to obtain a more general solution. The authors verified their theoretical analysis by the use of a finite element program PAFEC. Good comparisons were found between the analysis and the FEM program when shell elements were used, demonstrating the agreement between the analysis and thin plate and shell theory. When the authors used axisymmetric elements, small differences were apparent between the stresses at the load and support positions and between the displacements. It was suggested that the reason for this was that the distortion of the joint and local effects were not included in the models. The authors stated that the second model represented the best agreement with elastic theory. Cao and Bell noted that if the flange is relatively thin in comparison with the flange width, then the first model is a good approximation.

2.2.1.16. [Hyde *et al.* [25]]

Hyde (1994) continued their long term study of gasket-free joints by experimentally quantifying the sealing performance of conical (or taper) faced flanges in metal-to-metal contact. Both hydraulic and air pressure tests were carried out by the use of pressure transducers. The air pressure tests were conducted using a mains supply which passed through a rotating flowmeter. The only exit for the air was thus through the test joint. The main purpose of the hydraulic test was to determine the leakage pressure of the joint. Throughout all tests, four of the 24 bolts were strain gauged and measurements were recorded. During the hydraulic tests, the axial tension in the wall was reported to be proportional to the internal pressure. Hyde defined a leak from the joint as being a visible leak during a period of two minutes at a constant joint pressure. It was also noted that if the pressure was then increased further by a small amount then a leak would normally have been seen within the first five seconds. From these hydraulic tests Hyde concluded that the sealing efficiency of the joint was independent of the bolt load so long as the bolt load was less than that required to fully close the joint. The authors also found that if the bolt closure load was exceeded then the sealing efficiency decreases. The bolt closure load

could only be exceeded if the flanges were not sufficiently stiff, and so, leakage remains possible since a full contact circle does not exist. The sealing efficiencies for the reference and thin flanges used in the authors experiments were found to be 86% and 77% respectively when 24 bolts were used. For the air leakage tests the authors defined a perfect seal as a leakage of less than 0.01 litres per minute (185.72 cubic feet per year). From these tests, it was found that all of the joints were capable of sealing perfectly until the axial load was close to the total bolt load. Hyde noted that the cyclic bolt stresses and strains that were measured were very low up to and including the hydraulic leak pressure. The authors also noted that the scatter of the bolt loads was rather high at $\pm$10% although extreme caution had been taken. The discrepancy between the average and the lowest bolt loads was also found to be significant and did not change when the bolt load was increased to the closure load or the rated bolt load. In conclusion, the authors stated that the tapered flange is effective in sealing large diameter joints under the conditions of internal pressure and axial loading. However, the effectiveness of the joint decreases as the bolt spacing increases. The tapered flange also exhibited very small cyclic strains under the test conditions.

2.2.1.17. [Cao and Bell [26]]

Cao and Bell (1996) furthered their investigation of circular flange joints from before. The authors used the same flange geometry (i.e. exclusion of the hub and any gasket) for the determination of the bolt forces when the joint is under tension only. Finite element (ABAQUS) and analytical methods were used. The bolt forces could not be directly determined from the applied tension force because of the existence of a contact force between the flanges. The authors used axisymmetric and three dimensional models in this study and the three characteristics of bolt preload, tension force and joint geometry were varied and investigated. From the finite element study, the authors concluded that a uniform distribution of force applied at the bolt circle was a sufficiently accurate simplification for the bolts. It was noted by the authors that the contact area is limited to around the bolt hole when bolt preload is applied. Upon the application of a tensile force to the joint, the contact area moves towards the outside edges of the flanges. Cao and Bell stated that the contact force varied between joints from around 20% to 60% of the tension force. They found that the maximum bending stress in the tube was greater than that in the flange and that the tube at the junction with the flange would yield first. The authors also

noted that nearly all of the tube could reach a plastic state before the flange would start to yield. Cao and Bell stated that although bolt preload can significantly affect the behaviour of a joint at low-tension loads, this effect reduces as the tension load increases. The authors also created a mathematical model to simulate the results from the finite element study. This was achieved using the 'unit load method'. The mathematical model was then extended to calculate not only the bolt loads, but the deflection of the flange as well. After analysing a range of joints, Cao and Bell concluded that a good agreement had been achieved between their mathematical model and the results of the finite element analysis. The authors then simplified their formulae to give a small overestimation of the bolt force and to make the formulae easier to use.

2.2.2. Summary Points:

- Several small diameter bolts of high elasticity and stiff flanges with a thickness of at least four times the bolt diameter should be used. [10]
- The bolts should be pretensioned to above 80% of their minimum yield strength. [10]
- Pretensioning of the bolts increases the fatigue life of the flanged joint and does not induce significant stresses in the flanges. [11]
- Pretensioning of the bolts reduces flange separation and possible leakage. [11]
- When the bolting assembly is preloaded above a level that is dependent on the magnitude of the internal pressure, then changes in the bolt working loads will be insignificant. [14]
- The contact pressure between the flange faces and the bolt working loads increase with increasing tensile stiffness of the bolts. [14]
- As the bolt preload and flange tensile stiffness are increased then the flange deformation and bolt working load decrease. [14]
- The single plate assumption previously used when calculating the contact areas and pressure distribution leads to significant margins of error. [15]
- The size of the bolt hole does not affect the size of the contact region. [16]
- When the bolt spacing is less than 1.5 times the diameter of the contact region, then the contact regions will interact. [16]
- Hub stresses in compact flanges can be controlled by the angle of taper at the hub, but this also changes the minimum pressure for separation of the flange faces. [17]

- The compact flange is less sensitive to thermal shock than the conventional gasketed flange as it loses only one third of its bolt preload while the conventional flange loses all of its preload. [18]
- The use of high-grade heat treated fasteners with asymmetrical thread profiles increases the fatigue strength of the bolts by approximately 100%. [19]
- An indirect relationship exists between an applied torque and the bolt preload because of the presence of friction. [19]
- Machining the flange faces can reduce the initial leakage rate by an order of magnitude when compared to an 'as cast' flange face finish. [20]
- A small positive taper angle makes the initial leakage rate sensitive towards the bolt load, but a small negative taper angle causes the opposite reaction towards the bolt load. [20]
- A flanged joint with a negative taper angle exhibits less leakage than a flanged joint with nominally flat faces. [22]
- The effects of axial loading dominate over those caused by internal pressure. This dominance increases as the contact area decreases. [22]
- When an axial load and internal pressure are applied to a flanged joint, the size of the gap increases at the inside of the flange and decreases at the outside. [22]
- The sealing efficiency of a flanged joint is independent of the bolt load until sufficient bolt load is applied to fully close the joint. If this load is then increased further, then the sealing efficiency decreases. [25]
- The tapered flanged joints are effective in sealing large diameter joints when internal pressure and axial loads are applied. This effectiveness decreases as the bolt spacing increases. [25]

3. Methodology

3.1. Modelling of Flanged Pipe Joints –Modelling Options

As detailed in the literature survey, flanged pipe joints have already been modelled using finite element analysis by Hyde *et al.* (1988 and 1994), Webjörn (1985) and others. None of the previous finite element work has utilised a three-dimensional model which included modelling the bolt, and allowed for the analysis to predict the variation in the contact area and contact pressure. The use of a three-dimensional model eliminates the need for simplifications, such as removing the effects associated with the bolt hole or assumptions allowing the fillet at the hub/flange ring junction to be disregarded. These are perhaps the two main assumptions that have been frequently used to simplify the analyses of flanged pipe joints.

While these assumptions/simplifications are may be valid in certain situations, depending upon the main objective of the study, none of these can be applied to the present work. The reasons for this are based upon the desire to examine both the strength and sealing ability of the flanged joints. In order to do this, qualitative measures of strength and sealing ability must be employed. For the present study, the level and distribution of the various stress components, as well as the overall stress intensity, are used to quantify the comparative strength of the flanged joints. The contact, or interface, pressure is used as the main quantitative measure of the sealing ability of the three joint styles that will be subject to experimental validation in the future. This is discussed in Chapter 7.

For the purpose of finding the most suitable type of model, preliminary studies were conducted. The 'best type' of model was defined as one which provides sufficient detail of the stress distribution, together with additional information about the variation of contact between either the two flange faces or between the flange face and the gasket (or seal ring) if present.

A two-dimensional model is not suitable for this study since it is necessary to determine the effects, if any, which the bolt hole has on the contact and stress distributions. The use of three-dimensional general contact elements is necessary to provide the required information regarding the contact area and pressure. The main alternative to this would have been to constrain the two surfaces together and calculate the contact pressure from

the average of the nodal reaction forces (per element) and the element area. This process would not allow for any separation between the two surfaces and it would have been very time consuming. This was a numerical technique that was often used to evaluate contact effects prior to the advent of general contact element elements.

Fully parametric models were used throughout so that the time involved in building scaled geometry models of different sizes could be minimised. The meshing attributes of the models were also parametrically defined. Cross sectional drawings of the three flanged joints are shown in Figure 12-14 on pages 42-44. Explicit definitions of the parameters labelled in the figures can be found in the nomenclature.

It should be noted that only the VCF joint contains a washer. Although it is optional for a washer to be used in the ANSI flanged joint, it is not stated in ASME VIII Division 1 as being compulsory and so was not included for the purposes of this study. No washer is included with the Desflex flanged joint.

During the initial phase of the study, attempts were made to obtain as much information as possible from Destec Ltd., about the geometry; preloading methods and materials used in the Desflex flanged joint. Destec were willing to provide the vast majority of the geometry information required to build the finite element models. However, the company believed that the information about the geometry and material of the seal ring was commercially sensitive and they were not prepared to divulge such information to an external body. Shell (UK) provided a sample Desflex flanged joint, complete with seal ring as a scaled comparison for the models that were to be produced. It was then necessary to scale the size of the seal ring provided to suit the flanged models that were being made. Unfortunately, this procedure, which incorporated the use of a careful hand, a pair of callipers, a micrometer and a steel rule, was not very accurate and so a margin of error must exist. The scaling of the seal ring to the flange may not have been the same as that intended by Destec. For the reasons given above it is believed that some minor discrepancies may exist between this work and any other work where the exact dimensions of the seal ring are known.

A variety of parameters, including element type, mesh density, material model type and convergence options were investigated to optimise the parametric models used in the main investigation. A four inch $1500^{\#}$ class Verax compact flanged joint was used throughout this preliminary comparative study. In Chapter 3, sections 3.1.1-3.1.3 the

parameters mentioned above are discussed in detail. The results of these initial investigations are given in section 3.2.

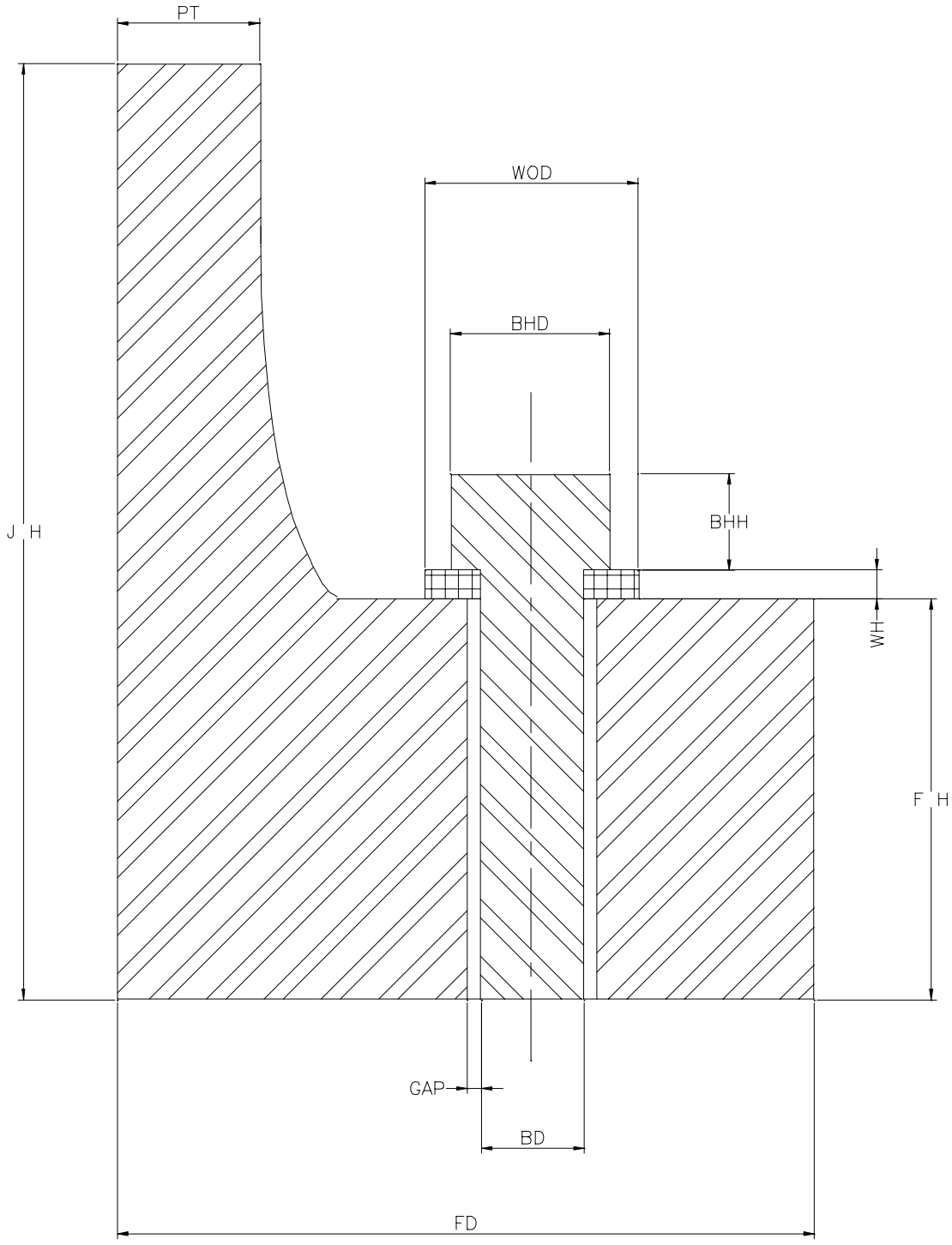

Figure 12: Cross Section of the Verax Compact Flanged Joint

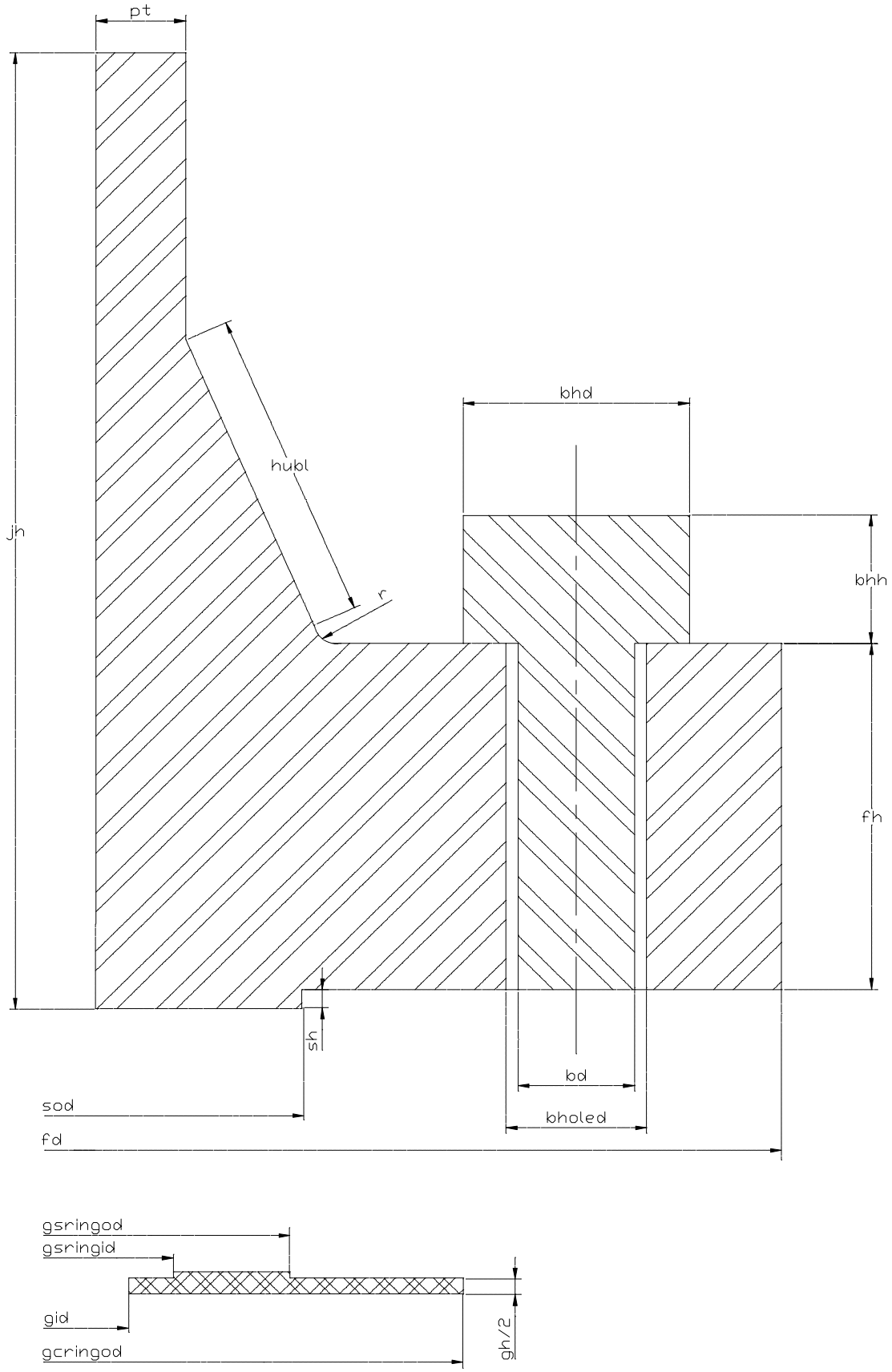

Figure 13: Cross Section of ANSI Flanged Joint

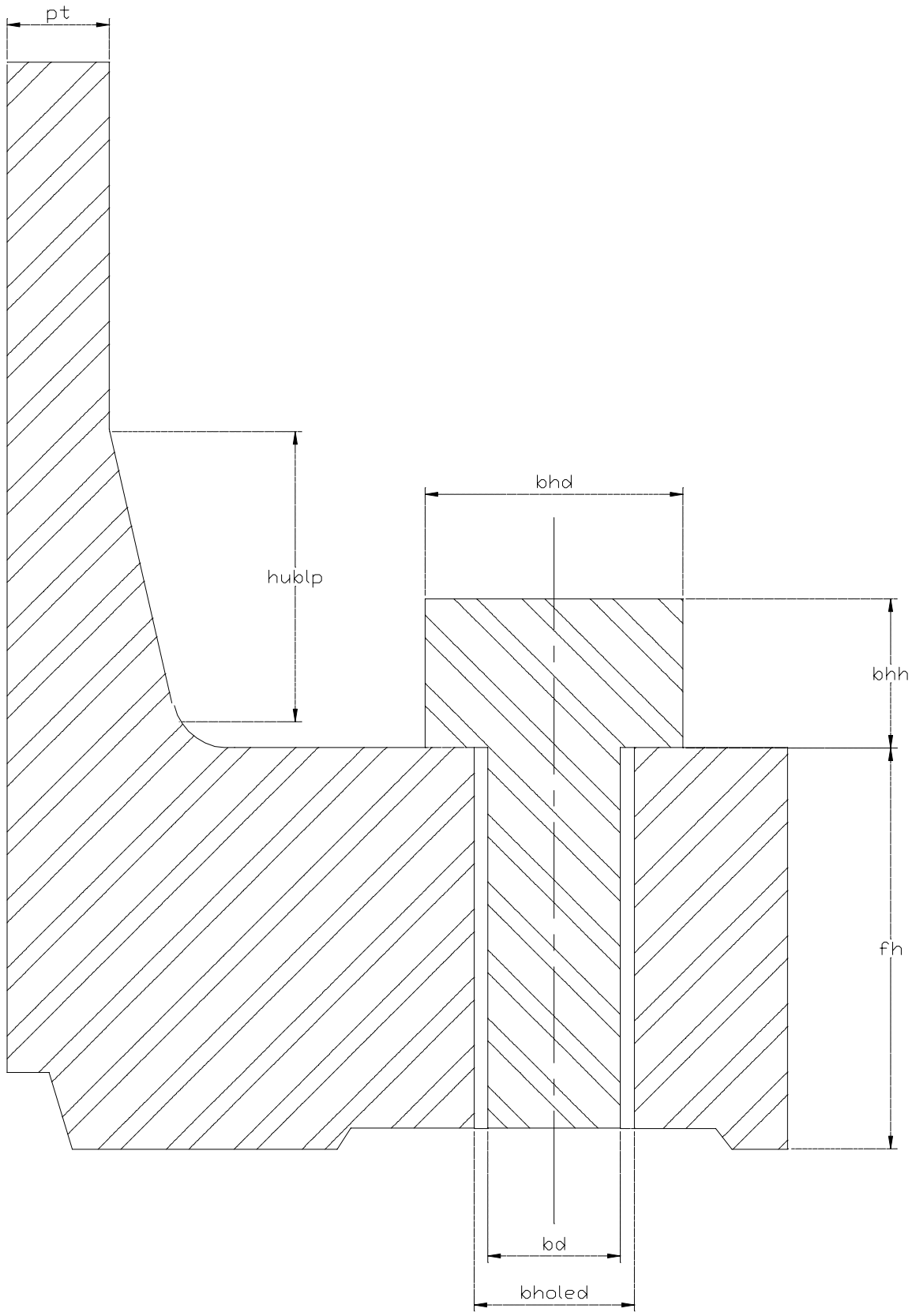

Figure 14: Cross Section of Desflex Flanged Joint

3.1.1. Element Choice

Since both stress and contact information were required outputs from this study, it was necessary to use two classes of element; solid elements to model the solid entities and contact elements to ensure that one of the solid entities did not penetrate through the other. The justification for the selection of the particular element type from each class is included in this section along with details of the element properties.

Solid Elements

The SOLID45 isoparametric structural element was used to model the flange, bolt and symmetry plane. The eight-noded SOLID45 element was initially chosen as a starting point since it has the fewest degrees of freedom whilst ensuring reasonable results and therefore allows the fastest solution times. This was thought to be of the greatest benefit as the emphasis at the early stage was on producing working models rather than on the accuracy of the results. Once a convergent solution had been achieved, and accurate results were later required, the results obtained using the SOLID45 element could be compared with those from the SOLID73 (an eight-noded element with translational and rotational degrees of freedom) or twenty-noded SOLID95 elements.

The SOLID45 is a three-dimensional element defined by eight nodes, each with three translational degrees of freedom (about the *x*, *y* and *z* axes). This element can undergo plasticity, creep, swelling, stress stiffening, large deflection and large strains. The SOLID45 element is shown below:

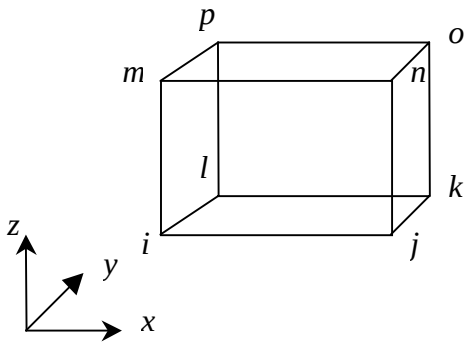

Figure 15 : The SOLID45 Element

The SOLID73 element also consists of eight nodes but each node has six degrees of freedom (translation and rotational in, and about the *x*, *y* and *z* axes). This element is

considered to give more accurate results than the SOLID45 without the large solution times of the SOLID95 element. The SOLID73 is not quite as accurate as the SOLID95 element for like numbered mesh densities.

The SOLID95 element is a high order structural quadratic solid element. This element consists of twenty nodes each having three translational degrees of freedom (about the *x*, *y* and *z* axes). Because of the increased number of nodes, the SOLID95 element has the larger solution times and requires a greater amount of processing power, but it is the more accurate. Like the SOLID45 and SOLID73 elements, the SOLID95 has the ability to demonstrate plasticity, creep, stress stiffening, large deflection, and large strains.

Contact Elements

In the past four to five years, commercial finite element software has introduced several types of contact element for both two-dimensional and three-dimensional applications. For both cases, contact elements can simulate 'point-to-point' contact and 'point-to-line' contact (for 2D) or 'point-to-surface' contact (for 3D). Since the general contact pattern between the flange and the gasket or flange and the symmetry plane could not be predicted, a general 'point-to-surface' contact element was required.

The three-dimensional 'point-to-surface' CONTAC49 contact elements were used between the flange face and reference (symmetry) surface to simulate contact distribution. The use of the CONTAC49 element type requires that the associated solid element used to model the flange and symmetry plane must not contain mid-side nodes. Therefore, the SOLID95 element is no longer suitable for this type of study.

The CONTAC49 element has the ability to represent contact and sliding between two surfaces. The element consists of one node (the point) on the 'contact' surface and four nodes that define the 'target' surface. The contact surface is displaced towards the 'target' surface until penetration between the point node and the 'target' surface occurs. A contact stiffness (*KN*) must be attributed to this element type. The contact stiffness quantifies the level of penetration that the 'target' surface will allow. If this value is too small, over penetration will occur and the results from the model will be inaccurate - too large a contact stiffness and the model will not converge towards a solution. The CONTAC49 element is shown overleaf:

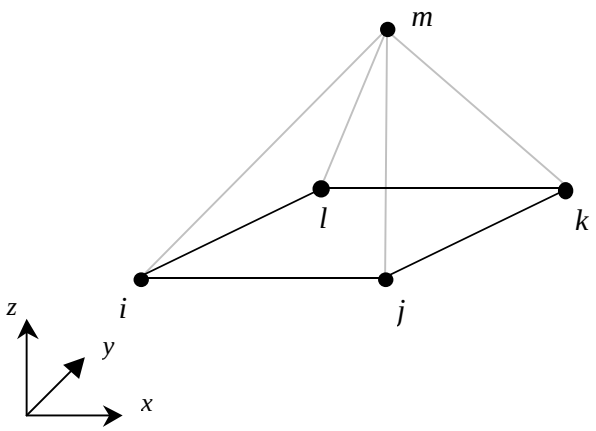

Figure 16: CONTAC49 Element

As shown in Figure 16 above, the contact node is denoted by the letter *m*, whilst the target area is defined by the nodes *i*, *j*, *k*, and *l*.

The normal contact stiffness, *KN*, is defined in the ANSYS Elements Manual[28] as:

$$KN = f\ E\ h$$

where, *f* is an arbitrary factor, *E* is Young's modulus of Elasticity, and *h* is a characteristic dimension, normally the average element edge length. Because *f* is an unknown factor, chosen by the user, which can vary between 0.1 and 100, a wide range of acceptable values for *KN* can be obtained. Since it is known that too small a value of *KN* causes a reduction in the accuracy of the results, it was decided that a suitable value of *KN* could be obtained by accepting the highest value of *f* that would allow the models to converge. By doing this, the highest degree of accuracy possible would be obtained at the cost of increased solution time.

The CONTAC49 element also has the ability to simulate levels of friction between two surfaces. In this study, no friction was employed between any of the surfaces, since the forces normal to the contact surfaces would be far greater than the shear forces. Therefore, this is a reasonable assumption.

After the CONTAC49 element has been used, a large volume of information is made available to the user about the status, position of contact, size of target area and various force components. The element output also supplies the size of any gap or over penetration that may exist. It should be noted that the position of contact between the

contact node and the target area is defined in a non-dimensional format as shown in Figure 17 below:

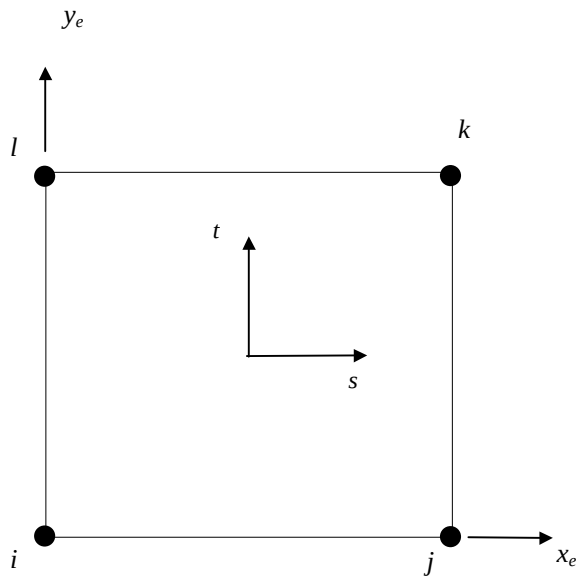

Figure 17: Target Co-ordinate System of the CONTAC49 Element.

The non-dimensional *s* and *t* axes are parallel to the element *x* and *y*-axes respectively. In the above co-ordinate system, node *i* is at location *(-1, -1)* and node *k* is at *(1,1)*.

3.1.2. Mesh Refinement

Two mesh densities were initially compared using the VCF joint as a case study. A basic mesh was compared with a mesh design that had been refined based on prior knowledge of the position of highly stressed areas and the stress distribution in ANSI flanged pipe joints. A second mesh was generated by refining around the upper surface of the flange ring, especially around the bolt hole and the hub/flange ring fillet. The mesh was also graded through the hub and attached pipe so that more elements were present near the outer surface of these components. The two mesh designs can be seen clearly in Figure 30 (unrefined mesh) and Figure 31 (refined mesh) on page 61.

Linear elastic material properties and the SOLID45 element type were used in these models, since this was a comparison of mesh density only. These properties allowed for the quickest solution times. The results from this comparison are contained in section 3.2 along with the results of the other preliminary model studies.

3.1.3. Material Properties

The material properties for the flanged joints were specified by Shell (UK). The properties for the specified materials are given in the tables below:

VCF	1500# Class			2500# Class		
	E (N/mm^2)	α	σ_{yield} (N/mm^2)	E (N/mm^2)	α	σ_{yield} (N/mm^2)
Flange/ Pipework	203395	0.3	248.2	195121	0.29	448.2
Bolt	210000	0.3	940	210000	0.3	940

Table 1: VCF Joint - Material Properties

ANSI	1500# Class			2500# Class		
	E (N/mm^2)	α	σ_{yield} (N/mm^2)	E (N/mm^2)	α	σ_{yield} (N/mm^2)
Flange/ Pipework	203395	0.3	248.2	195121	0.29	448.2
Bolt	204774	0.3	723.9	204774	0.3	723.9
Gasket	110000	0.16	111	195121	0.3	206.8

Table 2: ANSI Flanged Joint - Material Properties

DESFLEX	1500# Class			2500# Class		
	E (N/mm^2)	α	σ_{yield} (N/mm^2)	E (N/mm^2)	α	σ_{yield} (N/mm^2)
Flange/ Pipework	203395	0.3	248.2	195121	0.29	448.2
Bolt	204774	0.3	723.9	204774	0.3	723.9
Seal ring	202016	0.3	250	202016	0.3	250

Table 3: Desflex Flanged Joint - Material Properties

As a second phase of the preliminary studies, a comparison between two different types of material properties was made. The commonly used linear elastic properties were compared against bilinear kinematic hardening material properties. Both material models are shown in Figure 18 overleaf:

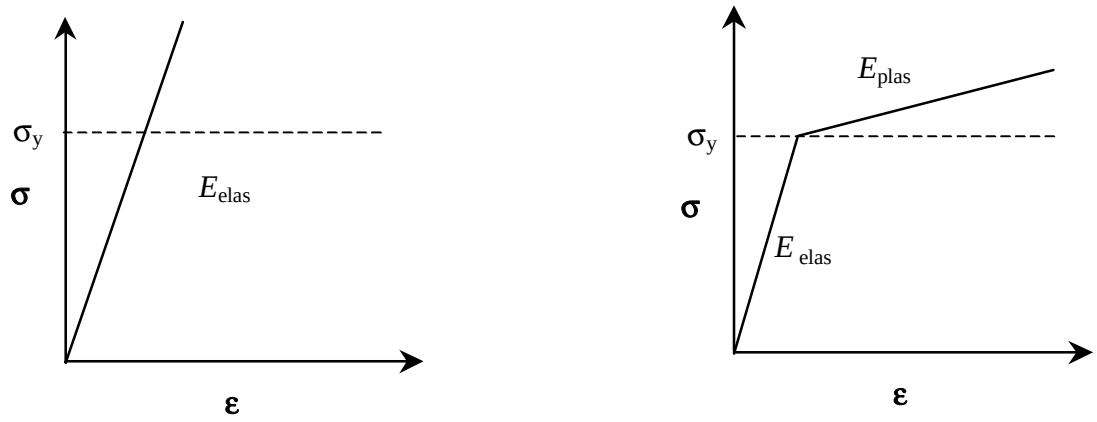

Figure 18: Material Properties - Linear Elastic versus Bilinear Kinematic

By definition, linear elastic materials contain no yield criterion. This suggests that the load carrying capacity of the material is independent of the magnitude of stress. The effect of this is that the modelled material that is subject to a stress greater than the yield stress of the actual material has the same load carrying capacity as the elastic material. This is known to be inaccurate especially when large quantities of plasticity occur. Therefore, this material model is satisfactory when only small quantities of the material are exposed to the yield stress or greater. The bilinear kinematic material model uses the Von-Mises yield criterion and a kinematic hardening and flow rule. Kinematic hardening assumes that the yield surface retains a constant size but moves in stress space with continued yielding. This is shown in Figure 19 on page 51. The flow rule determines the direction of plastic straining that will occur normal to the yield surface.

A bilinear material model consists of two sections each having a linear gradient. The first section, which models the elastic material, is valid until the yield stress is reached. The gradient of this section is the Young's Modulus of Elasticity. The second section which functions beyond the yield stress, and models the behaviour of the plastic material, has a gradient of the plastic tangent modulus, which for this study was 5% of the Young's Modulus of Elasticity. This value was determined from the stress-strain curve for a general purpose steel. It should be noted that this value is a general approximation and was not calculated for the materials listed in Table 1, 2 or 3 on page 49. No stress-strain curve was readily available for the specified materials.

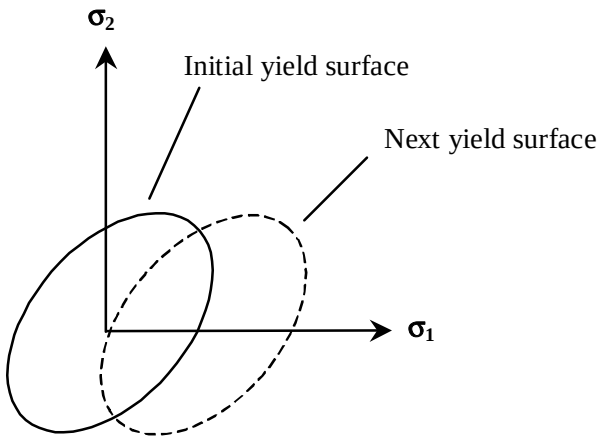

Figure 19: Bilinear Kinematic Hardening Rule

3.1.4. Loading Conditions

In order for a complete understanding of the loading that is exerted upon a flanged joint, a multi-loadstep procedure was used. This method permits an examination of the flanged joint at each stage of the loading process, i.e. at the initial contact step, the bolt-up step or the final step after the internal pressure has been applied. This allows for a better understanding of the complete installation procedure in terms of stressing and deformation rather than being limited to an analysis of the final condition only. The load steps are listed as follows:

- The 'contact' surface is brought into contact with the flange face by initiating penetration through a very small distance (nominally 0.1 microns). This distance is kept very small so that no significant additional stresses are present in the model.
  A solution is then obtained for this load step.
- A negative surface pressure is applied to the base of the bolt shaft. This surface pressure simulates the prestress normally applied by a torque wrench or hydraulic tensioner.
  A second solution is obtained for the combined effects of these load steps.
- The surface pressure is then removed and a zero displacement boundary condition is applied to the base of the bolt shaft.
- Internal pressure or other external loading is applied to the model.
  A third and final solution is obtained.

The applied preload for the VCF joint was specified by Webjörn as approximately 80% of the yield strength of the bolt material. As stated earlier, the yield strength of the bolt material was 940 N/mm^2 and so the applied bolt preload was 720 N/mm^2. Desflex specified a preload of 620 N/mm^2 for their flanged joint. This preload also remained the same for each joint size and pressure rating. A nominal preload of 50% yield was chosen for the ANSI flanged joint. The associated ASME standard does not specify a magnitude of preload for the bolts, only a minimum seating stress that relates to the gasket style and composition. The preload for the ANSI joint was based partially on the practical knowledge that most fitters of flanged joints tighten the bolts as hard as possible.

The magnitude of the internal pressure that was applied depended upon the pressure rating of the flanged joint, i.e. 1500$^{\#}$ or 2500$^{\#}$ class. The 1500$^{\#}$ class flanged joints were subject to a 240 Bar or 24 N/mm^2 internal pressure, while the 2500$^{\#}$ class joints were loaded with a 386 Bar or 38.6 N/mm^2 internal pressure. These pressures were supplied by Shell as design pressures. The application of the internal pressure also included the contribution from the end-cap loading. This was applied to the end of the pipework, a suitable distance away from the joint. The distance that was used was taken from Thomson [6] (Section 2.1.1.5 on page 17). A force balance calculation provided the magnitude of the end-cap loading:

Equivalent end-cap Force = Reaction Force in pipe wall

$$P_{internal} \times \pi \left(\frac{pid}{2} \right)^2 = P_{axial} \times \pi \left\{ \left(\frac{pod}{2} \right)^2 - \left(\frac{pid}{2} \right)^2 \right\}$$

$$\text{Therefore, } P_{axial} = \frac{P_{internal} \times pid^2}{pod^2 - pid^2}$$

The symbols used can be found in the nomenclature.

The boundary conditions remain the same for each of the load steps and flanged joint styles, as follows:

- Symmetry boundary conditions are applied to both sides of the flange ring and attached pipework, i.e. the surface with, and the opposite side from, the bolt hole.

- Symmetry boundary conditions are also applied to the bolt cross sectional area.

These boundary conditions remove the possibility of the restricted body displacing or rotating through any of the applied planes of symmetry.

3.2. Preliminary Model Studies

The four inch 1500# class VCF joint was modelled with different element types, mesh densities and material models in an effort to determine the best type model to use for the parametric study. A model was also tested with the same geometry but without the use of the contact analysis procedure. In this model, full contact was assumed between the two flange faces. Instead of applying the contact elements between the flange face and a second 'symmetry' surface, a zero (vertical) displacement boundary condition is applied to the base of the flange model. The second and third load steps of prestressing and applying any external loads remained the same for each model. This model provides a good reference with which to compare the contact analysis and would perhaps have been sufficient for the parametric study if the variation in contact pressure between the flange faces was not of direct importance.

The properties of the models that were used in the preliminary studies are summarised below:

Model #1: Linear elastic material properties, displacement constraint applied to base of flange ring instead of using contact elements, and an unrefined mesh. Model #1 was meshed using SOLID45 elements (described in section 3.1.1).

Model #2: Linear elastic material properties, displacement constraint applied to base of flange ring instead of using contact elements, and a refined mesh. Model #2 was meshed using SOLID45 elements.

Model #3: Linear elastic material properties, displacement constraint applied to base of flange ring instead of using contact elements, and a refined mesh using SOLID73 elements.

Model #4: Linear elastic material properties, CONTAC49 and SOLID45 elements were used, as well as a refined mesh.

Model #5: Bilinear kinematic material properties, CONTAC49 and SOLID45 elements were used, as well as a refined mesh.

Where possible, all of the convergence tools available within the ANSYS program were used. These tools are summarised below:

NEWTON-RAPHSON APPROACH

The Newton-Raphson approach repeatedly applies a linear approximation in small iterations until an equilibrium solution is obtained to within the applied tolerances. The convergence tolerance that was used throughout this study was $\pm$0.1%, i.e. the default value. The convergence of both the force and moment balance of the model was used.

AUTOMATIC TIME STEPPING

This option allows the best balance between accuracy and economy of time to be achieved. If the program solves a step of the load easily then it can increase the proportion on the load that can be applied in the following step. The program can also reduce the size of the next step if there was difficulty in reaching convergence, or bisect the current step if it fails to converge.

LINE SEARCH

Line search is an adaptive descent, convergence enhancement tool. If stress stiffening is detected, the size of the following step is decreased by a scaled factor (between 0 and 1).

The following pages present a number of stress intensity plots are included for each of the preliminary models for comparison purposes. The stress intensity was plotted instead of directional stresses so that the relative comparisons could be made using the minimum number of plots. The bolt and washer were removed from the flanged joint for Figure 25 to Figure 34 so that a closer examination of the bolt hole effects could be made.

The dimensions of the four inch 1500$^{\#}$ class VCF joint can be found in Appendix I starting on page 106.

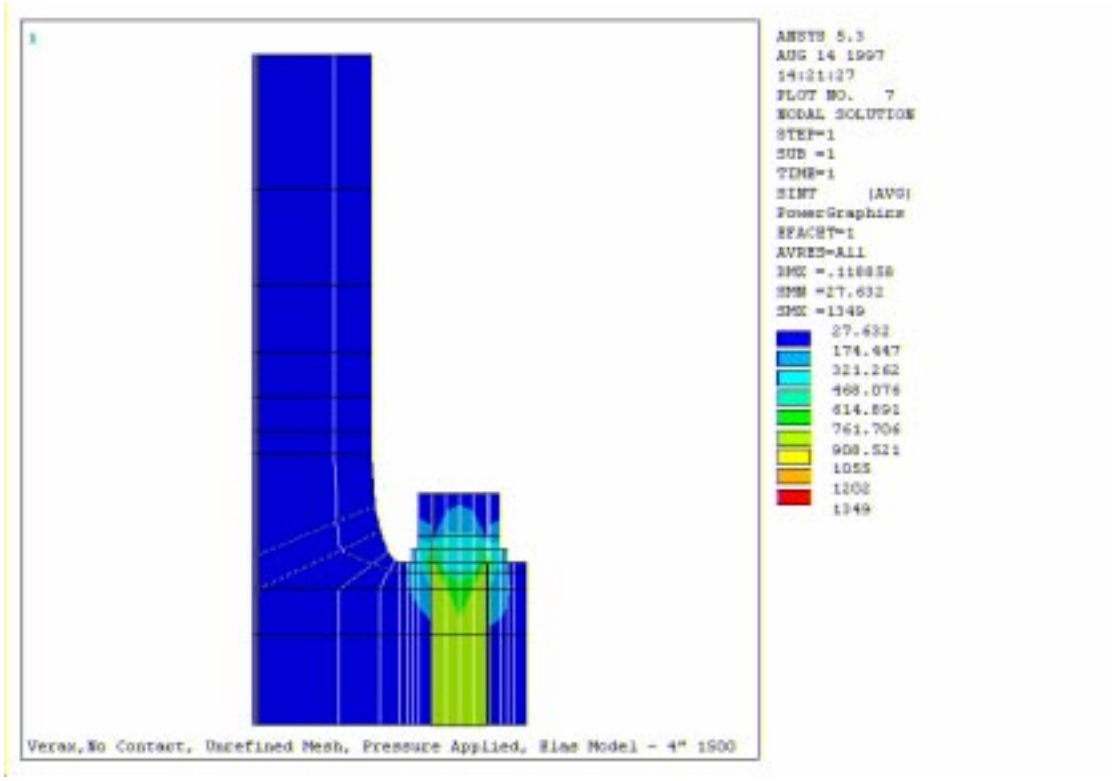

Figure 20: Preliminary Model #1, Complete Model - Stress Intensity Plot

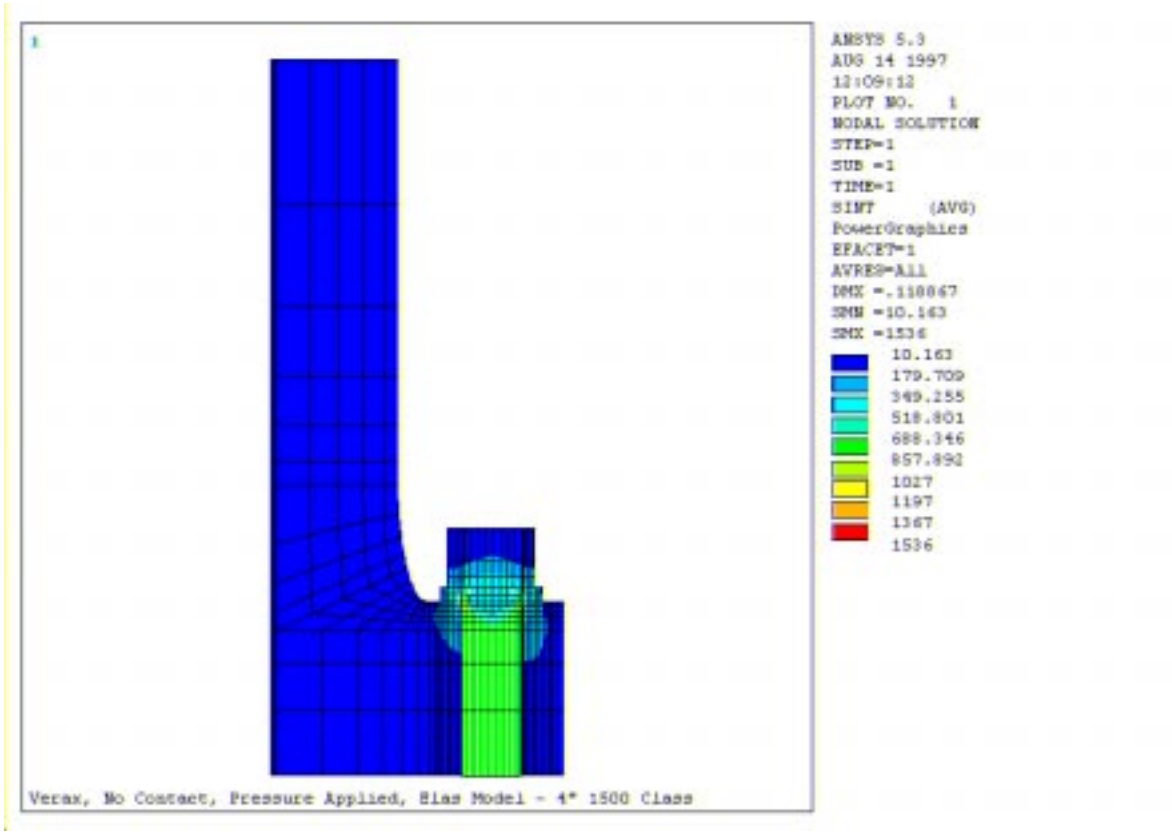

Figure 21: Preliminary Model #2, Complete Model - Stress Intensity Plot

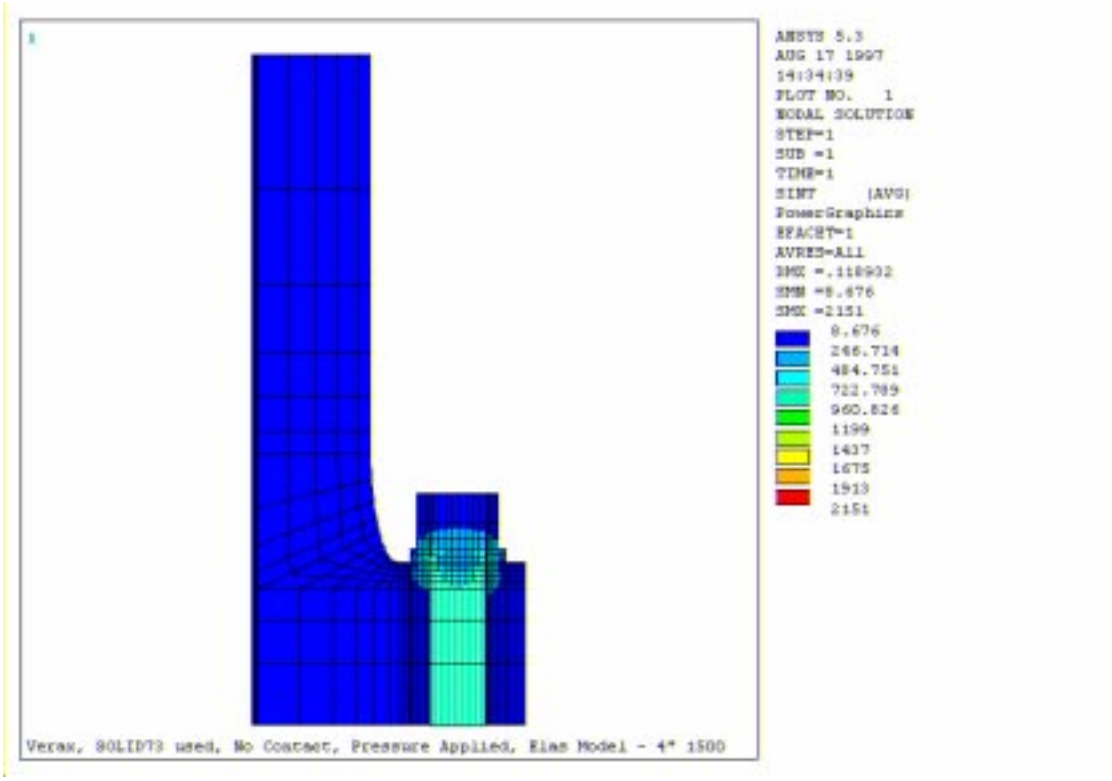

Figure 22: Preliminary Model #3, Complete Model - Stress Intensity Plot

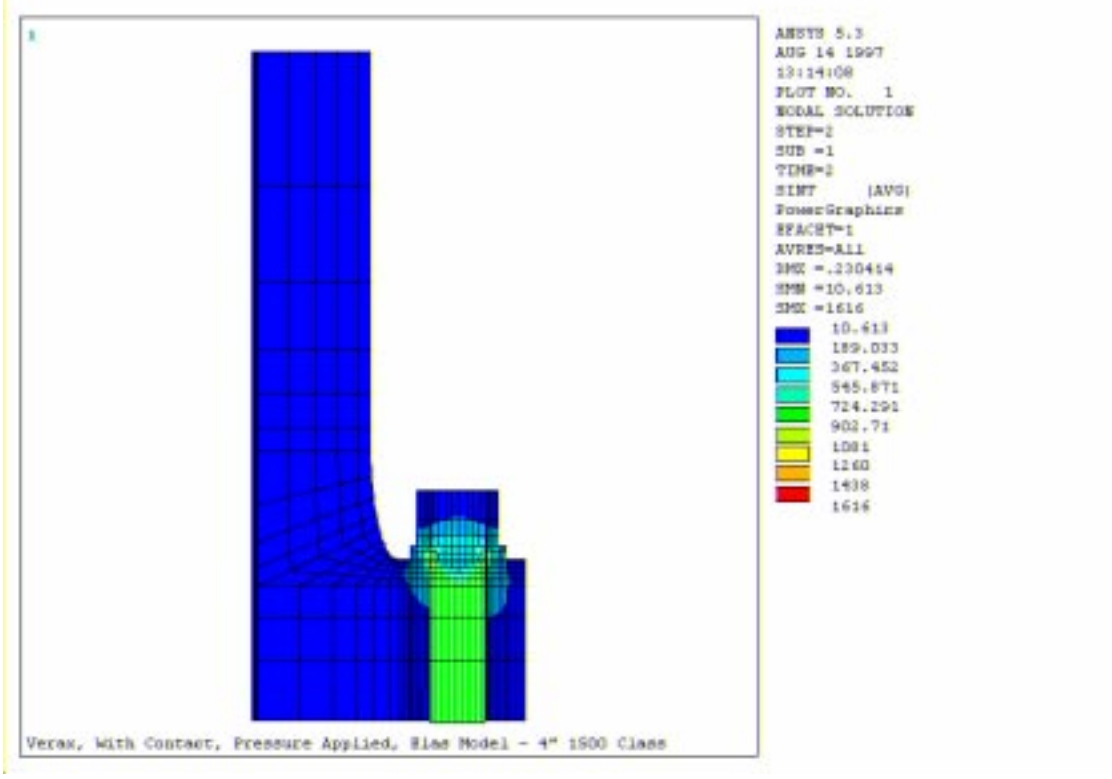

Figure 23: Preliminary Model #4, Complete Model - Stress Intensity Plot

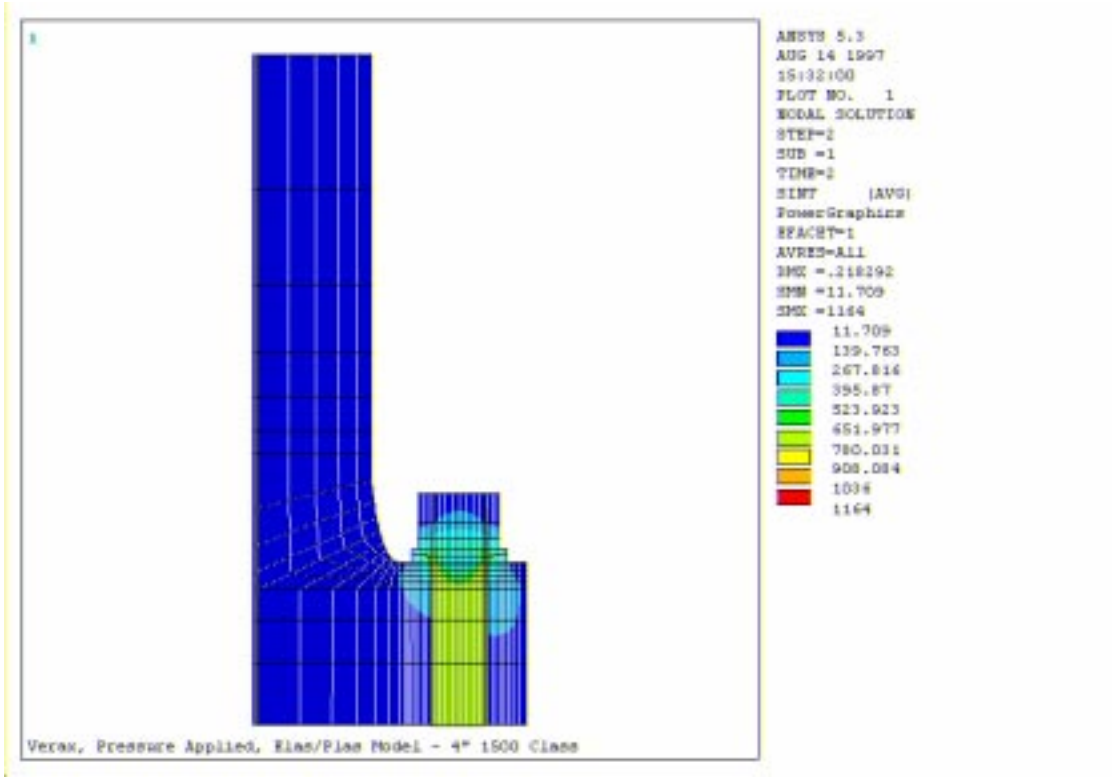

Figure 24: Preliminary Model #5, Complete Model - Stress Intensity Plot

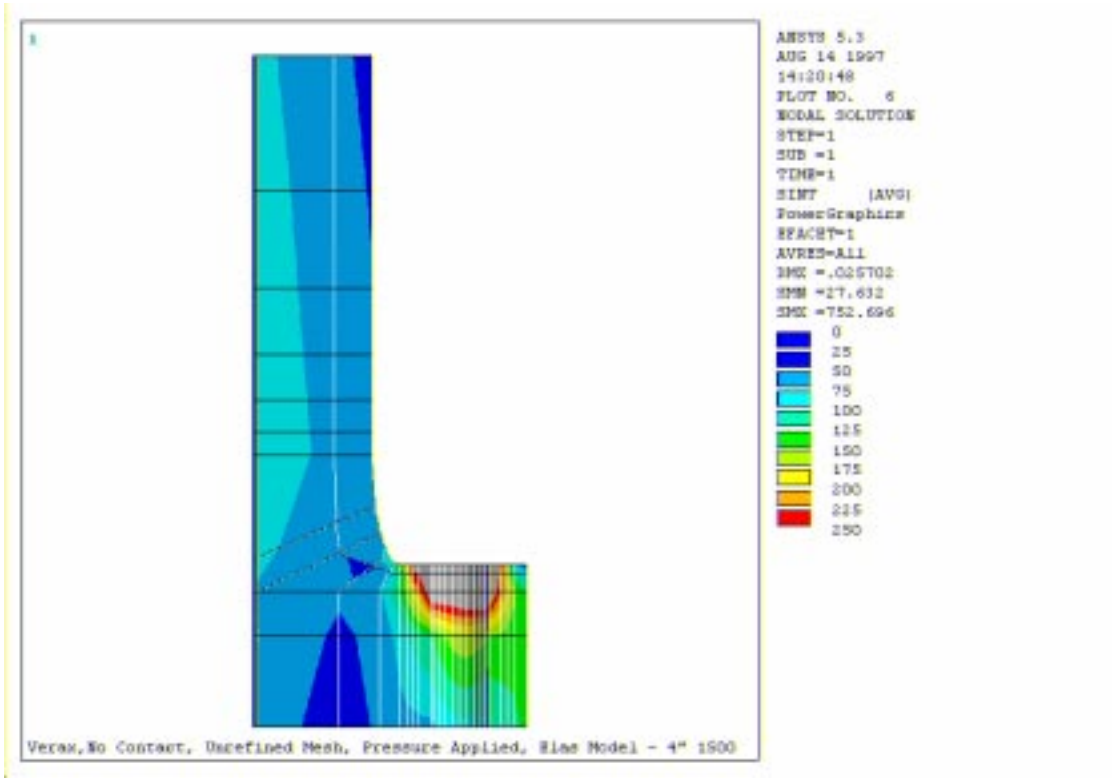

Figure 25: Preliminary Model #1, Flange/Pipe only - Stress Intensity Plot

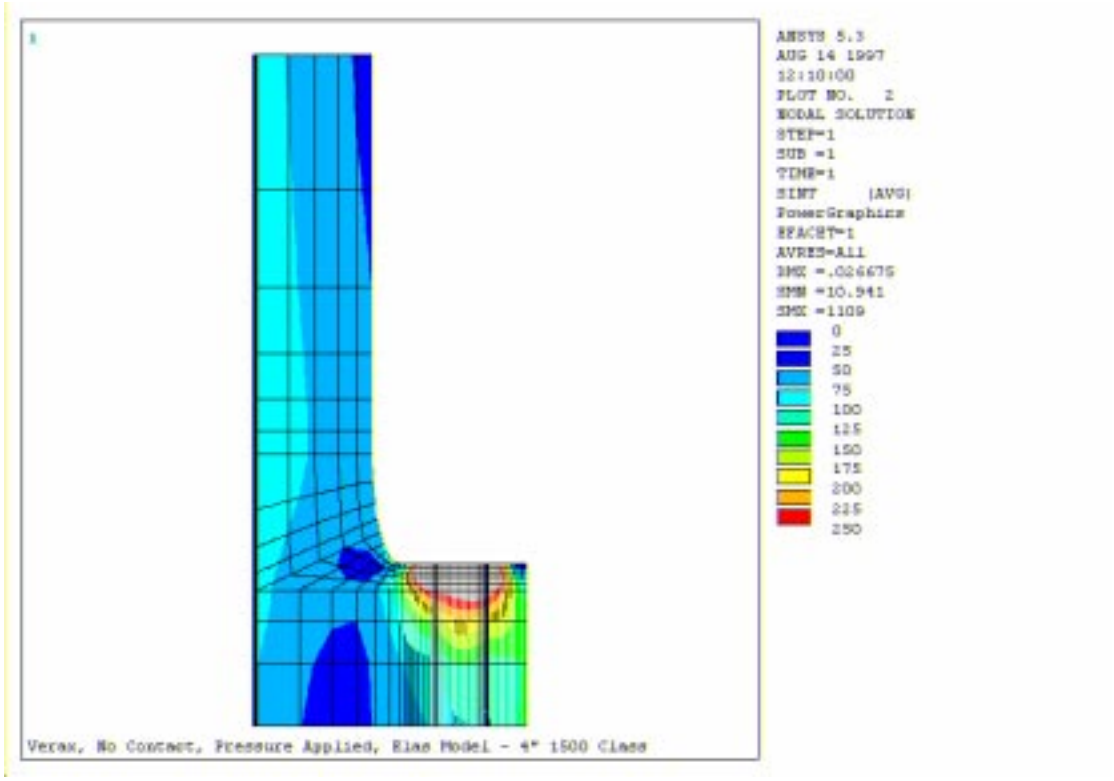

Figure 26: Preliminary Model #2, Flange/Pipe only - Stress Intensity Plot

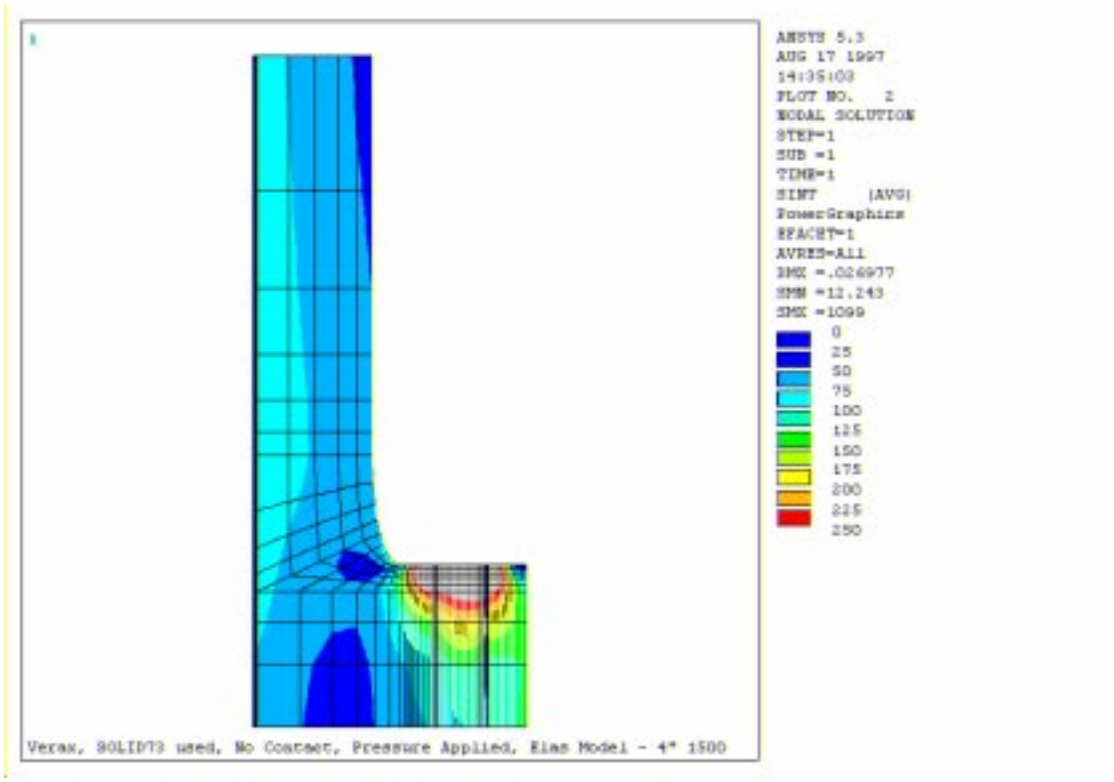

Figure 27: Preliminary Model #3, Flange/Pipe only - Stress Intensity Plot

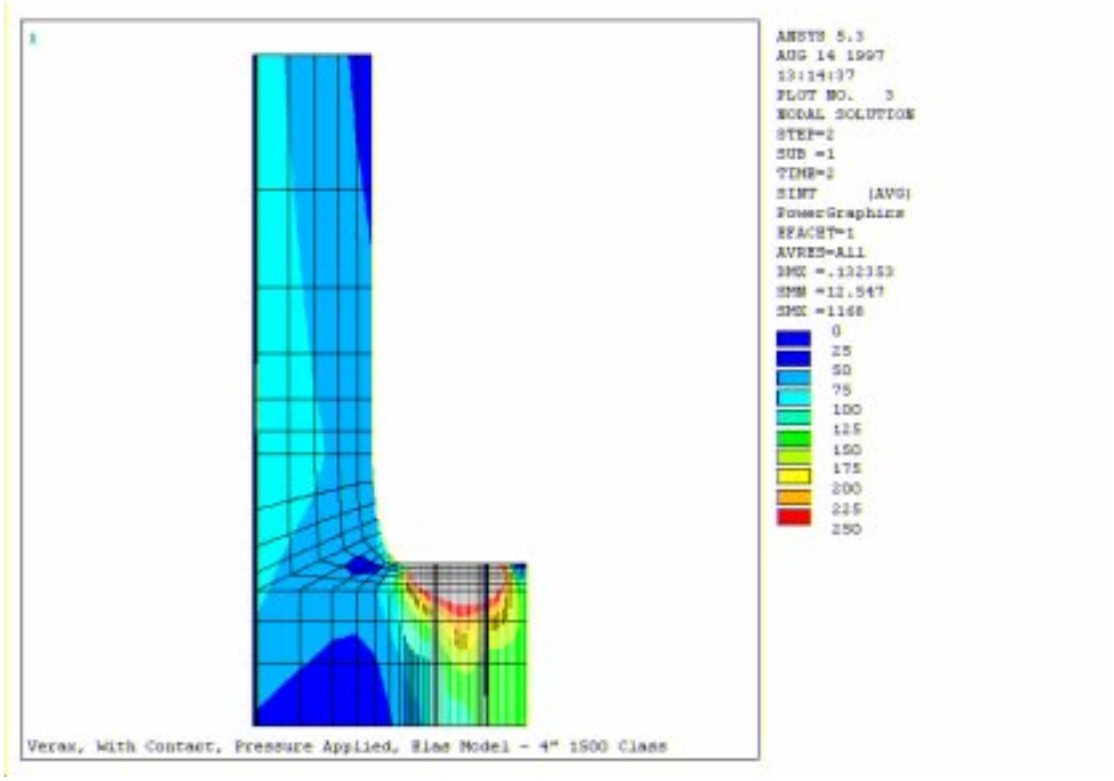

Figure 28: Preliminary Model #4, Flange/Pipe only - Stress Intensity Plot

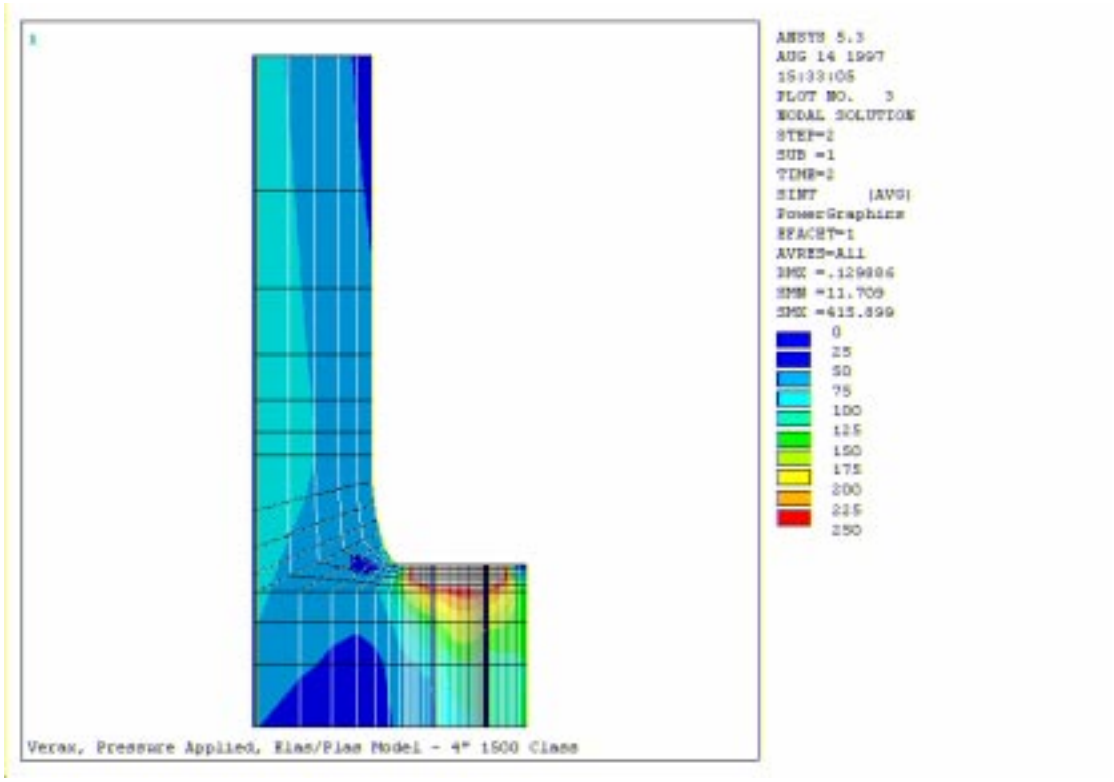

Figure 29: Preliminary Model #5, Flange/Pipe only - Stress Intensity Plot

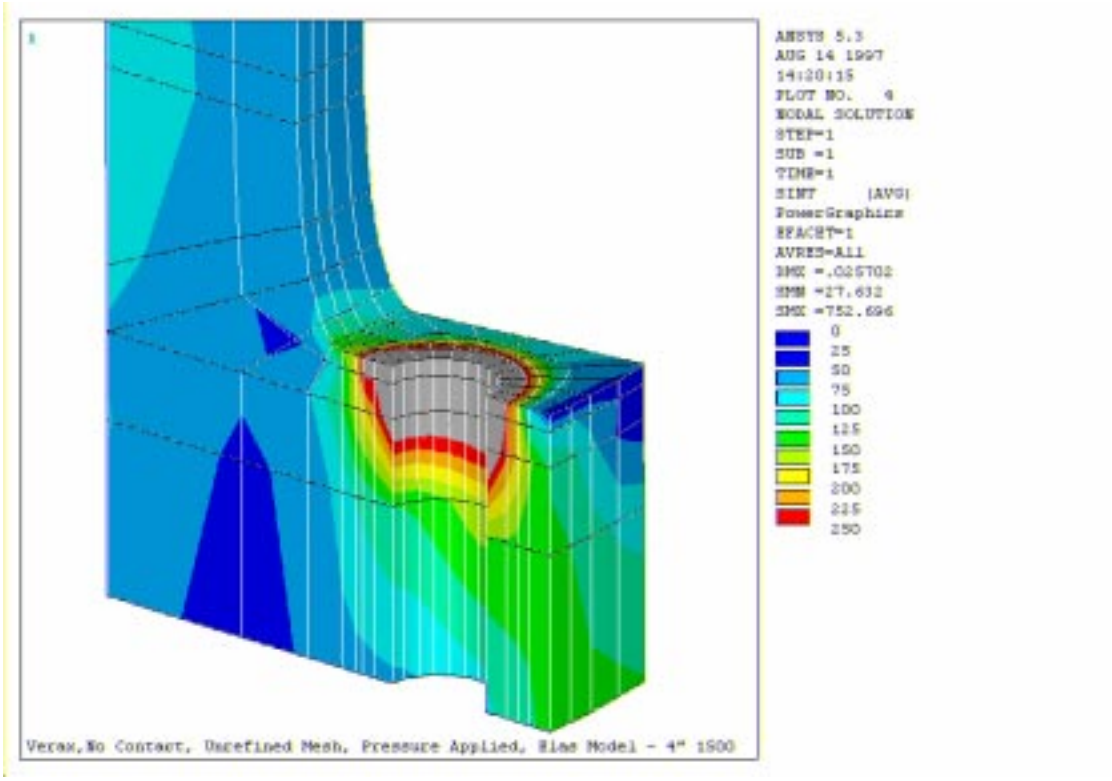

Figure 30: Preliminary Model #1, Flange/Pipe only - Magnified Stress Intensity Plot

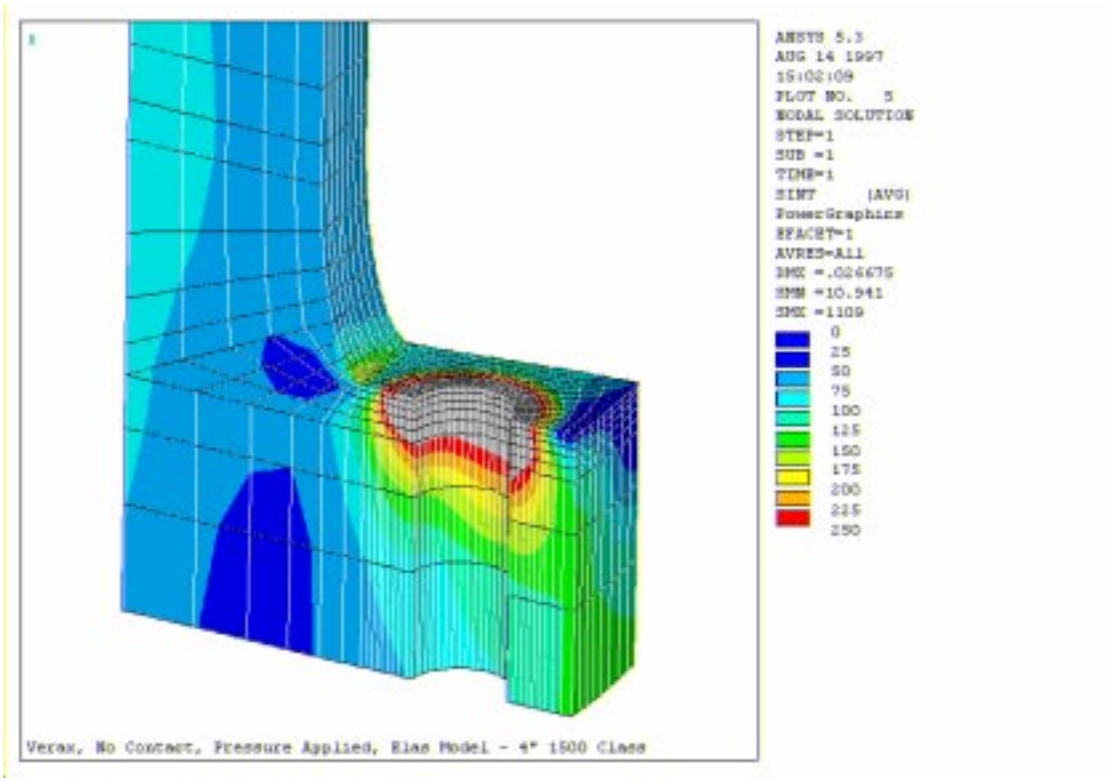

Figure 31: Preliminary Model #2, Flange/Pipe only - Magnified Stress Intensity Plot

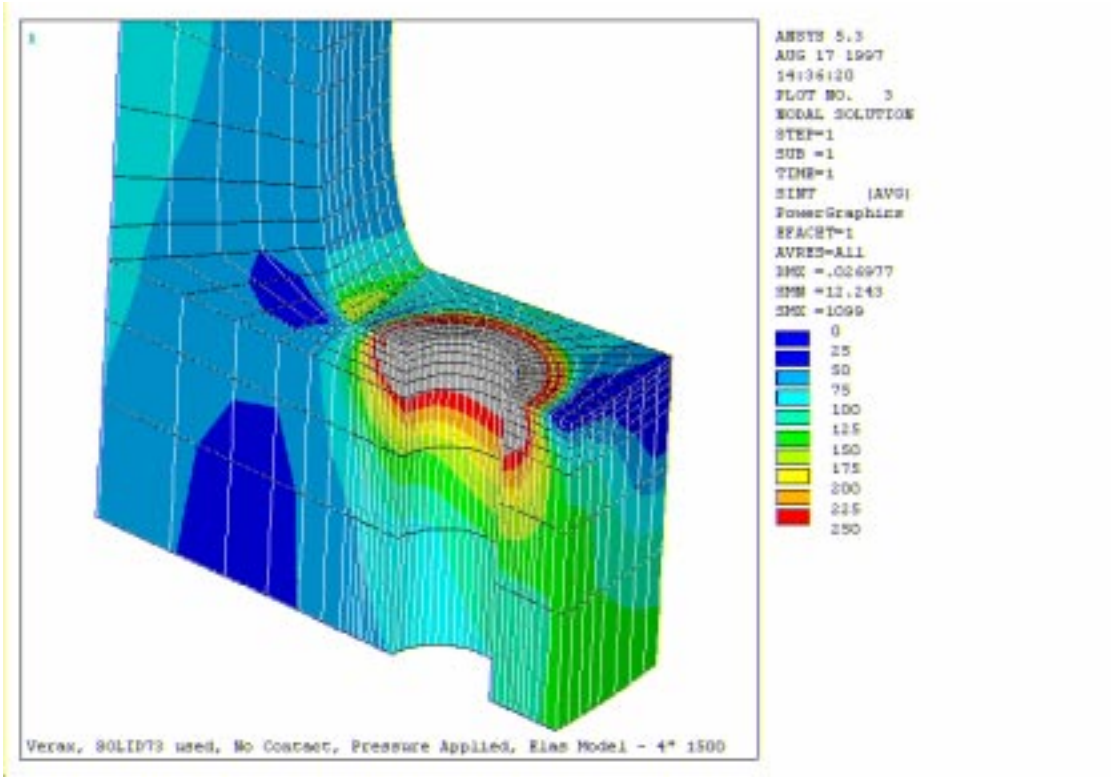

Figure 32: Preliminary Model #3, Flange/Pipe only - Magnified Stress Intensity Plot

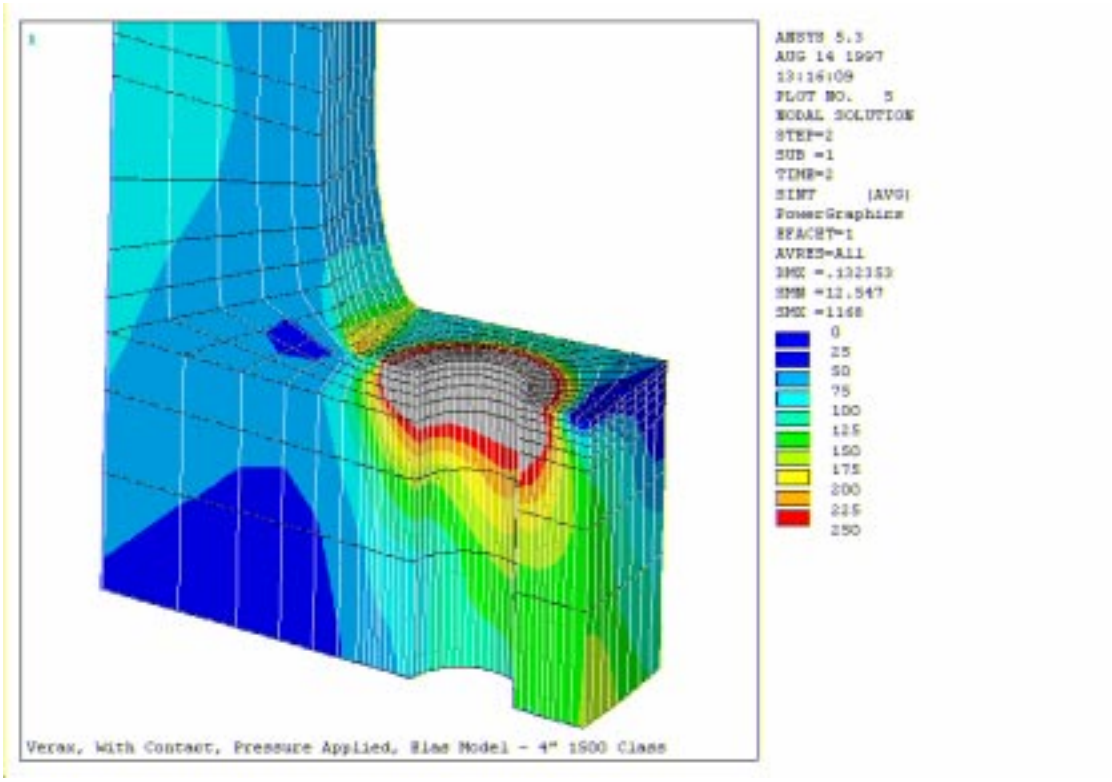

Figure 33: Preliminary Model #4, Flange/Pipe only - Magnified Stress Intensity Plot

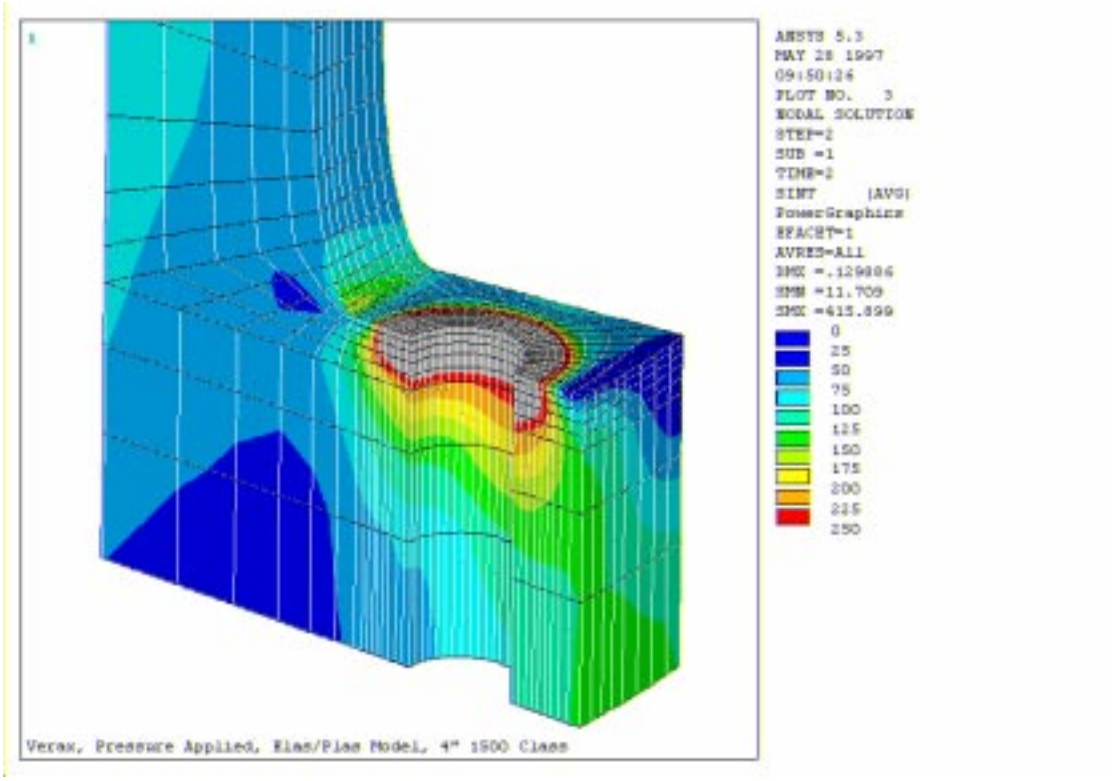

Figure 34: Preliminary Model #5, Flange/Pipe only - Magnified Stress Intensity Plot

3.2.1. Comparison of Mesh Densities

The stress intensity plots from the preliminary models #1 and #2 give a good comparison between an unrefined and a refined mesh. All of the other properties of these models are the same. The stress gradient through top of the bolt shaft shown in Figure 20, of the unrefined mesh, is quite different from that shown from the refined mesh in Figure 21. The increase in accuracy from the refined mesh is demonstrated again in the upper section of the flange ring. This is shown by comparing Figure 30 and Figure 31. Model #1, which contained the unrefined mesh, consisted of only 514 SOLID45 elements and 2,164 degrees of freedom. This model had a solution time of 173 CPU seconds on a R5000 150MHz Silicon Graphics Indy workstation. Comparatively, model #2 had 4,144 SOLID45 elements and 14,748 degrees of freedom. Model #2 took 642 CPU seconds to reach a solution. The solution of the more accurate model #2 was 3.71 times slower than model #1. The increase in time taken to solve was deemed acceptable in order to obtain improved accuracy.

3.2.2. Comparison of Element Types

Preliminary models #2 and #3 were used to compare the accuracy and solution times of the SOLID45 and SOLID73 elements. From Figure 21 and Figure 22, the maximum stress intensity differs greatly from 1536 N/mm^2 (model #2) to 2151 N/mm^2 (model #3). Although there is a large difference in magnitude, this is a very localised effect. Upon comparison of the plots of the flange/pipe section in Figure 26 and Figure 27, the stress distributions were almost identical. Similar observation is also found when the magnified stress intensity plots, Figure 31 and Figure 32, were compared. The preliminary model #3, which utilised the SOLID73 element, took 331 CPU seconds longer that model #2. This is a 51.5% increase in the solution time. It was therefore concluded that for this mesh density, there was no benefit in using the SOLID73 element over the SOLID45 element.

3.2.3. Effects on Stress Results from the use of Contact Elements

Figure 23 and Figure 24 shown the overall change in stress distribution between the model employing contact elements (preliminary model #4) and by using the fully constrained boundary condition (preliminary model #2). From these two plots of stress intensity there is very little difference in the stress distribution. By examining the flange ring and attached pipework (in Figure 26 and Figure 28), it is apparent that a small difference in the stress distribution through each model does exist at the base of the flange ring. It is believed that this is a result of the ability of the contact elements to separate from the symmetry plane, as would exist in a VCF joint. These plots demonstrate the unrealistic restriction that is imposed when the base of the flange is subject to a zero displacement boundary condition. The difference in stress distribution is shown clearly by comparing Figure 31 and Figure 33.

Model #4 took considerably longer to solve due to the increase in the total number of elements to 5544, compared with 4144 for model #2. This number of elements can be broken down to 4144 SOLID45 elements used for modelling the flange, pipe, bolt and washer, 280 SHELL63 elements which were used to model the symmetry plane and 1120 CONTAC49 elements. Model #4 consequently required more time to solve –

2353 CPU seconds (39 minutes and 13 seconds), a 266% increase compared with model #2.

3.2.4. Comparison of Results from Linear-Elastic and Bilinear Kinematic Material Models

Preliminary models #4 and #5 contained linear elastic and bilinear kinematic material properties respectively. These were used to determine if there was any benefit by using a more complex material model. The comparison between any pair of stress intensity plots for models #4 and #5 showed a different stress distribution through the flanged joint. Figure 23 and Figure 24 show a 27% reduction in the maximum stress in the joint from 1616 N/mm^2 to 1164 N/mm^2 by the incorporation of the bilinear material model. The difference in the stress distribution through the pipe and the inside of the flange ring, as shown in Figure 28 and Figure 29 is negligible. However, a comparison of Figure 33 and Figure 34 shows a significant difference in the magnitude of stress through the flange ring around the bolt hole. The level of stress at the hub/flange ring intersection is also reduced. The solution time was increased by 32.6% to 3120 CPU seconds (52 minutes). The reason for the increase in the solution time was for the redistribution of the stress from the material that had exceeded the specified yield limit.

3.3. Contact Pressure Evaluation

The CONTAC49 contact element supplies the user with a range of information from the analysis. This element details the new and old contact statuses, the total normal force for each element, the gap or penetration size, the target area for each element and the dimensionless location at which the 'contact' node breached the target area.
The procedure to generate a plot of the contact pressure over an area is detailed below:

1. All contact elements are selected,
2. An element table of the contact status of each element is generated,
3. All contact elements that were in contact are selected,
4. Element tables of the total normal force and target area are generated for the selected elements,
5. A specially written 'do' loop calculates the contact pressure from the total normal force exerted over each target area,
6. The contact pressure is then plotted.

The contact pressure distribution from the preliminary work was found to be very difficult to interpret and, as uncertainties existed about the procedure used to obtain the contact pressure distributions, a test model was constructed. The contact pressure evaluation procedure was tested by the use of a simple block problem. A quarter block was brought into contact with a flat surface. The Young's Modulus of the block (2,070 N/mm^2) was lower than that of the opposing surface (1E9 N/mm^2) so that the block would compress without the surface deflecting in any way. The value of the contact pressure is straightforward to calculate and the pressure contours are expected to be 20,700 N/mm^2.
The flat surface was intentionally made larger in area than the base of the flat block so that the complete base surface of the block would remain in contact with the opposing surface as the block was compressed. The quarter block model was ten millimetres long in each direction. If the opposing surface was of the same size as the base of the block then, when the block was compressed, the nodes at the outer edge of the block would have be displaced off the edge of the flat surface due to the Poisson effect. If this had

occurred then the associated contact elements would not have registered any contact between the two surfaces as having taken place.

The model is shown in Figure 35 overleaf:

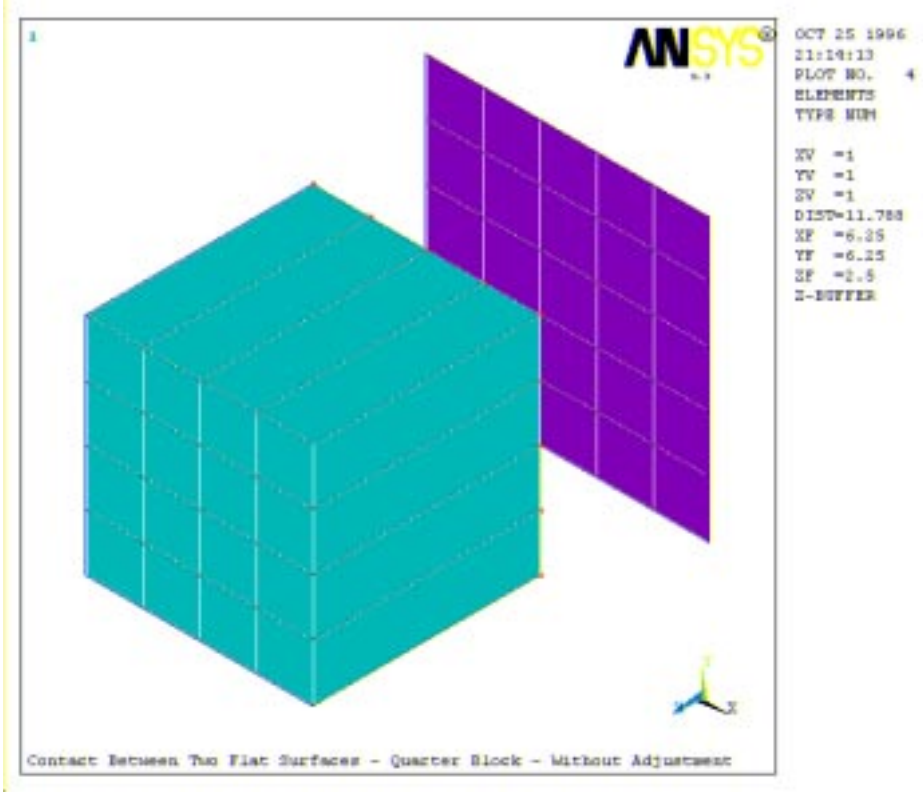

Figure 35: Test Model for Contact Pressure Evaluation - Quarter Block

As shown in Figure 35**,** the target areas of the elements on the flat surfaces were kept uniform for each mesh density.

Since a quarter of a larger square block was modelled, the bottom and left surfaces were constrained by symmetry in along both the *x* and *y*-axes. The opposing surface was also constrained along the same edges as well as being fully constrained in the *z* direction. The gap between the block and the surface was five millimetres. A uniform displacement of six millimetres was applied to the top surface of the block. This quantity of displacement allowed the block to compress by one tenth of its' original height therefore giving a strain of 0.1. As only a quarter block was being modelled, **an extra element was present on the base surface on two adjacent sides only (the top and right sides).**

From the Young's Modulus of Elasticity given above, it is simple to determine the expected uniform stress distribution from:

$$\sigma = \frac{E}{\varepsilon};$$

$$\text{Therefore, } \sigma = \frac{2070}{0.1} = 20700\, N/mm^2$$

Since the two contacting surfaces are flat and the applied load acts only in the *z* direction, then it is reasonable to expect the contact pressure and the stress distribution to be of the same magnitude.

Upon applying the simple procedure given above the test model to contact pressure plot shown in Figure 36 (below) was obtained:

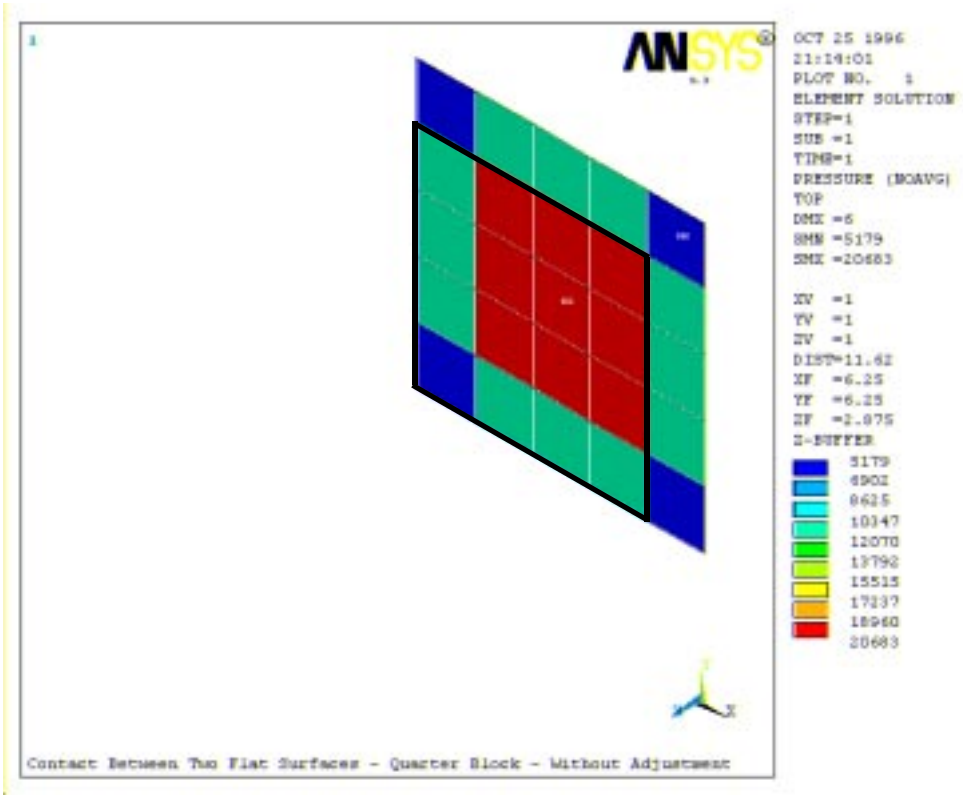

Figure 36: Contact Pressure Plot – Quarter Block - Without Adjustment

It is shown in Figure 36 that the contact pressure has been incorrectly calculated for the contact elements that lie along the left edge and the bottom edge. Since the model was constrained along these edges then the contact pressure should be equal to the stress calculation given previously. The projected contact area is outlined in black.

A second test case was then used to confirm the findings from the above model. A full block being compressed by a stiff flat surface was modelled in this test case. In this

case the same block and flat surface were used but the mesh and boundary conditions were changed. **An extra element was present all around the expected contact area of the block.** The flat surface was again fully constrained in the *z* direction. Both the flat surface and the block were constrained along the *y*-axis at *x*=5, i.e. midway along the *x*-axis of the block. This constraint was repeated for the *y*-axis of the block. The top surface of the block was uniformly displaced by six millimetres in the *z* direction. The model and resulting contact pressure plot, obtained by the same method as before, are shown in Figure 37 below, and Figure 38 on page 70:

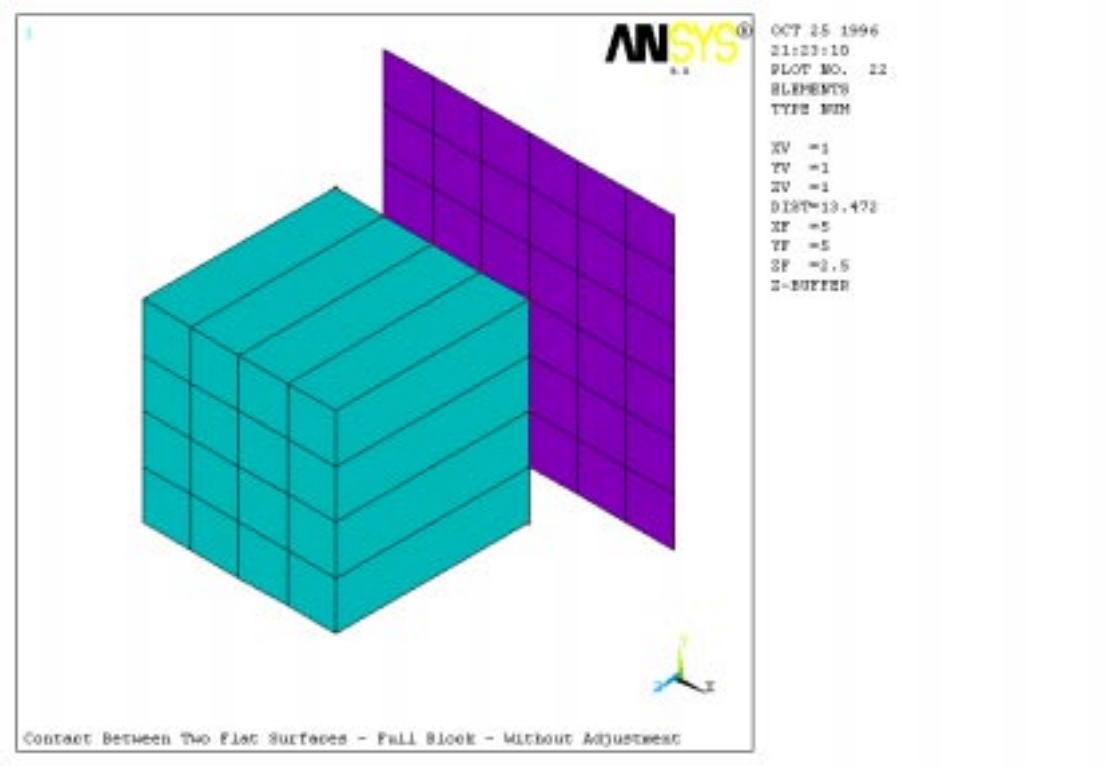

Figure 37: Second Test Model - Full Block

It is obvious from the two test cases that the internal calculation of the total normal force between the contact node and the target area is defective under certain circumstances.

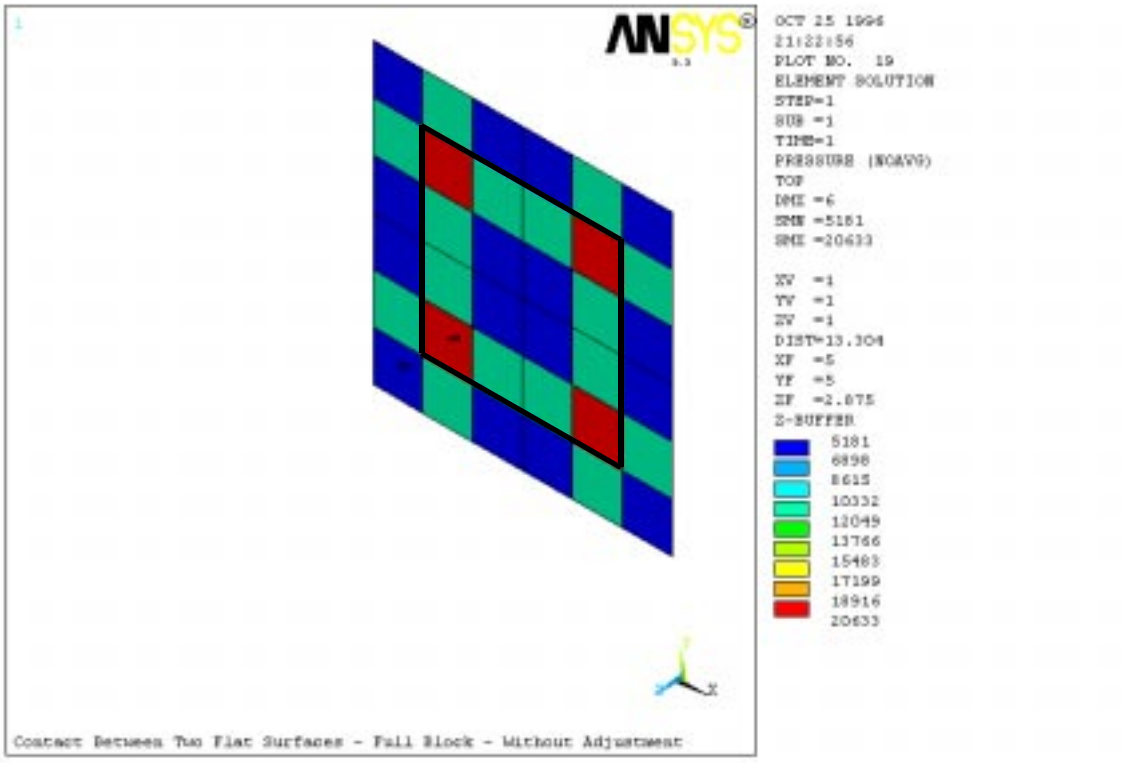

Figure 38: Contact Pressure Plot - Full Block - Without Adjustment

The projected contact area is outlined in black.

From the results of the test cases the following observations were made:

- If the 'contact node' were in contact within the boundaries of the target area then the normal force would have been correctly calculated. However, if the contact node came into contact on a node or edge defining the target area then the calculation of the contact pressure could be incorrect.
- When the displaced contact node rests on an edge of the target area, the normal force was consistently half of the predicted value.
- When the contact node came into contact with a node defining the target area, the normal force was found to be a quarter of the expected value.

As shown in Figure 36 and Figure 38, this type of situation is possible when the contact pressure near a constrained edge is sought.

3.4. New Contact Algorithm

To overcome the possibility of the contact pressure results obtained from the main comparative study being inaccurate, an algorithm was written to correct the problems that were found with the 'block' model test cases. The same models were also used to test the algorithm.

The algorithm consists of a set of instructions which are contained within a 'do' loop using the ANSYS parametric design language. The algorithm completes the set of instructions for every contact element that is in contact. Only those elements which contain a contact node that has come into contact with the boundary of the target area has the associated normal force modified. As mentioned in Section 3.1.1, this occurs when *s, t* or both are equal to ± 1. The set of instructions for the two possible situations are outlined in the flowcharts in Appendix II on page 109. The flowcharts detail the processes based on a contact node coinciding with a node which is shared by four target areas.

A simplified description of the procedure is given below:

- Select element in contact
- Determine node and element numbers together with the relative location to selected contact element.
- Find local direction of displacement using diagonally opposite contact nodes.
- Sum the contact forces to corresponding element in that direction.
- Re-adjust other contact forces.
- Select next element in contact.

The following figures demonstrate the improvement in the contact pressure plots for the two test cases. It should also be noted that the maximum contact pressure (displayed in red) is in close agreement with the simple analytical expression given earlier. The author believed that this was a distinct improvement and so the algorithm was applied to all of the contact pressure calculations conducted throughout the study.

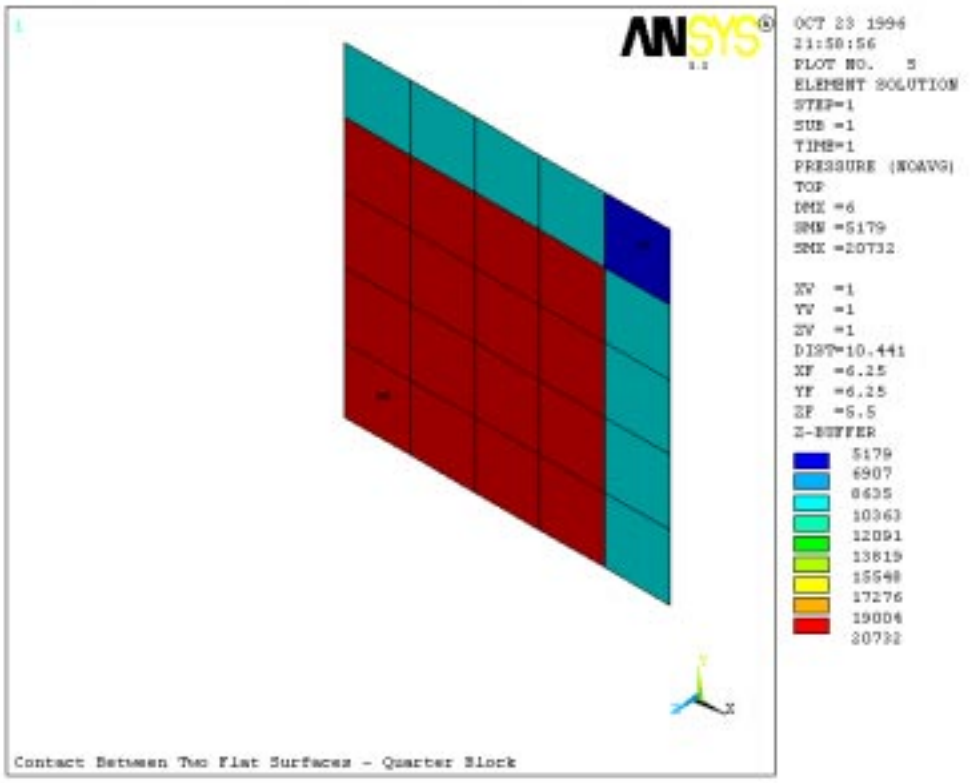

Figure 39: Quarter Block - Contact Pressure after Algorithm (unaveraged)

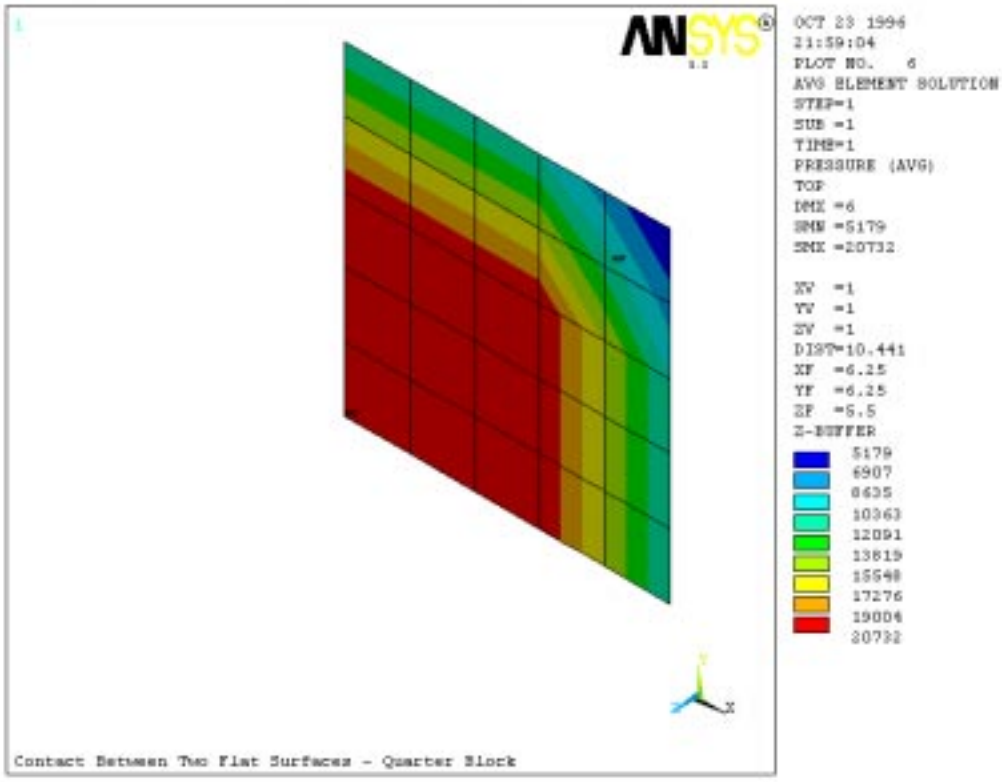

Figure 40: Quarter Block - Average Contact Pressure after Algorithm

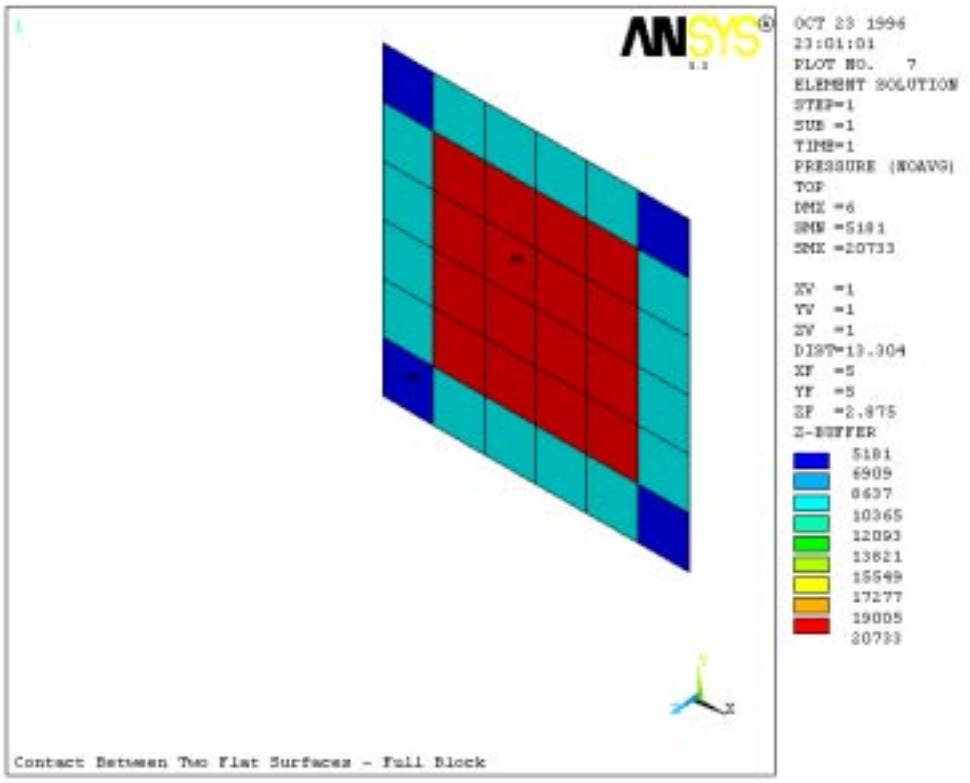

Figure 41: Full Block - Contact Pressure after Algorithm (unaveraged)

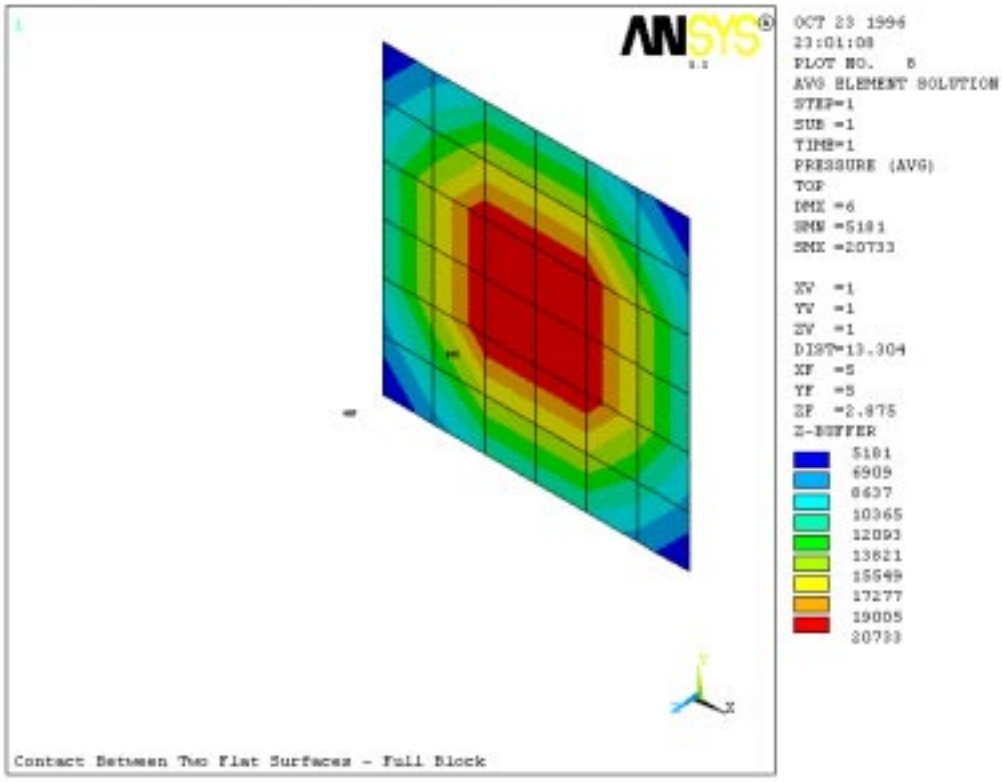

Figure 42: Full Block - Average Contact Pressure after Algorithm

4. Analysis Results

The parameter study undertaken has produced a large of quantity of results, therefore this section has been structured so that comparisons can be made between the three joint styles for each distinct component of the flanged pipe joint. Three areas of interest are examined during the comparisons, these correspond to possible failure indicators; the **flange ring and pipework**, the **bolts**, including any washers and finally, the **contact/interface pressure**. Each component section has been subdivided first by pressure rating and then by nominal bore.

Due to the large number of plot available, this section only contains selected figures from the three types of four inch 1500# class flanged joint. A complete set of figures can be found in Appendix III starting on page 113. The plots shown in this section, and in Appendix III, have been scaled to maximise the size of the joint in the available viewing area. The sizes of the different flanged joint styles are not directly comparable using these plots. An example of the relative difference in the size of the various joint styles is given in section Figure 53 on page 93.

It should also be noted that the legend for the stress intensity plots has been scaled such that a blue colour indicated a low level of stress, red indicated a high stress present within the elastic region, and grey indicated that the material has exceeded the prescribed elastic limit.

4.1. Flange Ring / Pipework

The following finite element plots are zoomed plots of the hub and flange ring. This type of plot was used to present greater detail of the stress distribution through both the hub and flange ring. The stress distribution in the rest of the pipe wall is similar to the section shown in the figures contained in this section and Appendix III.

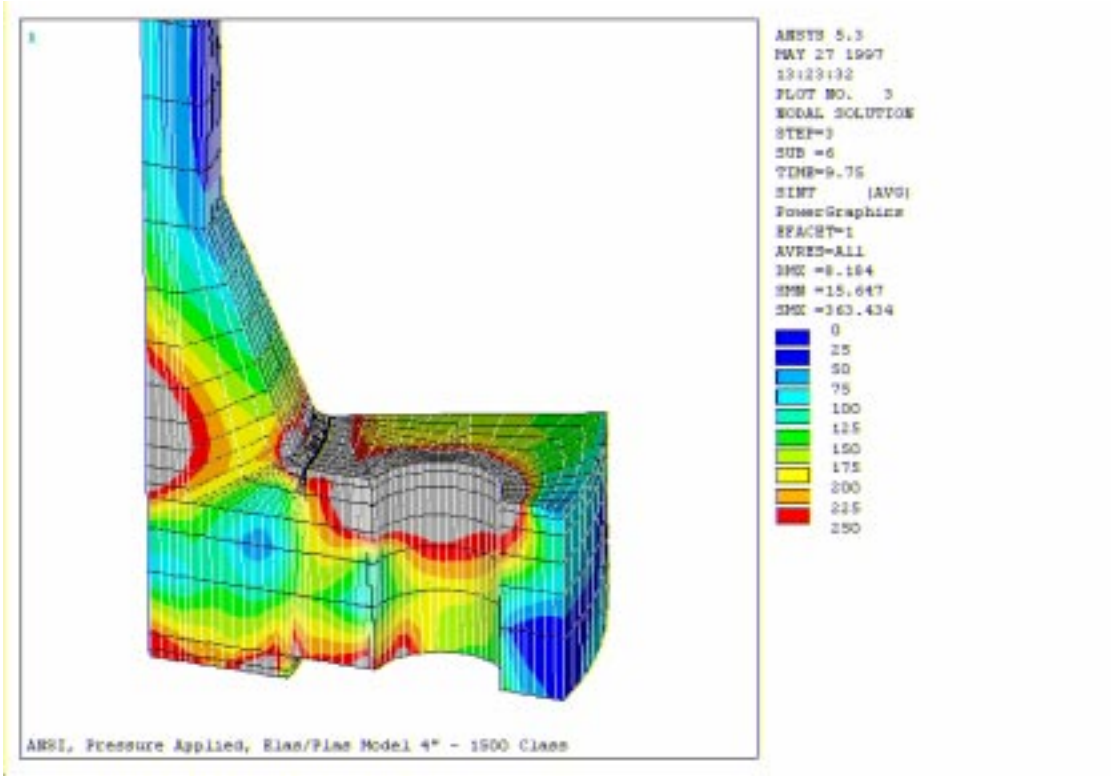

Figure 43: ANSI 4" 1500# Class, Isometric View - Stress Intensity Plot

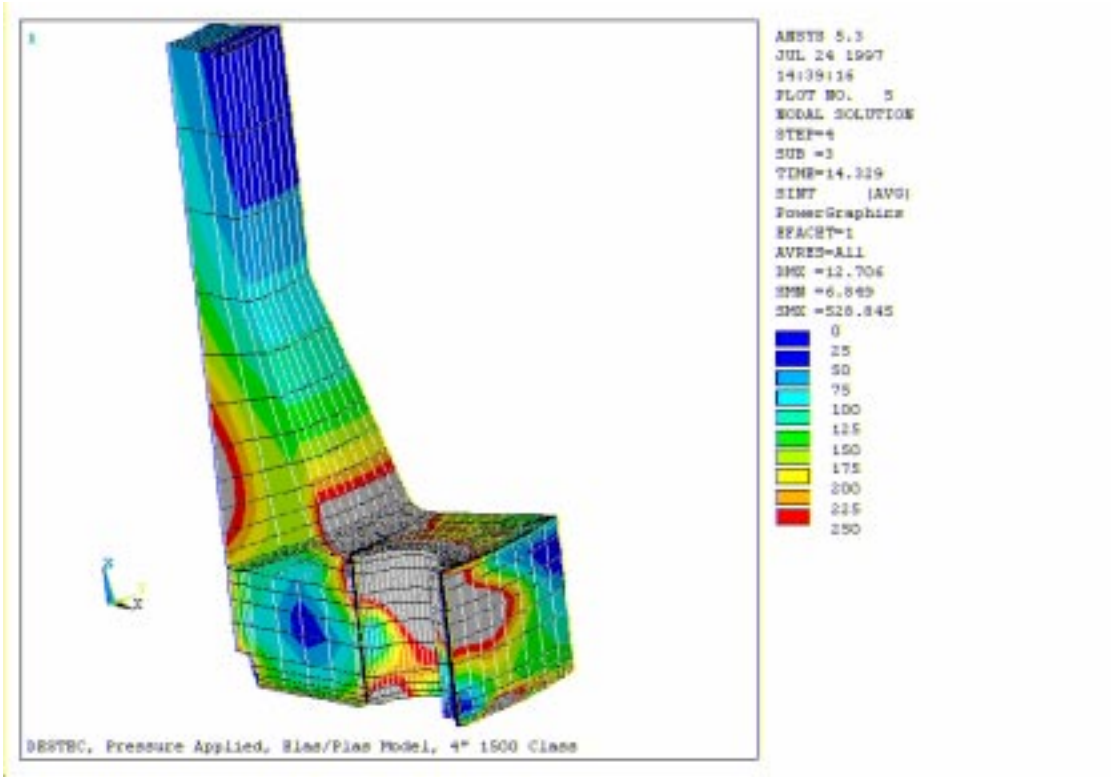

Figure 44: DESFLEX 4" 1500# Class, Isometric View - Stress Intensity Plot

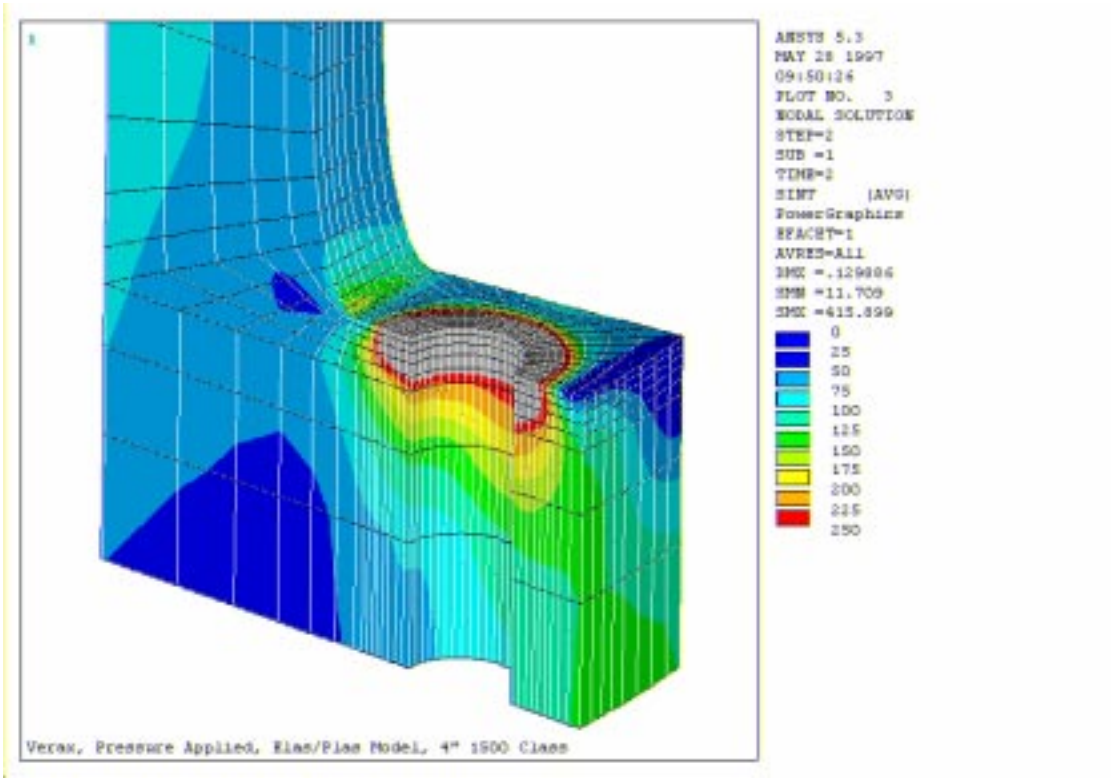

Figure 45: VCF 4" 1500# Class, Isometric View - Stress Intensity Plot

Examination of the results from the flange ring, hub and attached pipework for the three flanged joint styles brought about a number of observations. These observations have been grouped by flanged joint type. However, Section 5 contains a comparative discussion of the flanged joints and their characteristics.

4.1.1. The ANSI Flanged Joint – Flange/Pipework

In general, the 1500# class of ANSI flanged joint displayed yielding in several specific locations. These comprise the inside surface of the hub, the junction between the hub and the flange ring, around the bolt hole, and, in some cases, on the flange shoulder where contact was made with the gasket. Flange rotation, a commonly known problem associated with the ANSI joint, was observed in all cases. The relative magnitude of rotation is given in Table 4. For approximate measurement of the above rotations, it was assumed that rotation occurred about the outside edge of the shoulder for all of the cases.

The relative magnitude of rotation was measured as the difference in the axial displacement of a node on the outer edge of the shoulder from that of a node on the outer diameter of the flange ring.

	Angle of Rotation (degrees)	
Nominal Bore	1500# Class	2500# Class
Four Inch	0.2400	0.1981
Eight Inch	0.2097	0.1869
Twelve Inch	0.2153	0.1744

Table 4 : Rotation of the ANSI Flanged Joint

The four inch 1500# class joint contained a very high level of plasticity, especially at the inside of the hub and through the flange ring around the bolt hole. This size of joint also rotated through the largest angle. This rotation of the flange ring caused a large compressive stress in the inside of the hub while a tensile stress was causing yielding of the hub/flange ring junction. This is shown in the axial stress plot in Figure 46:

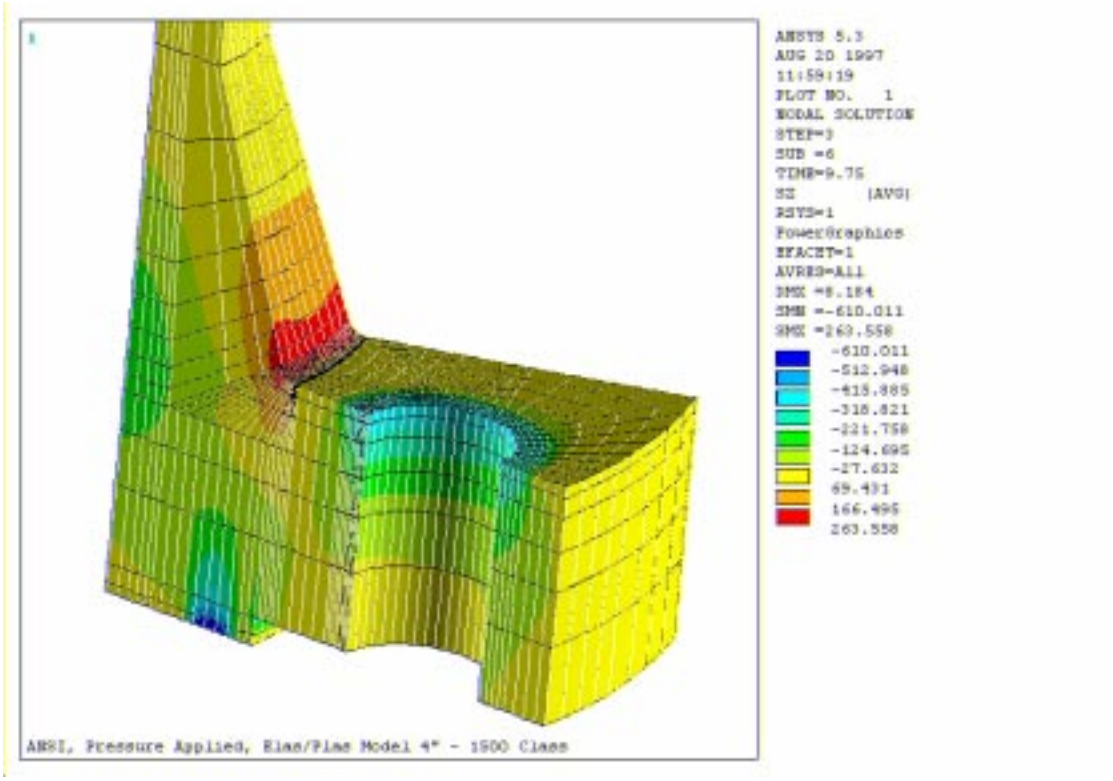

Figure 46 : ANSI 4" 1500# Class - Axial Stress Plot of Flange Ring

Figure 46 also shows the high compressive stress present at the point on the shoulder where the flange comes into contact with the gasket seal ring. The compressive stress from the bolt load, which appears to only be present under the bolt head area on the top surface of the flange ring, is also shown clearly.

A region of yielding was also present on the base of the flange ring at the radially inner edge of the bolt hole. This was due to the combined radial and circumferential compressive stresses that were also due to the rotation of the flanged joint.

The eight and twelve inch 1500# ANSI joints displayed similar stress distribution patterns to the four inch 1500# joint with a few small differences. The magnitude of plasticity in the hub of the eight and twelve inch nominal bore joints was less as well as the degree of yielding around the bolt hole. These joints also rotated 12.5% and 10.3% less, respectively, than the four inch 1500# class joint.

The characteristics of the 2500# class ANSI joints were quite different to those of the 1500# class. In general, the three sizes of 2500# class joint displayed far less yielding. The four inch nominal bore joint displayed only a small area of surface yielding was present at the hub/flange ring junction while no yielding was present on the inside of the hub. The quantity of plasticity caused by the bolt head was also far lass than that shown

by any of the 1500# class ANSI joints. The general level of stress in, and degree of rotation of, the flange ring of each of the ANSI 2500# class joints was significantly less than that of the ANSI 1500# class joints.

4.1.2. The DESFLEX Flanged Joint – Flange/Pipework

The stress distribution through the Desflex four inch 1500# class flange ring and hub were similar to that of the equivalent ANSI flanged joint with some additional effects from the two recesses in the base of the flange ring. The magnitude of yielding at the inner surface of the hub was less, but still about 1/5 of the hub thickness. The front of the hub, where the hub meets the flange ring, also contained some yielding due to a tensile stress. This yielding covered the entire fillet between these two sections but did not continue too deeply into the flanged joint. A characteristic that was only observed with the Desflex flanged joint was yielding at the flange outer diameter. This phenomenon was present for all of the Desflex 1500# class flanged joints but was only present in very small areas in the 2500# Class joints. In the case of the four inch 1500# class joint, the yielding at the hub/flange ring and the yielding at the flange diameter were connected with extensive compressive yielding around the bolt hole. The plasticity at the bolt hole continued to around two thirds of the flange height. On the base of the flange ring, a small quantity of tensile yielding was present at the inner radius of the bolt hole.

These observations confirm that the Desflex flange ring behaves, when in line with the bolt hole, similarly to a simple thick beam loaded with a compressive force on the top surface.

With the exception of the four inch 1500# Class Desflex flanged joint, none of the other Desflex joints that were examined showed any noteworthy levels of yielding in the hub. The four inch 1500# class joint also displayed the highest magnitude of plasticity in the flange ring, both around the bolt hole and at the flange diameter.

In general, the 2500# class Desflex joints yielded only around the bolt hole. The yielding in this area also decreased as the nominal bore increased.

4.1.3. The VCF Joint – Flange/Pipework

The VCF joint demonstrated no yielding or high levels of stress at the inner surface of the hub, and in the worst case, only slight surface yielding of the hub/flange ring connection. Around the bolt hole, yielding was present in an area comparable to that of the washer. This yielding extended to around 20% of the flange height in the four inch 1500# class joint. The stress distribution that extended from the yielding around the bolt hole extended towards the outer diameter indicating the resistance of the joint to the bending effects of the internal pressure. At the base of the flange ring, a quantity of material at the inner diameter of the pipe was subject to very low levels of stress. The behaviour of the other sizes of joint in this class was also very similar. The 2500# class joints displayed far less significant levels of stress than the equivalent 1500# class joints. No yielding was observed in the hub section of any of the 2500# class joints. The maximum stress intensity that was present in the hub was approximately 50% of the yield stress. This was the case for each of the three sizes. As with the 1500# class VCF joints, a large quantity of material located near the inside pipe diameter at the base of the flange ring was subject to low levels of stress intensity (i.e. less that 1/3 yield stress) showing excessive unused material. However, this deceased as the nominal bore increased.

4.2. Bolt and Washer

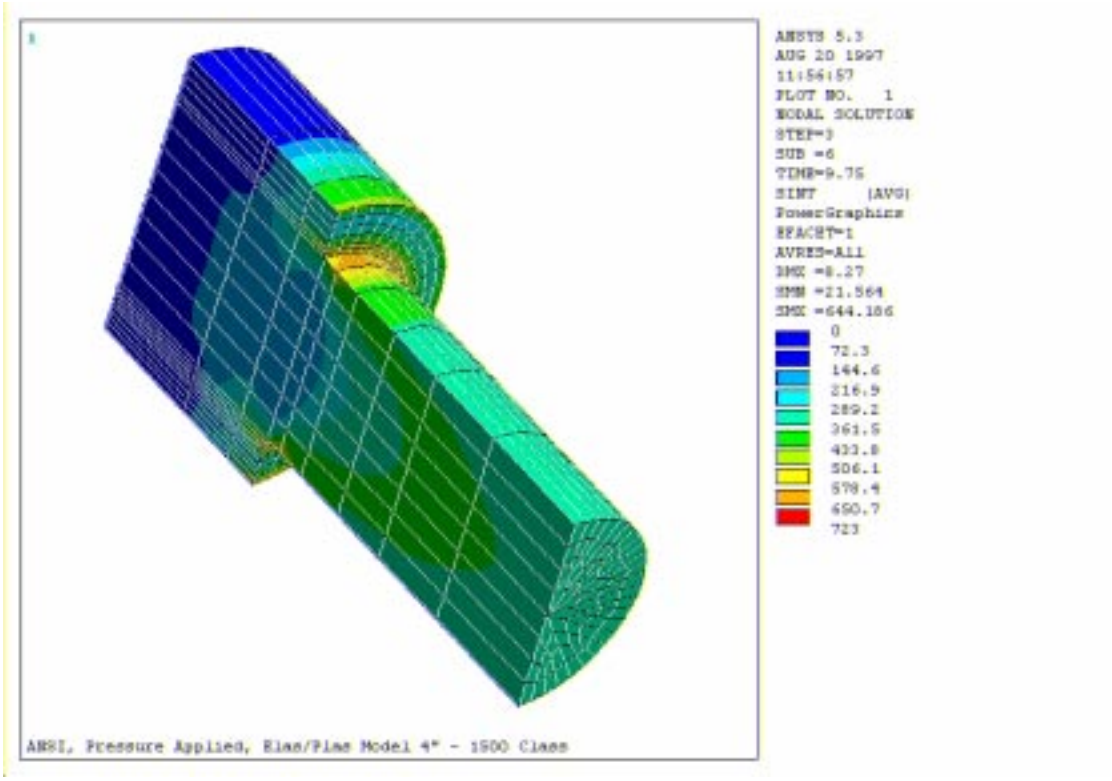

Figure 47: ANSI 4" 1500# Class, Bolt Only, Stress Intensity Plot

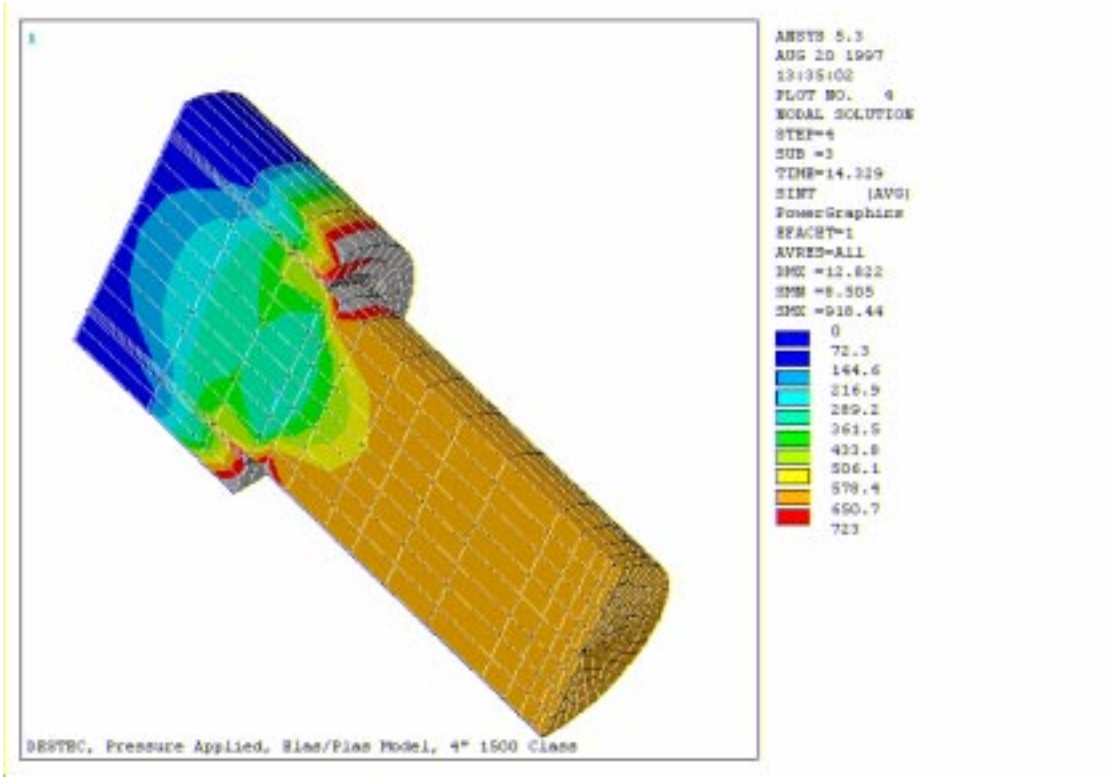

Figure 48: DESFLEX 4" 1500# Class, Bolt Only, Stress Intensity Plot

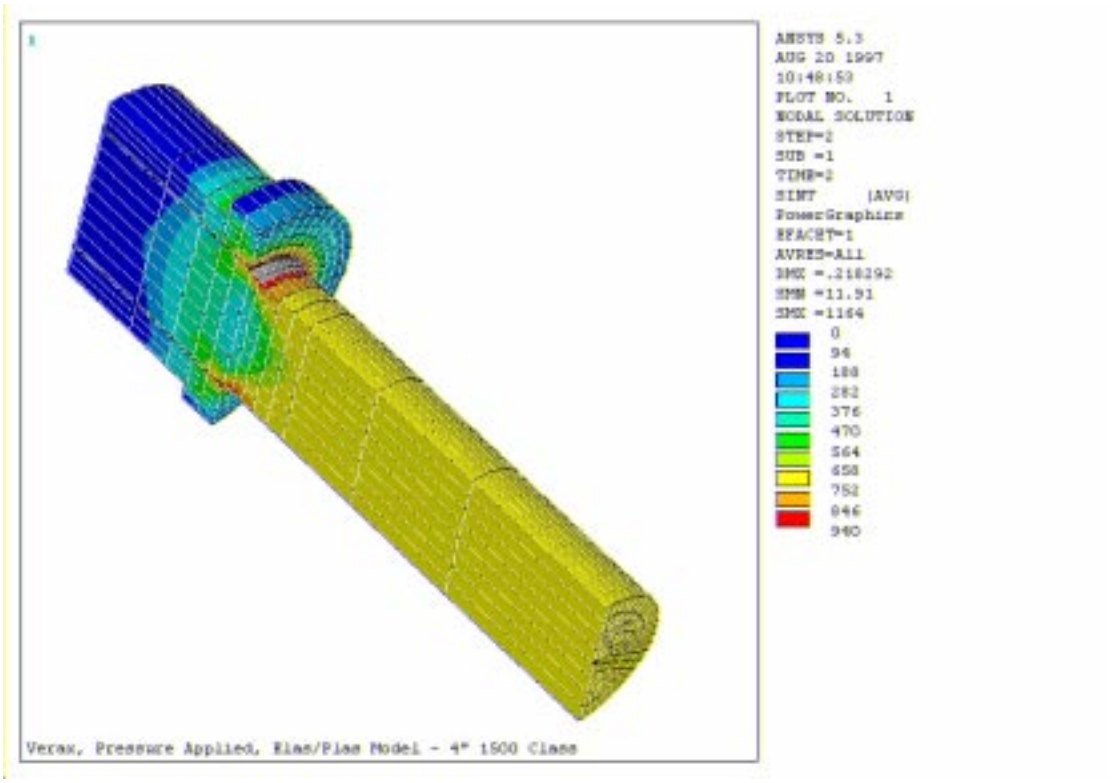

Figure 49: VCF 4" 1500# Class, Bolt and Washer, Stress Intensity Plot

4.2.1. The ANSI Flanged Joint - Bolt

In contrast to the magnitude of yielding of the hub/flange ring component of the ANSI flanged joint, no yielding was found on any of the bolts. The 1500# class flanged joints did not yield their bolts anywhere. The most highly stressed area of the bolt was found at the corner where the bolt head is attached to the bolt shaft. In this area the stress intensity reached 580 N/mm^2 (80% of the yield stress) for both the four and eight inch 1500# class joints. The bolts of the twelve inch 1500# class joint were subject to a maximum stress of 520 N/mm^2 which is approximately 72% of the yield stress.

The bolts of the three ANSI 2500# class joints were not subject to any yielding either. The maximum percentage of the yield stress observed in the bols of the 2500# class joints was less than that of the 1500# class joints. The maximum stress in the four inch 2500# class joint was 508 N/mm^2 (70.2% of the yield stress). Similar maximum stresses were found in the bolts of the eight and twelve inch joints. The stress contained within the bolt head decreased to a minimal value within about half of the bolt head height.

4.2.2. The DESFLEX Flanged Joint - Bolt

The four inch 1500# class Desflex flanged joint stressed the bolts beyond the yield stress in two main areas. These areas were at the top of the bolt shaft and under the base of the bolt head. The yielding of the bolt shaft was mainly on the surface and extended only a small distance into the bolt shaft. The yielding on the base of the bolt head was more extensive, especially at the outside edge. The stress distribution in the bolt was symmetrical about the centre. A high magnitude of stress intensity was observed through the lower half of the bolt head, while at the centre of the bolt the contours continue to almost the top of the bolt. The eight and twelve inch 1500# class Desflex joint demonstrated less yielding than the equivalent four inch joint on the underside of the bolt head. The magnitude of yielding in the bolt shaft of both the eight and twelve inch joints was very similar to that observed in the four inch joint. On the base of the bolt head, the quantity of yielding decreased as the nominal bore of the Desflex 1500# class joints increased.

The four inch 2500# class Desflex joint displayed a similar quantity of surface yielding as those of the 1500# class. However, significantly more yielding was observed on the base of the bolt head and at the corner where the bolt head meets the bolt shaft. Yielding was only present on the bolt shaft of the eight and twelve inch 2500# class Desflex joints. Apart from the lack of yielding on the underside of the bolt head the stress distribution through the bolt was the same as that found in the four inch joint.

4.2.3. The VCF Joint - Bolt

All of the VCF joints displayed very similar stress distributions. A small quantity of surface yielding was observed at the top of the bolt shaft. No yielding was observed on the underside of the washer or the bolt head due to the high yield stress of the material. The stress distribution in the bolt head extended only through the lower half while almost the entire washer was subject to an extent from the effect of the bolt loading. The twelve inch 1500# class VCF joint demonstrated a very slight change in stress intensity across the diameter of the bolt. Examination determined that this was not of a significant magnitude and was only highlighted by the scale of the legend. The four inch and twelve inch 2500# class joints demonstrated the least magnitude of stress through the thickness of the washer in comparison to the rest of the VCF joints.

4.3. Contact / Interface Pressure

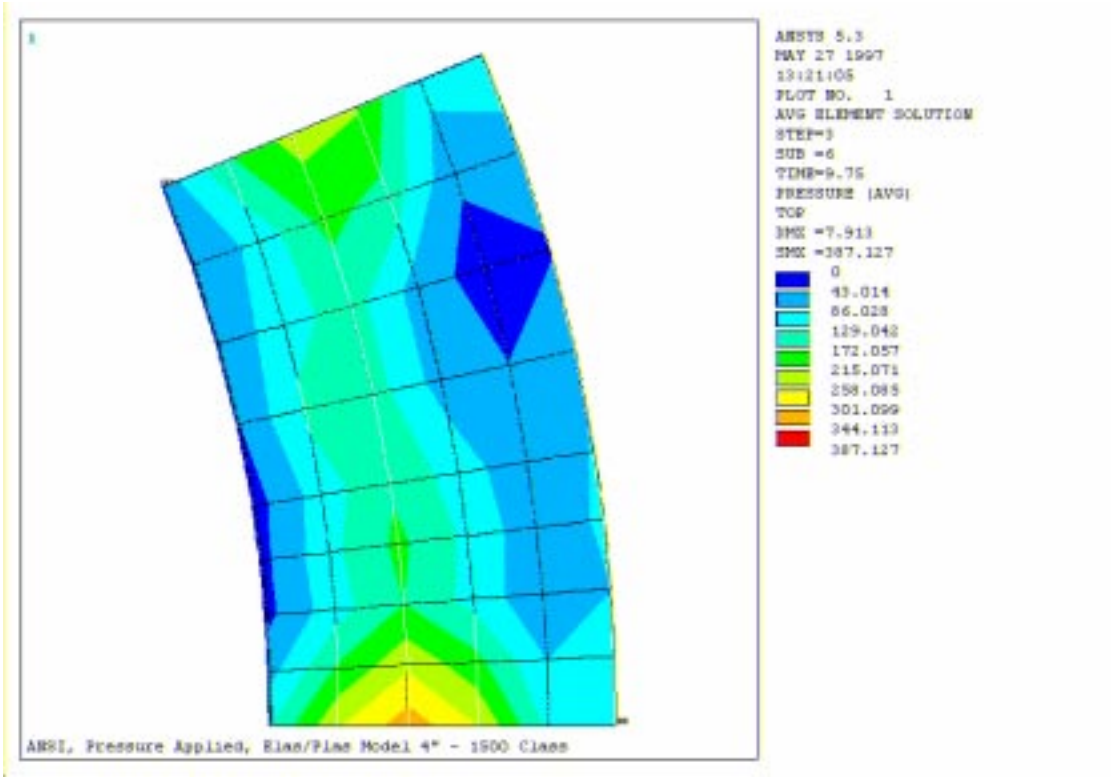

Figure 50: ANSI 4" 1500# Class - Contact Pressure Plot

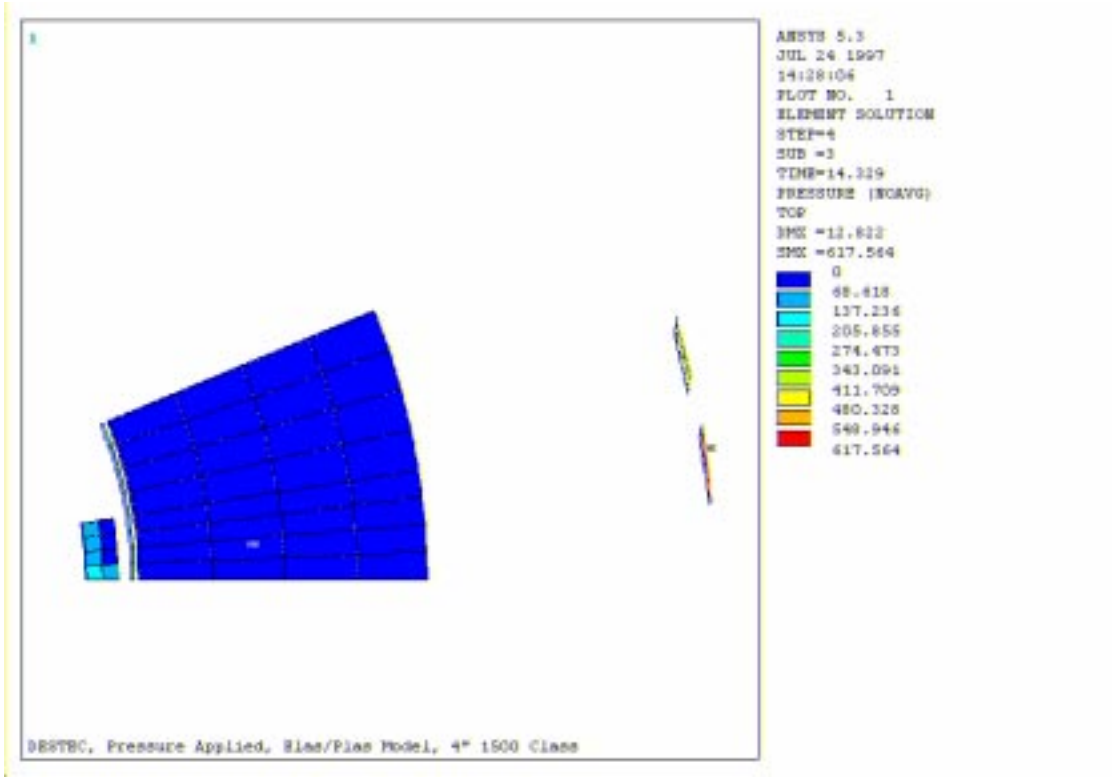

Figure 51: DESFLEX 4" 1500# Class - Contact Pressure Plot

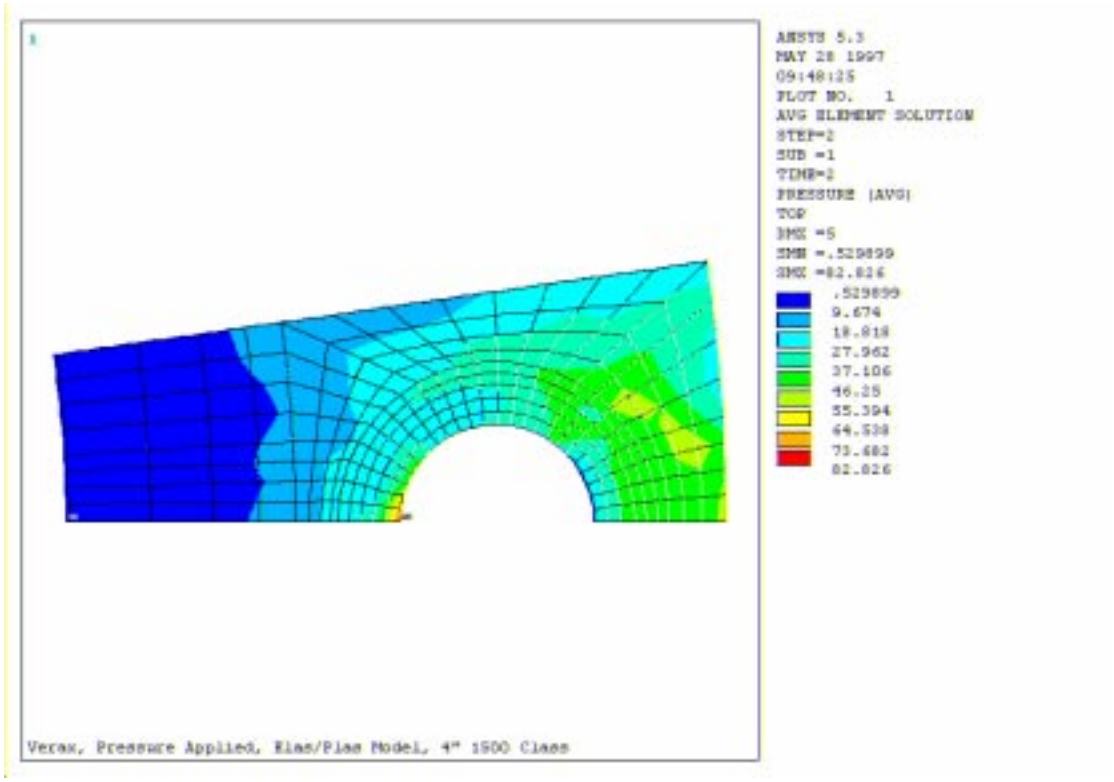

Figure 52: VCF 4" 1500# Class - Contact Pressure Plot

4.3.1. The ANSI Flanged Joint – Contact Pressure

The ANSI flanged joints in general generated a contact surface between the shoulder of the flange ring and the seal ring of the gasket. The four inch 1500# class ANSI joint displayed circumferencial rings of contact pressure across the contact area. The magnitude of the contact pressure did exceed the yield stress of the gasket over approximately 20% of the contact area. The eight inch 1500# joint contact pressure plot contained a number of voids or missing contact elements which would have been expected to display some value of contact pressure. These voids were explained by the ANSYS support engineer as numerical problems with the generation of the contact matrix and could not be corrected by the user. From the remaining elements, the pressure distribution was similar to that of the four inch 1500# flanged joint. The magnitude of the contact pressure was a minimum of twice the yield stress of the gasket. The area over which the contact between the gasket and the flange ring was made was still limited to the area of the seal ring of the gasket. The twelve inch 1500# joint contact pressure plot was dominated by maximum stresses at the corners of the inner edge of the gasket seal ring. This lead to a large contact pressure being observed at the inner edge of the seal ring and a much smaller contact pressure at the outside edge.

The 2500# class ANSI joints all displayed a number of missing elements similar to the eight inch 1500# flanged joint. A high contact pressure was observed in the four inch 2500# ANSI joint, a minimum of three times the yield of the gasket. This pressure decreased as distance from the axis throught the centre of the bolt hole increased. A very small area of contact was observed; approximately 60% of the width of the seal ring. The eight inch 2500# flanged joint also displayed the same contact pressure distribution as the four inch equivalent with a minimum contact pressure of approximately three times the yield of the gasket material. The twelve inch 2500# joint displaed a greater area of contact than any of the other ANSI flanged joints. Areas of the gasket centering ring close to either side of the seal ring were found to be in contact with the shoulder of the flange ring. The minimum contact pressure between the two surfaces was again above the yield of the gasket material.

4.3.2. The DESFLEX Flanged Joint – Contact Pressure

The sharp corner at the outer edge of the Desflex seal ring generated a ring of contact around the four inch 1500# class joint. The corner of the seal ring generated a contact pressure of 70 N/mm^2.

Contact was also observed between the seal ring and bolt hole recesses in the base of the flange ring. Indiscriminate areas of high contact pressure were also found at the outer edge of the flange ring. The top surface of the seal ring only displayed a small area of contact with the under surface of the flange ring. This was the same for the eight inch 1500# class Desflex joint. The outside edge of the seal ring created a much smaller contact pressure in the twelve inch 1500# flanged joint of 22 N/mm^2, but contact was still present around the whole edge of the seal ring. At the outer diameter of the flange ring, only a small contact pressure was observed with a maximum value of 18 N/mm^2. The area between the two recesses in the base of the flange ring also displayed contact between the two flange rings but only a very small contact pressure was present; up to 5 N/mm^2. The four inch 2500# class joint displayed no contact between the seal ring and the recess in the flange ring. However, a high contact pressure (400 N/mm^2) was present between the top of the contact seal ring and the base of the flange ring. The outer edge of the flange ring displayed a high contact pressure between the two flange rings in the range of 108-278 N/mm^2. The contact between the sharp corner and the recess in the base of the flange ring was evident in the eight and twelve inch 2500# class joints. The twelve inch joint displayed a higher contact pressure of over 120 N/mm^2. Both of the eight and twelve inch 2500# class joints also showed a significant contact pressure between the outer edges of their flange rings.

4.3.3. The VCF Joint – Contact Pressure

All of the VCF joints demonstrated a significant contact pressure on the outer half of the flange ring area. The four inch 1500# class joint displayed contact over a large percentage of the flange face with no contact being shown at the inner edge of the flange ring. The area of highest contact pressure was observed outside of the bolt circle, while a ring of contact pressure of 25 N/mm^2 enclosed the bolt hole. This ring of pressure continued across the face of the flange ring. The eight inch 1500# class flanged

joint displayed no contact over the inner third of the flange face. Elsewhere, a contact pressure, similar to that of the four inch 1500# class joint, was observed. An area of higher contact pressure, between 30 and 45 N/mm^2 was exhibited outside of the bolt hole slightly offset from the axis of symmetry passing through the centre of the bolt hole. A similar distribution was also found on the flange face of the twelve inch 1500# class joint. The four inch 2500# class VCF joint displayed contact over the full flange face. The same ring of higher contact pressure (approximately 40 N/mm^2) existed around the bolt hole while a larger ring of between 10 and 18 N/mm^2 was present across the outer area of the flange face. The eight and twelve inch 2500# class joints exhibited contact only over the outer half of the flange face. The eight inch joint displayed a contact pressure of between 17 and 35 N/mm^2 over the rest of the flange face while the twelve inch joint displayed a minimum contact pressure of 20 N/mm^2 over the outer third of the flange face.

5. Fundamental Joint Characteristics

In this chapter, a comparative discussion is presented for the three styles of flanged joint detailing the advantages and disadvantages of each. Specific emphasis is given to the strength and to the possible sealing characteristics of the joint. Sealing ability can not be determined directly from this finite element work since no direct correlation to leakage has been made. Hence, any comments about the sealing ability of the flanged joints will be based upon the contact pressure and areas determined from this study. It is therefore assumed that a direct linear relationship exists between the sealing ability and the quantity and distribution of the contact pressure. Further experimental work is obviously required to determine any relationship between the contact pressure and sealing ability of flanged joints but this will be discussed in more detail in chapter 7.

5.1. Joint Strength

From the observations made in the previous chapter, the ANSI flanged joint displayed, in some cases, significant yielding of the flange hub. This yielding occurred on the inner surface and at the hub/flange ring connection. The concentration of a tensile stress caused by the rotation of the flange ring only weakens this area. If any imperfections, i.e. cracks or voids, were to exist in the weld, the possibility of propagating these imperfections would be increased. The four inch 1500# class Desflex flanged joint also demonstrated this tensile stress at the hub/flange ring connection. However, the stress intensity at this point was reduced to a surface effect in the larger sizes of the 1500# class Desflex joints. At the hub of the VCF joints, at worst, only a small quantity of surface yielding could be observed. This would demonstrate a greater proportion of the original joint strength being available in the hub/flange ring connection of the VCF rather than the ANSI or Desflex flanged joints.

The bolt holes of the three flanged joint styles display another area where the flange joint styles differ in available strength. Considering the 1500# class joints, the yielding of the VCF joint was similar for each size. The Desflex joints displayed large quantities of yielding around the bolt hole and significant yielding at the outer diameter of the flange ring. The ANSI flanged joints displayed similar levels of yielding to that of the Desflex flanged joints around the bolt holes but did not display any yielding at the outer diameter of the flange ring. This may be related to the quantity of rotation of these two

types of joint. The Desflex joint resists rotation of the flange ring by generating contact between the two flange rings at the outer edge of the flange ring. In contrast, the ANSI flange ring freely rotates, and for the cases reported, did not cause any direct contact between the two flange rings.

Although extensive yielding of the flange ring around the bolt holes is not normally associated with failure, this quantity of yielding does bring concern about the reusability of the joints. Assuming that it were necessary to gain access to the system for maintenance via a flanged joint, then from the results of this study the quantity of available strength of the resealed Desflex or ANSI joint may be significantly less that the original strength of the joint. Comparing the extensive yielding of the Desflex and ANSI 1500# class joints to that of the VCF joints, it could be reasoned that the VCF joints would retain more of their original strength should the joint require opening and resealing during the operational life of the joint.

Considering the 2500# class joints, very little yielding, if any, occurs in any of the three flange joint styles. The thickness of the flange ring in particular could be considered oversized in the case of the ANSI and VCF joint styles. The Desflex flanged joint makes the best use of the available strength of the flange ring without causing any significant yielding.

The level of yielding of the bolts associated with the three different flange joint styles was quite similar. All of the bolts displayed a maximum stress at the top of the bolt shaft, and any yielding was only present on the surface of the bolt. This means that a high percentage of the original bolt strength was available for any additional loading for each flange joint style. Perhaps the only consideration relating to the bolting of the flanged joints could be that the use of the washer. The VCF joint achieved the goal of diffusing the applied bolt load over a wider surface area of the flange ring by using a washer. The washer could be associated with the lower level of yielding that was present through the thickness of the flange ring of the VCF joint. The 2500# class of VCF joint did not use this property of the washer fully. It may have been possible to generate the same level of stress in the bolt shaft without the use of a washer and only a small additional amount of yielding of the flange ring being present.

5.2. Sealing Capability

The difference between the quantity contact area and pressure of the three flanged joint styles is quite large. In general, the ANSI flanged joint only created an area of significant contact over the seal ring portion of the gasket. The effective width of the seal ring (for the cases examined in this study) varies between seven and fifteen millimetres. Even if the widest sealing area is used, then fifteen millimetres is still considered to be a very small width over which to generate a seal to withstand the internal pressure contained within the flanged joint. The ANSI flanged joint exerted a very high contact pressure upon the gasket. This may cause cracking of the seal ring or tearing of the seal ring from the rest of the gasket. These effects result from creating a high pressure seal on a relatively low strength gasket (compared to the strength of the flange rings) and must be taken into consideration. The Desflex flanged joint generated a seal between a recess in the base of the flange ring and a seal ring. This seal ring was of greater strength than the ANSI gasket but it to yielded completely when subject to both the bolt load and the internal pressure. This is shown in Figure 71 (in Appendix II). This type of joint also generated a contact area at the outside edge of the flange ring. Between these two contact areas, a circumferential ring of a medium contact pressure was obtained. It is the authors' belief that the three-dimensional contact elements had difficulty in modelling the contact characteristics between the outer edge of the seal ring and the recess in the base of the flange ring. This is due to the very small areas of contact that are present in this area. The larger areas of contact that were generated between the two flange rings were subject to a very small contact pressure. Because of this low contact pressure, it is believed that these areas of contact would have little significance in the sealing capabilities of the Desflex flanged joint. The VCF joint demonstrated consistently larger areas of contact that were subject to medium levels of contact pressure. Most of the contact pressure existed outside of the bolt circle, but retained a complete contact circle round the circumference of the flange ring. In the worst case, the twelve inch $2500^{\#}$ class joint, some separation of the flange rings was noted at the inner diameter of the flange ring. However, even in this case, good contact was present outside of the bolt circle. It is that authors belief that a marginal increase in the taper angle applied to the flange faces could have a beneficial effect upon the magnitude of both the contact area and pressure.

5.3. Other Factors

Several commercial factors should be considered when comparing the three types of flanged joint, other than the comparison of the technical capabilities of each joint. These other factors include the size and weight of the joints, the amount of time required for installation and maintenance and the overall cost of the joint.

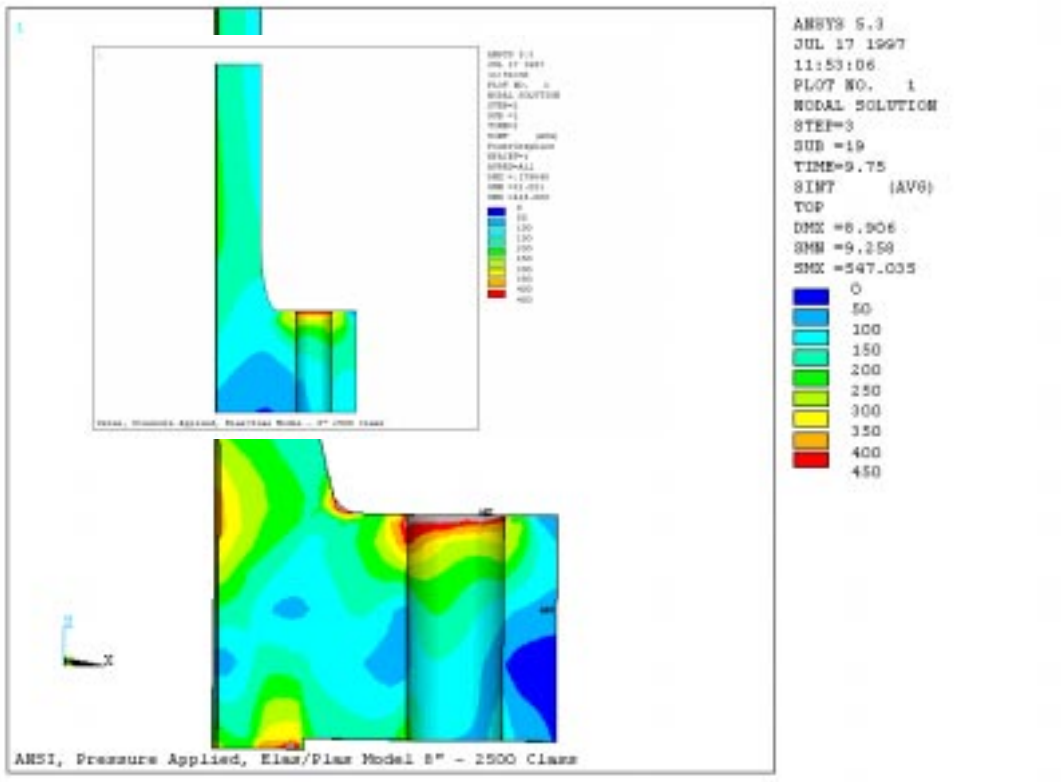

Figure 53: Scaled figure of ANSI and VCF joints

Figure 53 above, demonstrates the true size difference between the VCF and the ANSI style of flanged joint. The figure uses the eight inch 2500# Class joint as an example. Quantifying this difference in scale by comparing the actual percentage difference in weight produced the following results:

The VCF joint weights approximately 12% of the ANSI flanged joint while the Desflex joint weighs 27.2%. With both the Desflex and the VCF joints a substantial weight saving is made. In the case of the VCF joint, the actual saving in weight is 72 kilograms. When this magnitude of weight saving is multiplied by the number of joints that are to be used on, for example, an oil or gas platform, a substantial reduction in the

overall weight of the platform can be made. This would also have a direct influence on the need for structural support in certain areas of the platform.

From a brief examination of these joints, it is assumed that the more bolts the joint has, the longer it will take to install the joint. It is also assumed that the time required to align a gasket or seal ring is not significant in comparison to the time required to correctly tension the bolts. On this basis, it is believed that the VCF joint will require the most time to install considering that it has significantly more bolts. The difference in the installation time is greatest at the smaller diameters and in the 1500# pressure class. From the maintenance viewpoint, the ANSI flanged joint is expected to require the most time for the inspection and repair of damaged gaskets. This is detrimental from a commercial viewpoint when an installation would have to be shutdown for a flanged joint to be opened and a gasket replaced. Since the VCF joint does not contain a supplementary sealing medium, it is believed that most, if not all, of this downtime can be eliminated. The comparative cost to manufacture and install the three types of joint is small in comparison to the maintenance cost of repairing a leaking joint. Therefore the a comparison of the actual cost of purchase is of very little concern in comparison to the reduction in downtime that a technically superior flanged joint may save. For this reason, a comparison of the actual purchase price of these joints has not been supplied.

6. Conclusions

In conclusion, the following points have been made:

6.1. The ANSI Joint

- The ANSI style of flanged joint that is in common use throughout the oil and gas industries is of a poor and inconsistent design. The joint is overdesigned in some situations, and subject to significant yielding in others.
- The ANSI joint provides a very high pressure seal over, what is considered, a small sealing area. Any scratching or other damage to the sealing surface of the gasket could result in the loss of the seal.

6.2. The Desflex Joint

- The Desflex joint, like the ANSI joint, is also subject to an inconsistent design that allows large quantities of yielding in some situations.
- The Desflex joint contains an improved sealing mechanism compared to the soft gasket of the ANSI joint.

6.3. The VCF Joint

- The VCF 1500$^{\#}$ class flanged joint has the highest proportion of the original flanged joint strength available after being subject to an internal pressure.
- The available material of the hub and flange ring section of the 2500$^{\#}$ class joints are not fully utilised in any of the three styles. A design optimisation of this area, based on the joints ability to withstand the 386Bar internal pressure, could be made resulting in a further reduction in the cost of raw material and overall weight of the joint.

In general, the VCF joint provides the best balance between the quantity of contact area and the magnitude of the contact pressure whilst providing a constant seal between the flange faces. The VCF joint also contains the lowest levels of stress in the areas of

importance whilst minimising the weight of the joint. The low levels of stress in these areas, especially at the hub, allow the joint to withstand other external loads that may have caused the other joint styles to fail.

It is possible to encounter a number of difficulties when attempting to conduct this type of analysis that incorporates geometric nonlinearities. A substantial amount of time is required to obtain the correct contact stiffness for a particular model. It should be noted that a contact stiffness that produces good results for one size of a geometrically similar model (with an identical mesh) would not necessarily do the same for a different size. This means that the contact stiffness has to be re-evaluated for each size of each flange style model. As the VCF joint models require only around two hours to solve, this is not a substantial obstacle, but only an inconvenience. The Desflex model, on the other hand, which requires almost 3 days to reach a solution, encounters this problem then a significant amount of time is wasted.

The solution times of the three types of model that were examined in this work varied greatly. The VCF joint required about 2-3 hours depending on the geometric size of the model. The smaller the size of the model, the longer the model required to solve. The ANSI flanged joint models required approximately 10-12 hours and the Desflex joint models required between two and three days of CPU time. It is the authors belief that as the VCF joint required contact between two relatively hard and almost parallel surfaces. In this case, contact was caused by a displacement normal to the two surfaces. This type of contact analysis was straightforward and so the solution time was low. The ANSI model contained two flat surfaces, one of which was relatively soft (the gasket) and caused the contact by a displacement normal to the contact surfaces. It is believed that the ease of deformation of the gasket material increased the difficulty of the problem. The Desflex model, however, contained a seal ring that was of an unusual shape. Only the top surface of the seal ring was parallel to the underside of the flange ring. The seal ring also contained an angled surface that came into contact with the flange ring. The author believes this angled slope caused the large increase in the solution times of the Desflex models compared to the other flanged joint styles. In particular, the sliding of the angled slope against the underside of the flange ring would have required a significant amount of solution time.

7. Future Work

7.1. Experimental Validation

The validation of this finite element work by conducting a set of experiments is essential to validate the results discussed in this report. Two main types of experiment are required to validate both the strength and contact analysis results. In order for the strength of the joints to be measured, strain gauges should be used at important locations on the flanged joint. The hub and the hub/flange ring connection of the flanged joint should receive a number of gauges, both inline with, and midway between, the centre of the bolt holes. These are is not only of importance in demonstrating the differences between the strength of the three styles of flanged joint, but they are also accessible locations for the application of the strain gauges. Strain gauges should also be applied to the shaft of several of the bolts. By strain gauging several bolts, a better understanding of the tolerances involved with the applcation of the bolt tensioning procedure can be obtained. Ideally, hydraulic tensioners, or some other calibrated bolt tensioning equipment should be used to apply the correct torque to the bolts. A margin of uncertainty may exist in this area if the threads of the bolts are of poor quality. It may be possible for the hydraulic tensioner to register a high torque in the bolt when it is actually the threads of the bolt that have jammed.

The determination of the leakage characteristics of a flanged joint will also require the use of accurate and well-calibrated equipment. The magnitude of leakage could be detected by extracting a vacuum around the joint before internal pressure is applied to the joint. This vacuum would then be measured, and using a large number of small steps, the magnitude of the internal pressure should be increased in the joint. At each step, the internal pressure should be help for a specified length of time and the pressure within the vacuum chamber should be measured. This process should be repeated until it is obvious that the flanged joint is leaking significantly, or until the design pressure of the joint has been reached. It may also be of value to find at what magnitude of internal pressure a specified leakage rate exists. It would not be possible to correlate this type of leakage rate to the contact pressure distribution between two flange faces, in the case of the VCF joint. However, it may be possible to correlate the experimental results with the minimum contact pressure that exists around the circumference of the flange ring.

This may be possible as it is at the area of lowest contact pressure that it is most likely for a leak to exist.

7.2. External Loads

As a result of the work detailed in this thesis, a further study has been initiated investigating the effects of pipe bending on the strength of a flanged pipe joint which is subject to internal pressure. In this study, a comparison of the VCF and ANSI twelve inch 1500# class joints is conducted. A 'half joint' model has been used for the study, including all of the associated bolts. A plot of the models is given Figure 54 and Figure 55.

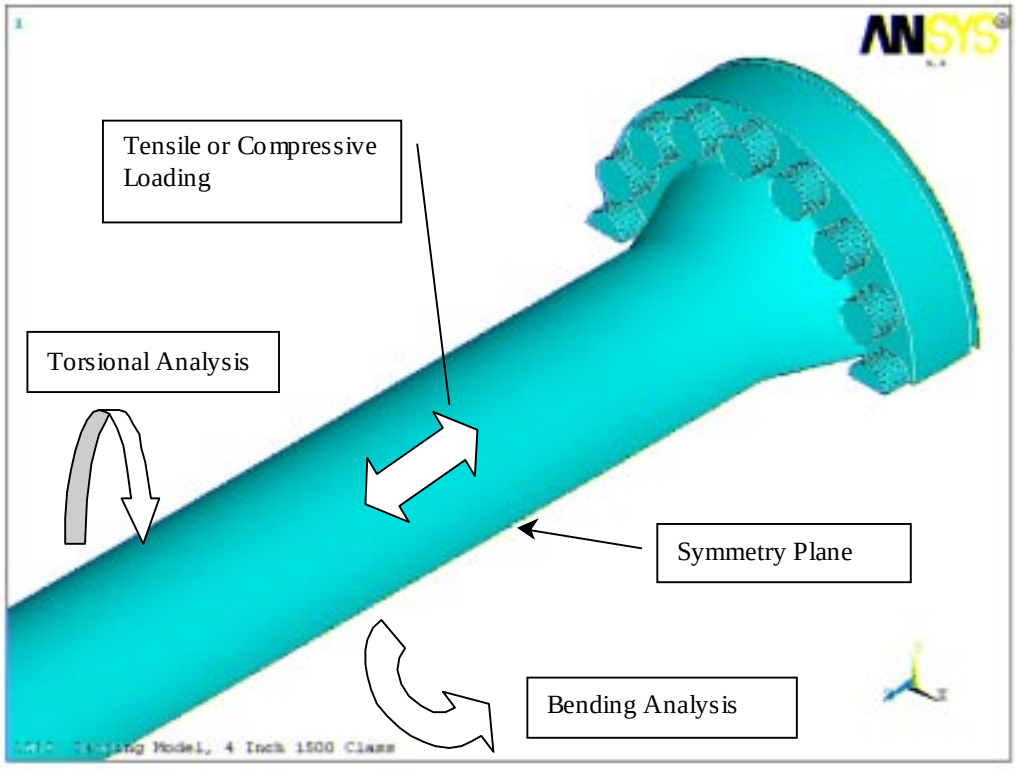

Figure 54: Plot of ANSI Model for Combined Loading Analysis

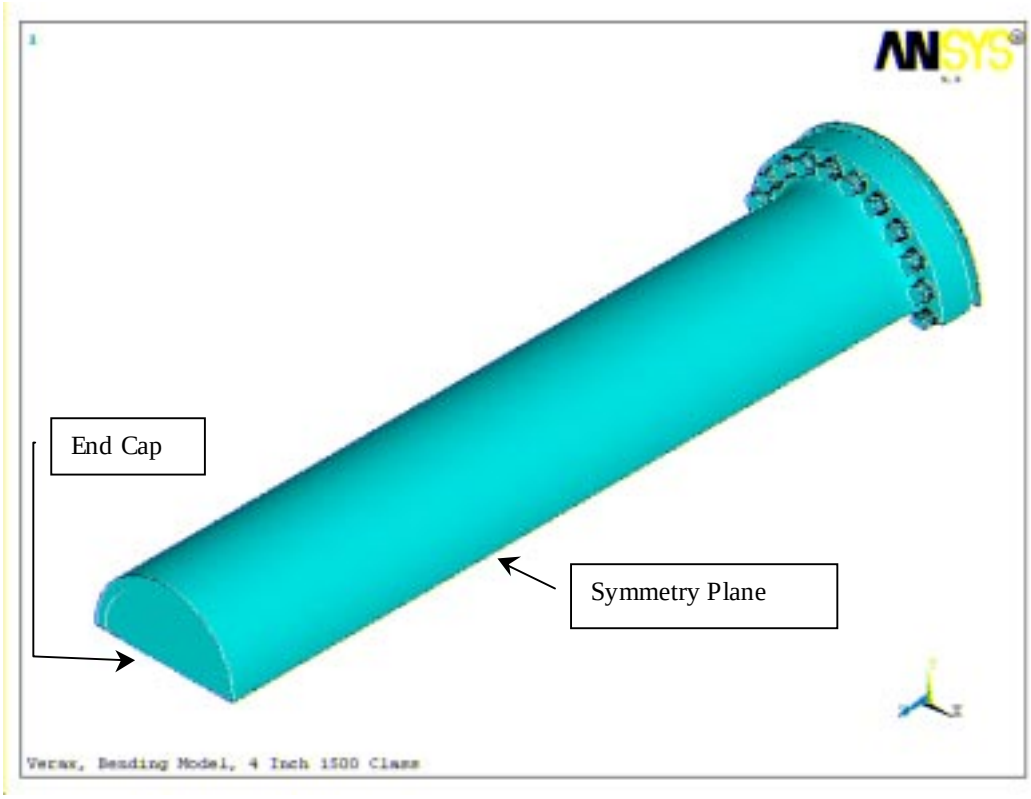

Figure 55: Plot of VCF Model for Combined Loading Analysis

The initial loading steps were as detailed above in section 3.1.4. A further load step was added in order for the bending moment to be applied.

The magnitude of the bending moment was based upon the required moment to cause the surface of a pipe, of equivalent length and wall thickness, to begin yielding at the outer surface. This was accomplished by the use of the fundamental relationship between bending stress, moment and geometry:

$$\frac{M}{I}=\frac{\sigma}{y}=\frac{E}{R}$$

From this relationship, an initial value was obtained for comparison purposes with the strength of the flanged joint. The applied bending load was applied in small fractions of the calculated load for two reasons:

- a processing time limit existed on the workstation where this analysis was carried out and,
- The applications of small fractions would allow for examination of the results at many stages before the calculated value is reached. This could be of great benefit in

demonstrating the increasing effect of a bending load on the variation in contact area and pressure.

This bending analysis would determine if the flanged joint, were weaker than the surrounding pipework when a bending load is present. It would also quantify the difference between the various types of flanged joint in terms of the bending load required to cause separation of the flange faces (or flange to gasket seal) over a predetermined area.

It is however; necessary to note the computational power that is required to conduct such an analysis. Using an R5000 150MHz Silicon Graphics Indy workstation with 128MB memory, the above bending analysis would take 30 CPU days and require 3GB of free disk space.

A similar method to this could be used to analyse the effect of a torsional load on the flanged joint that is subject to internal pressure. From this, a study into the combined external loading of torsion and bending moment could be studied.

7.3. Design Optimisation

A large quantities of material exist in the VCF joint, especially in the 2500# class, which is not fully utilised. It is believed that a design optimisation of this joint would be beneficial. Removal of some of this material as shown in the Figure 56 would not only result in a further weight saving in comparison to the ANSI joint style, but it would mean an increase in the contact pressure between the flange faces.

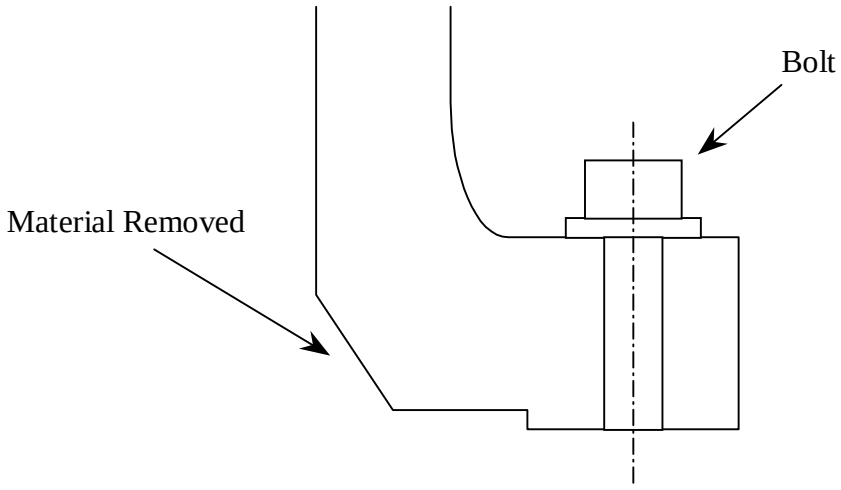

Figure 56: Proposed Optimisation of VCF Joint

The increase in contact pressure would be caused by the reduction in the contact area. It is also believed that an increase in the present positive taper angle (as defined in Figure 8) over the new contact area would result in a redistribution of the contact pressure. The redistribution would increase the contact pressure at the inner diameter and reduce the contact pressure at the outer diameter. Since the contact area would still exist between the inner and outer diameters of the washer, no rotation of the flange ring would exist, other than that caused by the taper angle. The effect of the induced rotation upon the fillet between the hub and the flange ring would have to be investigated. It would be expected that an increase in the tensile stress at the fillet would result from the increase in the taper angle.

The flow characteristics of fluids passing through a joint of this shape would have to be carefully examined so that no ill effects occur. In order to eliminate the possibility of poor fluid flow characteristics, a 'filler' material would be used to replace the removed flange ring material. The filler material would only serve the purpose of filling the vacant space where the internal flanged joint profile had been altered. The filler material would require no significant strength characteristics but would need to be resistant to any corrosion or deterioration from the exposure to the contained fluid.

8. References

1. Waters, E. O., and Taylor, J. H., 1927, "The Strength of Pipe Flanges," Transactions of Mechanical Engineering, Vol. 49, pp. 531-542.

2. Waters, E. O., Wesstrom, D. B., Rossheim, D. B., and Williams, F. S. G., 1937, "Formulas for Stresses in Bolted Flanged Connections," Transactions of ASME, Vol. 59, p 161.

3. Almen, J. O., 1944, "Tightening Is Vital Factor in Bolt Endurance," Machine Design, February 1944, pp. 158-162.

4. Murray, N. W., and Stewart, D. G., 1961, "Behaviour of Large Taper Hub Flanges," *Proc. Symp. Pressure Vessel Research Towards Better Design*, Institute of Mechanical Engineers, p. 133.

5. Keer, L. M., Dundurs, J., and Tsai, K. C., 1972, "Problems Involving a Receding Contact Between a Layer and a Half Space," Journal of Applied Mechanics, Vol. 39, No. 4, pp. 1115-1120.

6. Thomson, G., 1988, "Strength and Flexibility of Pressurised Taper Hub Flanged Joints," Applied Solid Mechanics - 2, Editors, Tooth, A. S., and Spence, J., Ch. 13, Elsevier Applied Science Publications, London.

7. Sawa, T., Higurashi, N., and Akagawa, H., 1991, "A Stress Analysis of Pipe Flange Connections," Journal of Pressure Vessel Technology, Vol. 113, pp.497-503.

8. Laviolette, D., Nica, A., Chaaban, A., Marchand, L., and Shirazi-Adl, A., 1996, "Mechanical Behaviour of Pressurised Bolted Joints Subjected to External Bending Loads," International Conference on Pressure Technology, Vol. 2, pp. 117-122.

9. Price, J. W. H., and Chanana, A., 1996, “The Leakage of Bolted Flanged Joints in High Temperature Systems,” International Conference on Pressure Technology, Vol. 2, pp. 133-139.

10. Webjörn, J., 1967, “Flange Design in Sweden,” Proceedings of the Petrochemical Mechanical Engineering Conference, American Society of Mechanical Engineers, Philadelphia PA, September 17-20 1967. Paper 67-PET-20.

11. Schneider, R. W., 1968, “Flat Face Flanges with Metal-to-Metal Contact Beyond the Bolt Circle,” Transactions of ASME, Journal of Engineering for Power, Series A, Vol. 90, No. 1, pp. 82-88.

12. Waters, E. O., and Schneider, R. W., 1969, “Axisymmetric, Nonidentical, Flat Face Flanges with Metal-to-Metal Contact Beyond the Bolt Circle,” Transactions of ASME, Journal of Engineering for Industry, Vol. 91, Series B, No. 3, pp. 615-622.

13. Meck, H. R., 1969, “Analysis of Bolt Spacing for Flange Sealing,” Journal of Engineering for Industry, Technical Briefs, February 1969, pp. 290-292.

14. Pindera, J. T., and Sze, Y., 1972, “Influence of the Bolt System on the Response of the Face-to-Face Flanged Connections,” Proceedings of the 2nd International Conference on Structural Mechanics in Reactor Technology, Vol. G, paper 2/6.

15. Gould, H. H., and Mikic, B. B., 1972, “Areas of Contact and Pressure Distribution in Bolted Joints,” Journal of Engineering for Industry, Vol. 94, No. 3, pp. 864-870.

16. Thompson, J. C., Sze, Y., Strevel, D. G., and Jofriet, J. C., 1976, “The Interface Boundary Conditions for Bolted Flanged Connections,” Journal of Pressure Vessel Technology, November 1976, pp. 277-282.

17. Webjörn J., and Schneider, R. W., 1980, “Functional Test of a Vessel with Compact Flanges in Metal-to-Metal Contact,” Bulletin of the Welding Research Council, No. 262, pp. 10-16.

18. Webjörn, J., 1983, “The Effect of Thermal Shock in Pipe Connections with Compact Flanges,” ASME, Paper No. 83-WA/PVP-6.

19. Junker, G. H., and Wallace, P. W., 1984, “The Bolted Joint: Economy of Design Through Improved Analysis and Assembly Methods,” Proceedings of the Institution of Mechanical Engineers, Vol. 198B No.14. pp. 255-266.

20. Lewis, L. V., Fessler, H., and Hyde, T. H., 1987, “Determination of the Initial Gaps Between Flat Flanges Without Gaskets,” Proceedings of the Institute of Mechanical Engineers, Part A, Vol. 201, pp. 267-277.

21. Fessler, H., Hyde, T. H., and Lewis, L. V., 1988, “Leakage Through Loaded Flat-Flanged Joints Without Gaskets,” Proceedings of the Institute of Mechanical Engineers, Part A, Vol. 202, pp. 1-13.

22. Hyde, T. H., Lewis, L. V., and Fessler, H., 1988, “Bolting and Loss of Contact Between Cylindrical Flat-Flanged Joints Without Gaskets,” Journal of Strain Analysis, Vol. 23, pp. 1-8.

23. Webjörn, J., 1989, “The Theoretical Background to the Verax Compact Flange System,” ASME, PVP - Vol. 158, Advances in Bolt Technology, pp. 7-11.

24. Cao, J., and Bell, A. J., 1993, “Elastic Analysis of a Circular Flange Joint Subjected to an Axial Force,” International Journal of Pressure Vessels and Piping, Vol. 55, pp. 435-449.

25. Hyde, T. H., Fessler, H., and Lewis, L. V., 1994, “The Sealing of Conical Faced Flanges Without Gaskets,” Seventh ICPVT, pp. 105-118.

26. Cao, J., and Bell, A. J., 1996, “Determination of Bolt Forces in a Circular Flange Joint Under Tension Force,” International Journal of Pressure Vessels and Piping, Vol. 68, pp. 63-71.

27. Webjörn, J., 1985, “The Bolted Joint – a Series of Problems,” Linköping Studies in Science and Technology, Dissertation No. 130, Appendix A.

28. ANSYS Inc., 1996, *ANSYS Elements Manual*, Seventh Edition, Chapter 4, Section 49 – The CONTAC49 Element, pp. 339-345.

29. ANSYS Inc., 1996, *ANSYS Theory Manual*, Seventh Edition, Chapter 4, Section 1 – Rate Dependant Plasticity, pp. 4-24.

9. Appendix I – Model Parameters

Listed in the following tables are the parameters that were used in the flanged joint models. A definition of the parameters can also be found in the nomenclature.

VCF MODEL PARAMETERS						
	1500# Class			2500# Class		
	4" NB	8" NB	12" NB	4" NB	8" NB	12" NB
taperang*	0.0705	0.0779	0.888	0.03896	0.0487	0.05844
fd	160	298	425	182	320	458
fh	24	42	54	36	54	72
pt	17.1	24	34	13.48	23.012	33.33
pod	114.3	219.1	323.9	114.3	219.1	323.9
pcd	140	263	380	152	275	398
bd	8	14	18	12	18	24
nbolts	22	24	28	16	20	24
gap	0.25	0.4	0.5	0.35	0.5	0.5
jh	98.7	164.9	219.5	118.7	184.7	249.5

* Measured in degrees. All other dimensions are in millimetres.

Table 5 : VCF Joint Model Parameters

DESFLEX MODEL PARAMETERS						
	1500# Class			2500# Class		
	4” NB	8” NB	12” NB	4” NB	8” NB	12” NB
jh	146.9	215.34	298.1	156.5	247.1	333.0
fd	219	356	508	225	403	578
fh	34.9	57.2	80.9	44.5	85.7	210.7
pod	114	219	323.9	114	219	323.9
pt	17.1	24	34	13.48	23.012	33.33
pcd	181	304.8	438.2	187.3	333.4	476.3
bd	19.05	25.4	34.9	19.05	34.9	50.8
r	6	8	10	6	15	15
hubang*	19	15	15.7	23.2	18.8	16.2
hubht	57.1	65.7	90.8	58.6	70.5	85.91
nbolts	8	16	16	12	12	12

* Measured in degrees. All other dimensions are in millimetres.

Table 6: DESFLEX Joint Model Parameters

ANSI MODEL PARAMETERS						
	1500# Class			2500# Class		
	4” NB	8” NB	12” NB	4” NB	8” NB	12” NB
jh	481.4	923.8	1510.6	477.6	1001.1	1668.9
hubht	123.8	212.7	282.6	190.5	317.5	463.6
pod	114	219	323.9	114	219	323.9
wth	17.1	24	34	13.48	23.012	33.33
fh	54	92.1	123.8	76.2	127	184
fod	311	482	673	356	552	762
hod	162	292	451	165	305	441
hdw	114	219	323.9	114	219	323.9
r	5	6.5	11	9.5	15.5	15.5
sh	6.4	6.4	6.4	6.4	6.4	6.4
sod	157.2	269.9	381	157.2	269.2	381
gth	3.2	3.2	3.2	3.2	3.2	3.2
gid	103.2	203.2	303.2	103.2	203.2	303.2
gsringid	120.3	225	333	117.1	215.5	323.5
gsringod	149.6	263.9	375.1	149.6	263.9	375.1
gsringht	4.5	4.5	4.5	4.5	4.5	4.5
gcringod	201.5	341.5	507.2	225.5	373.8	530.5
bd	31.75	41.275	50.8	38.1	50.8	69.85
gap	1.575	1.5625	1.6	1.6	1.6	1.575
nbolts	8	12	16	8	12	12

All dimensions are measured in millimetres.

Table 7: ANSI Joint Model Parameters

10. Appendix II – Contact Pressure Algorithm Flowchart

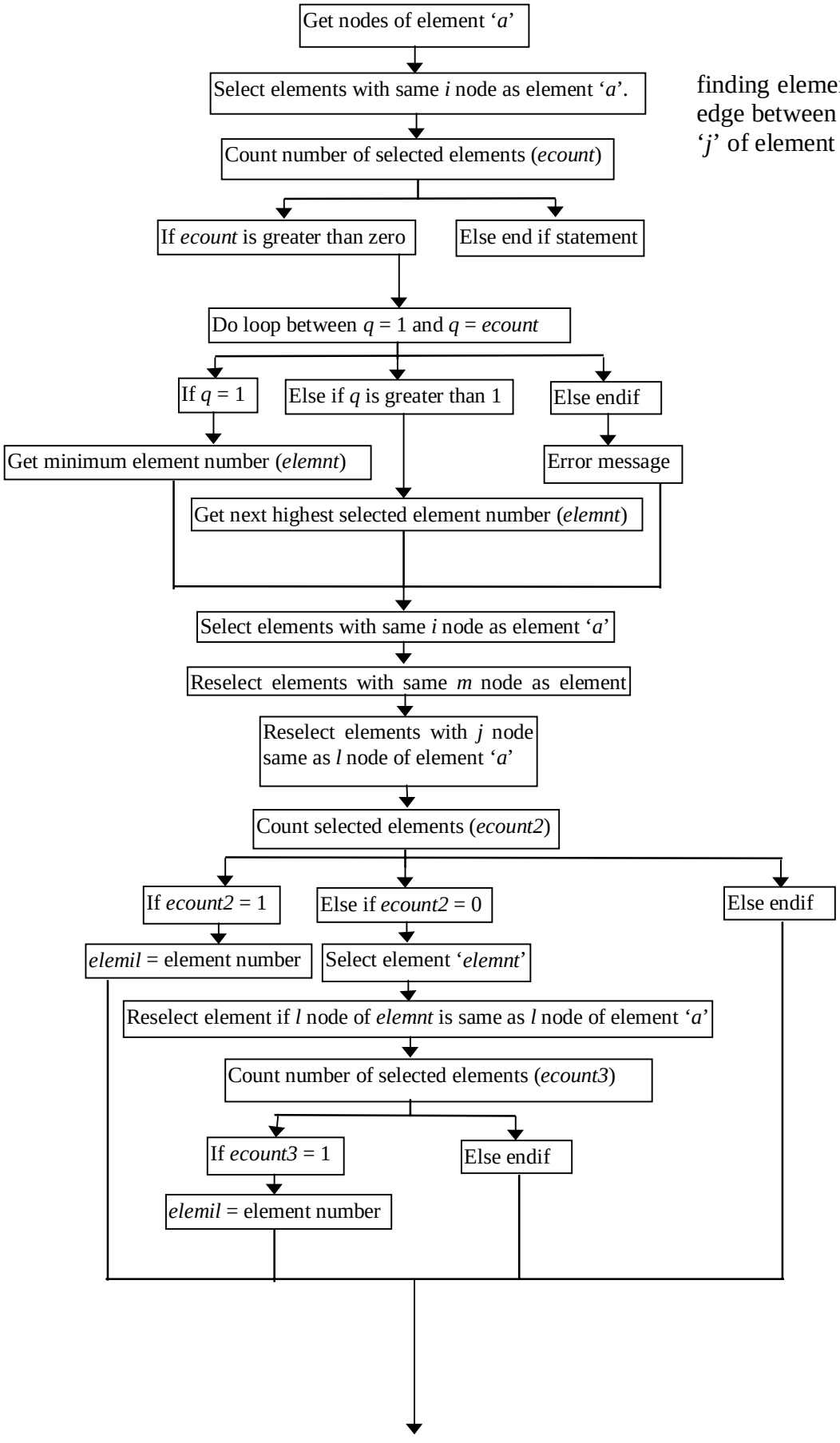

finding element sharing the edge between nodes ‘*i*’ and ‘*j*’ of element ‘*a*’.

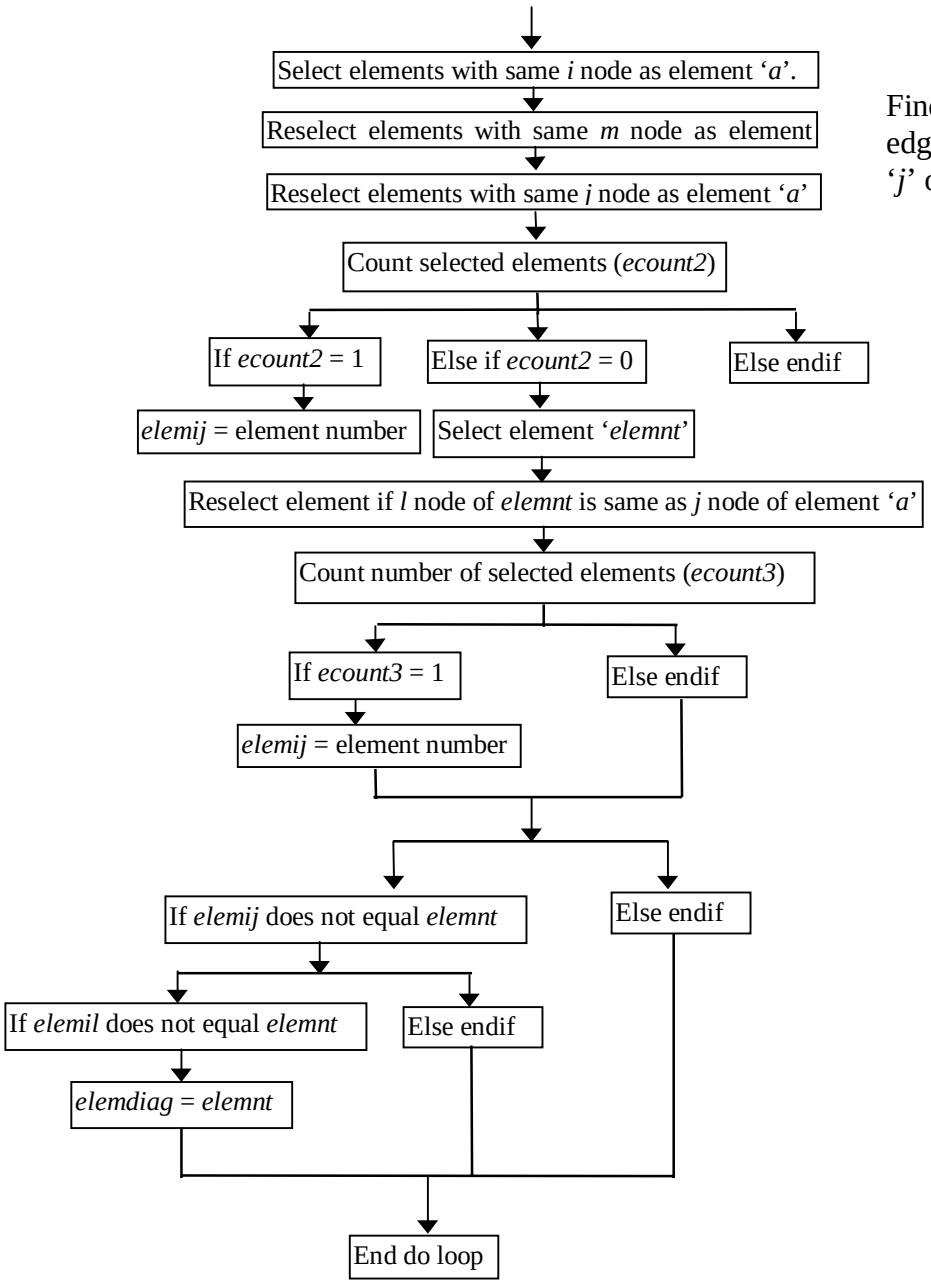

Find element sharing the edge between nodes '*i*' and '*j*' of element '*a*'.

This procedure is repeated for adjacent elements that have their *j*, *k* and *l* nodes as the same the node as the *i* node of element '*a*'.

Once this has been completed, the following procedure that redistributes the contact force is carried out:

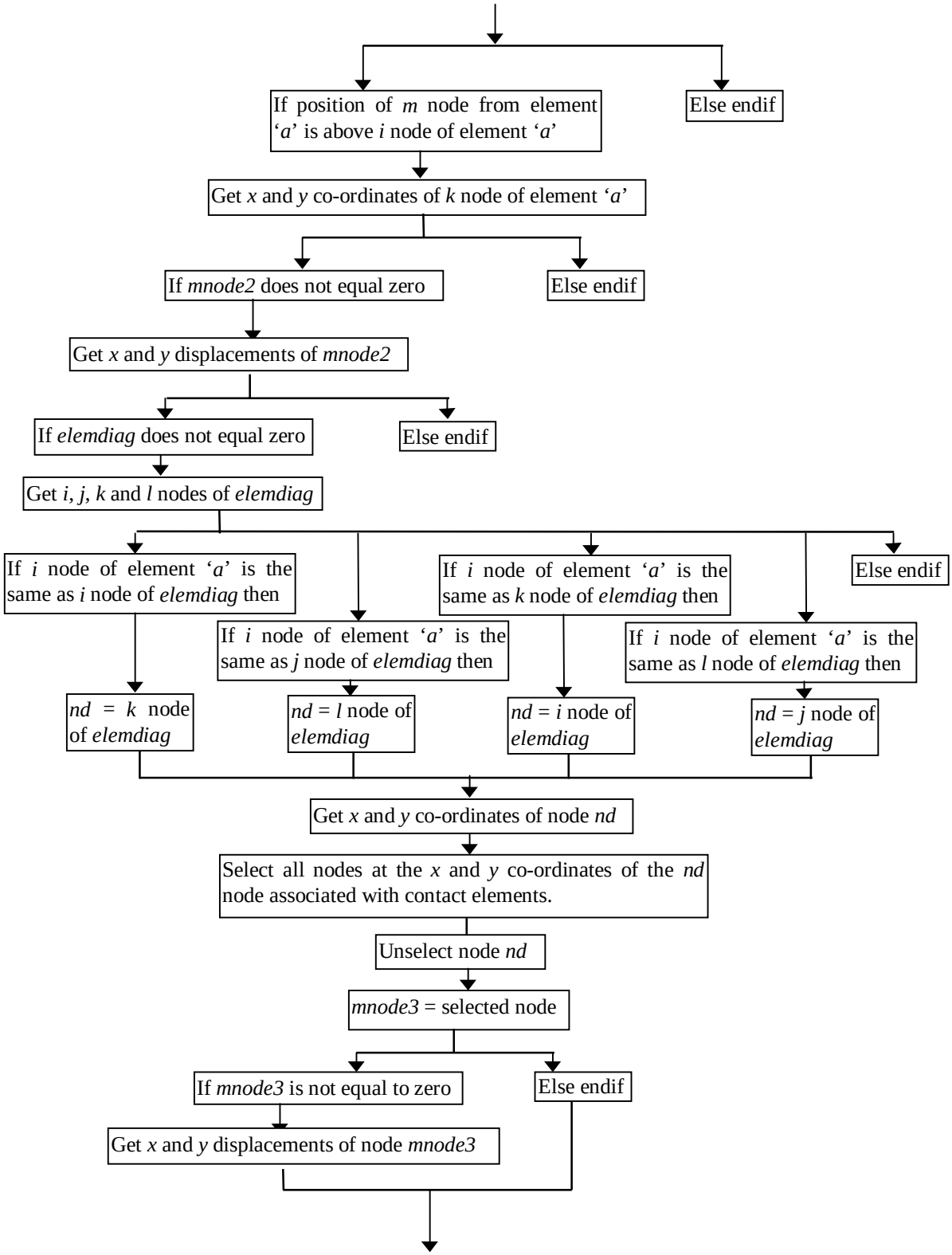
If position of *m* node from element '*a*' is above *i* node of element '*a*'
Else endif
Get *x* and *y* co-ordinates of *k* node of element '*a*'
If *mnode2* does not equal zero
Else endif
Get *x* and *y* displacements of *mnode2*
If *elemdiag* does not equal zero
Else endif
Get *i*, *j*, *k* and *l* nodes of *elemdiag*
If *i* node of element '*a*' is the same as *i* node of *elemdiag* then
If *i* node of element '*a*' is the same as *j* node of *elemdiag* then
If *i* node of element '*a*' is the same as *k* node of *elemdiag* then
If *i* node of element '*a*' is the same as *l* node of *elemdiag* then
Else endif
nd = *k* node of *elemdiag*
nd = *l* node of *elemdiag*
nd = *i* node of *elemdiag*
nd = *j* node of *elemdiag*
Get *x* and *y* co-ordinates of node *nd*
Select all nodes at the *x* and *y* co-ordinates of the *nd* node associated with contact elements.
Unselect node *nd*
mnode3 = selected node
If *mnode3* is not equal to zero
Else endif
Get *x* and *y* displacements of node *mnode3*

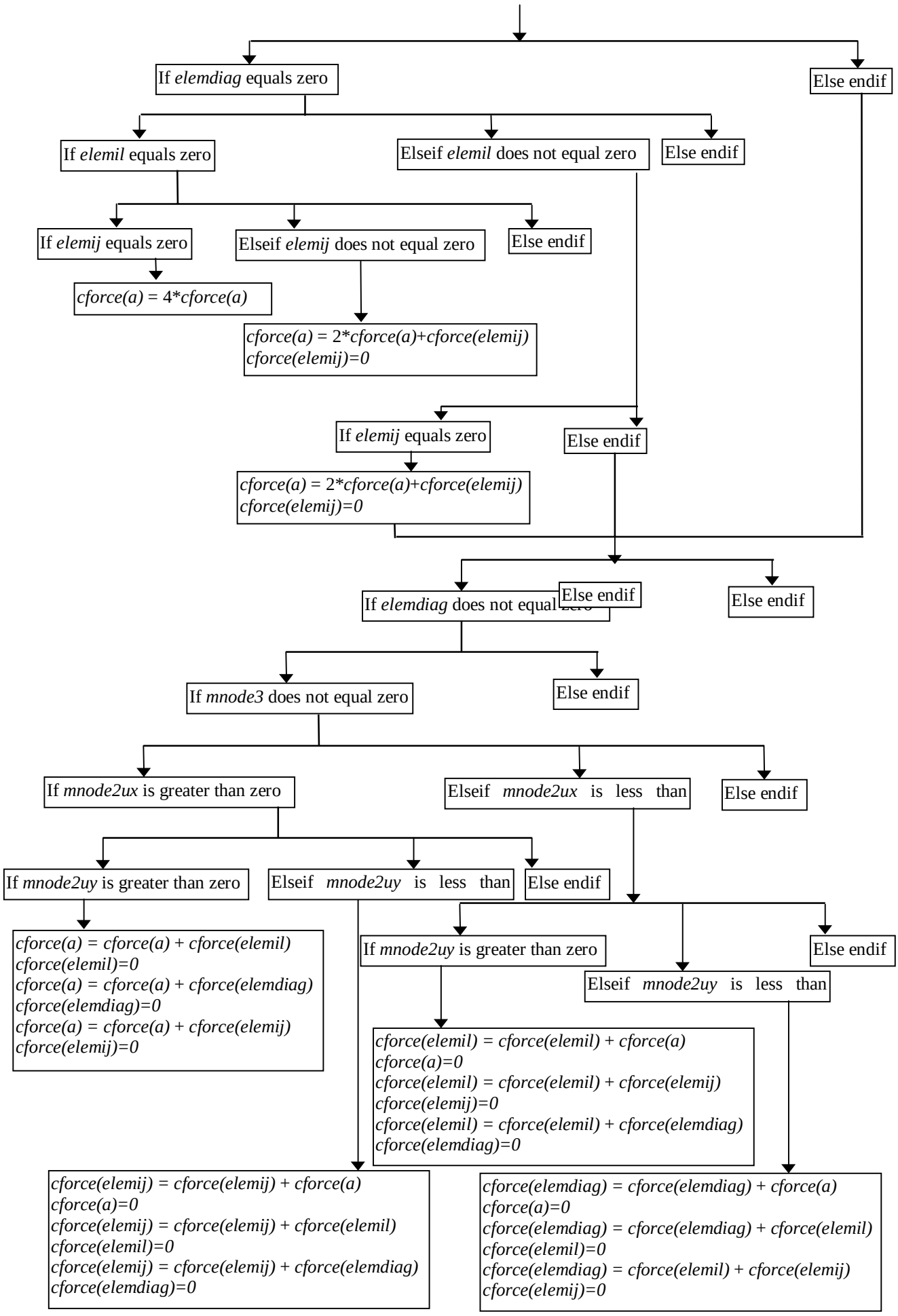
If *elemdiag* equals zero
Else endif
If *elemil* equals zero
Elseif *elemil* does not equal zero
Else endif
If *elemij* equals zero
Elseif *elemij* does not equal zero
Else endif
cforce(a) = 4**cforce(a)*
cforce(a) = 2**cforce(a)*+*cforce(elemij)*
cforce(elemij)=0
If *elemij* equals zero
Else endif
cforce(a) = 2**cforce(a)*+*cforce(elemij)*
cforce(elemij)=0
If *elemdiag* does not equal zero
Else endif
Else endif
If *mnode3* does not equal zero
Else endif
If *mnode2ux* is greater than zero
Elseif *mnode2ux* is less than
Else endif
If *mnode2uy* is greater than zero
Elseif *mnode2uy* is less than
Else endif
cforce(a) = cforce(a) + cforce(elemil)
cforce(elemil)=0
cforce(a) = cforce(a) + cforce(elemdiag)
cforce(elemdiag)=0
cforce(a) = cforce(a) + cforce(elemij)
cforce(elemij)=0
If *mnode2uy* is greater than zero
Elseif *mnode2uy* is less than
Else endif
cforce(elemil) = cforce(elemil) + cforce(a)
cforce(a)=0
cforce(elemil) = cforce(elemil) + cforce(elemij)
cforce(elemij)=0
cforce(elemil) = cforce(elemil) + cforce(elemdiag)
cforce(elemdiag)=0
cforce(elemij) = cforce(elemij) + cforce(a)
cforce(a)=0
cforce(elemij) = cforce(elemij) + cforce(elemil)
cforce(elemil)=0
cforce(elemij) = cforce(elemij) + cforce(elemdiag)
cforce(elemdiag)=0
cforce(elemdiag) = cforce(elemdiag) + cforce(a)
cforce(a)=0
cforce(elemdiag) = cforce(elemdiag) + cforce(elemil)
cforce(elemil)=0
cforce(elemdiag) = cforce(elemil) + cforce(elemij)
cforce(elemij)=0

11. Appendix III – Finite Element Plots

Below is a list of the complete set of finite element plots that are contained in this appendix. This list was not presented as part of the Table of Figures due to the volume of plots.

11.1. Flange Ring / Pipework

11.1.1. 1500# Class

11.1.1.1. Four Inch Nominal Bore

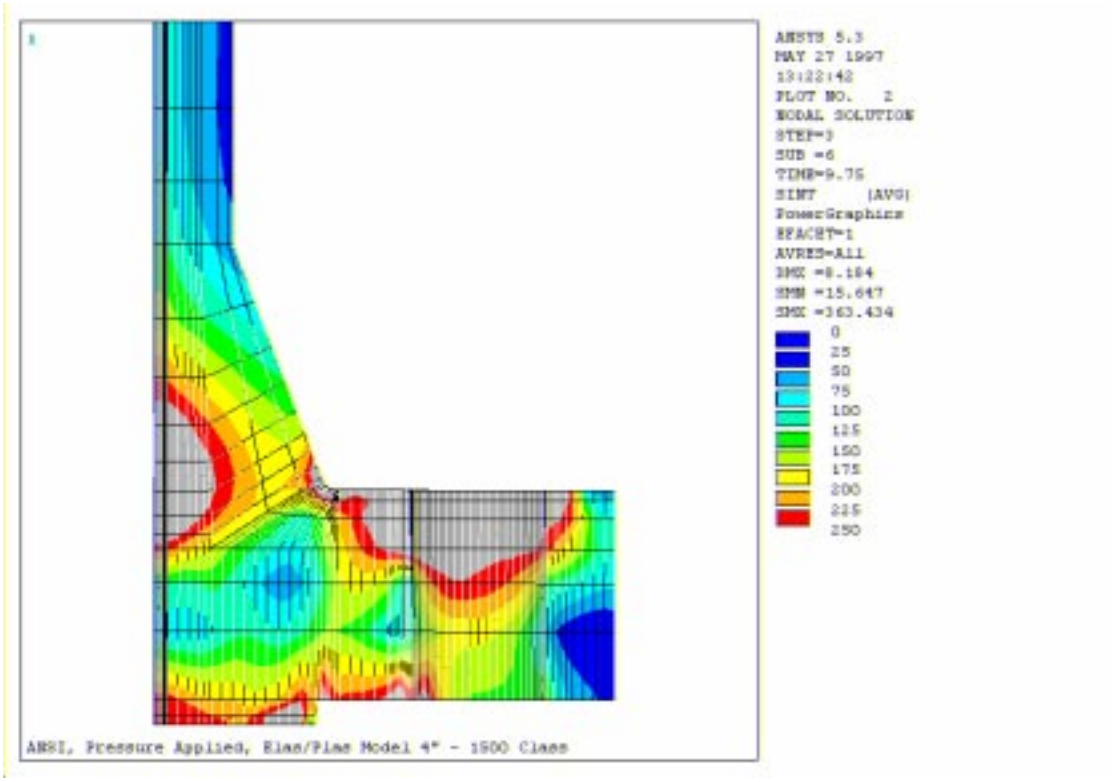

Figure 57: ANSI 4" 1500# Class, Flange/Pipe Cross Section - Stress Intensity Plot

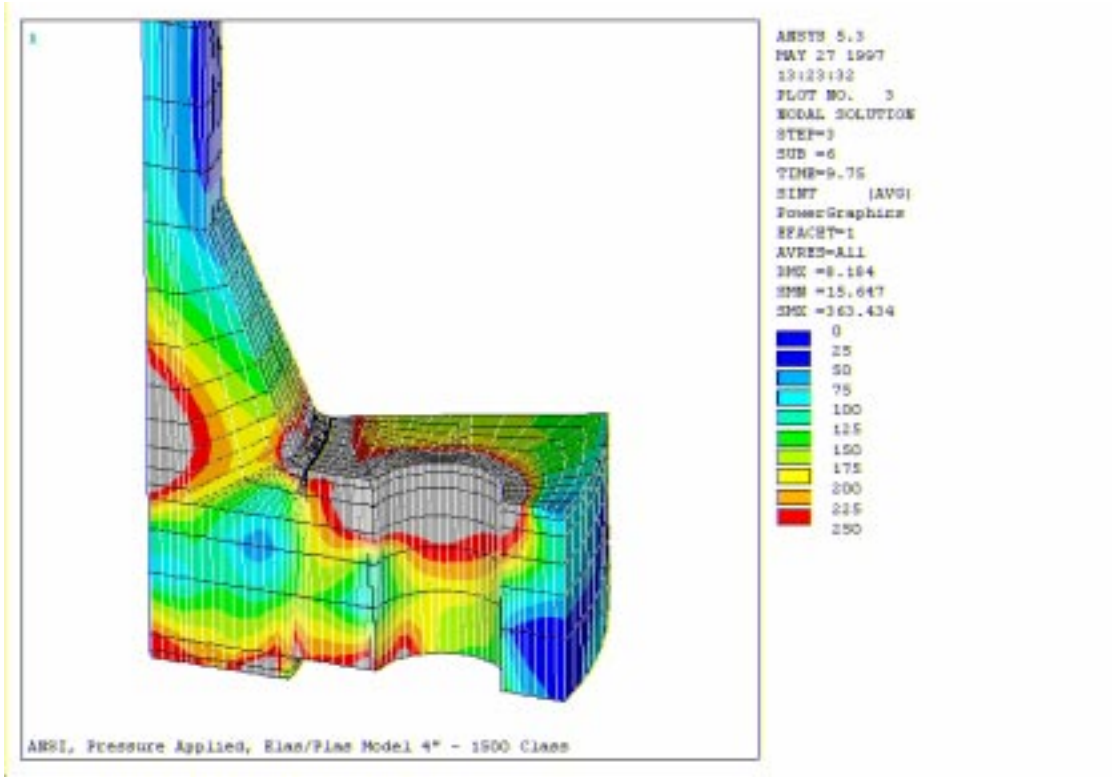

Figure 58: ANSI 4" 1500# Class, Flange/Pipe Isometric View - Stress Intensity Plot

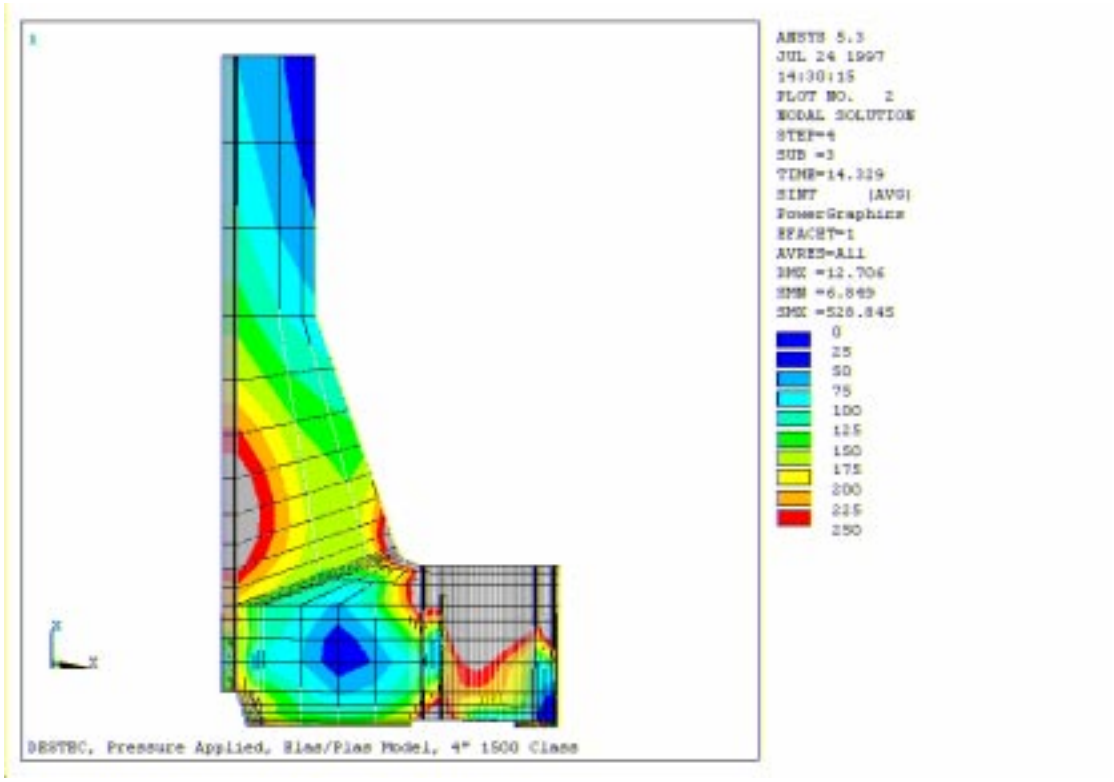

Figure 59: DESFLEX 4" 1500# Class, Flange/Pipe Cross Section - Stress Intensity Plot

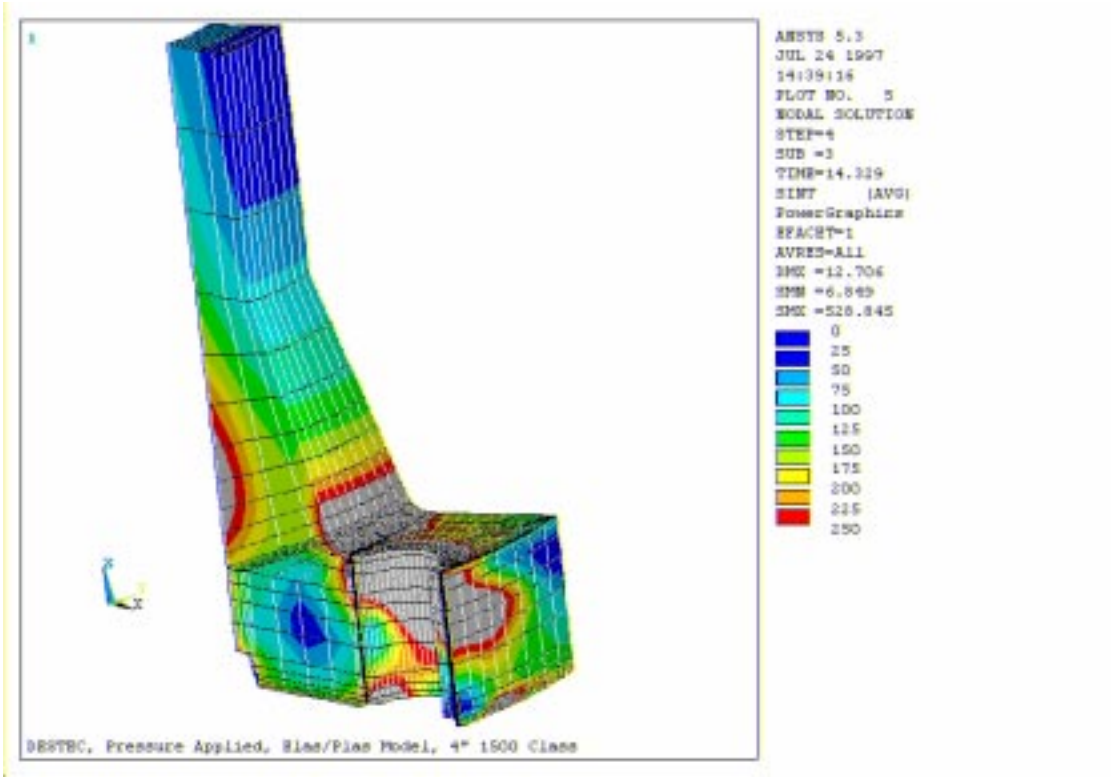

Figure 60: DESFLEX 4" 1500# Class, Flange/Pipe Isometric View - Stress Intensity Plot

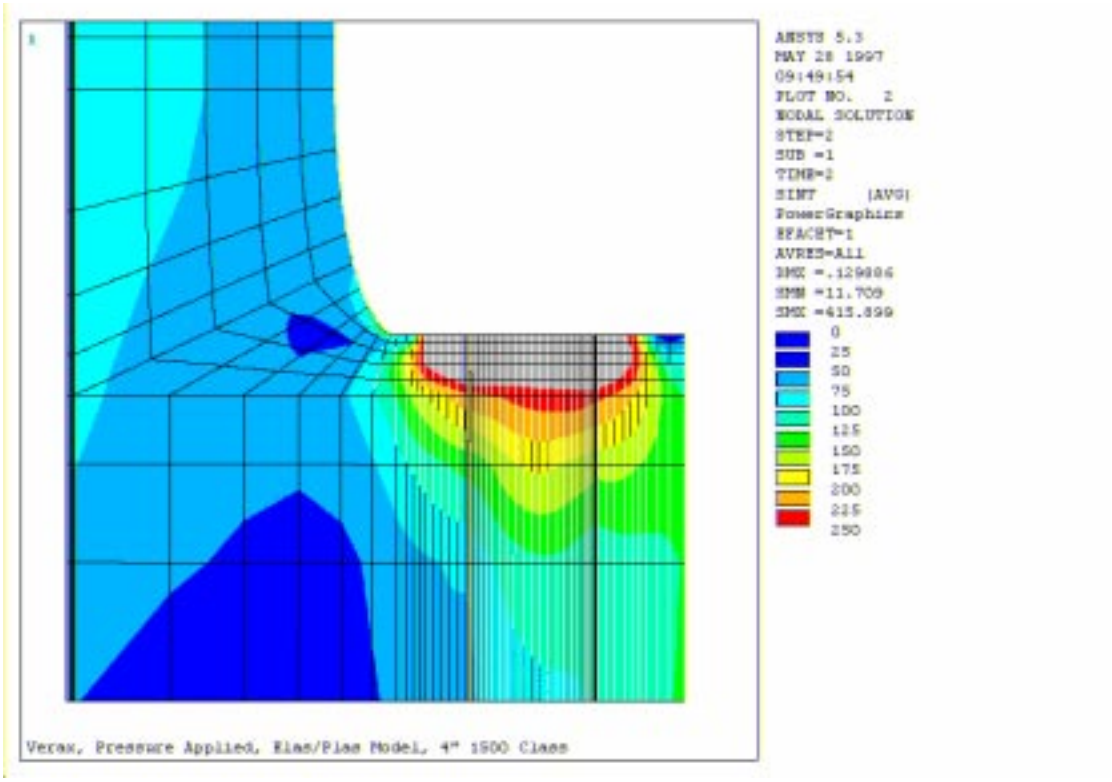

Figure 61: VCF 4" 1500# Class, Flange/Pipe Cross Section - Stress Intensity Plot

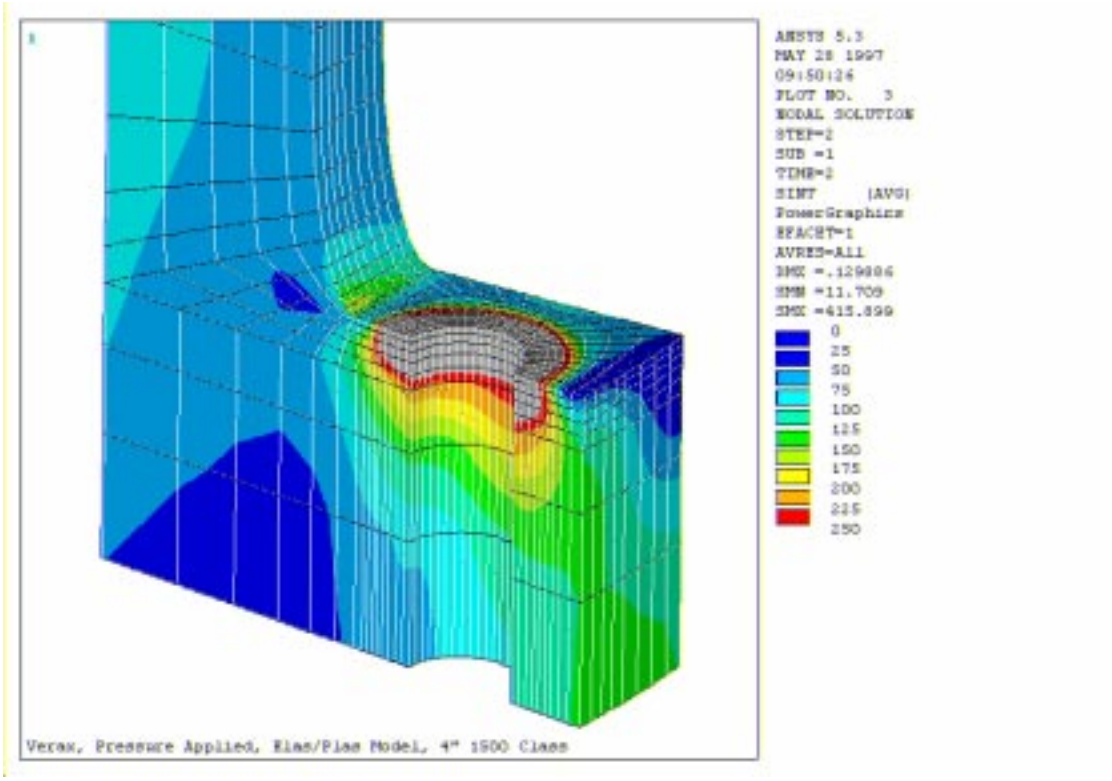

Figure 62: VCF 4" 1500# Class, Flange/Pipe Isometric View - Stress Intensity Plot

11.1.1.2. Eight Inch Nominal Bore

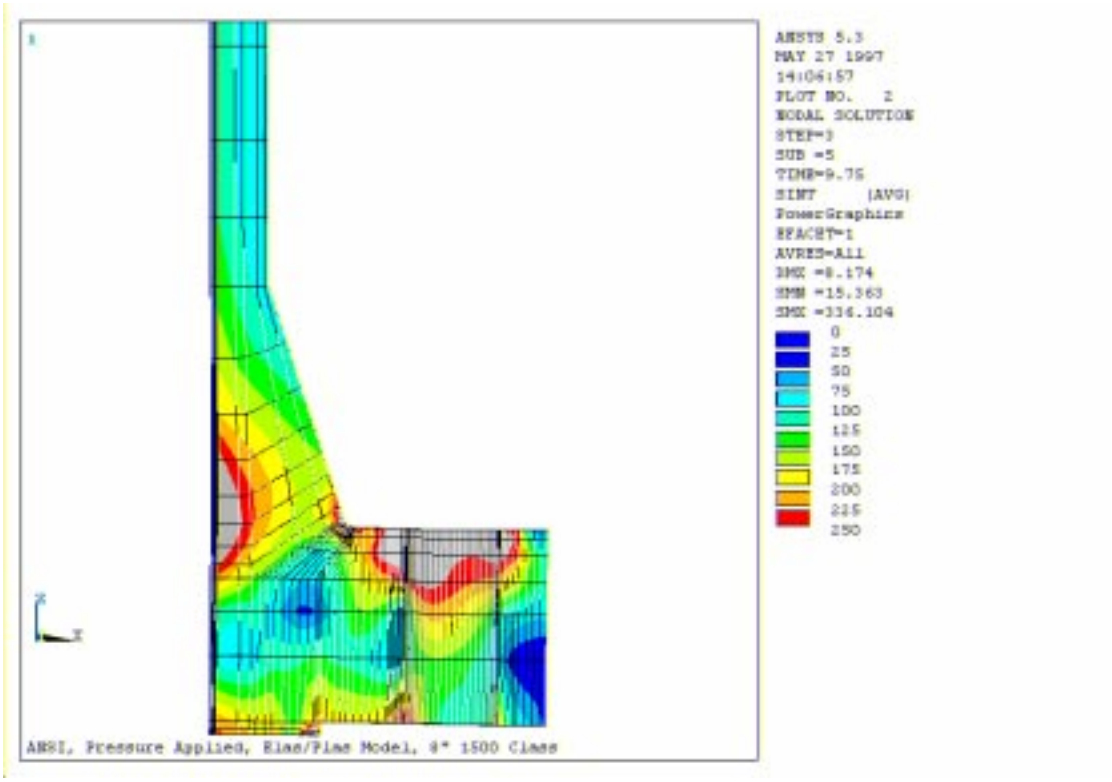

Figure 63: ANSI 8" 1500# Class, Flange/Pipe Cross Section - Stress Intensity Plot

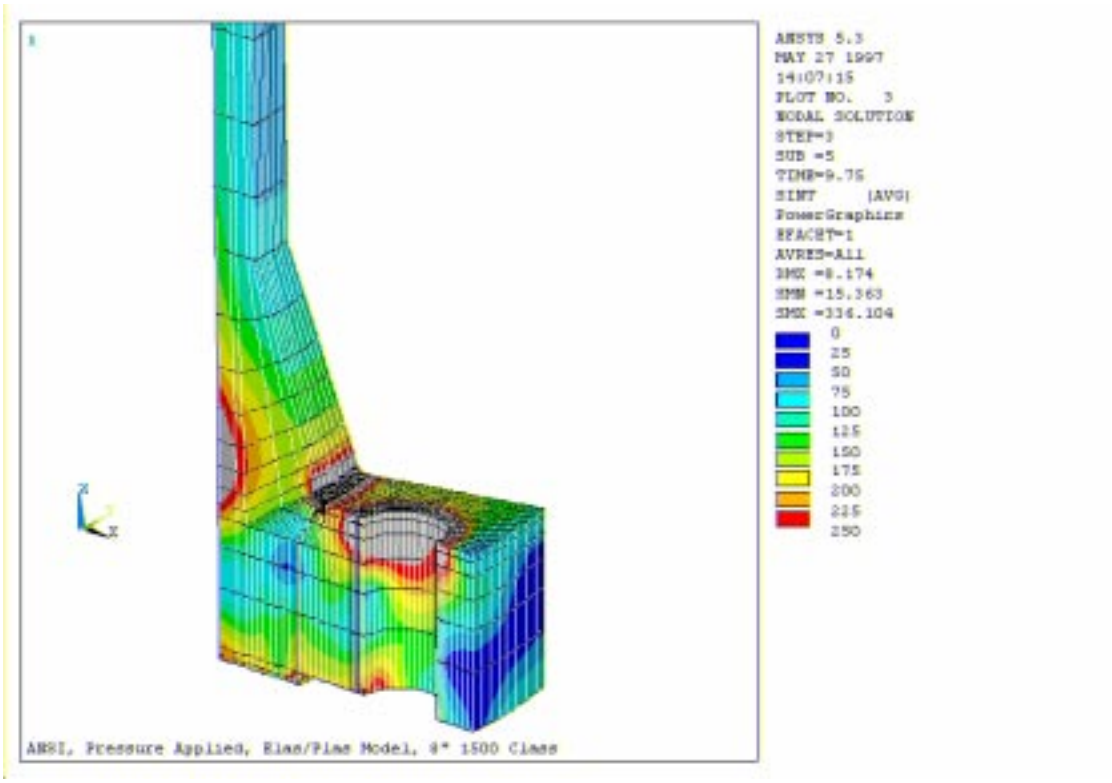

Figure 64: ANSI 8" 1500#, Flange/Pipe Isometric View - Stress Intensity Plot

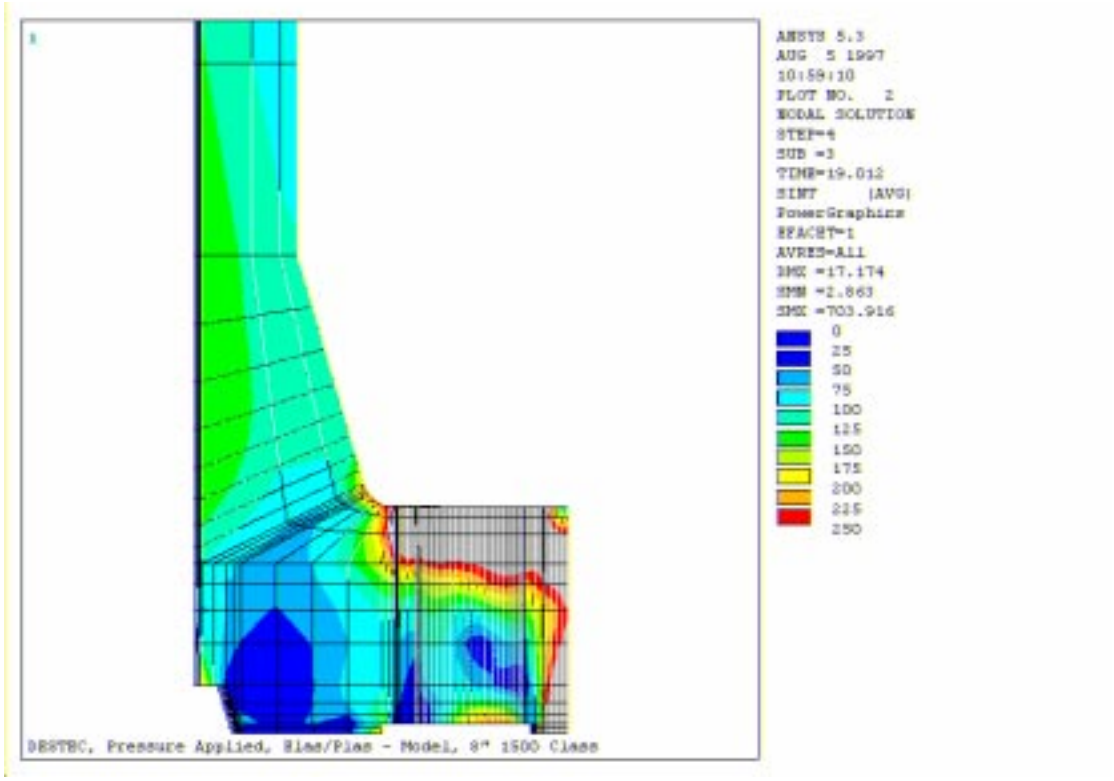

Figure 65: DESFLEX 8" 1500# Class, Flange/Pipe Cross Section - Stress Intensity Plot

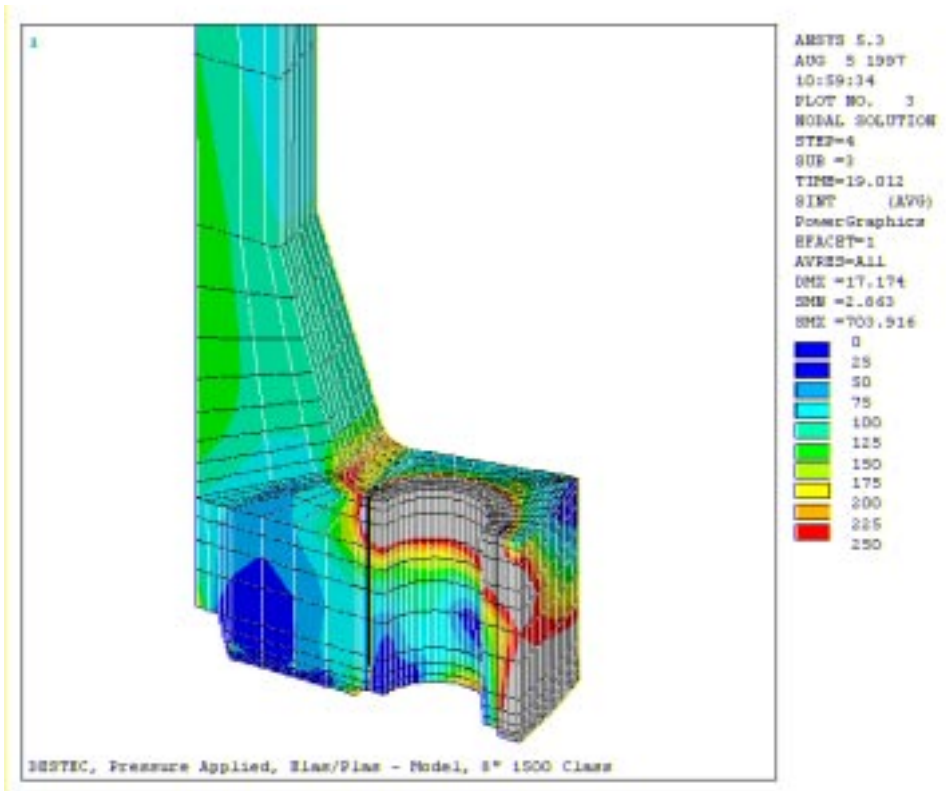

Figure 66: DESFLEX 8" 1500# Class, Flange/Pipe Isometric View - Stress Intensity Plot

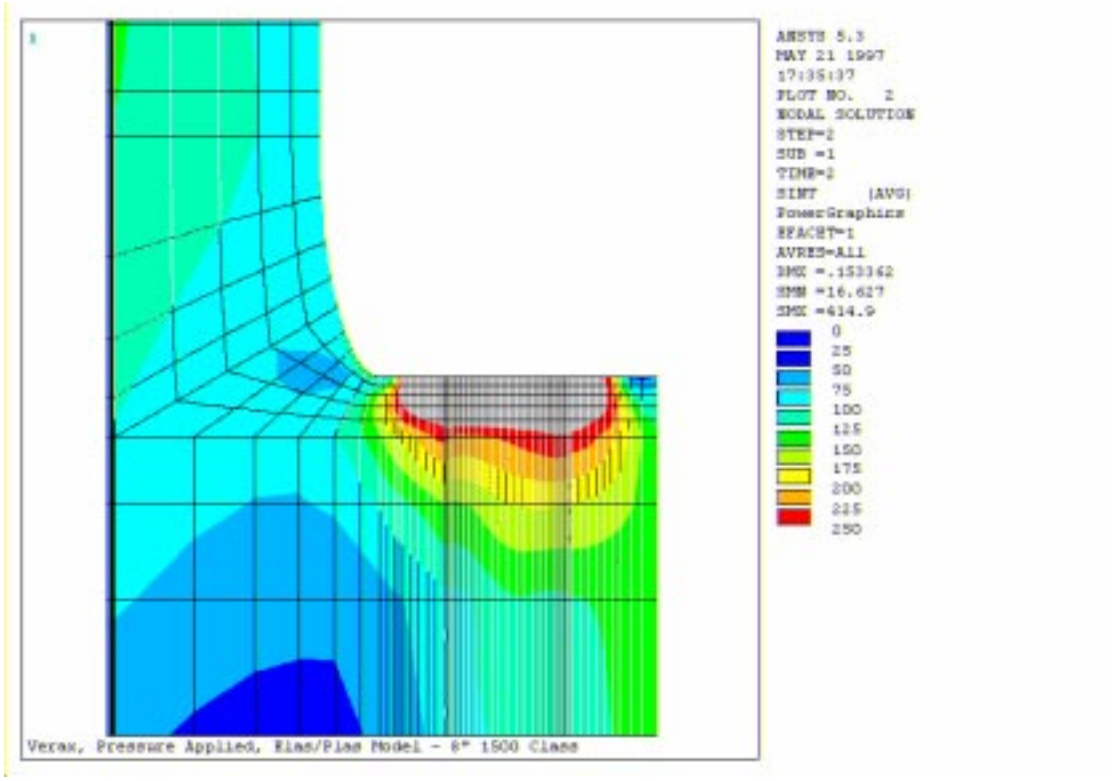

Figure 67: VCF 8" 1500# Class, Flange/Pipe Cross Section - Stress Intensity Plot

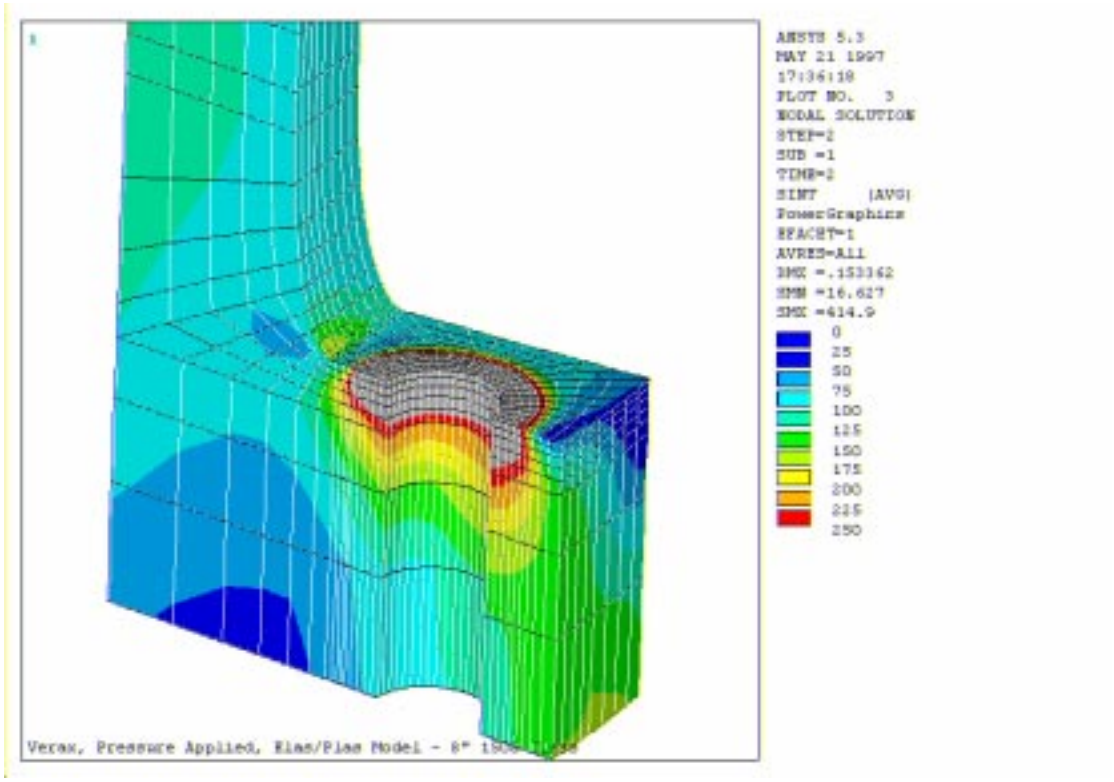

Figure 68: VCF 8" 1500# Class, Flange/Pipe Isometric View - Stress Intensity Plot

11.1.1.3. Twelve Inch Nominal Bore

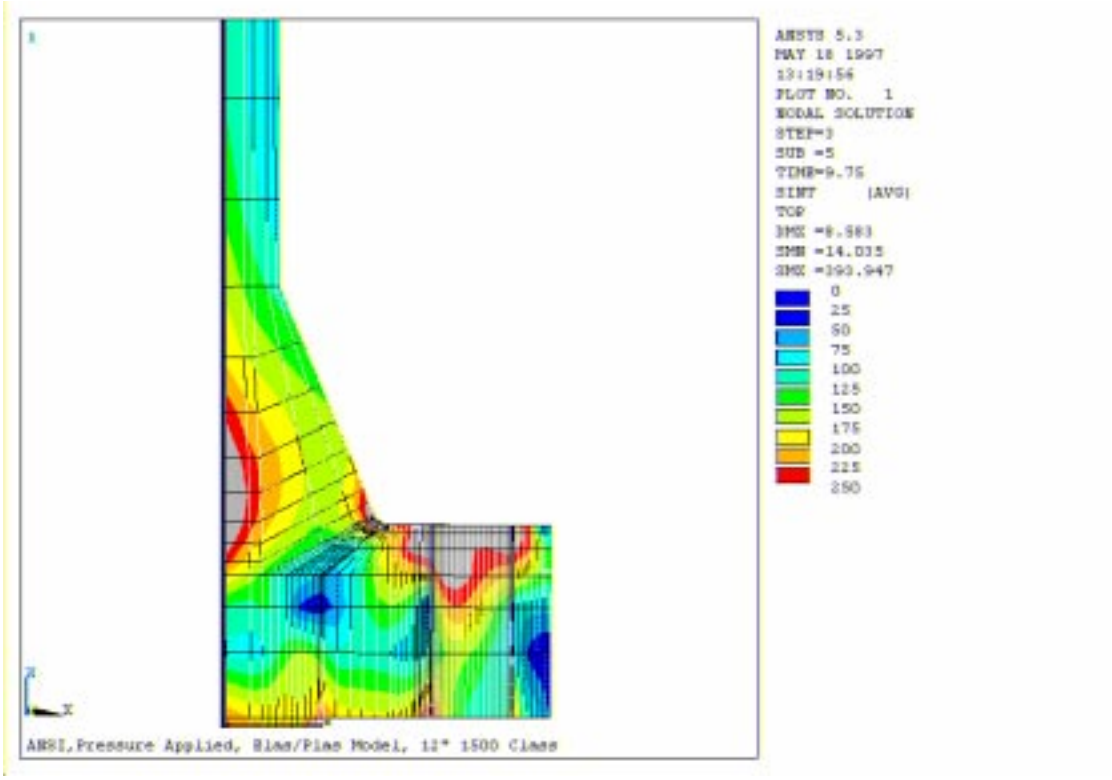

Figure 69: ANSI 12" 1500# Class, Flange/Pipe Cross Section - Stress Intensity Plot

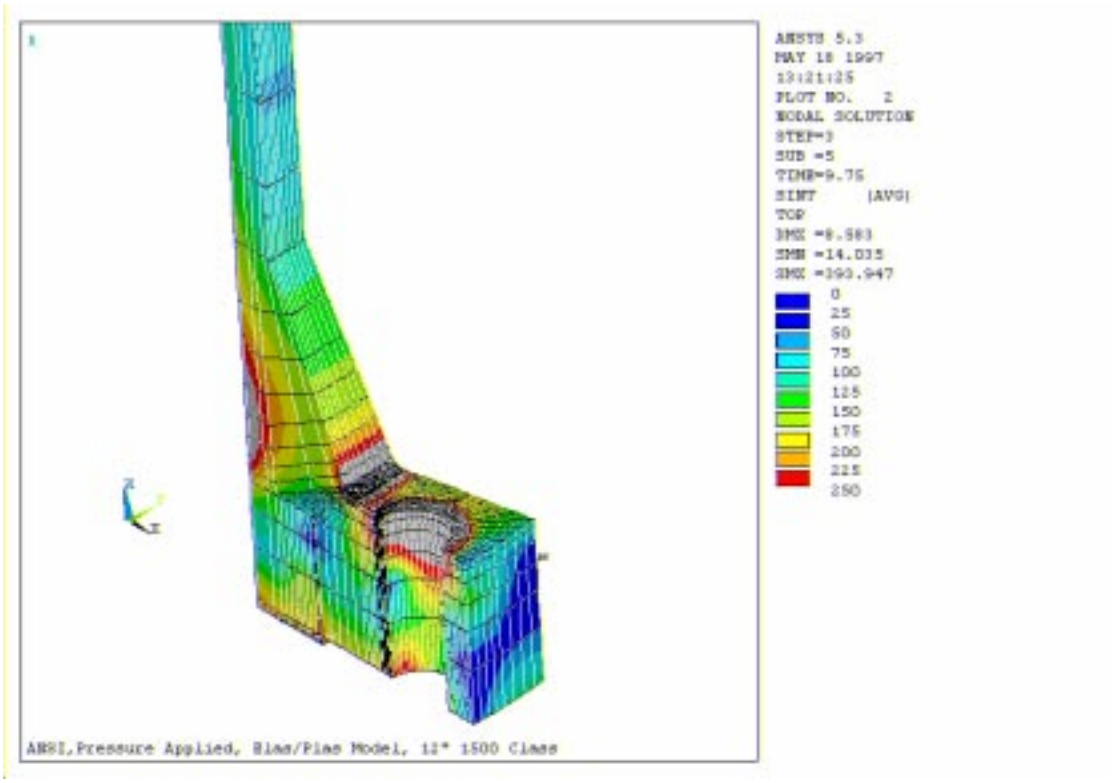

Figure 70: ANSI 12" 1500# Class, Flange/Pipe Isometric View - Stress Intensity Plot

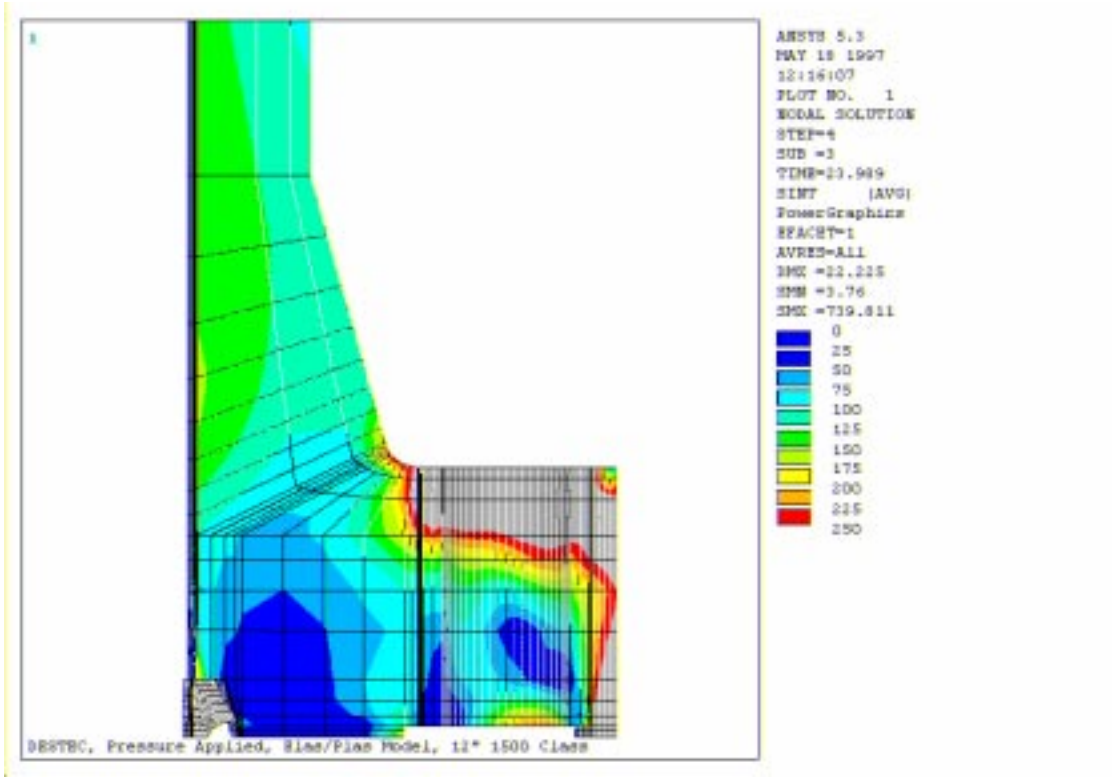

Figure 71: DESFLEX 12" 1500# Class, Flange/Pipe Cross Section - Stress Intensity Plot

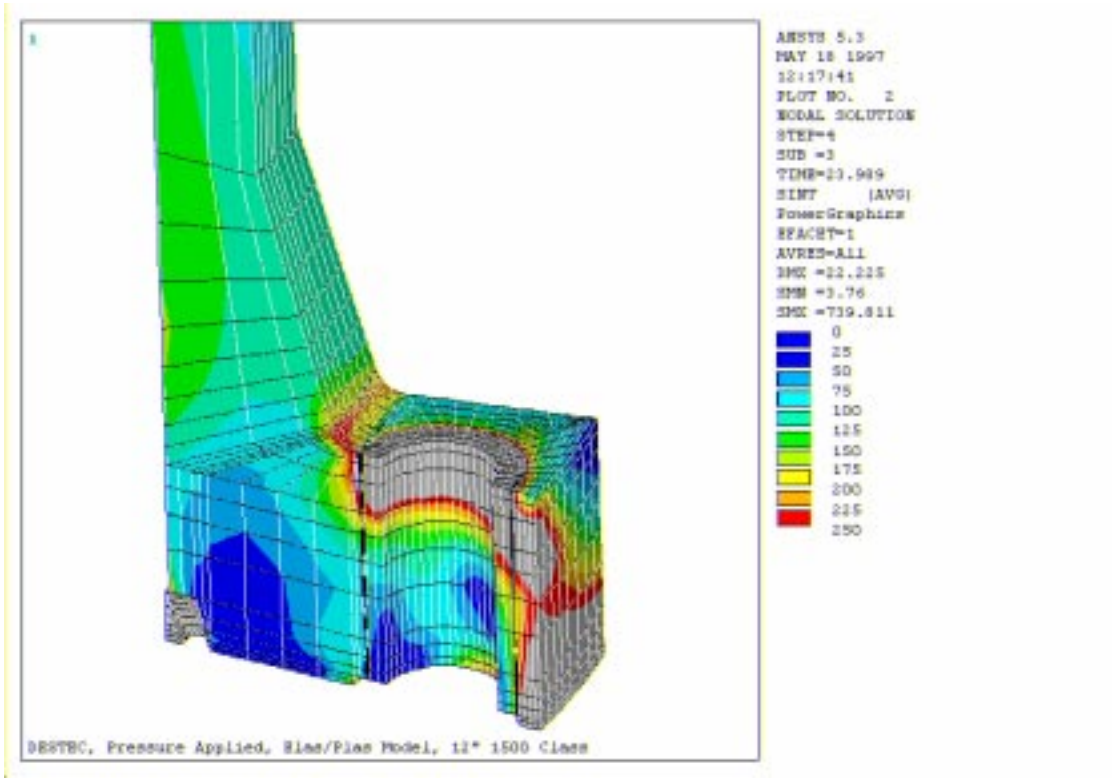

Figure 72: DESFLEX 12" 1500# Class, Flange/Pipe Isometric View - Stress Intensity Plot

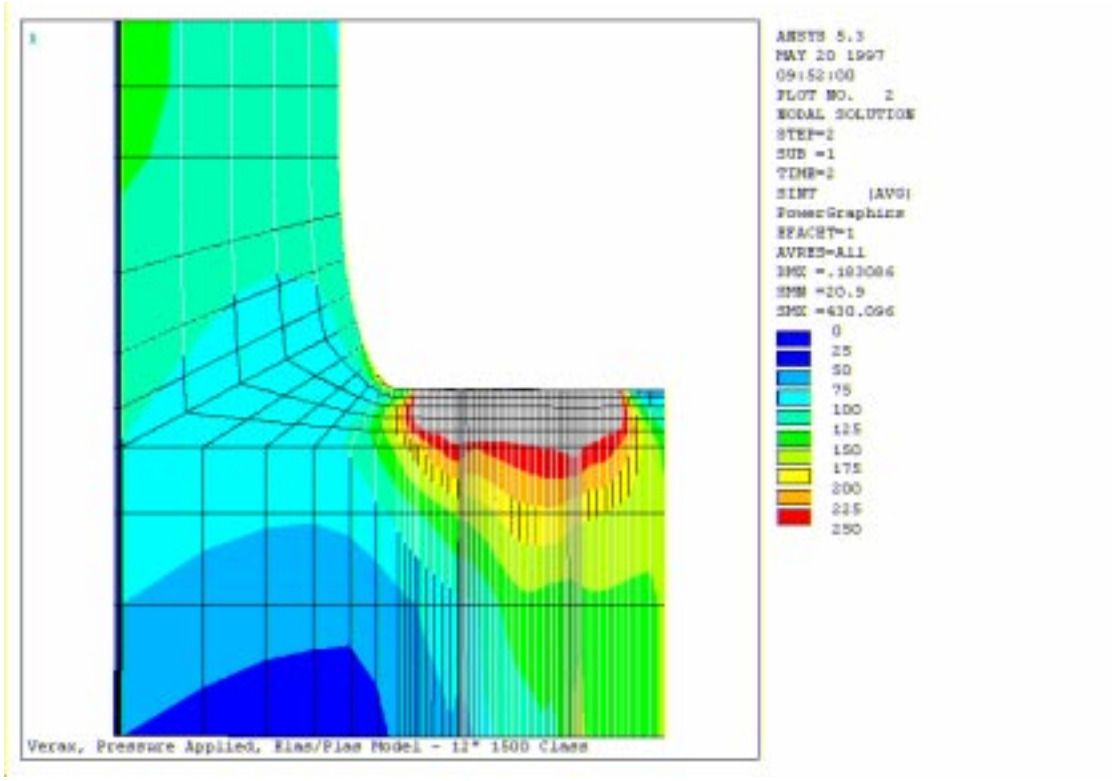

Figure 73: VCF 12" 1500# Class, Flange/Pipe Cross Section - Stress Intensity Plot

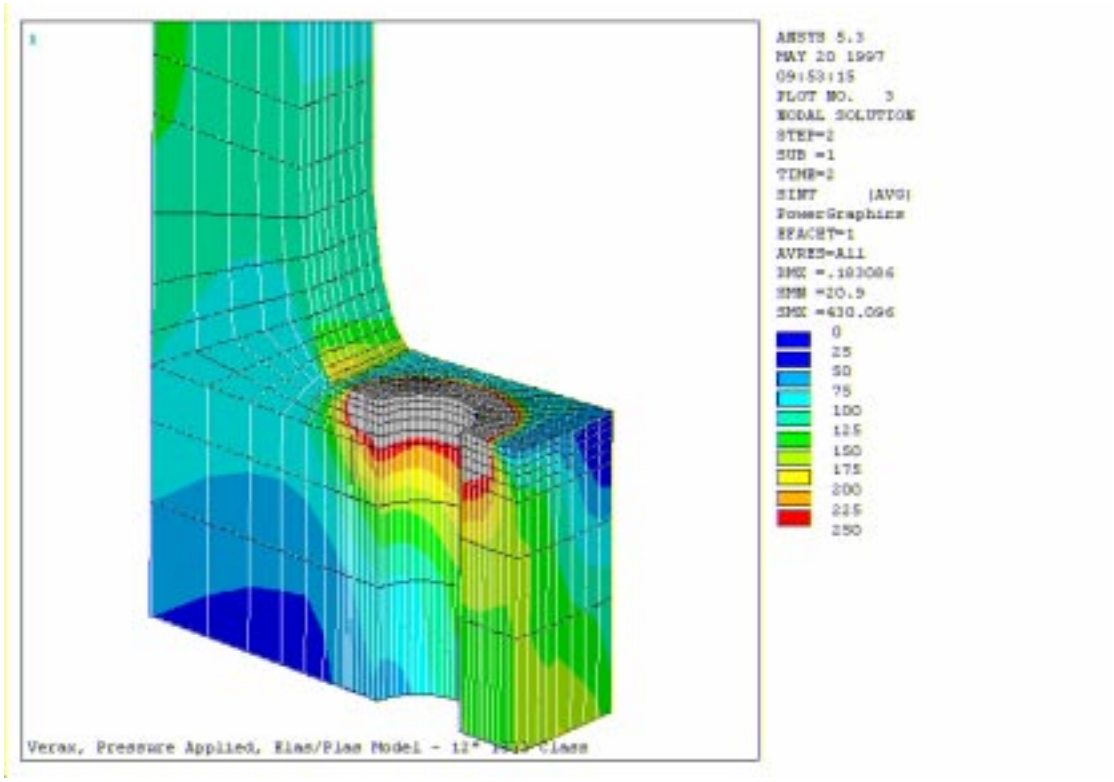

Figure 74: VCF 12" 1500# Class, Flange/Pipe Isometric View - Stress Intensity Plot

11.1.2. 2500# Class

11.1.2.1. Four Inch Nominal Bore

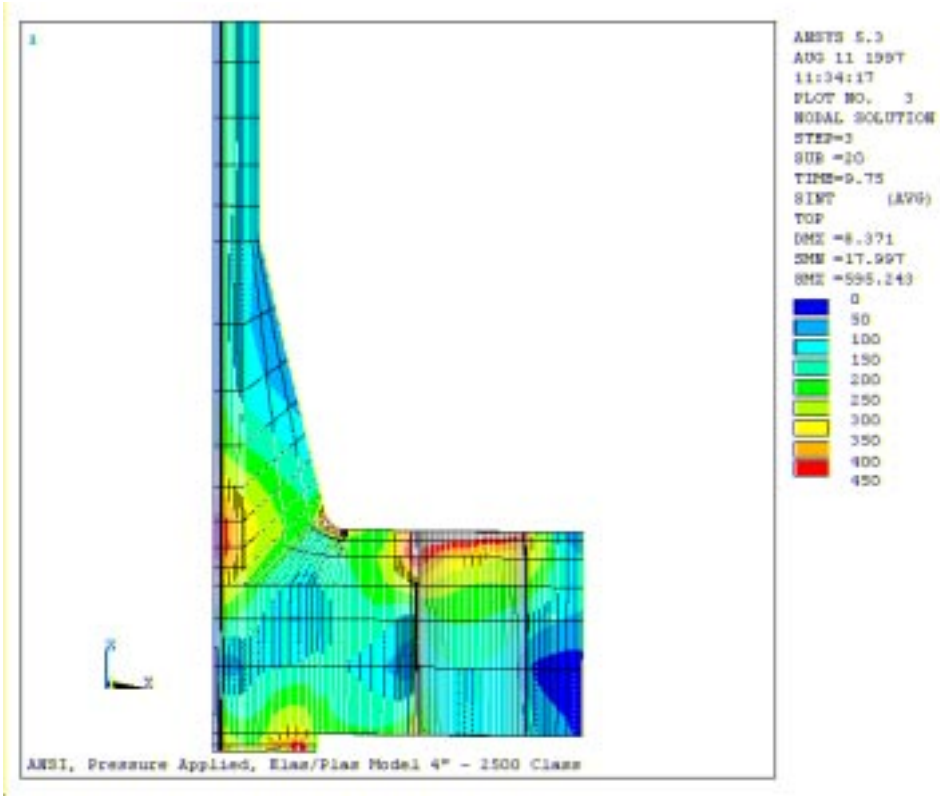

Figure 75: ANSI 4" 2500# Class, Flange/Pipe Cross Section - Stress Intensity Plot

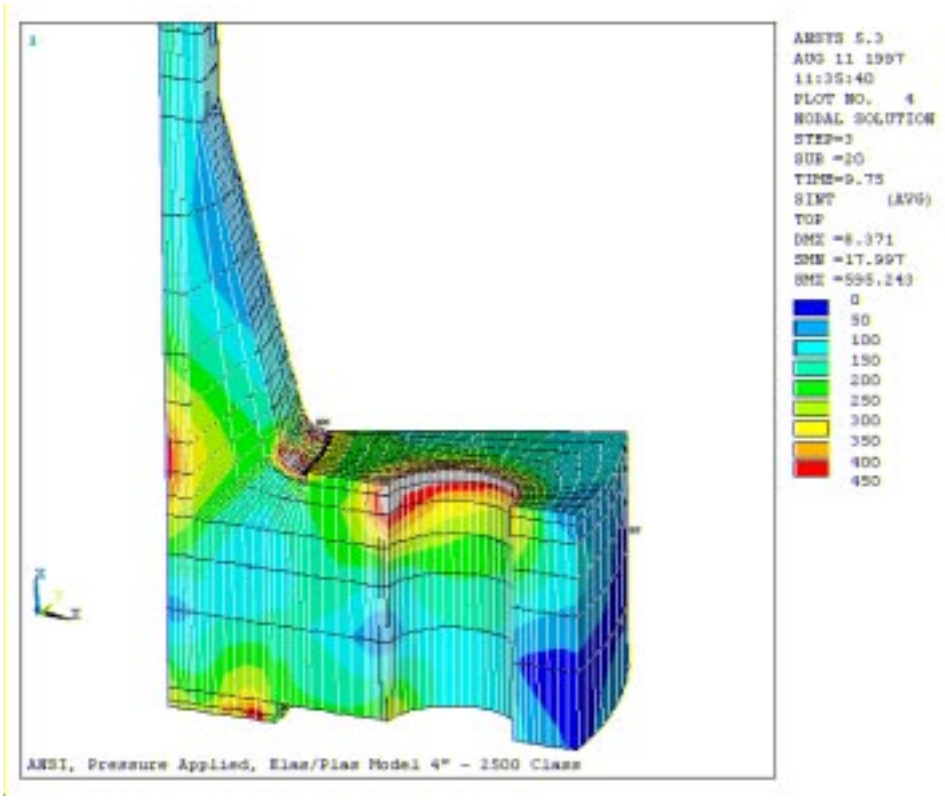

Figure 76: ANSI 4" 2500# Class, Flange/Pipe Isometric View - Stress Intensity Plot

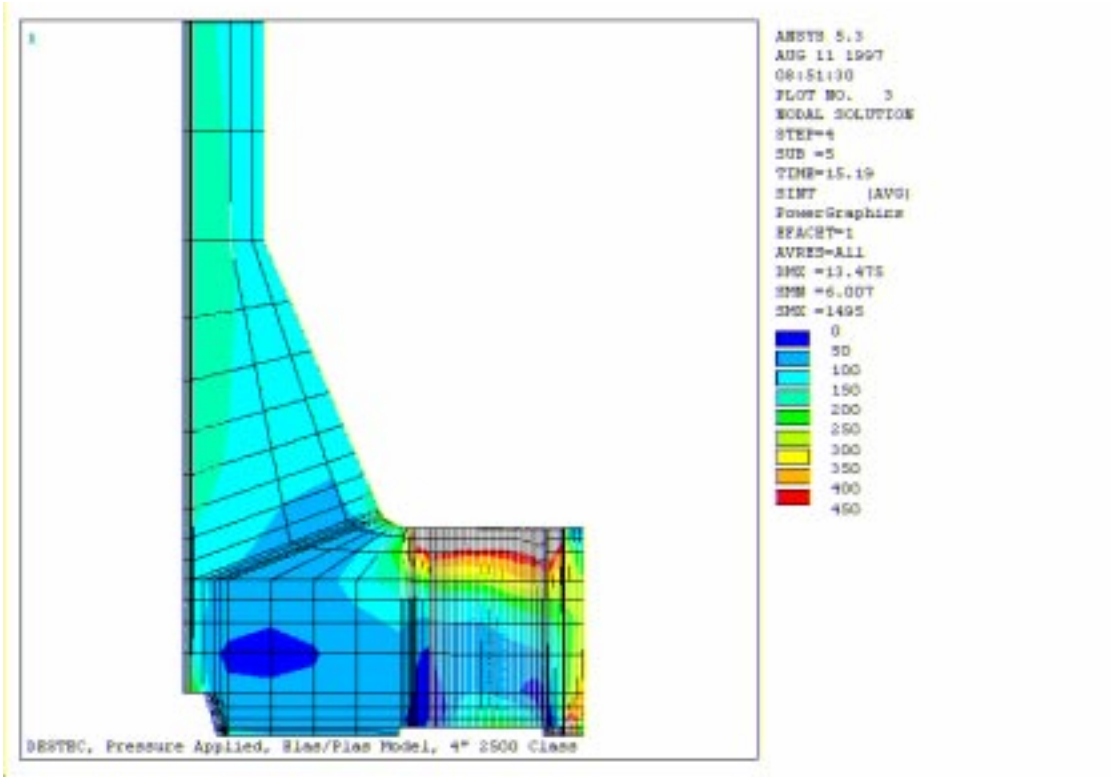

Figure 77: DESFLEX 4" 2500# Class, Flange/Pipe Cross Section - Stress Intensity Plot

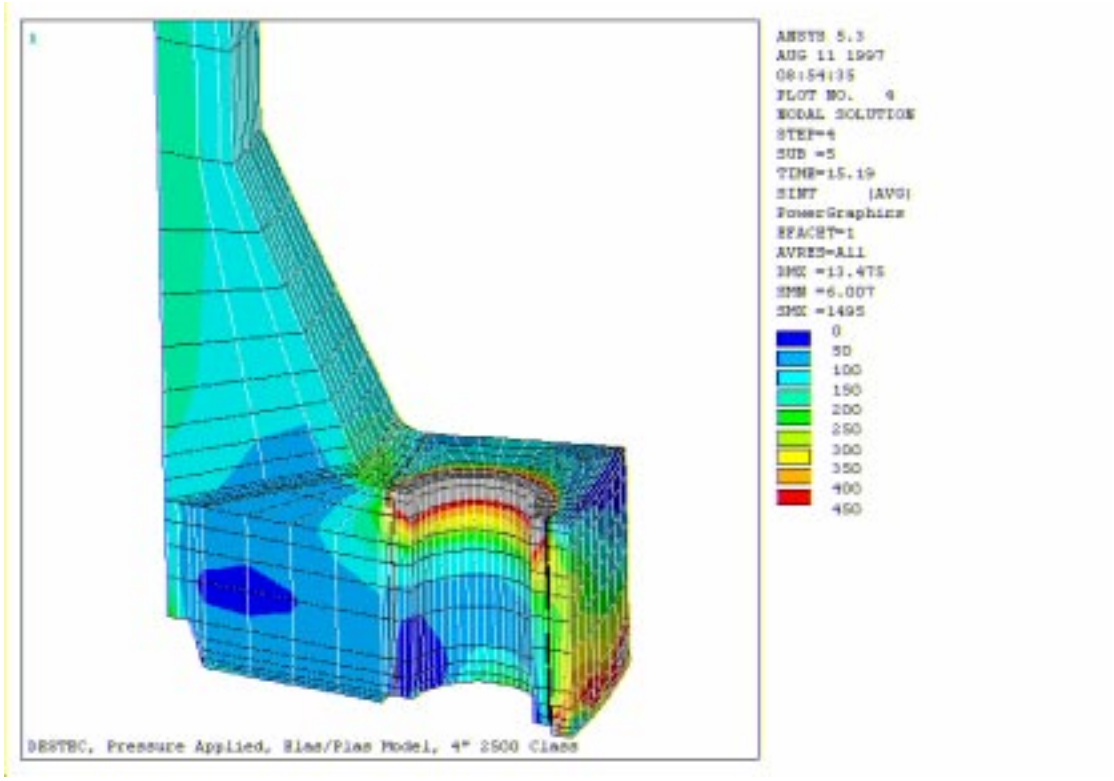

Figure 78: DESFLEX 4" 2500# Class, Flange/Pipe Isometric View - Stress Intensity Plot

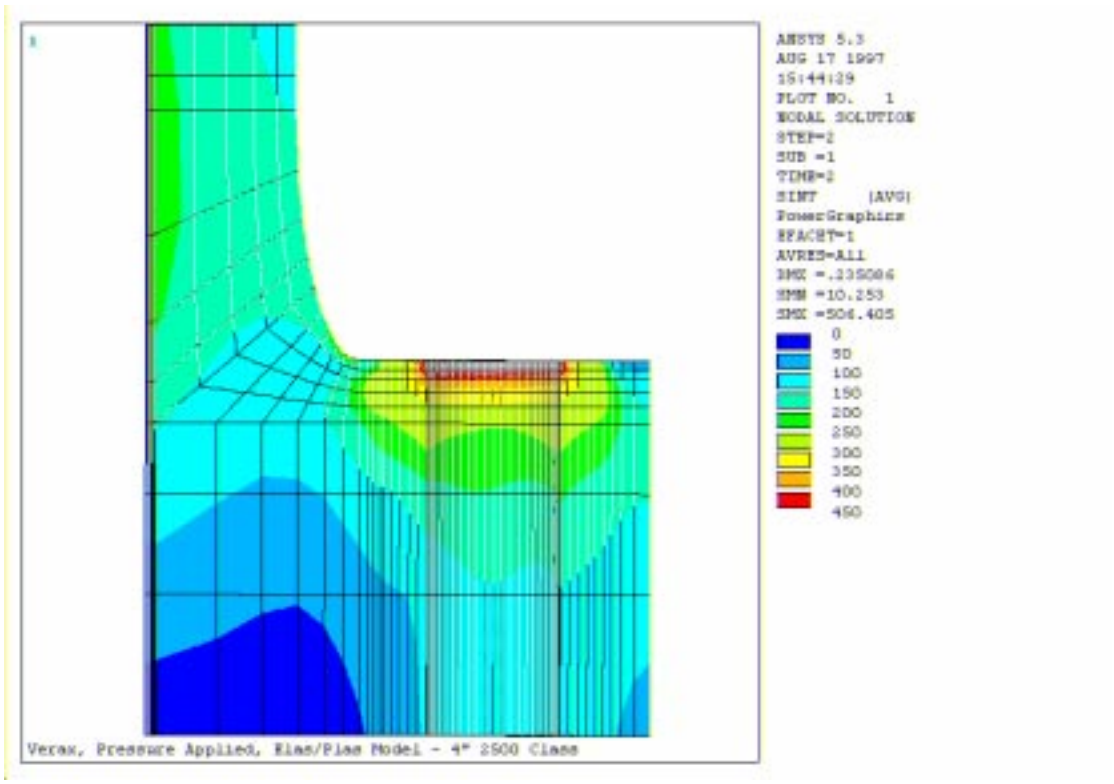

Figure 79: VCF 4" 2500# Class, Flange/Pipe Cross Section - Stress Intensity Plot

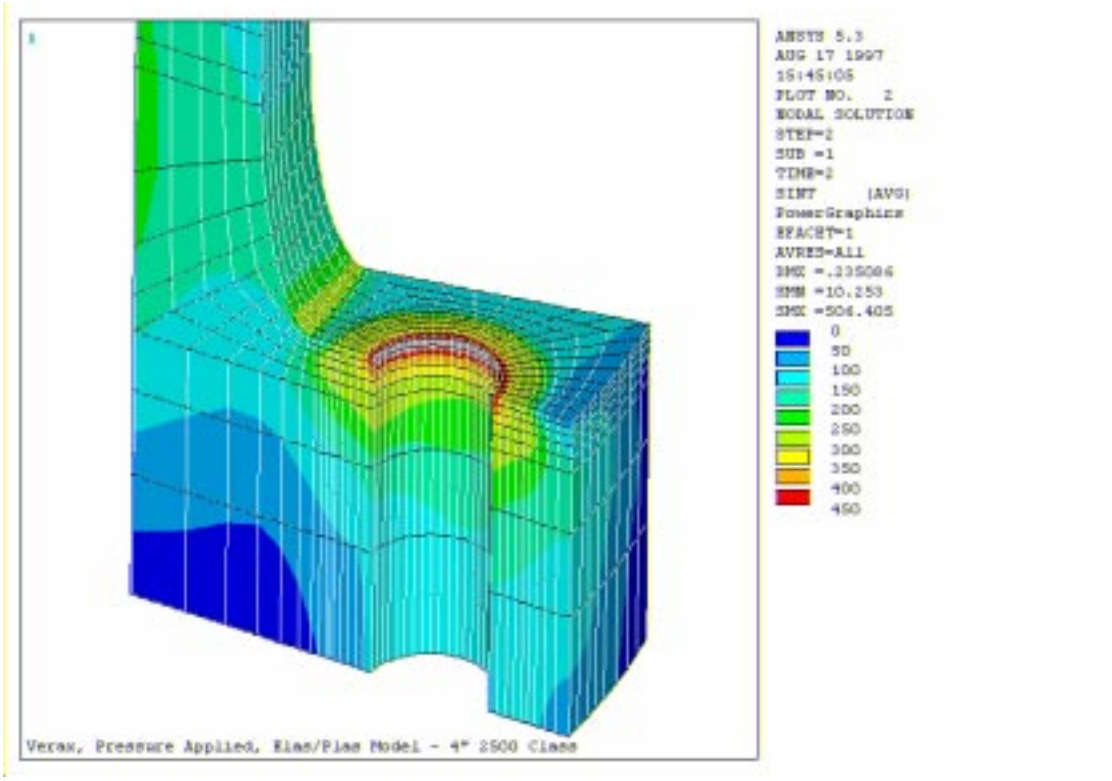

Figure 80: VCF 4" 2500# Class, Flange/Pipe Isometric View - Stress Intensity Plot

11.1.2.2. Eight Inch Nominal Bore

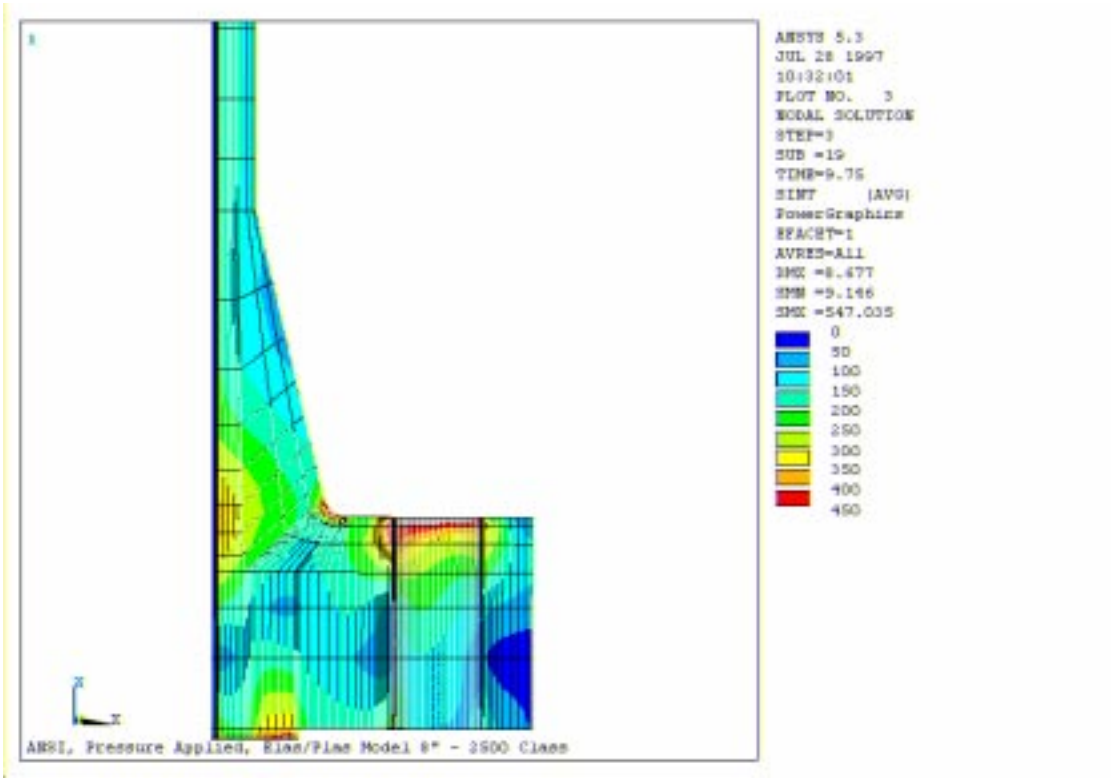

Figure 81: ANSI 8" 2500# Class, Flange/Pipe Cross Section - Stress Intensity Plot

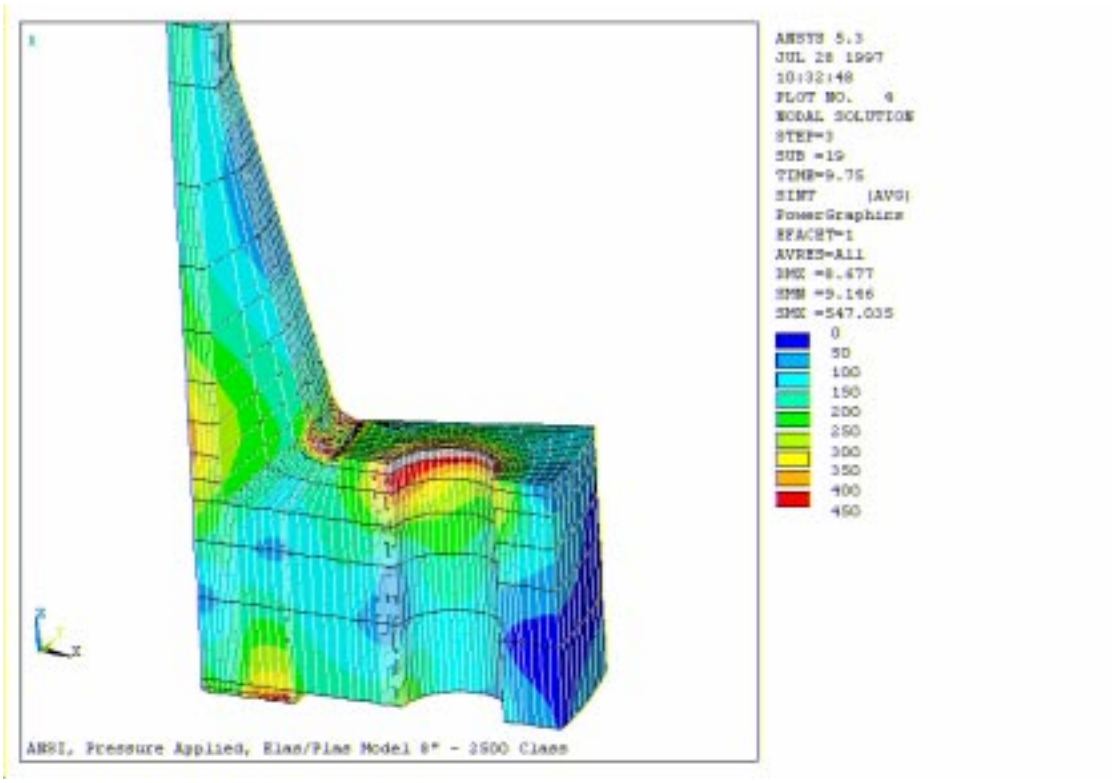

Figure 82: ANSI 8" 2500# Class, Flange/Pipe Isometric View - Stress Intensity Plot

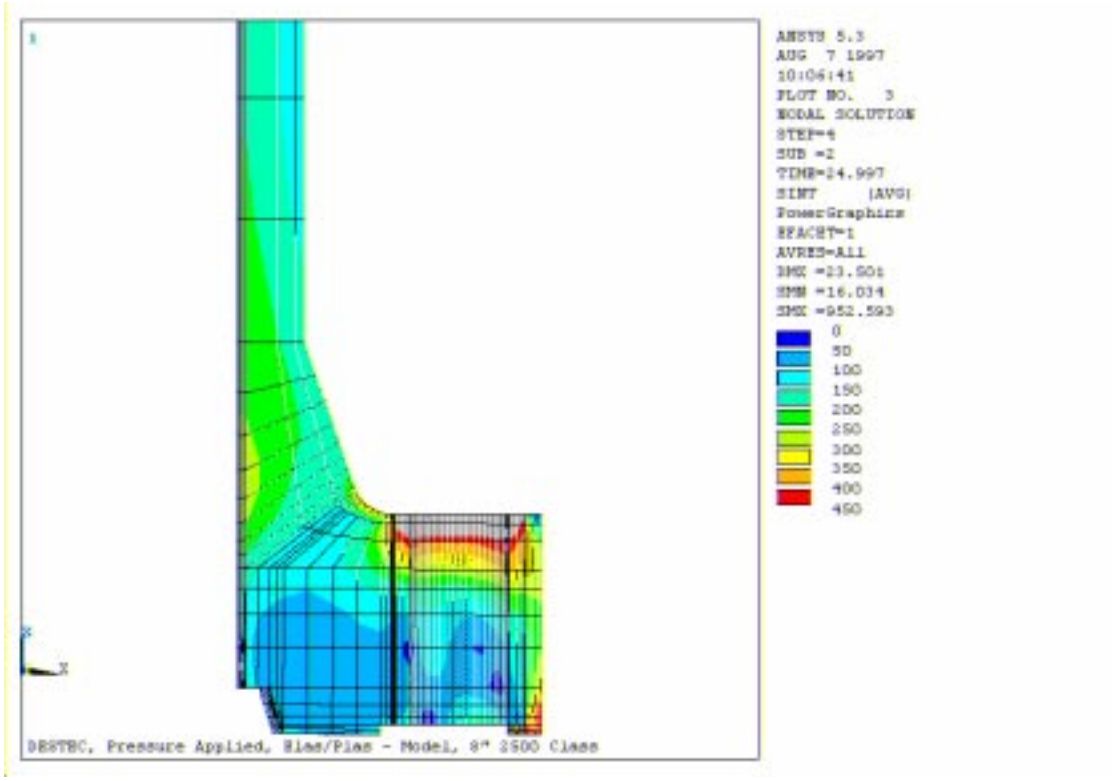

Figure 83: DESFLEX 8" 2500# Class, Flange/Pipe Cross Section - Stress Intensity Plot

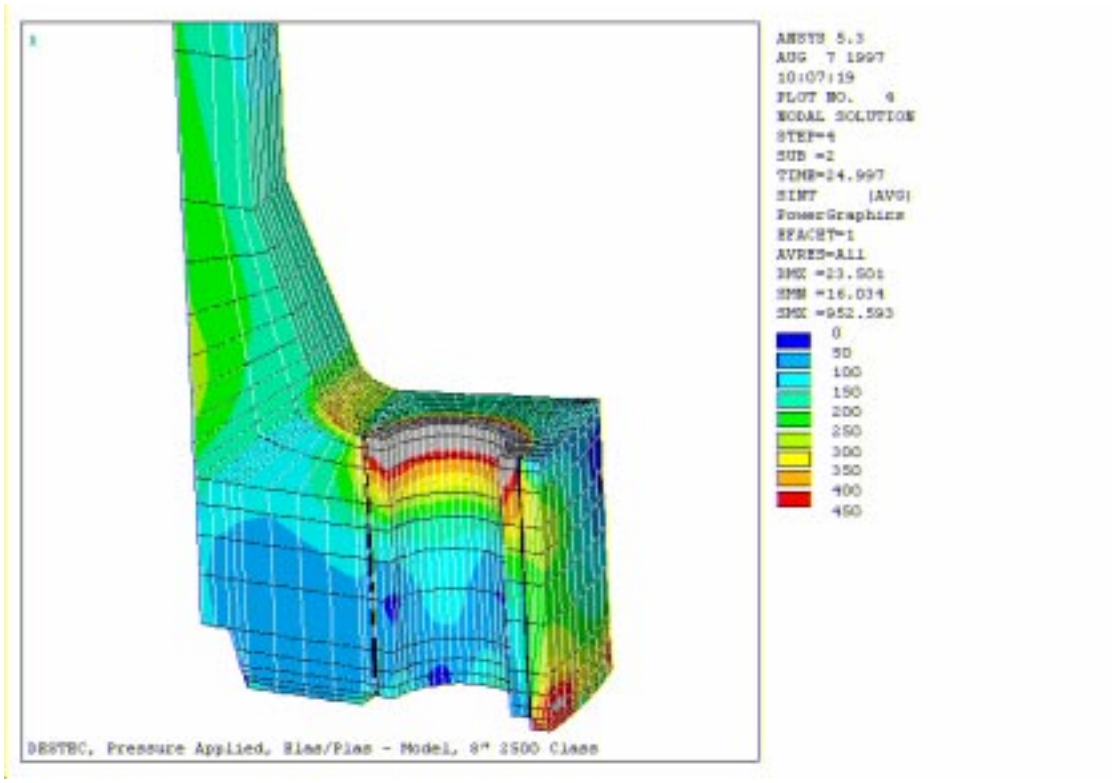

Figure 84: DESFLEX 8" 2500# Class, Flange/Pipe Isometric View - Stress Intensity Plot

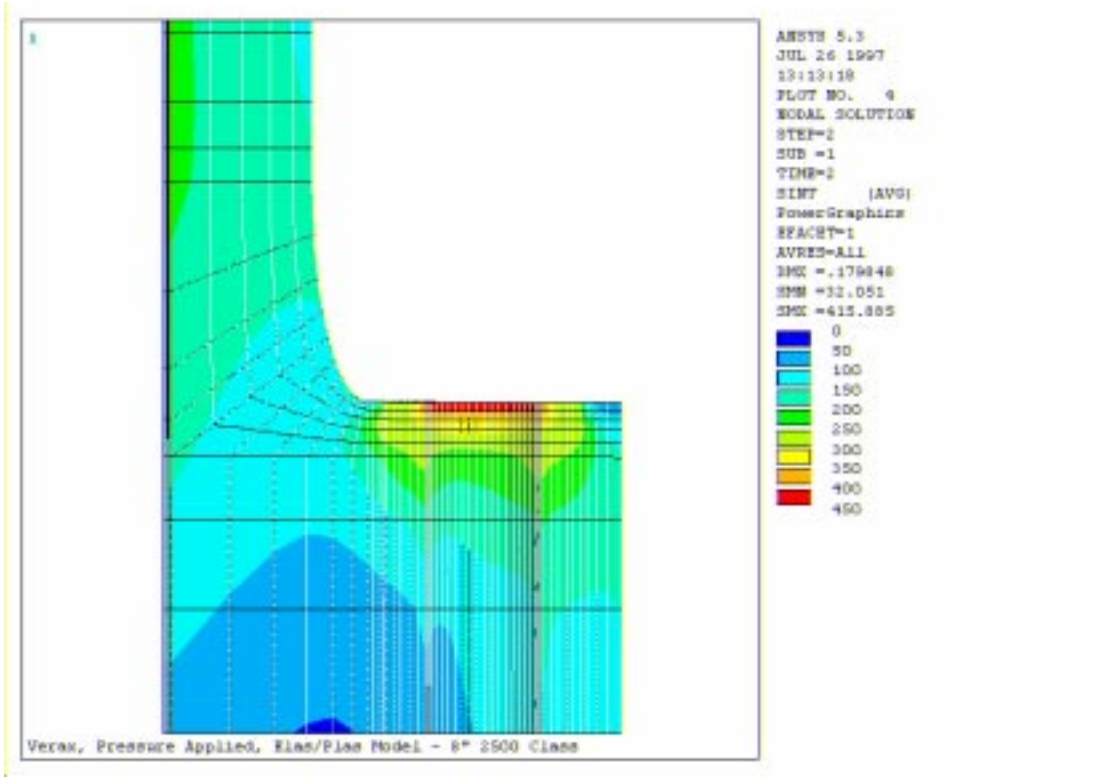

Figure 85: VCF 8" 2500# Class, Flange/Pipe Cross Section - Stress Intensity Plot

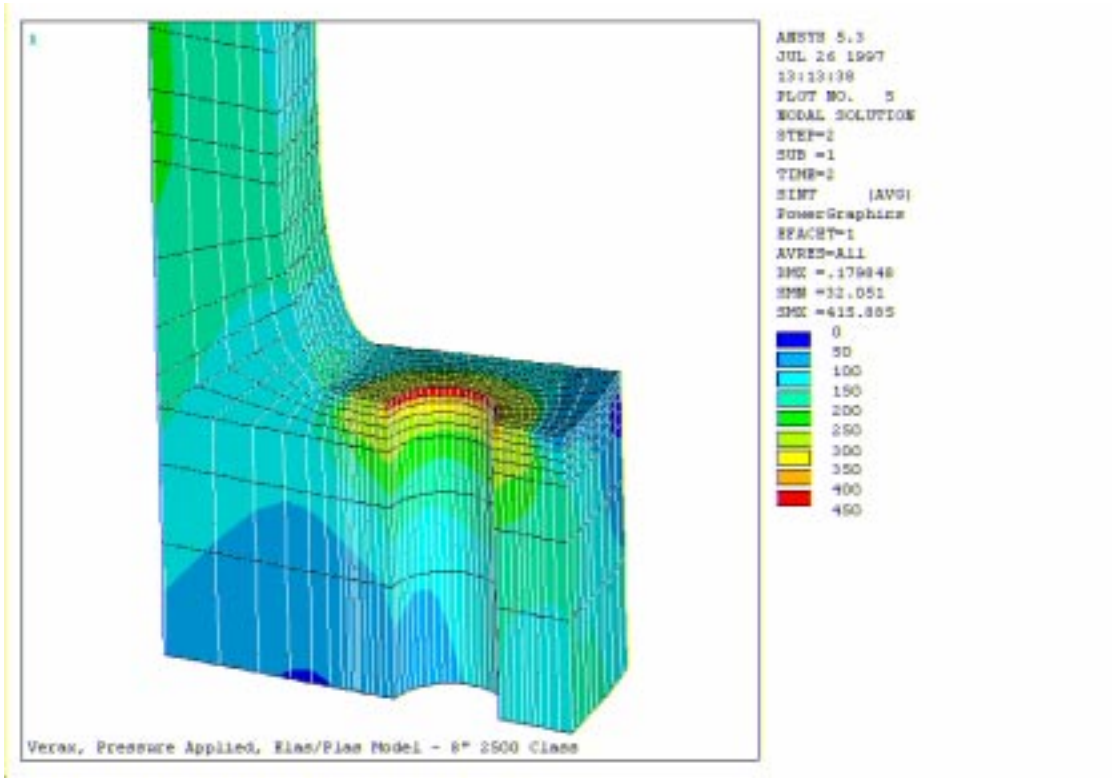

Figure 86: VCF 8" 2500# Class, Flange/Pipe Isometric View - Stress Intensity Plot

11.1.2.3. Twelve Inch Nominal Bore

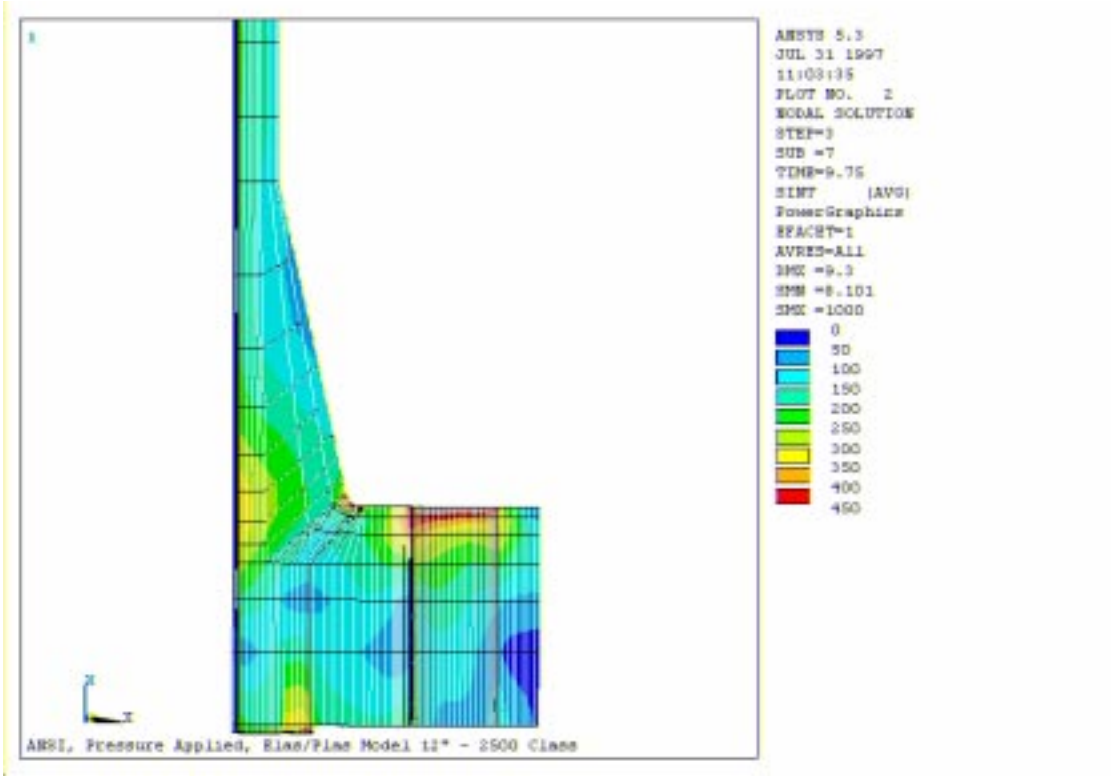

Figure 87: ANSI 12" 2500# Class, Flange/Pipe Cross Section - Stress Intensity Plot

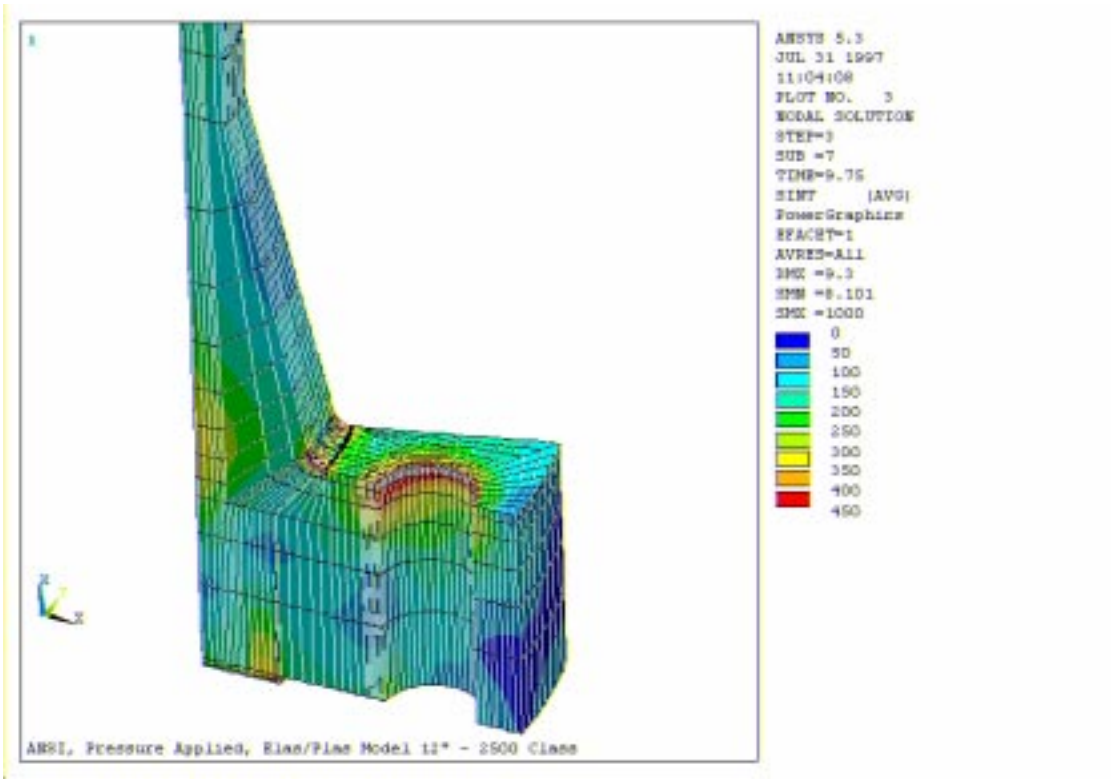

Figure 88: ANSI 12" 2500# Class, Flange/Pipe Isometric View - Stress Intensity Plot

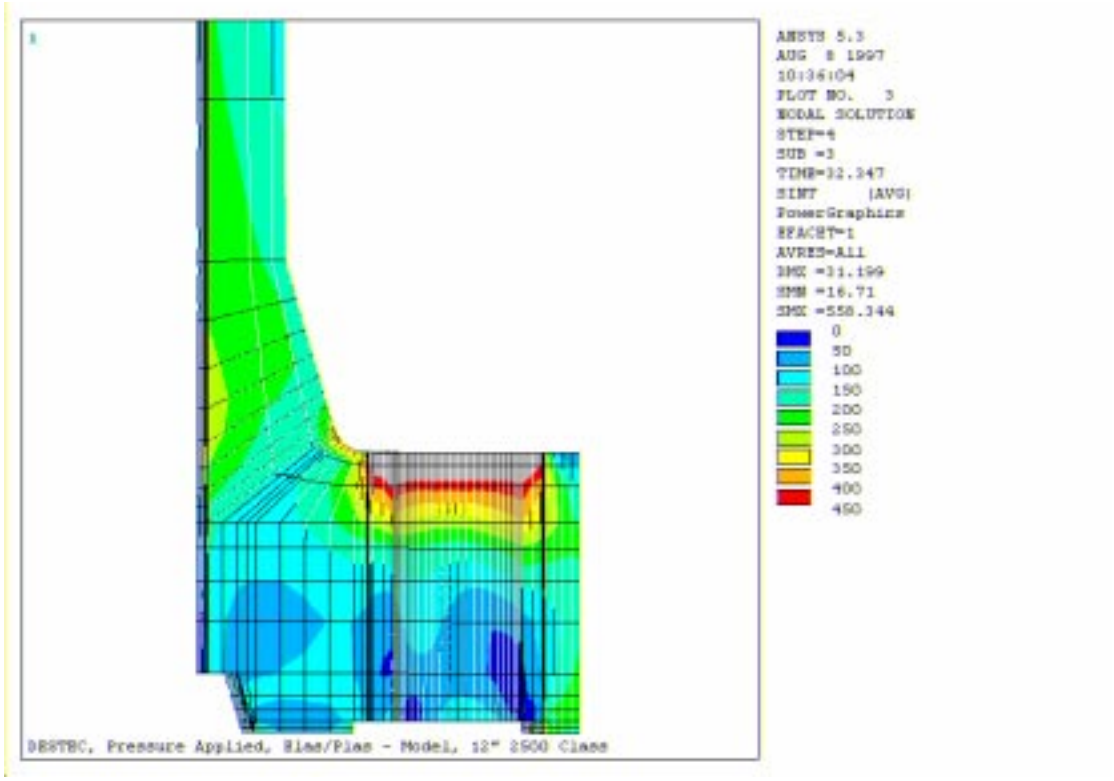

Figure 89: DESFLEX 12" 2500# Class, Flange/Pipe Cross Section - Stress Intensity Plot

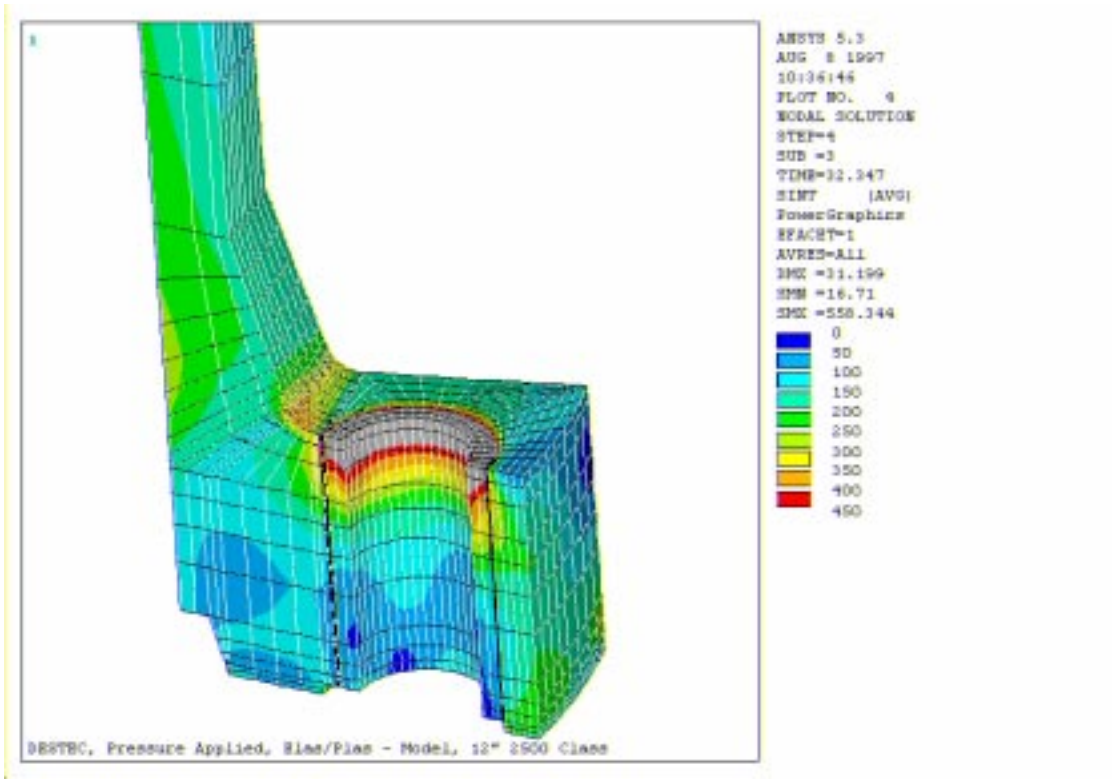

Figure 90: DESFLEX 12" 2500# Class, Flange/Pipe Isometric View - Stress Intensity Plot

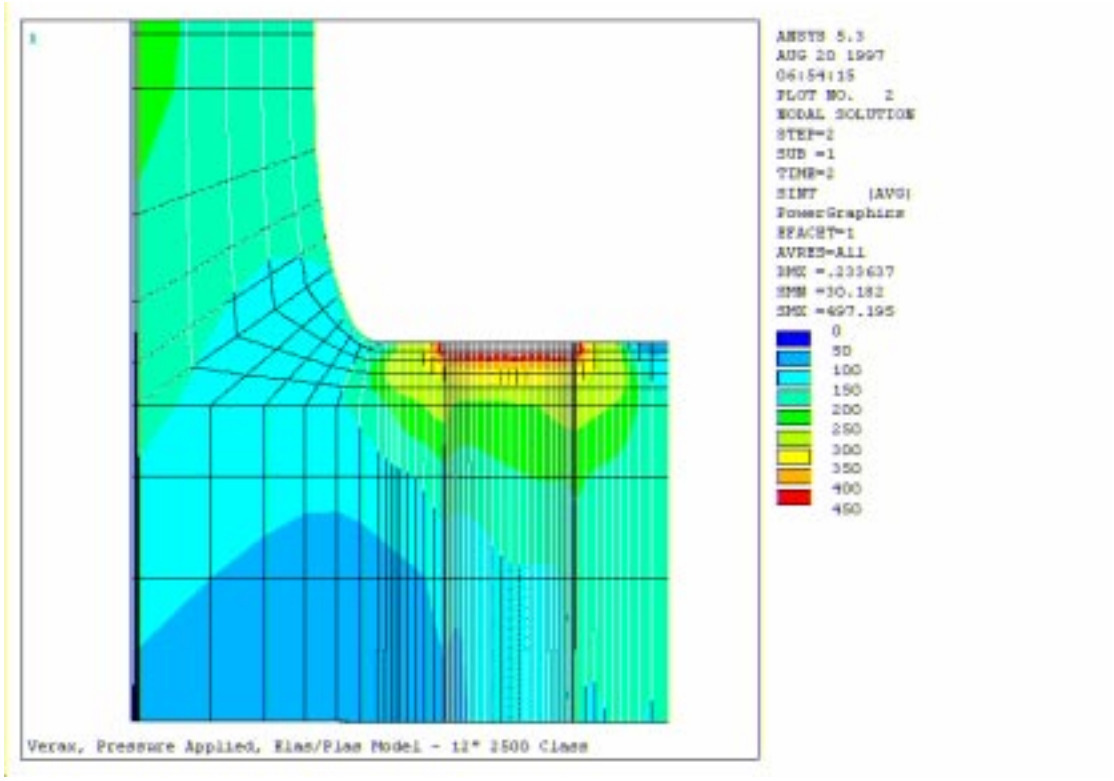

Figure 91: VCF 12" 2500# Class, Flange/Pipe Cross Section - Stress Intensity Plot

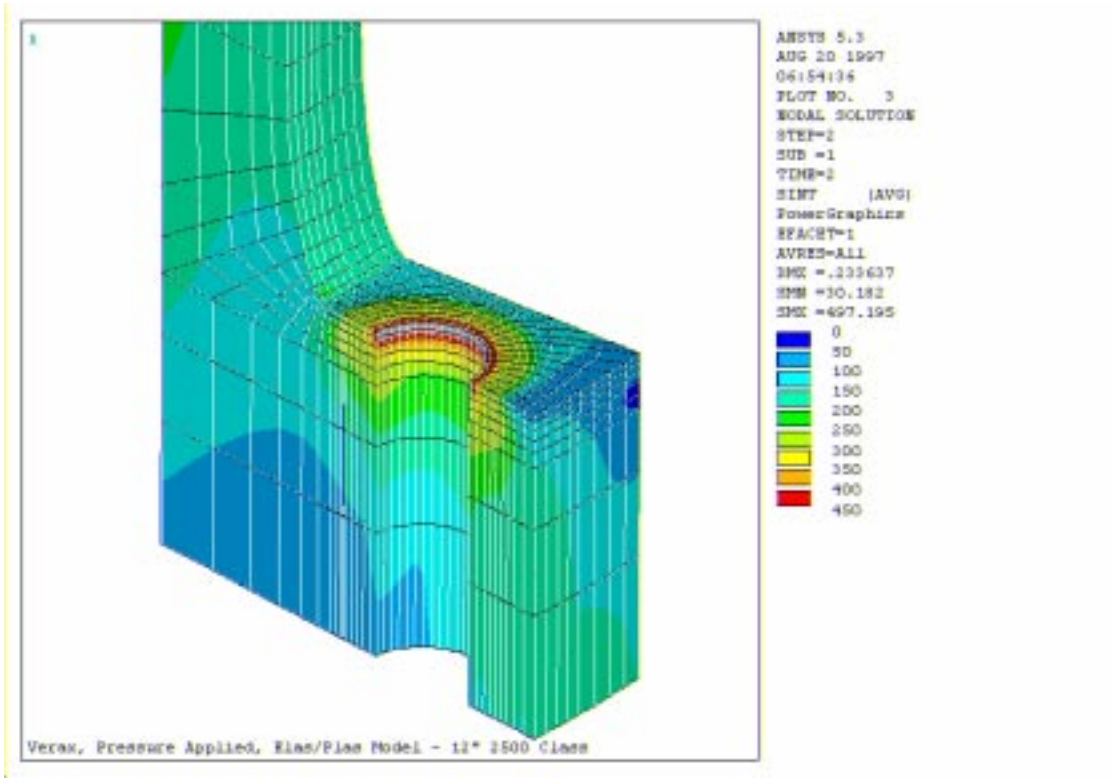

Figure 92: VCF 12" 2500# Class, Flange/Pipe Isometric View - Stress Intensity Plot

11.2. Bolt and Washer

11.2.1. 1500# Class

11.2.1.1. Four Inch Nominal Bore

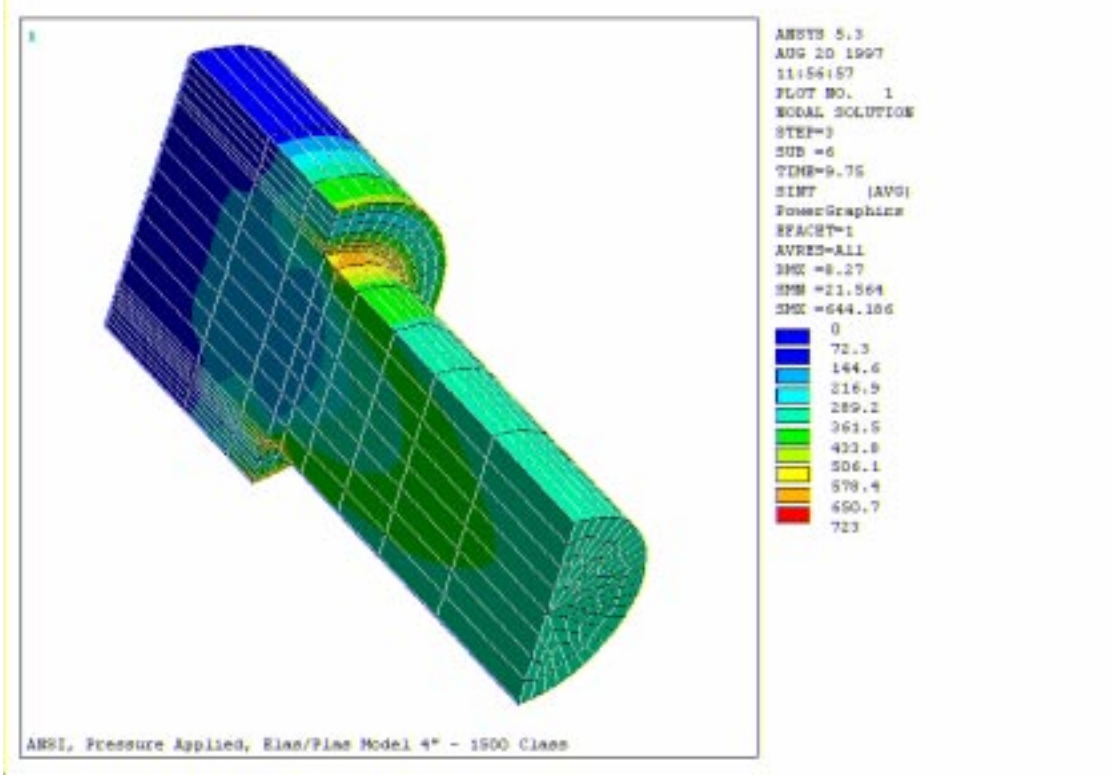

Figure 93: ANSI 4" 1500# Class, Bolt Only - Stress Intensity Plot

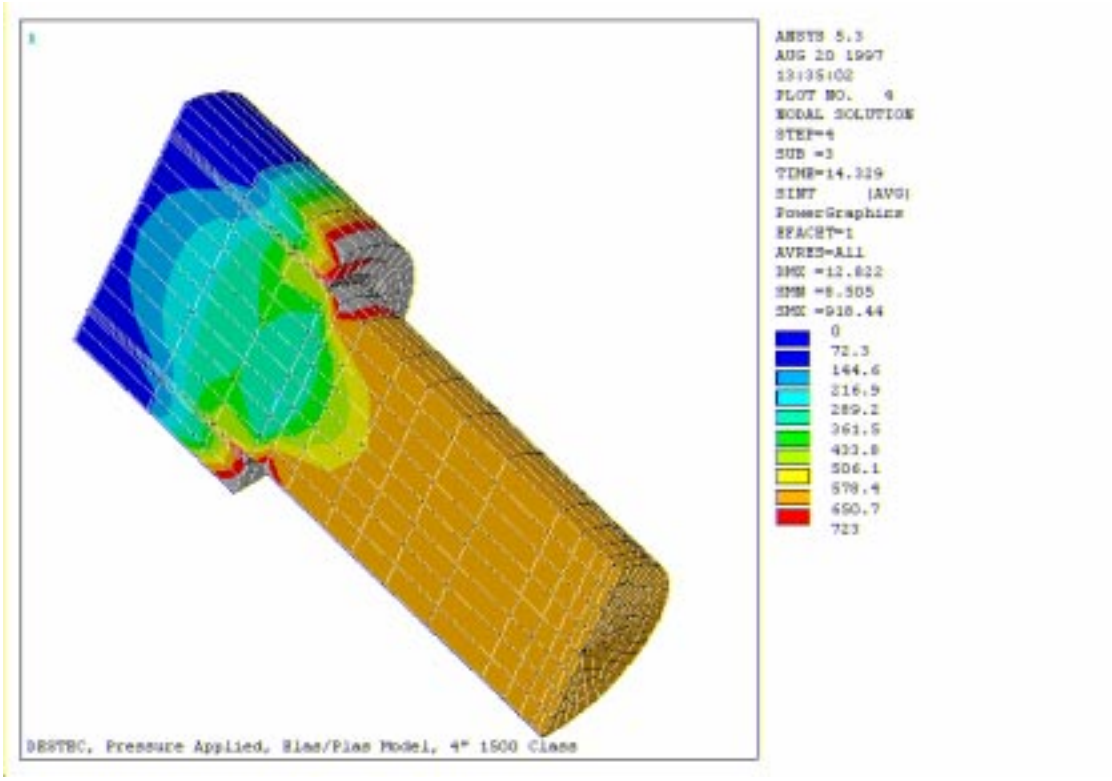

Figure 94: DESFLEX 4" 1500# Class, Bolt Only - Stress Intensity Plot

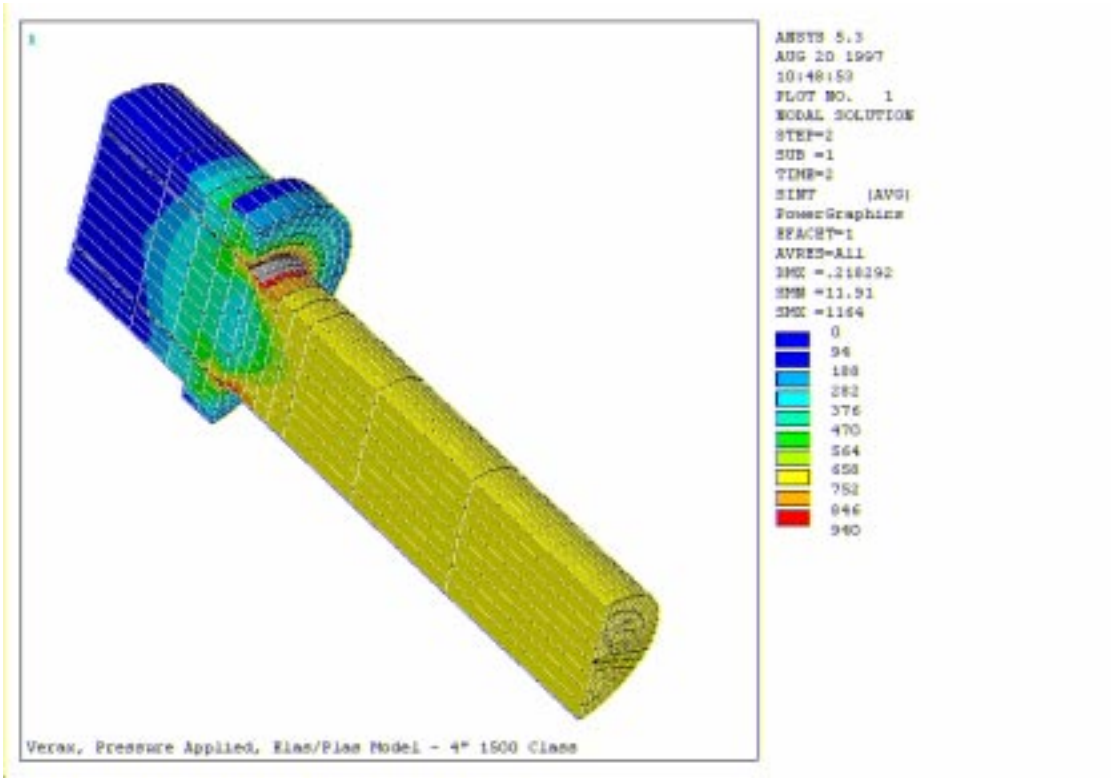

Figure 95: VCF 4" 1500# Class, Bolt and Washer - Stress Intensity Plot

11.2.1.2. Eight Inch Nominal Bore

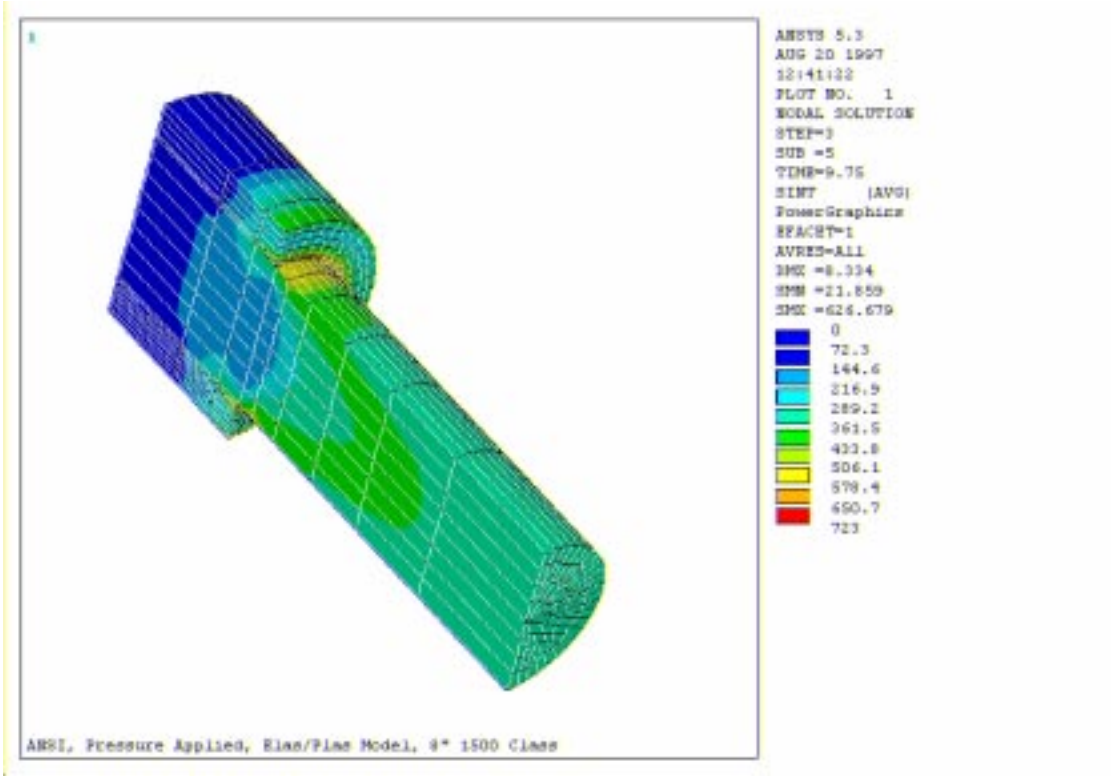

Figure 96: ANSI 8" 1500# Class, Bolt Only - Stress Intensity Plot

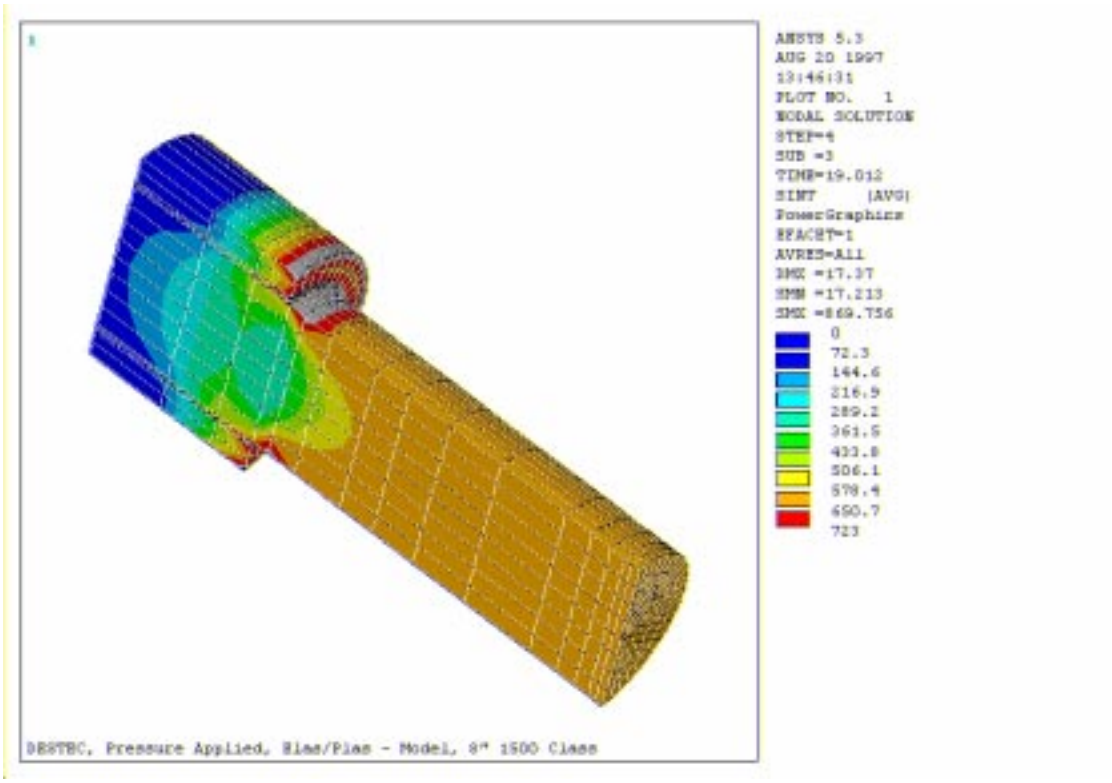

Figure 97: DESFLEX 8" 1500# Class, Bolt Only - Stress Intensity Plot

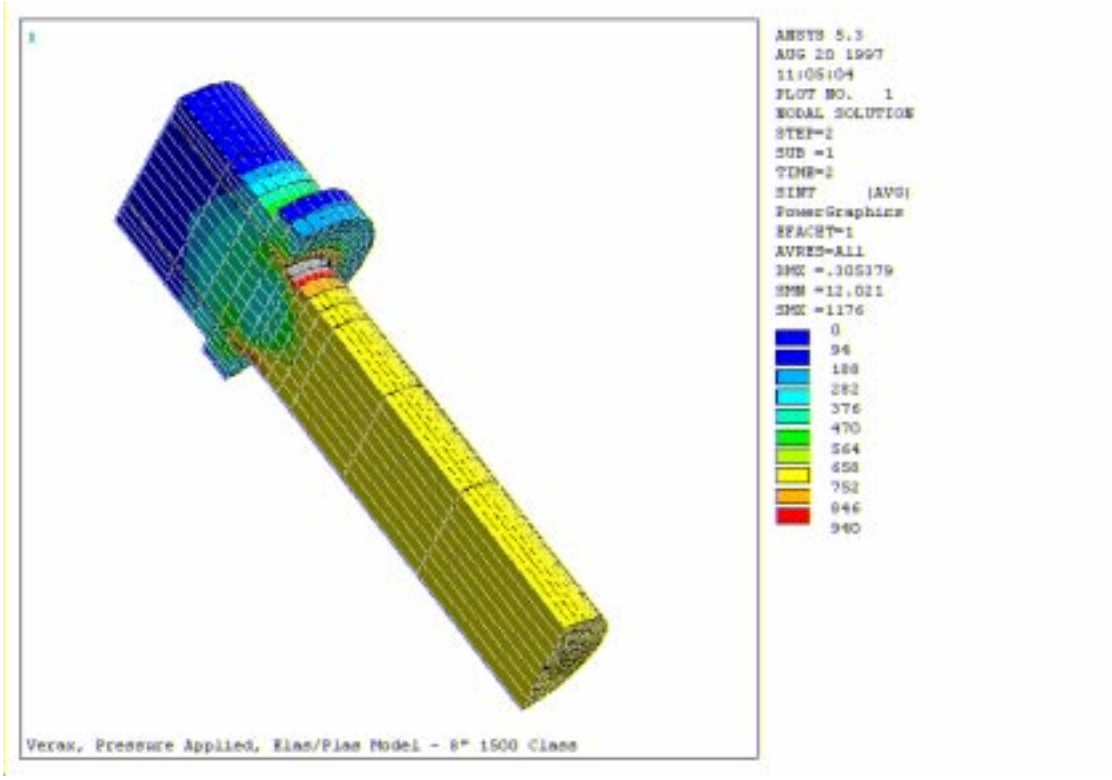

Figure 98: VCF 8" 1500# Class, Bolt and Washer - Stress Intensity Plot

11.2.1.3. Twelve Inch Nominal Bore

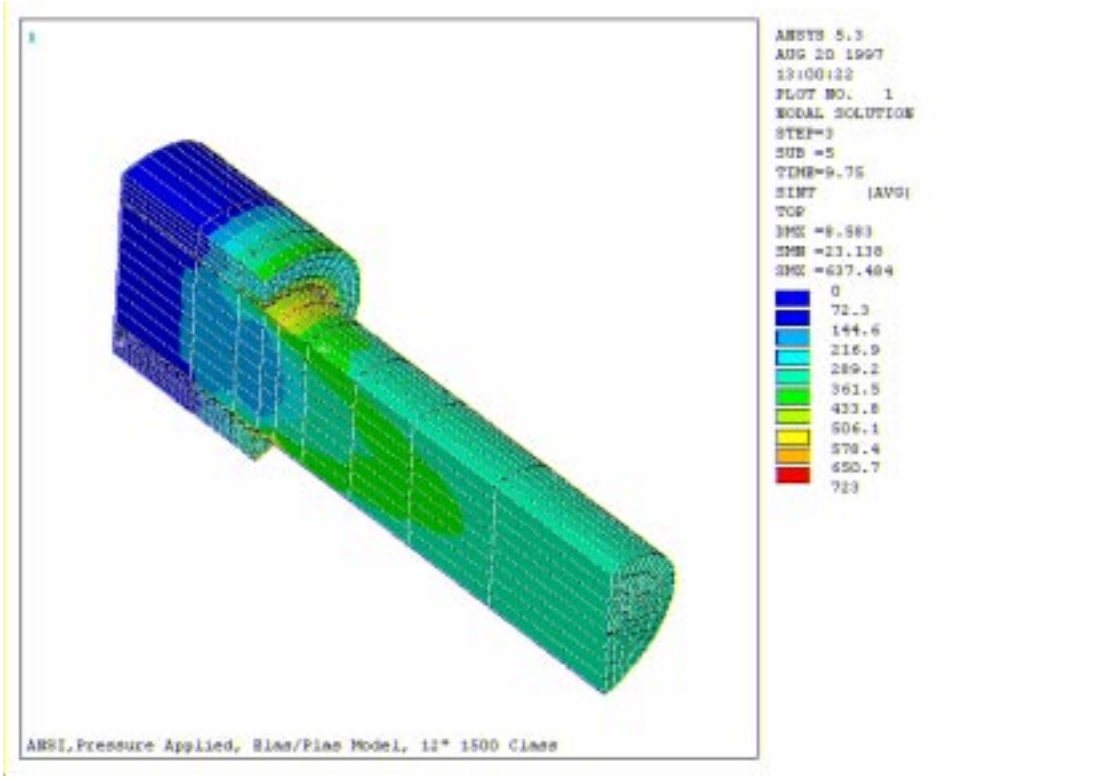

Figure 99: ANSI 12" 1500# Class, Bolt Only - Stress Intensity Plot

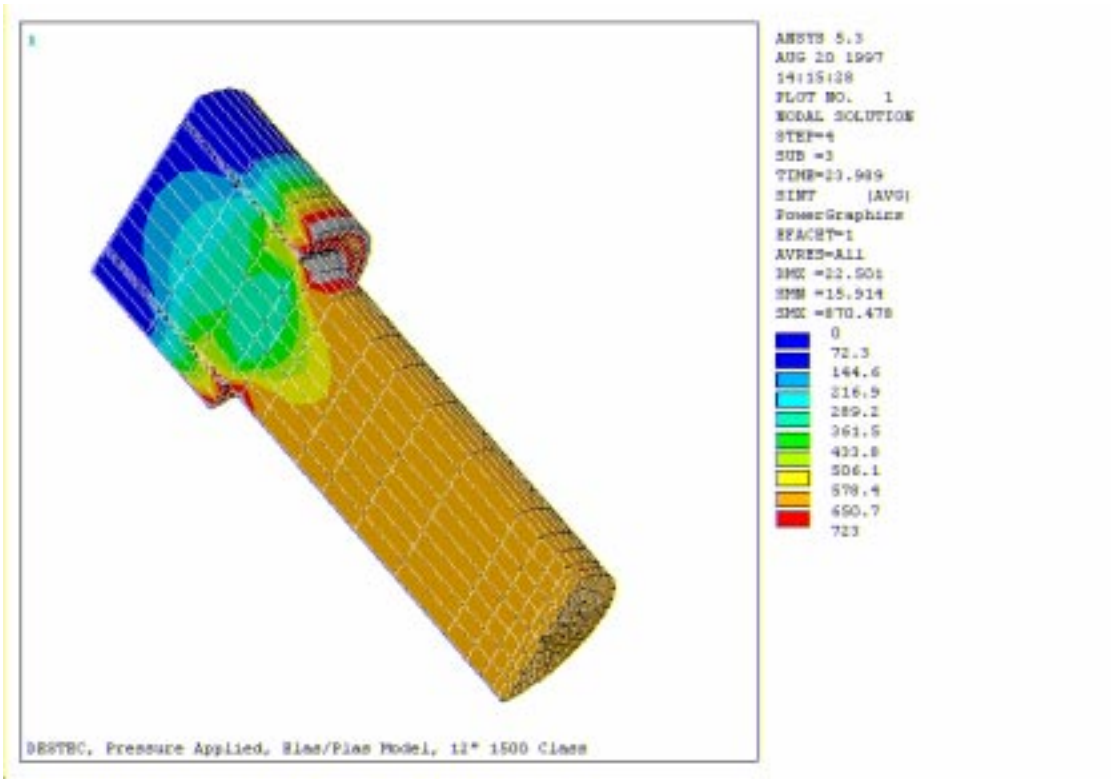

Figure 100: DESFLEX 12" 1500# Class, Bolt Only - Stress Intensity Plot

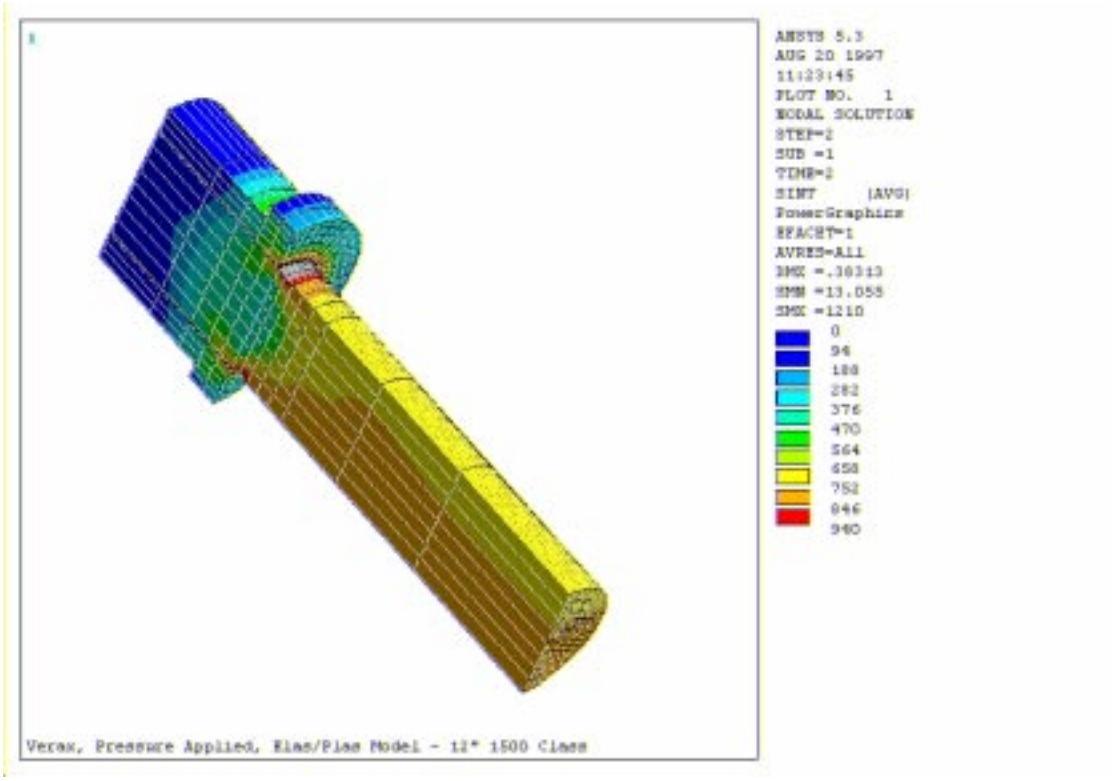

Figure 101: VCF 12" 1500# Class, Bolt and Washer - Stress Intensity Plot

11.2.2. 2500# Class

11.2.2.1. Four Inch Nominal Bore

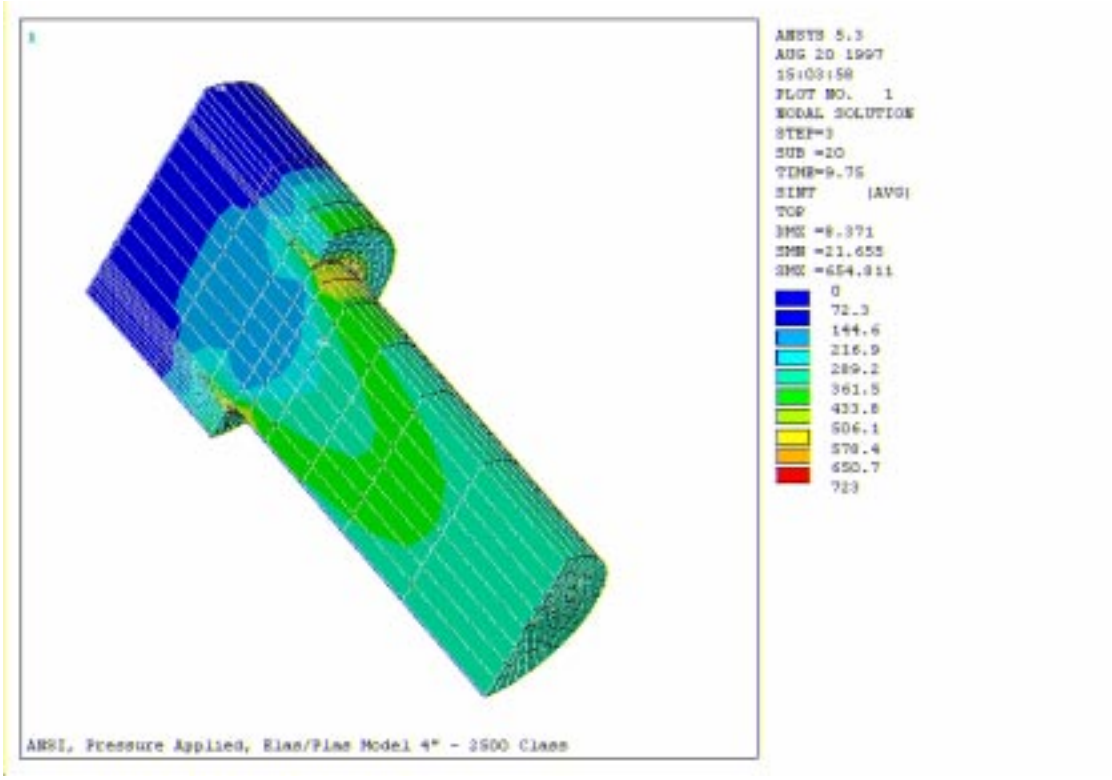

Figure 102: ANSI 4" 2500# Class, Bolt Only - Stress Intensity Plot

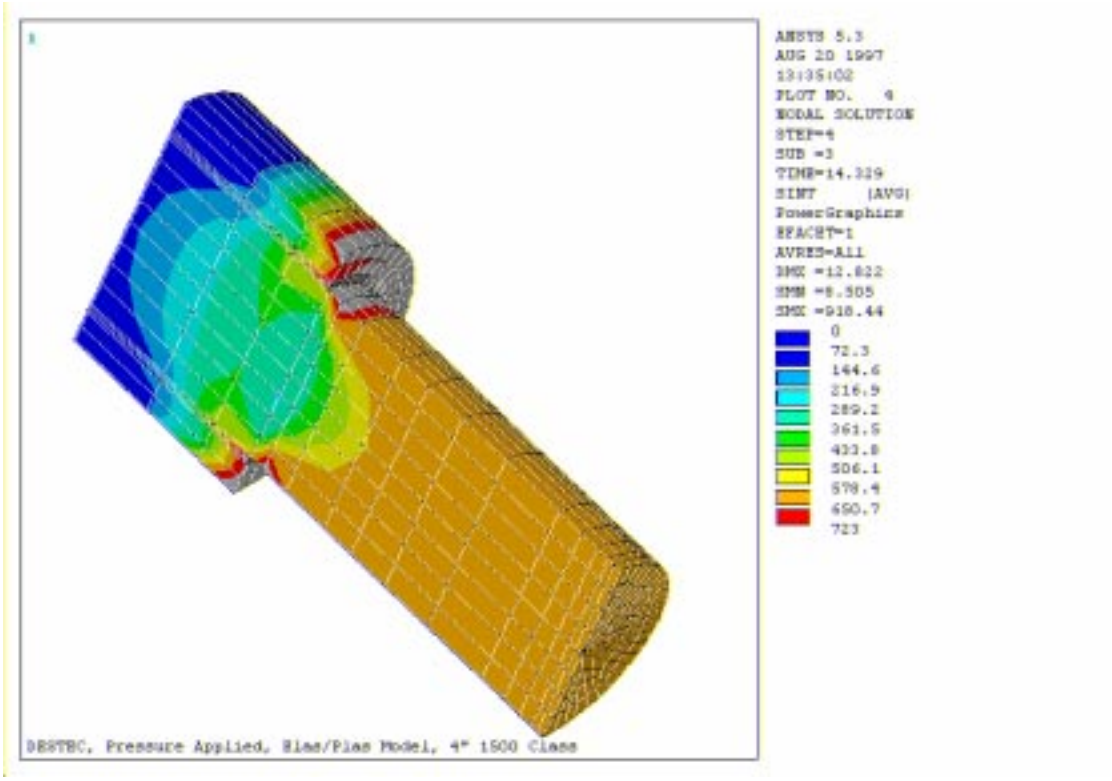

Figure 103: DESFLEX 4" 2500# Class, Bolt Only - Stress Intensity Plot

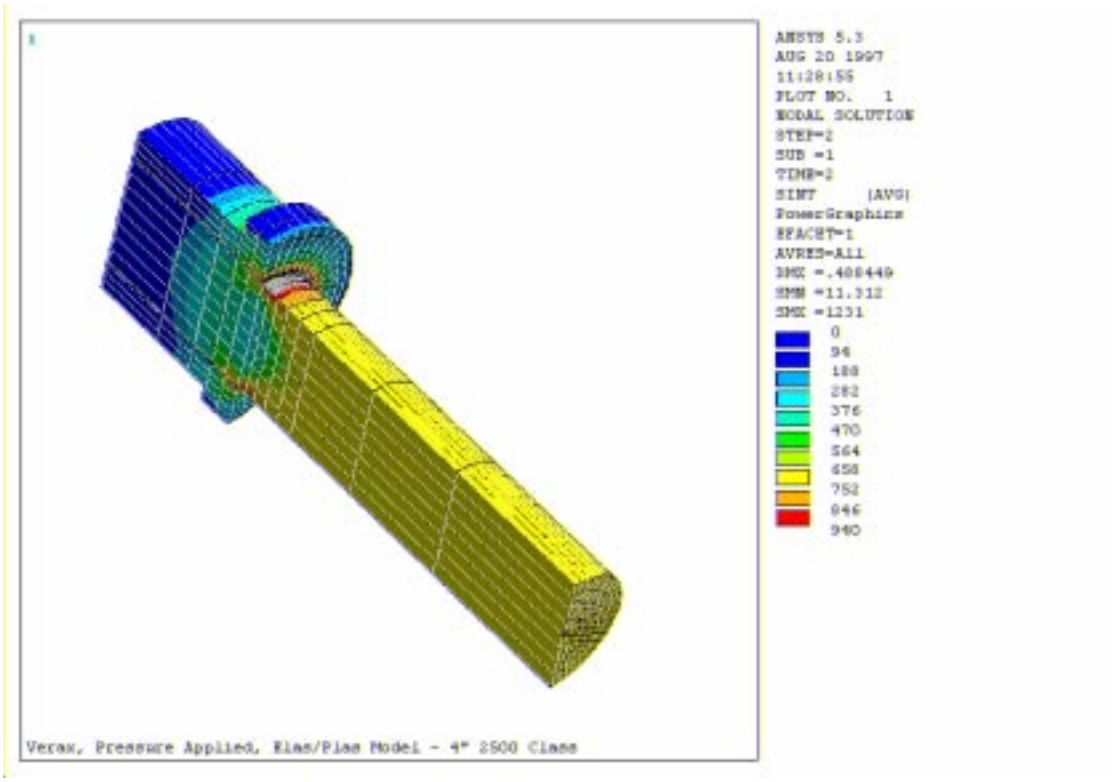

Figure 104: VCF 4" 2500# Class, Bolt and Washer - Stress Intensity Plot

11.2.2.2. Eight Inch Nominal Bore

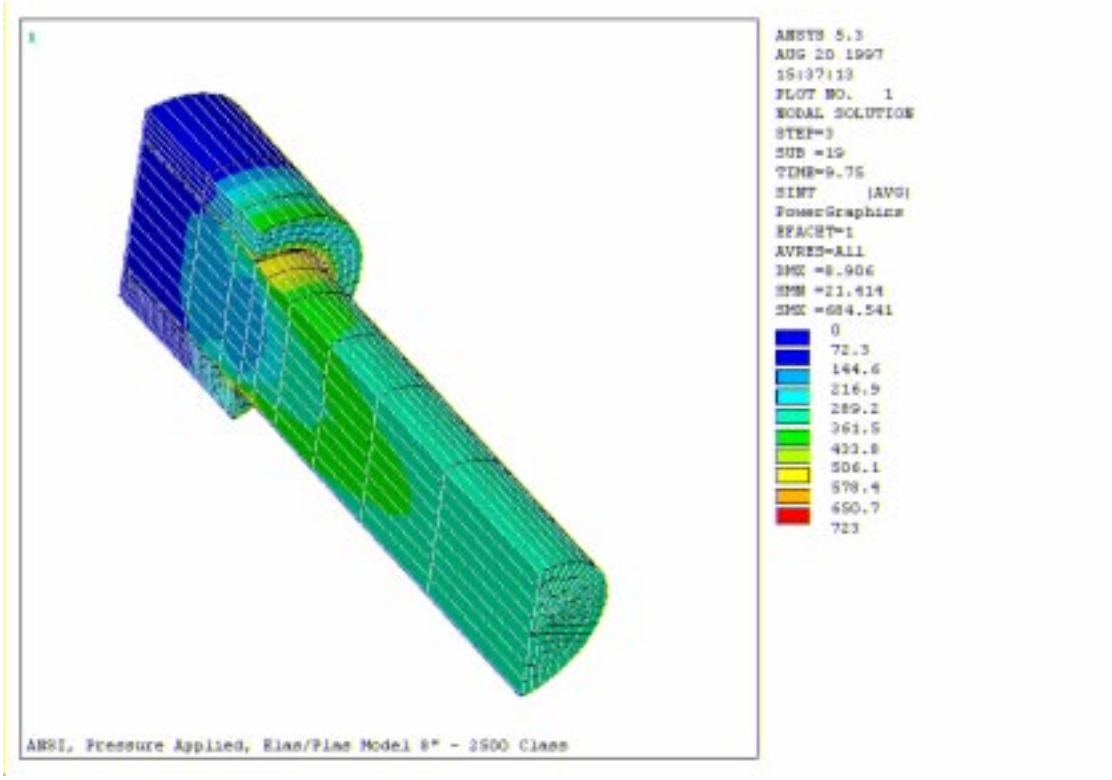

Figure 105: ANSI 8" 2500# Class, Bolt Only - Stress Intensity Plot

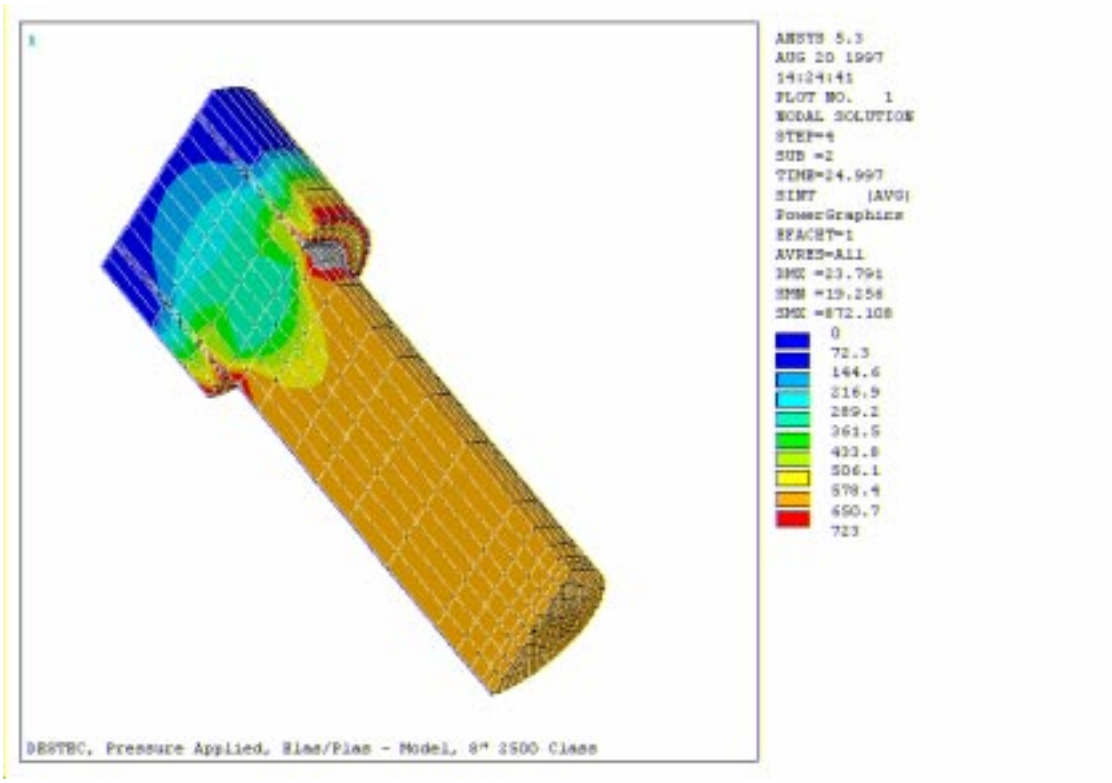

Figure 106: DESFLEX 8" 2500# Class, Bolt Only - Stress Intensity Plot

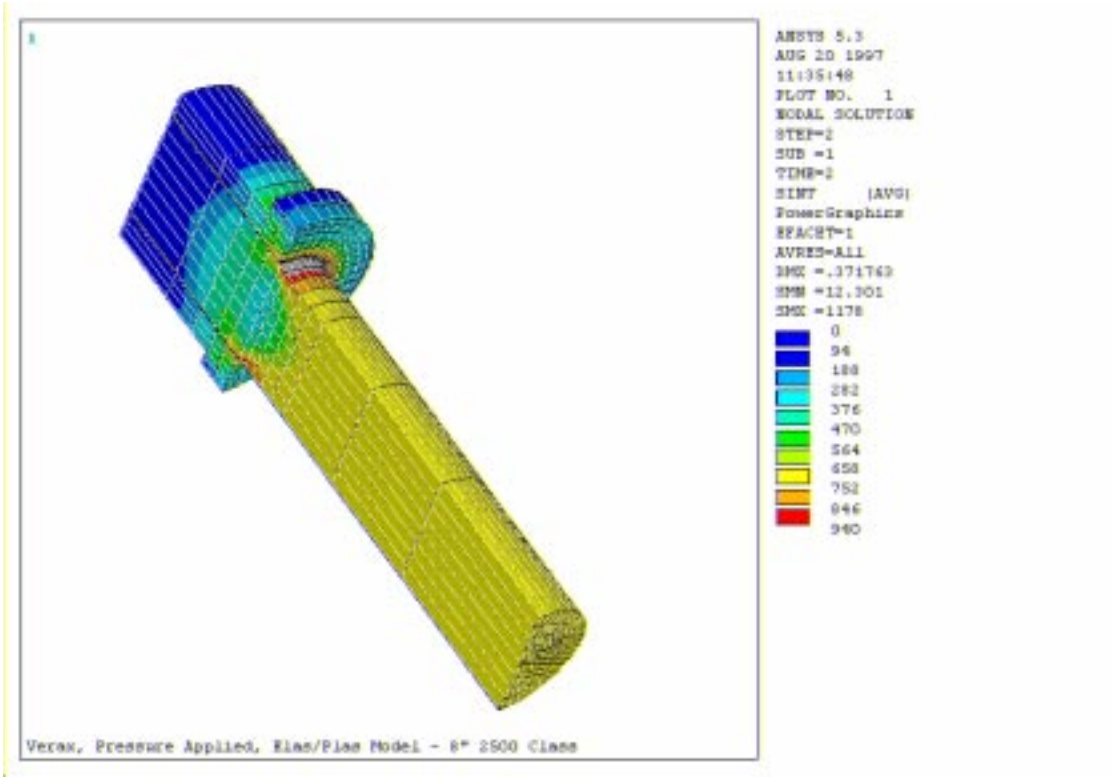

Figure 107: VCF 8" 2500# Class, Bolt and Washer - Stress Intensity Plot

11.2.2.3. Twelve Inch Nominal Bore

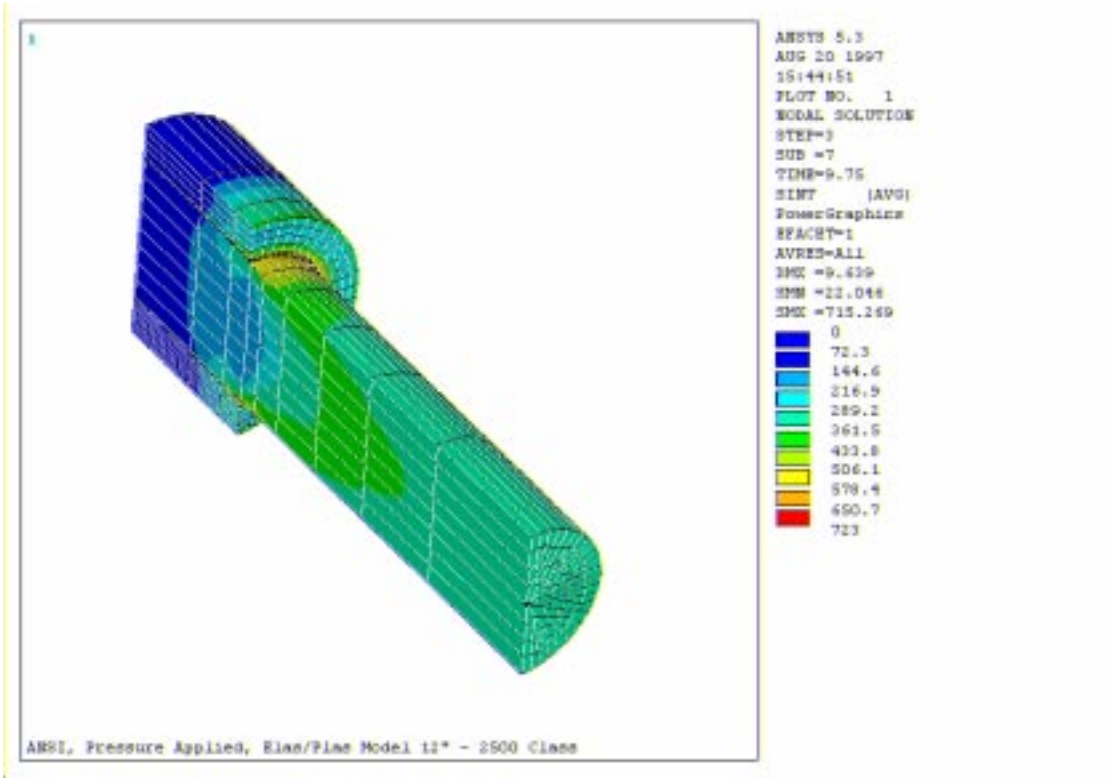

Figure 108: ANSI 12" 2500# Class, Bolt Only - Stress Intensity Plot

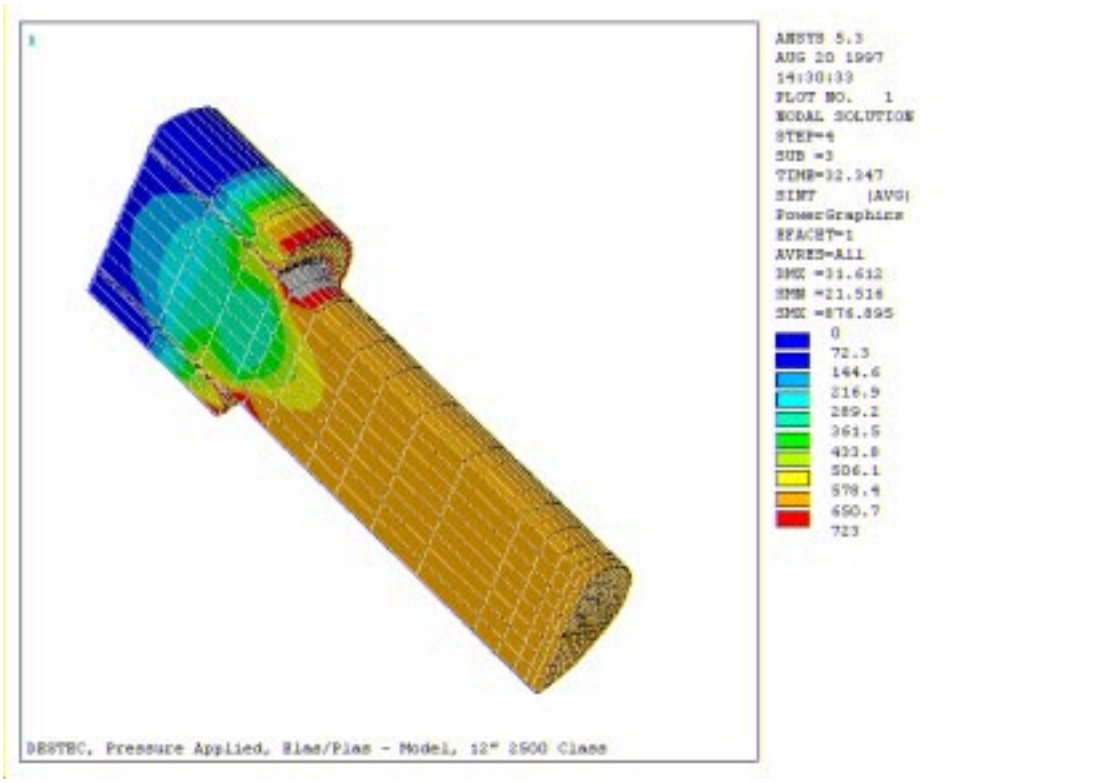

Figure 109: DESFLEX 12" 2500# Class, Bolt Only - Stress Intensity Plot

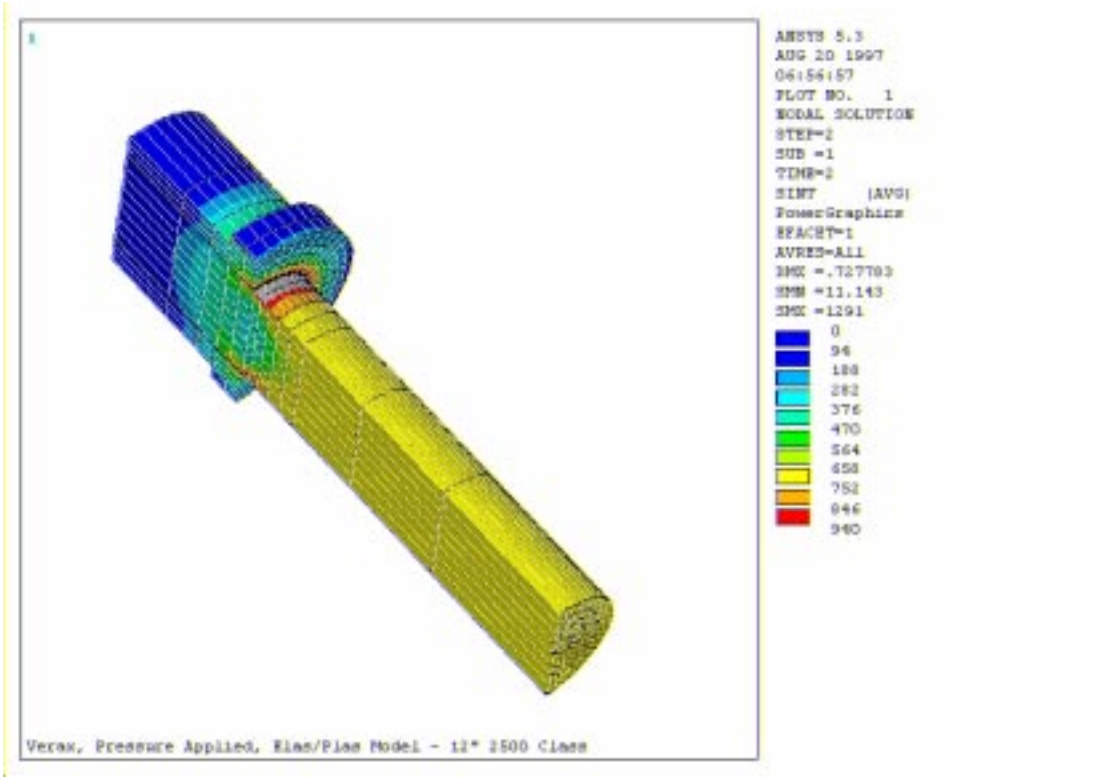

Figure 110: VCF 12" 2500# Class, Bolt and Washer - Stress Intensity Plot

11.3. Contact Pressure

11.3.1. 1500# Class

11.3.1.1. Four Inch Nominal Bore

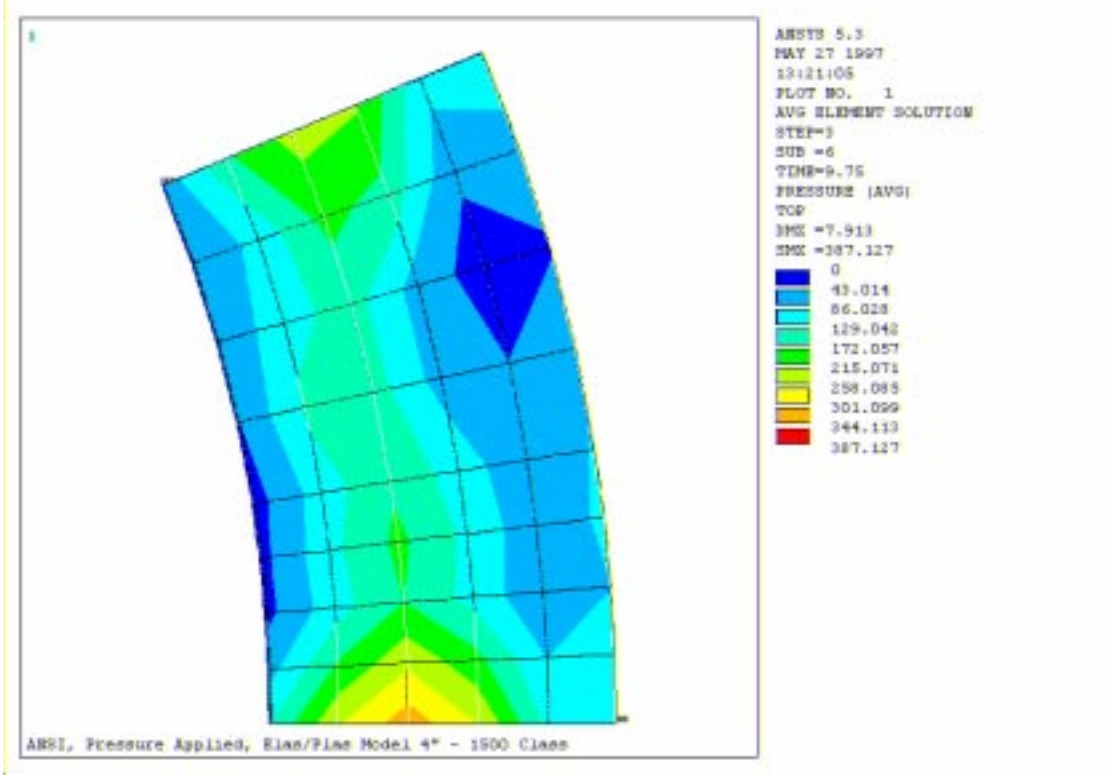

Figure 111: ANSI 4" 1500# Class - Contact Pressure Plot

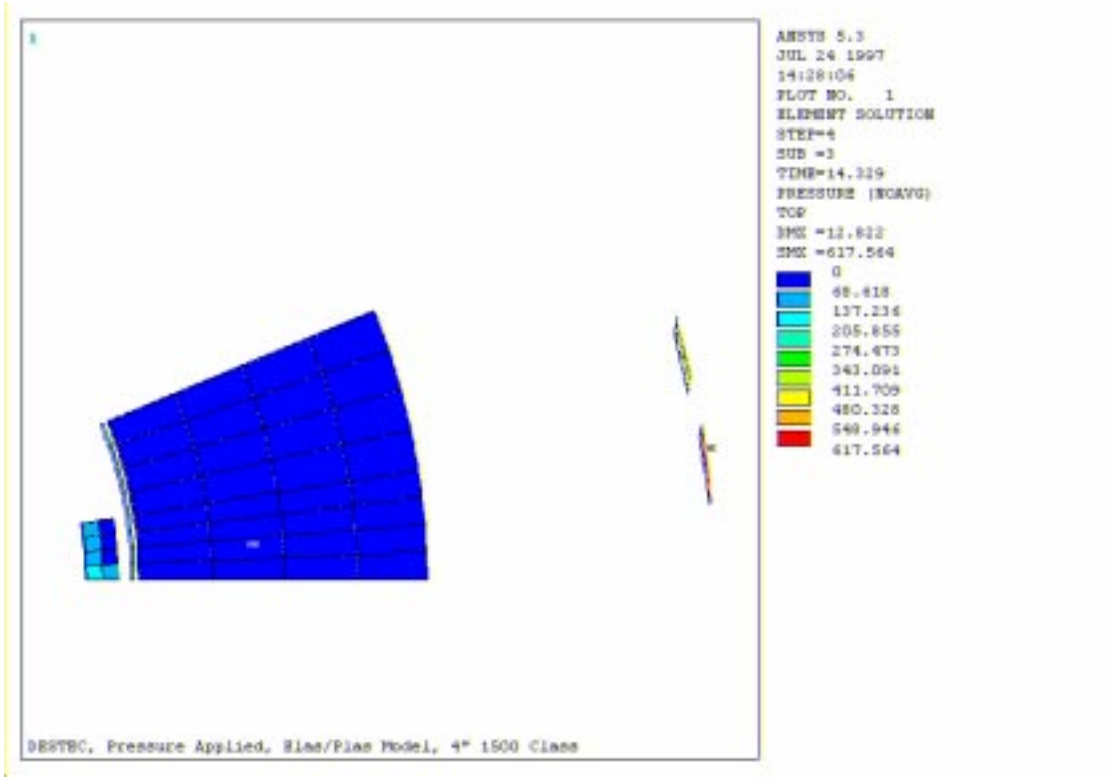

Figure 112: DESFLEX 4" 1500# Class - Contact Pressure Plot

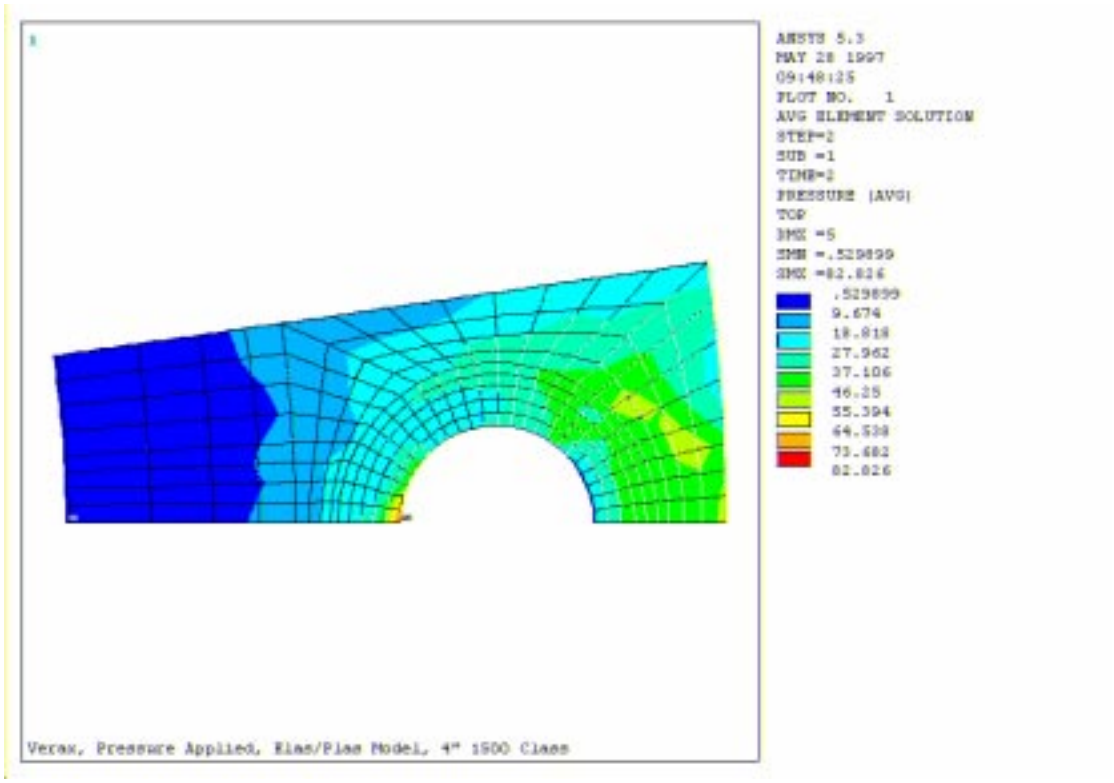

Figure 113: VCF 4" 1500# Class - Contact Pressure Plot

11.3.1.2. Eight Inch Nominal Bore

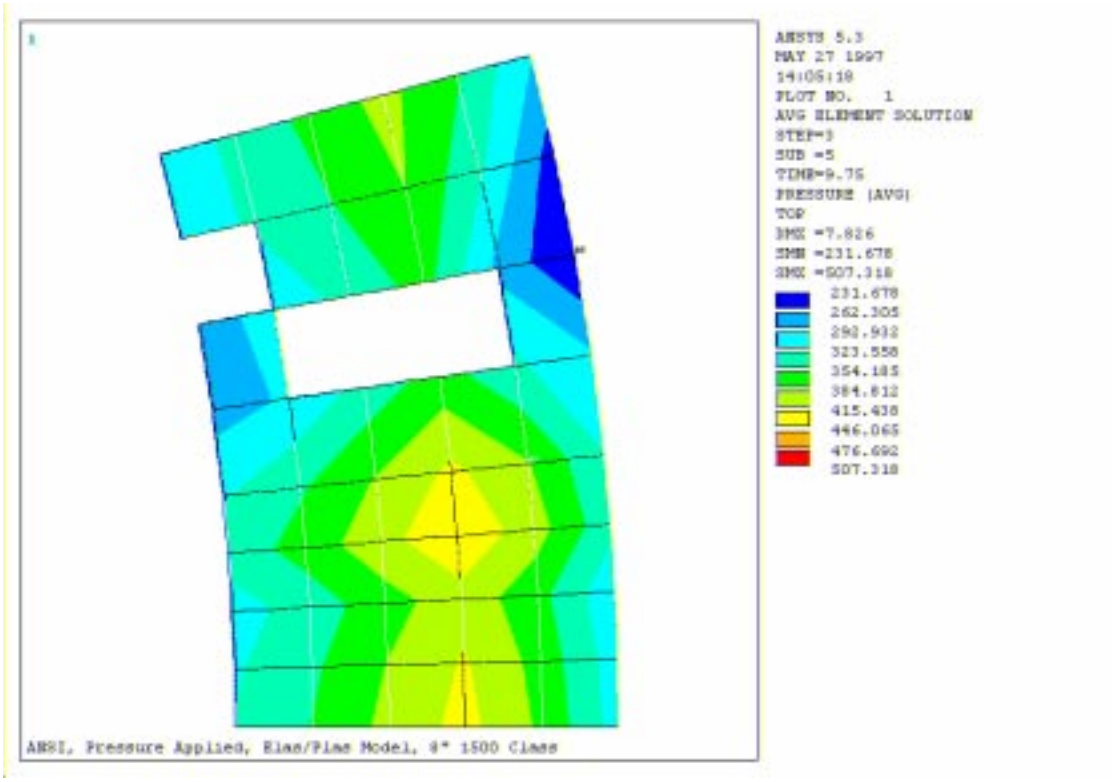

Figure 114: ANSI 8" 1500# Class - Contact Pressure Plot

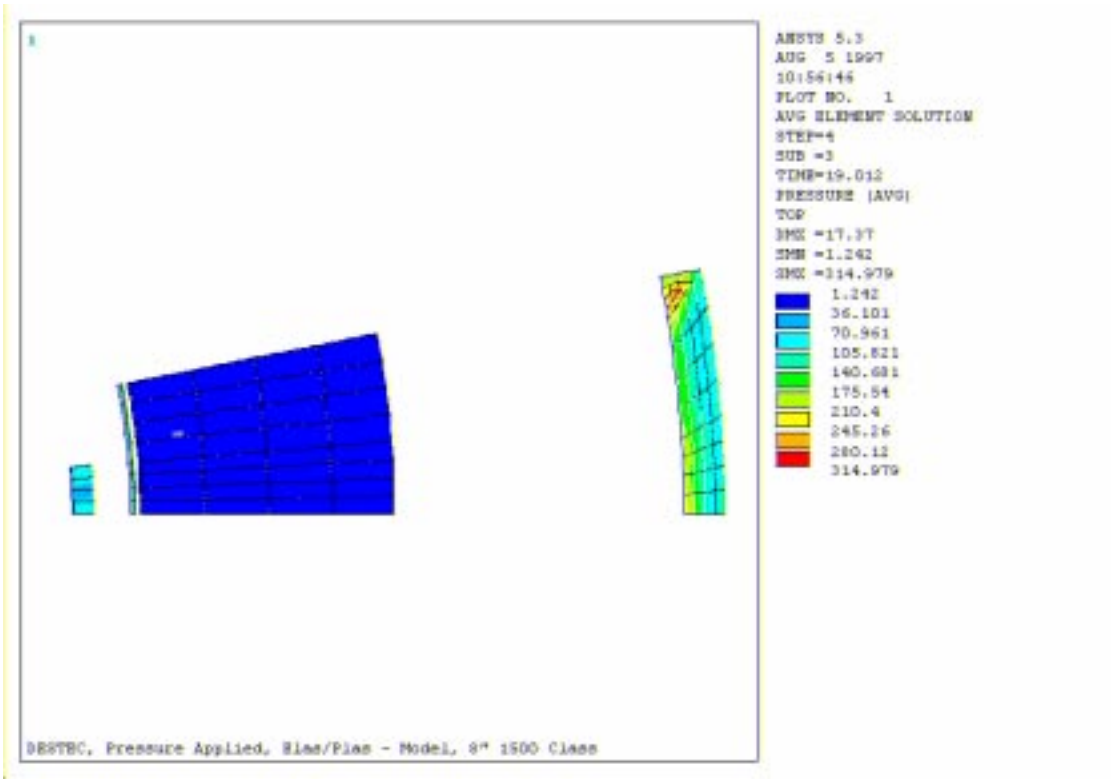

Figure 115: DESFLEX 8" 1500# Class - Contact Pressure Plot

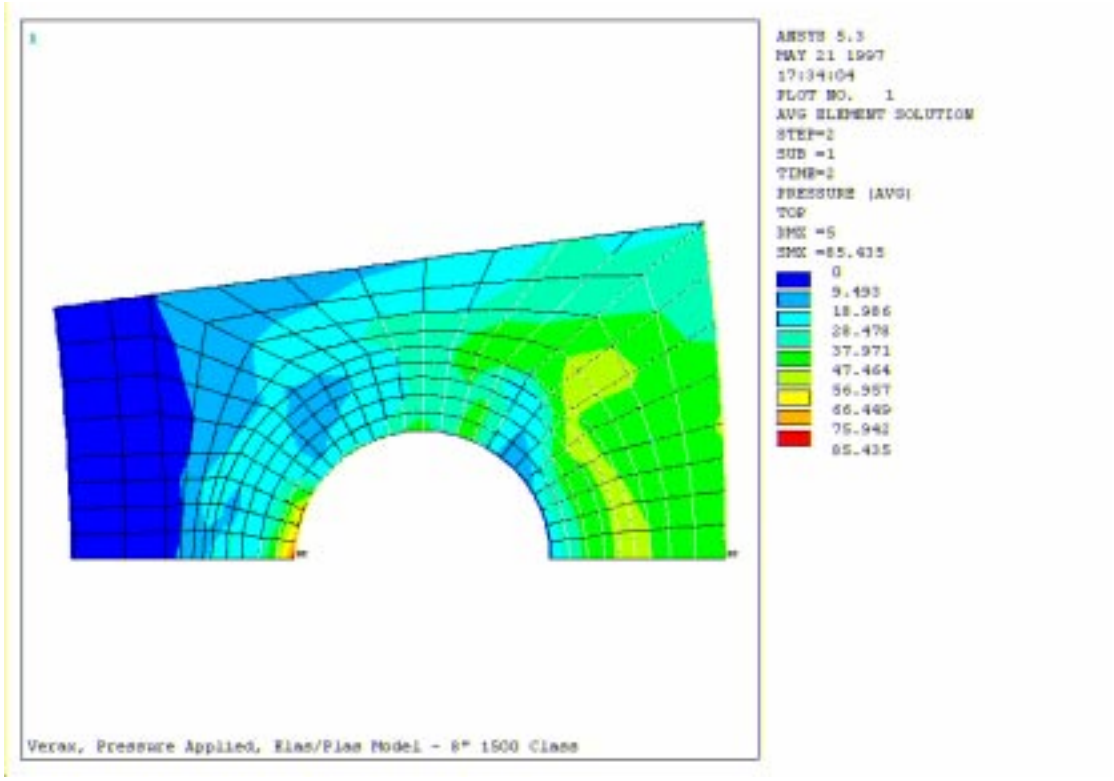

Figure 116: VCF 8" 1500# Class - Contact Pressure Plot

11.3.1.3. Twelve Inch Nominal Bore

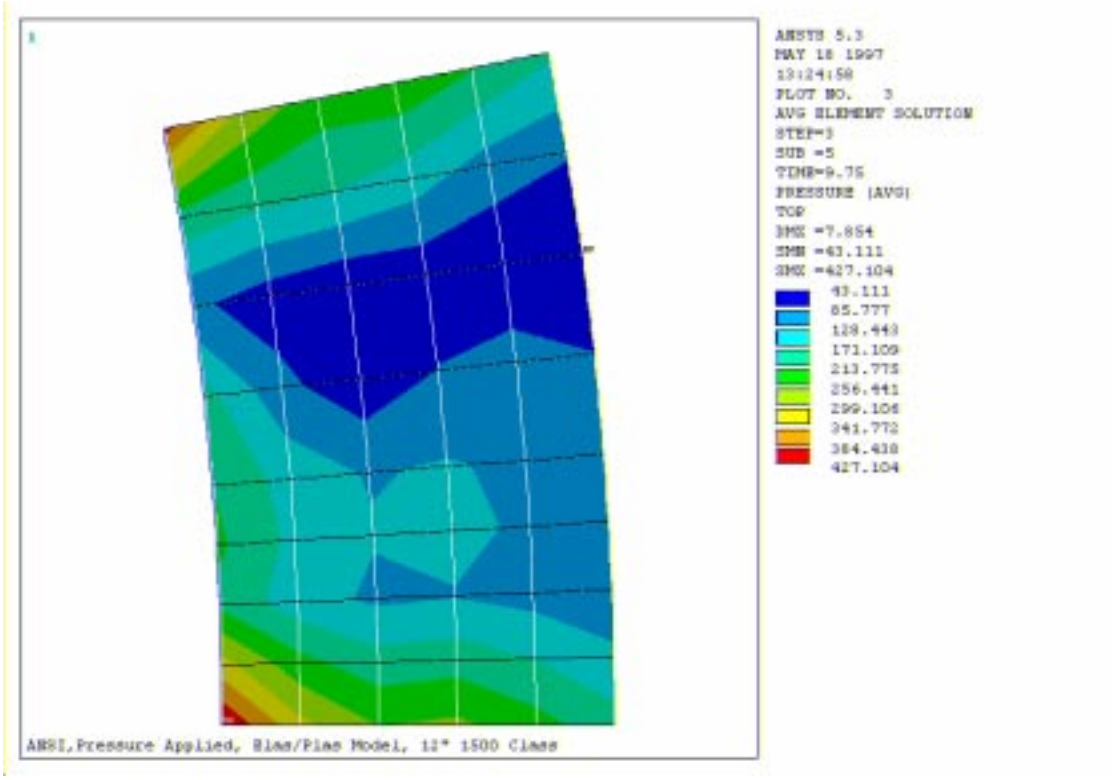

Figure 117: ANSI 12" 1500# Class - Contact Pressure Plot

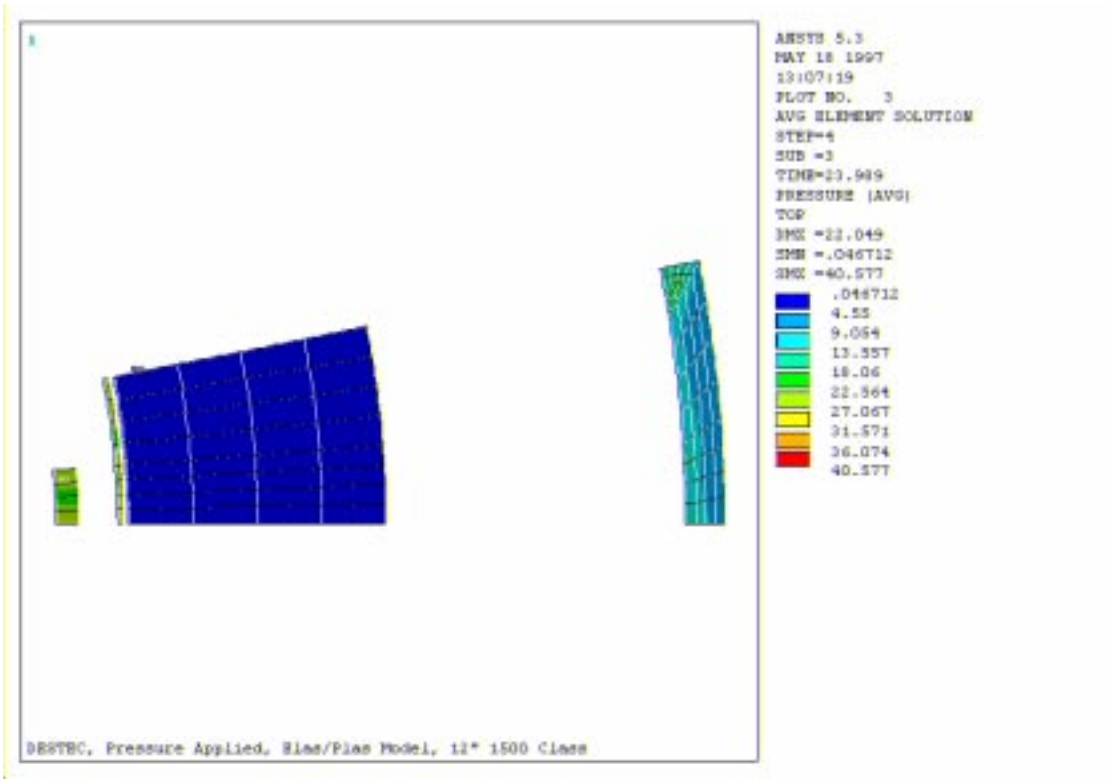

Figure 118: DESFLEX 12" 1500# Class - Contact Pressure Plot

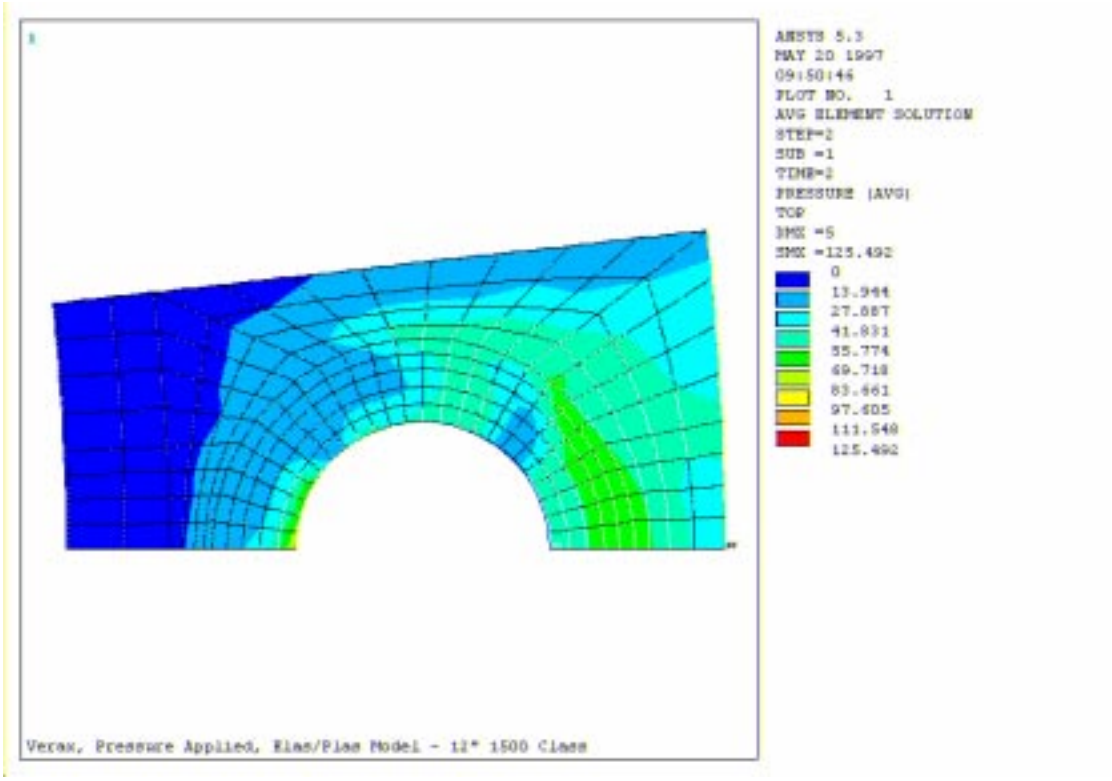

Figure 119: VCF 12" 1500# Class - Contact Pressure Plot

11.3.2. 2500# Class

11.3.2.1. Four Inch Nominal Bore

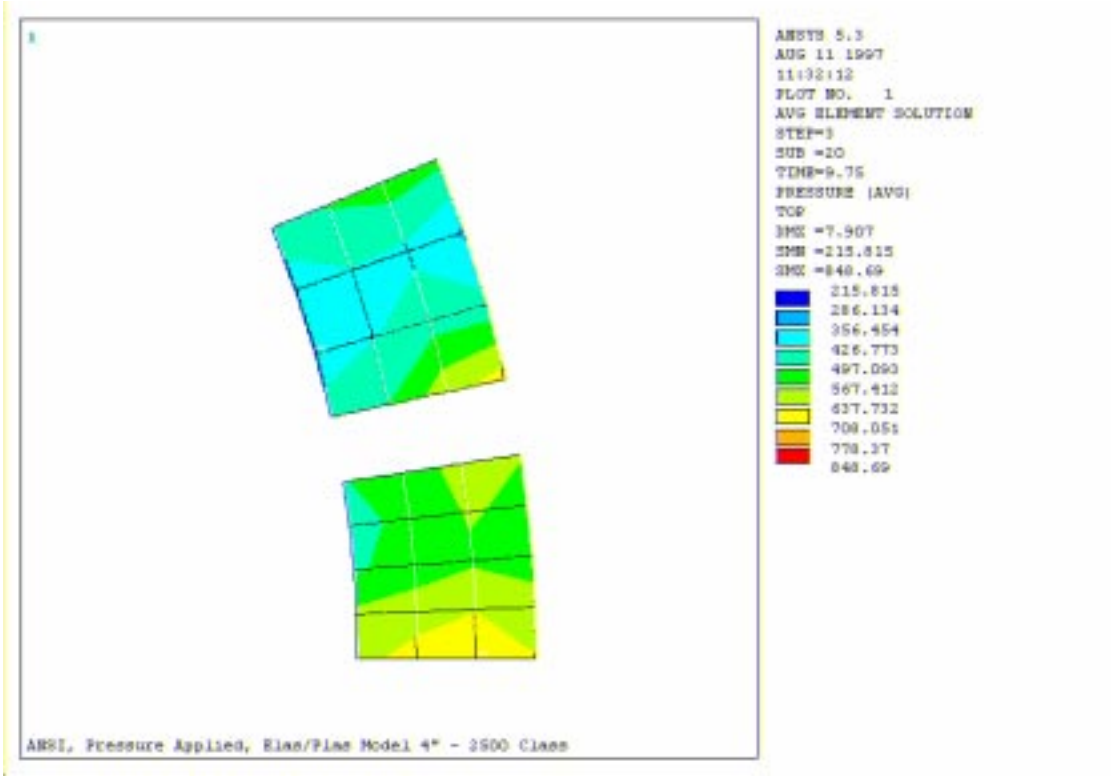

Figure 120: ANSI 4" 2500# Class - Contact Pressure Plot

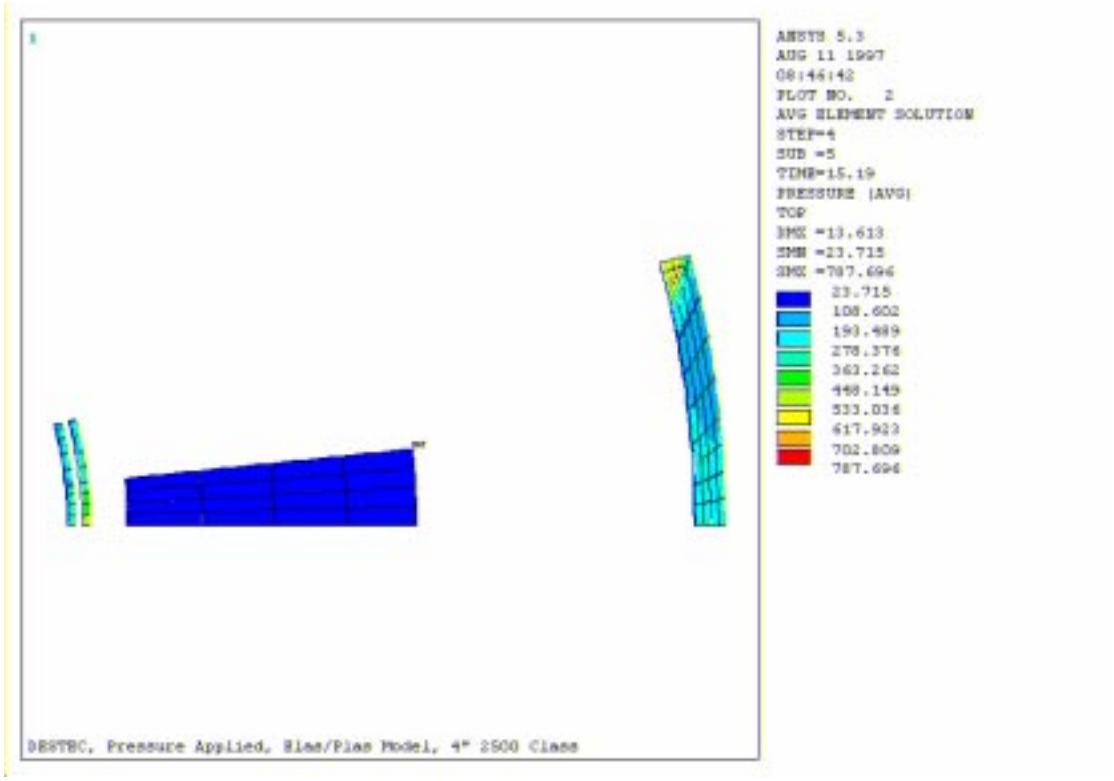

Figure 121: DESFLEX 4" 2500# Class Contact Pressure Plot

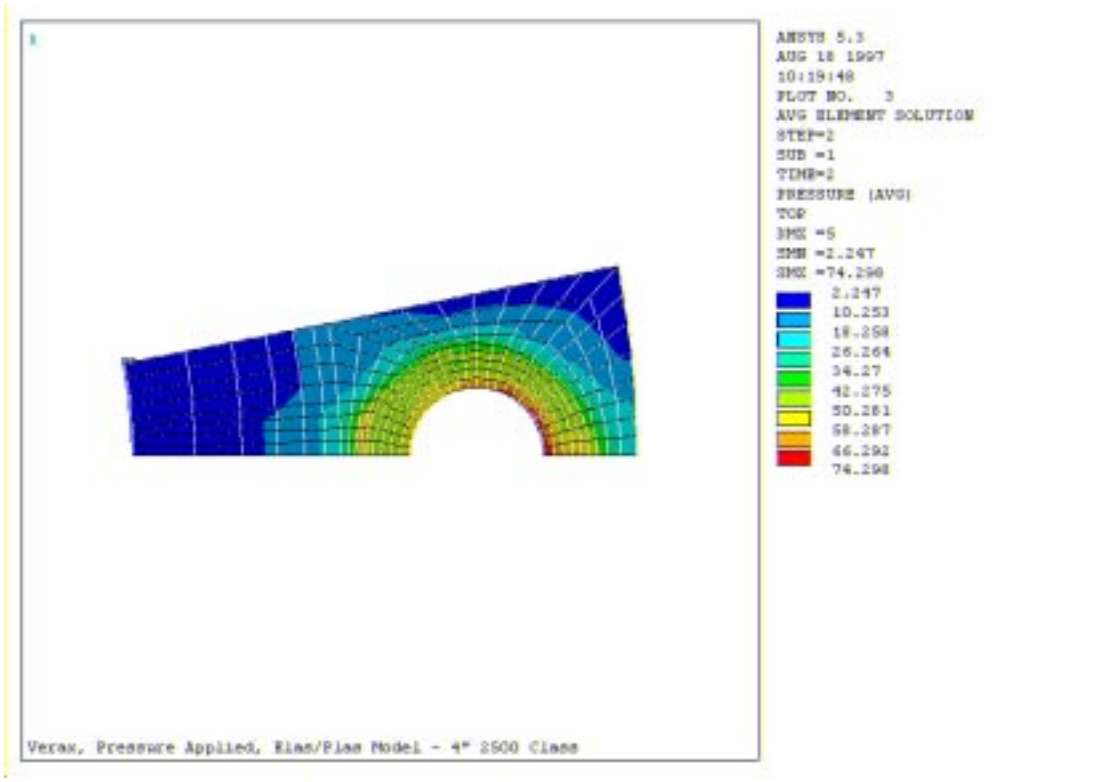

Figure 122: VCF 4" 2500# Class - Contact Pressure Plot

11.3.2.2. Eight Inch Nominal Bore

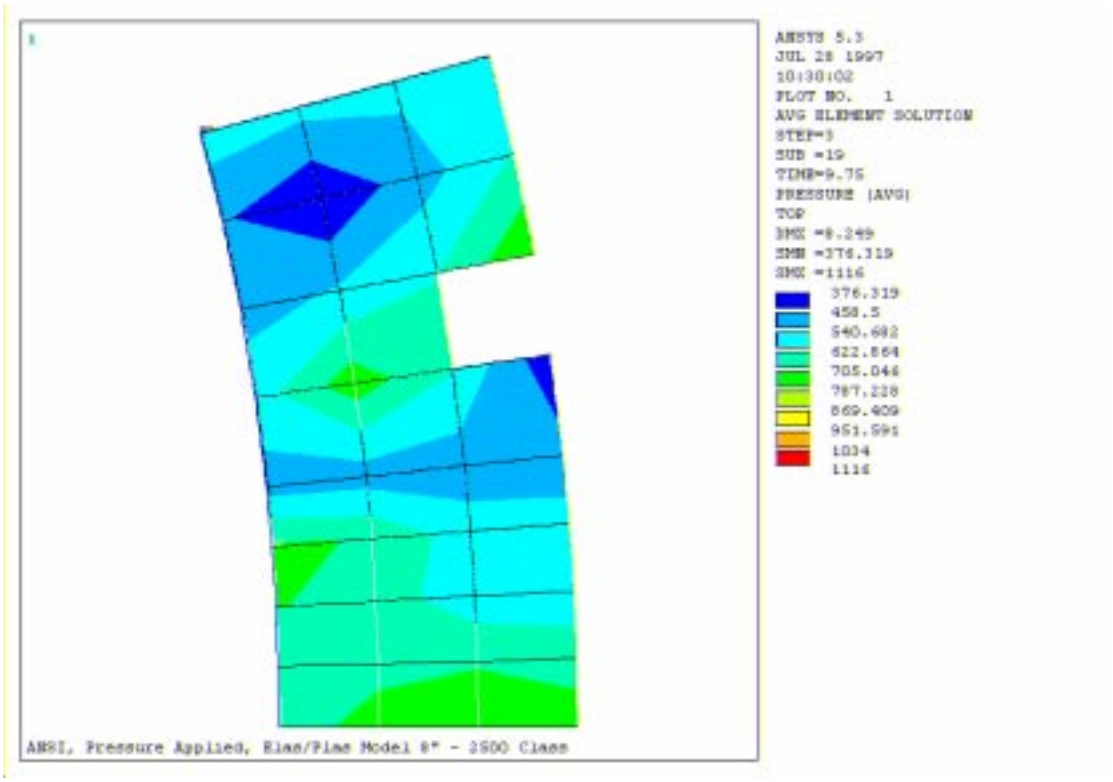

Figure 123: ANSI 8" 2500# Class - Contact Pressure Plot

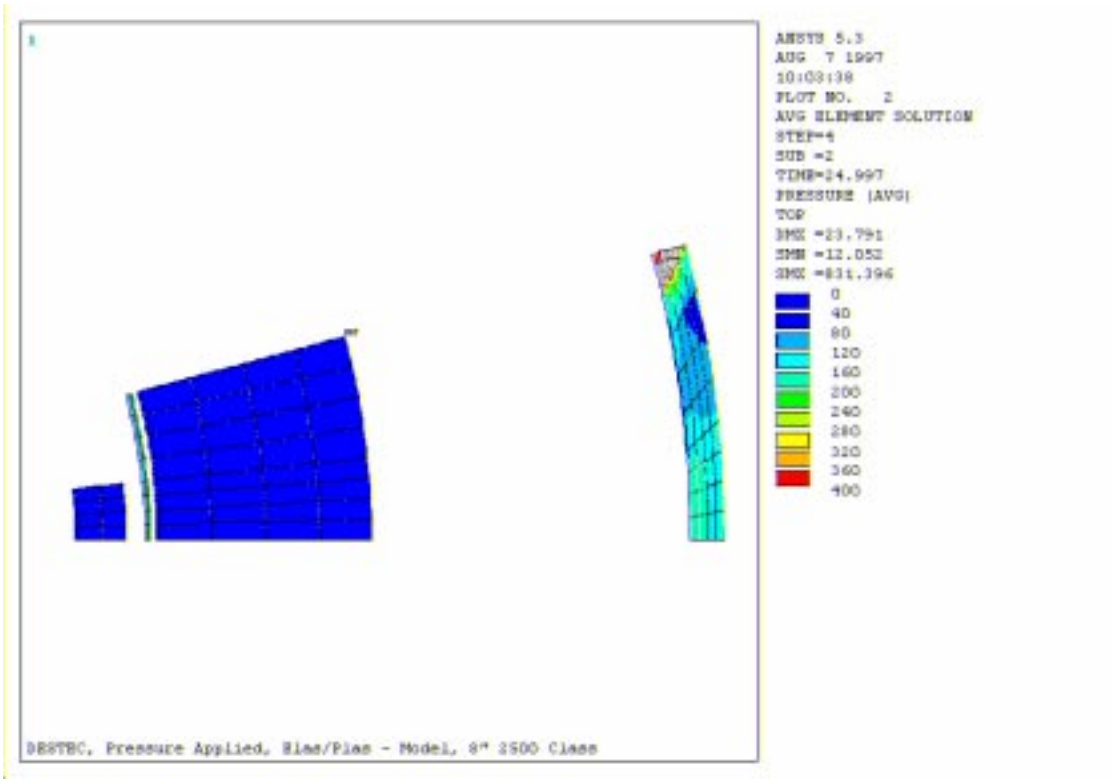

Figure 124: DESFLEX 8" 2500# Class - Contact Pressure Plot

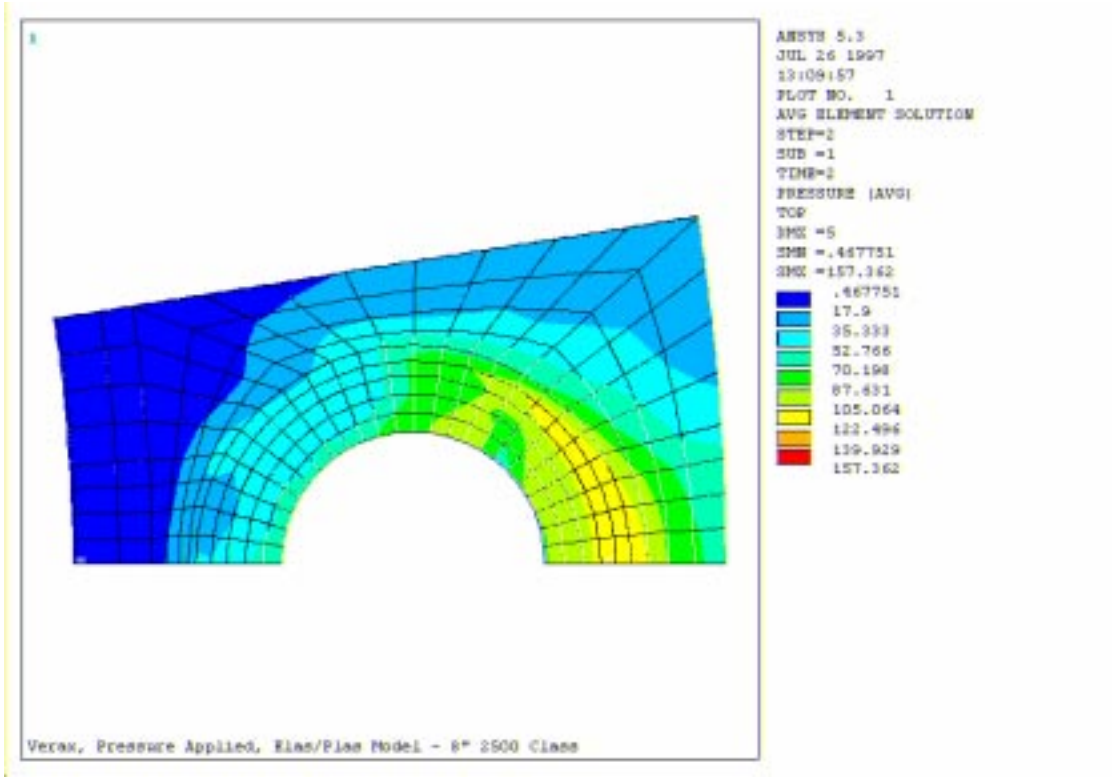

Figure 125: VCF 8" 2500# Class - Contact Pressure Plot

11.3.2.3. Twelve Inch Nominal Bore

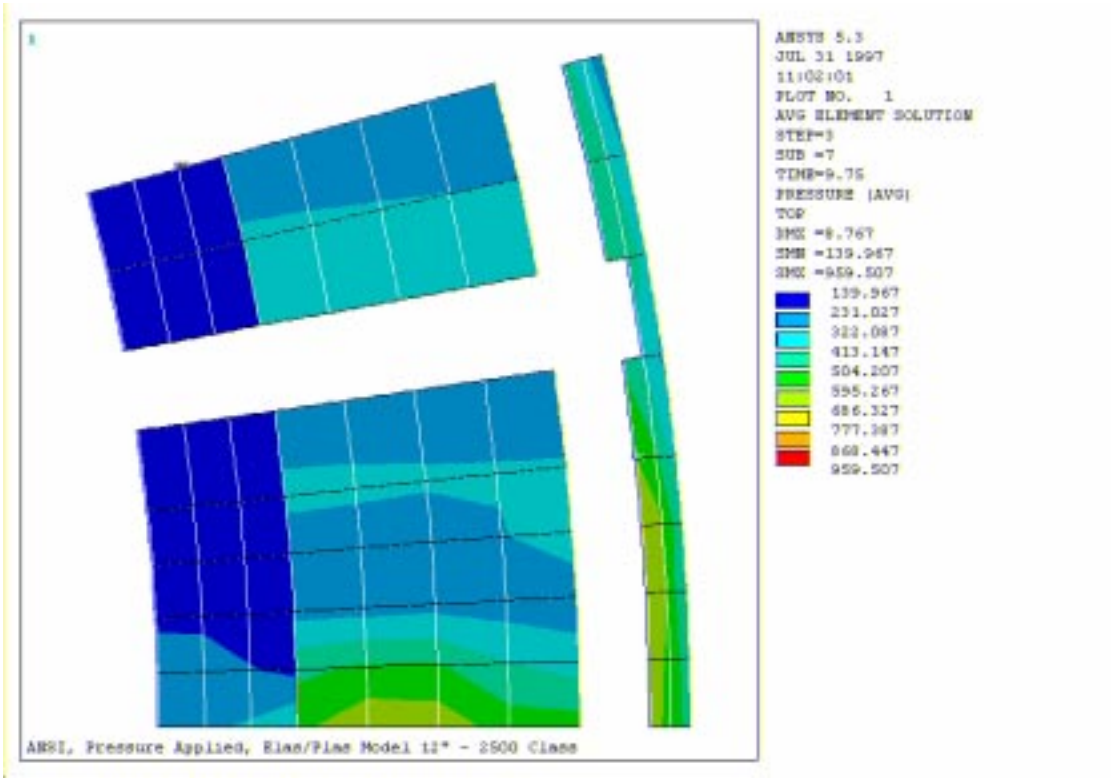

Figure 126: ANSI 12" 2500# Class - Contact Pressure Plot

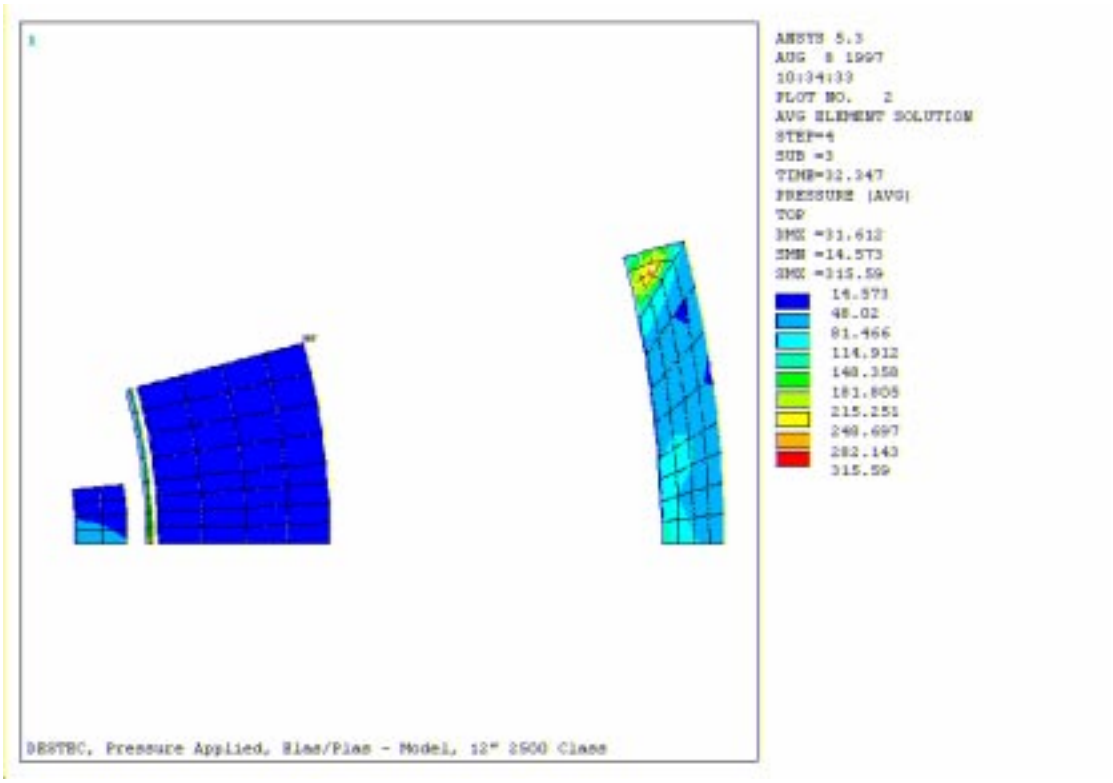

Figure 127: DESFLEX 12" 2500# Class - Contact Pressure Plot

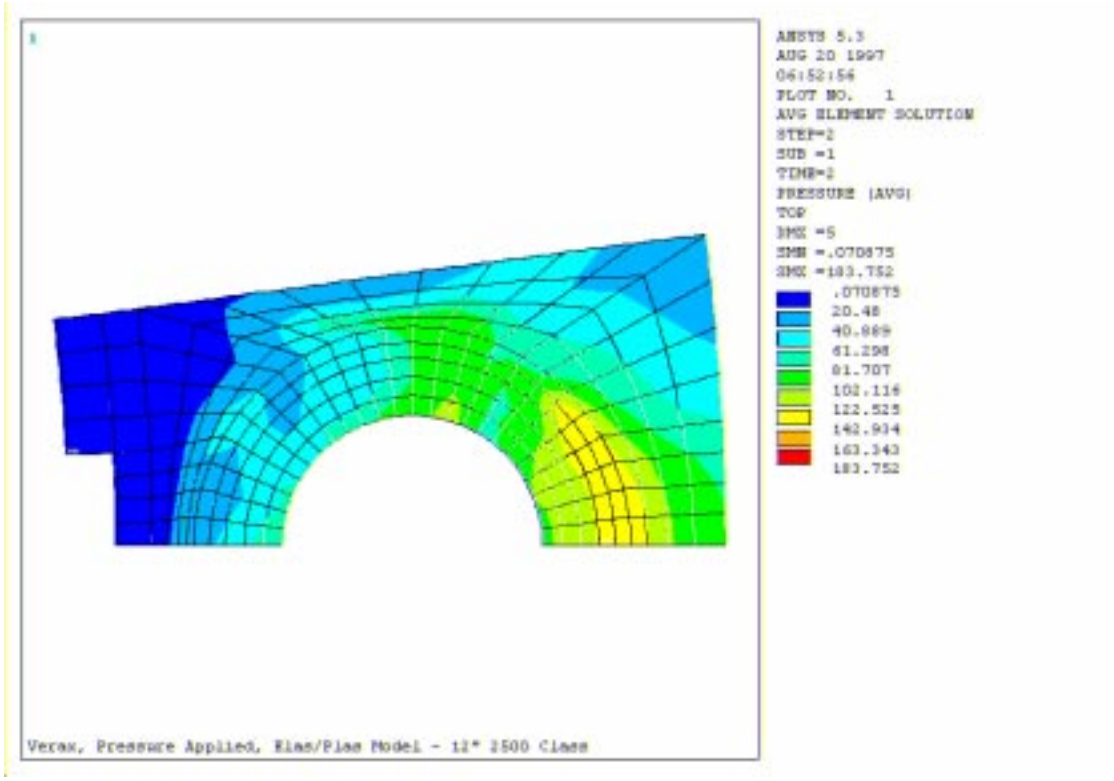

Figure 128: VCF 12" 2500# Class - Contact Pressure Plot

12. Appendix IV – Input File

This appendix contains an input file for the four inch 1500 class VCF joint model. This model incorporates a refined mesh, SOLID45 and CONTAC49 elements and a bi-linear kinematic material model. The input file also details the multiple loadsteps that were used. The text size has been reduced because of the length of the input file.

```
/NERR,5,100000,
/UIS,MSGPOP,3
/filnam,v41testp2      ! eqv. of 10.9 class bolts
/config,nproc,2
/title,Contact used, Pressure Applied, Elas/Plas Model – 4” 1500 Class
/user,1
/dscale,1,1
!*
/PREP7
!*
PI=3.1415926
!*
*set,taperang,0.0705  ! Taper angle (degrees)
*set,fd,160    ! Flange Diameter
*set,fh,24     ! Flange Height
*set,pt,17     ! Pipe Thickness
*set,pod,114.3 ! Pipe Outside Diameter
*set,pid,(pod-2*pt)    ! Pipe Inside Diameter
*set,pcd,140   ! Pitch Circle Diameter
*set,bd,8      ! Bolt Diameter
*set,bhd,1.5*bd        ! Bolt Head Diameter
*set,bhh,1*bd  ! Bolt Head Height
*set,wod,1.75*bd       ! Washer Outside Diameter
*set,wh,0.25*bd        ! Washer Height
*set,r,bd/2    ! Radius of hub/flange connection
*set,nbolts,22 ! Number of Bolts
*set,nsegm,(180/nbolts)       ! Number of Segments
*set,nsegm1,nsegm/2.5  ! Proportion of the two segments
*set,nsegm2,(1.5*nsegm1)
*set,gap,0.25  ! gap between bolt and flange
*set,jh,98.72  ! Joint Height-incl 3*sqrt(Rt) for pipe length
pint=24
!
elmlnth=0.2    ! used for contact pressure  calculation
!
!*
! Material Properties
!*
YM_F=203395            ! Youngs modulus of flange (N/mm2)
P_YM_F=0.1*YM_F        ! Plastic Youngs Modulus for flange
PR_F=0.3       ! Poissons Ratio of flange
YIELD_F=248.2  ! Yield stress for flange (N/mm2)
!*
YM_B=210e3             ! Youngs modulus of bolt (N/mm2)
P_YM_B=0.1*YM_B        ! Plastic Youngs Modulus for bolt
```

```
PR_B=0.3       ! Poissons Ratio of bolt
YIELD_B=940    ! Yield stress for bolt (N/mm2)
!*
YM_W=YM_B              ! Youngs modulus of washer (N/mm2)
P_YM_W=0.1*YM_W        ! Plastic Youngs Modulus for washer
PR_W=0.3       ! Poissons Ratio of washer
YIELD_W=940    ! Yield stress for washer (N/mm2)
!*
!*
! Contact Information
!*
curv_el=2      ! Cylinder curved lines
C=0.3          ! Correction Factor
KN=C*YM_F      ! Normal Stiffness of Contact Elements
!*
! Element Types
!*
ET,1,SOLID45
ET,2,SHELL63
ET,3,CONTAC49
KEYOPT,3,7,1
!*
! Material Properties
!*
MP,EX,1,YM_F     ! Material 1 = Flange
MP,NUXY,1,PR_F   ! EX=Youngs Mod., NUXY= Poissons Ratio !*
MP,EX,2,YM_B      ! Material 2 = Bolt
MP,NUXY,2,PR_B
!*
MP,EX,3,YM_W     ! Material 3 = Washer
MP,NUXY,3,PR_W
!*
MP,EX,4,0
MP,MU,4,0   ! Coefficient of friction (const=0)
!*
MP,EX,5,2000000   ! Youngs Mod for shell elements
!*
TB,BKIN,1,1,2
TBDATA,1,YIELD_F,P_YM_F
TB,BKIN,2,1,2
TBDATA,1,YIELD_B,P_YM_B
TB,BKIN,3,1,2
TBDATA,1,YIELD_W,P_YM_W
!*
! Real Constants
!*
R,1,2,2,2,2
!*
R,2,KN,,,,1     ! Real Constant = contact stiffness
!*              ! and Target length tolerance=1
! Geometry
!*
k,1,0,0,0
k,2,,,jh
k,3,pid/2
k,4,(pod/2)+r
```

```
k,10,fd/2
k,50,pcd/2
k,5,fd/2,,fh
k,60,pcd/2,,fh
k,6,(pod/2)+r,,fh
k,7,(pod/2)+r,,(fh+4*r)
k,8,(pod/2),,(fh+4*r)
k,9,(pod/2),,jh
k,11,(pid/2),,jh
k,12,(pid/2),,(fh+4*r)
k,13,(pod/2)+r,,fh-r
k,14,(pid/2),,fh-r
k,15,(fd/2),,fh-r
k,55,(pcd/2),,fh-r
!*
l,3,4
l,4,10
l,10,15
l,15,5
l,5,6
l,15,13
l,4,13
l,13,6
l,3,14
l,14,13
l,14,12
l,12,8
l,12,11
l,8,9
l,11,9
KWPAVE,       7
wpstyle,0.05,1,-1,10,0.003,1,0,,5
KWPLAN,-1,7,8,6
CSWPLA,11,1,4,1,
l,6,8
WPAVE,0,0,0
CSYS,0
ldiv,16,0.33333,,,0
l,14,16
a,3,4,13,14
a,14,13,6,16
a,14,16,8,12
a,12,8,9,11
a,4,10,15,13
a,13,15,5,6
vrotat,1,2,3,4,,,1,2,nsegm1
vrotat,11,15,19,23,,,1,2,nsegm2
arotat,3,4,,,,,1,2,nsegm1
arotat,65,66,,,,,1,2,nsegm2
l,31,42
l,29,41
l,28,40
adele,5,6
ldele,5,6
ldele,2
a,31,42,41,29
```

```
a,19,21,39,38
adele,6
a,28,29,41,40
ldele,2,5,3
ldiv,75,0.5,,,0
ldiv,76,0.5,,,0
ldiv,77,0.5,,,0
circle,50,bd/2,55,10,180,6
circle,50,(bd/2)+gap,55,10,180,6
circle,50,bhd/2,55,10,180,6
circle,50,wod/2,55,10,180,6
circle,55,bd/2,60,10,180,6
circle,55,(bd/2)+gap,60,10,180,6
circle,55,bhd/2,60,10,180,6
circle,55,wod/2,60,10,180,6
circle,60,bd/2,55,6,180,6
circle,60,(bd/2)+gap,55,6,180,6
circle,60,bhd/2,55,6,180,6
circle,60,wod/2,55,6,180,6
l,53,62
l,52,61
l,51,59
l,49,58
l,48,57
l,47,56
l,46,54
l,62,69
l,61,68
l,59,67
l,58,66
l,57,65
l,56,64
l,54,63
l,69,76
l,68,75
l,67,74
l,66,73
l,65,72
l,64,71
l,63,70
l,76,4
l,75,18
l,74,28
l,73,45
l,72,40
l,71,37
l,70,10
l,53,55
ldele,178
l,53,50
l,52,50
l,51,50
l,49,50
l,48,50
l,47,50
l,46,50
```

```
l,83,90
l,82,89
l,81,88
l,80,87
l,79,86
l,78,85
l,77,84
l,90,97
l,89,96
l,88,95
l,87,94
l,86,93
l,85,92
l,84,91
l,97,104
l,96,103
l,95,102
l,94,101
l,93,100
l,92,99
l,91,98
l,104,13
l,103,19
l,102,29
l,101,44
l,100,41
l,99,38
l,98,15
l,83,55
l,82,55
l,81,55
l,80,55
l,79,55
l,78,55
l,77,55
l,105,112
l,106,113
l,107,114
l,108,115
l,109,116
l,110,117
l,111,118
l,112,119
l,113,120
l,114,121
l,115,122
l,116,123
l,117,124
l,118,125
l,119,126
l,120,127
l,121,128
l,122,129
l,123,130
l,124,131
l,125,132
```

```
l,126,6
l,127,21
l,128,31
l,129,43
l,130,42
l,131,39
l,132,5
l,105,60
l,106,60
l,107,60
l,108,60
l,109,60
l,110,60
l,111,60
!*
a,50,53,52
a,50,51,52
a,50,49,51
a,50,48,49
a,50,47,48
a,50,46,47
a,53,52,61,62
a,52,61,59,51
a,51,59,58,49
a,49,58,57,48
a,48,57,56,47
a,47,56,54,46
a,62,69,68,61
a,61,68,67,59
a,59,67,66,58
a,58,66,65,57
a,57,65,64,56
a,56,64,63,54
a,59,76,75,68
adele,63
ldele,255,256
a,69,76,75,68
a,68,75,74,67
a,67,74,73,66
a,66,73,72,65
a,65,72,71,64
a,64,71,70,63
a,76,4,18,75
a,75,18,28,74
a,74,28,45,73
a,73,45,40,72
a,72,40,37,71
a,71,37,10,70
l,50,55
l,53,83
l,52,82
l,51,81
l,50,80
l,49,69
ldele,260
ldele,259
```

```
l,49,80
l,48,79
l,47,78
l,46,77
l,62,90
l,61,89
l,59,89
ldele,265
l,59,88
l,58,87
l,57,86
l,56,85
l,54,85
ldele,269
l,54,84
l,69,97
l,68,96
l,67,95
l,66,94
l,65,93
l,64,92
l,63,91
l,76,104
l,75,103
l,74,102
l,73,101
l,72,100
l,78,99
ldele,282
l,71,99
l,70,98
lsel,s,,,78,283
lsel,all
a,76,75,103,104
a,75,74,102,103
a,74,73,101,102
a,73,72,100,101
a,72,71,99,100
a,71,70,98,99
a,69,68,96,97
a,68,67,95,96
a,67,66,94,95
a,66,65,93,94
a,65,64,92,93
a,64,63,91,92
a,62,61,89,90
a,61,59,88,89
a,59,58,87,88
a,58,57,86,87
a,57,56,85,86
a,56,54,84,85
a,53,52,82,83
a,51,52,82,81
a,51,49,80,81
a,49,48,79,80
a,48,47,78,79
```

```
a,47,46,77,78
nummrg,kp
a,76,69,97,104
a,75,68,96,103
a,74,67,95,102
a,73,66,94,101
a,65,72,100,93
a,64,71,99,92
a,63,70,98,91
a,69,62,90,97
a,68,61,89,96
a,67,59,88,95
a,58,66,87,80
a,57,65,93,86
a,56,64,92,85
a,54,63,91,84
a,62,53,83,90
a,52,61,89,92
adele,114
a,52,61,89,82
a,51,59,88,81
a,49,58,87,80
a,48,57,86,79
a,47,56,85,78
a,46,54,84,77
a,53,50,55,83
a,52,50,55,82
a,51,50,55,81
a,49,50,55,80
a,48,50,55,79
a,47,50,55,78
a,46,50,55,77
a,97,96,103,104
a,96,95,102,103
a,95,94,101,102
a,94,93,100,101
a,93,92,99,100
a,92,91,98,99
a,90,89,96,97
a,89,88,95,96
a,88,87,94,95
a,87,86,93,94
a,86,85,92,93
a,85,84,91,92
a,83,82,89,90
a,82,81,88,89
a,81,80,87,88
a,87,86,79,80
a,86,85,78,79
a,85,84,77,78
a,83,55,82
a,82,55,81
a,81,55,80
a,80,55,79
a,79,55,78
a,78,55,77
```

```
a,104,13,19,103
a,103,19,29,102
a,102,101,44,29
a,101,44,41,100
a,100,41,38,99
a,99,38,15,98
a,70,10,15,98
asel,u,,,127,151
a,99,38,37,71
a,100,41,40,72
a,101,44,45,73
a,102,29,28,74
a,103,19,18,4
adele,162
a,103,19,18,75
a,104,13,4,76
asel,all
ldele,289
ldele,286
ldele,287
l,55,60
l,83,105
l,82,106
l,81,107
l,80,108
l,79,109
l,78,110
l,77,111
l,90,112
l,89,113
l,88,114
l,87,115
l,86,116
l,85,117
l,84,118
l,97,119
l,96,120
l,95,121
l,94,122
l,93,123
l,92,124
l,91,125
l,104,126
l,103,127
l,102,128
l,101,129
l,100,130
l,99,131
l,98,132
a,104,103,127,126
a,103,102,128,127
a,102,101,129,128
a,101,100,130,129
a,100,99,131,130
a,99,98,132,131
a,97,96,120,119
```

```
a,96,95,121,120
a,95,95,122,121
adele,172
a,95,94,122,121
a,94,93,123,122
a,93,92,124,123
a,92,91,125,124
a,90,89,113,112
a,89,88,114,113
a,88,87,15,114
adele,178
ldele,317
a,88,87,115,114
a,87,86,116,115
a,86,85,117,116
a,85,84,118,117
a,83,82,106,105
a,82,81,107,106
a,81,80,108,107
a,80,79,109,108
a,79,78,110,109
a,78,77,111,110
a,104,97,119,126
a,103,96,120,127
a,102,95,121,128
a,101,94,122,129
a,100,93,123,130
a,99,92,124,131
a,91,98,132,125
a,97,90,112,119
a,96,89,113,120
a,95,88,114,121
a,94,87,115,122
a,86,93,123,116
a,85,92,124,117
a,84,91,125,118
a,90,83,105,112
a,89,82,106,113
a,88,81,107,114
a,87,80,108,115
a,86,79,109,116
a,78,85,117,110
a,77,84,118,111
a,83,55,60,105
a,82,55,60,106
a,81,55,60,107
a,80,55,60,108
a,79,55,60,109
a,78,55,60,110
a,77,55,60,111
a,13,104,126,6
a,103,19,21,127
a,102,29,31,128
a,101,129,43,44
a,100,130,42,41
a,99,131,39,38
```

```
a,98,15,5,132
a,128,127,120,119
adele,228
adele,223
a,126,127,120,119
a,127,128,121,120
a,129,129,122,121
adele,225
a,128,129,122,121
a,129,130,123,122
a,130,131,124,123
a,124,131,132,125
a,119,120,113,112
a,120,121,114,113
a,121,122,115,114
a,122,123,116,115
a,123,124,117,116
a,117,124,125,118
a,112,113,106,105
a,113,114,107,106
a,114,115,108,107
a,115,116,109,108
a,116,117,110,109
a,110,117,118,111
a,105,60,106
a,106,60,107
a,107,60,108
a,108,60,109
a,109,60,110
a,110,60,111
a,126,6,21,127
a,127,128,31,21
a,128,129,43,31
a,129,130,42,43
a,130,131,39,42
a,131,132,5,39
/GRAPHICS,POWER
/TYPE,1,6
/CPLANE,0
/SHADE,1,1
adele,5,6
a,42,41,44,43
a,43,44,29,31
a,40,45,44,41
a,45,28,29,44
va,8,151,163,162,69,75
va,162,25,161,152,70,76
va,161,160,153,254,71,77
va,160,159,154,253,72,78
va,159,158,155,43,73,79
va,80,158,157,156,41,74
va,216,12,247,217,151,164
va,217,218,248,29,152,165
va,218,219,249,6,153,166
va,219,220,250,5,154,167
va,220,251,221,44,155,168
```

```
va,221,252,222,42,156,169
va,75,81,99,100,127,63
va,128,64,100,101,76,82
va,101,102,77,83,129,65
va,102,103,78,84,130,66
va,103,104,79,85,131,67
va,104,105,80,86,132,68
va,133,57,106,107,81,87
va,134,58,107,108,82,88
adele,109
a,66,94,87,58
ldele,322
ldele,323
!***
va,59,83,135,109,108,89
va,136,60,109,110,84,90
va,137,61,110,111,85,91
va,138,62,111,112,86,92
va,139,51,113,114,87,93
va,140,52,114,115,88,94
va,141,53,115,116,89,95
va,142,54,116,117,90,96
va,143,55,117,118,91,97
va,144,56,118,119,92,98
va,145,45,120,121,93
va,146,46,121,122,94
va,147,47,122,123,95
va,148,48,123,124,96
va,149,49,124,125,97
va,150,50,125,126,98
va,127,223,164,170,188,189
va,128,224,165,171,189,190
va,129,225,166,172,190,191
va,130,226,167,173,191,192
va,131,227,168,174,192,193
va,132,228,169,175,193,194
va,229,133,170,176,195,196
va,230,134,171,177,196,197
va,231,135,172,178,197,198
va,232,136,173,179,198,199
va,233,137,174,180,199,200
va,234,138,175,181,200,201
va,235,139,202,203,176,182
va,236,140,203,204,177,183
va,237,141,204,205,178,184
va,238,142,205,206,179,185
va,239,143,206,207,180,186
va,240,144,207,208,181,187
va,241,145,209,210,182
va,242,146,210,211,183
va,243,147,211,212,184
va,244,148,212,213,185
va,245,149,213,214,186
va,246,150,214,215,187
k,,pcd/2,,(fh+wh)
circle,133,bd/2,60,6,180,6
```

```
circle,133,(bd/2)+gap,60,6,180,6
circle,133,bhd/2,60,6,180,6
circle,133,wod/2,60,6,180,6
ldele,319
ldele,318
l,134,141
l,135,142
l,136,143
l,137,144
l,138,145
l,139,146
l,140,147
l,141,148
l,142,149
l,143,150
l,144,151
l,145,152
l,146,153
l,147,154
l,148,155
l,149,156
l,150,157
l,151,158
l,152,159
l,153,160
l,154,161
l,134,133
l,135,133
l,136,133
l,137,133
l,138,133
l,139,133
l,140,133
a,155,148,149,156
a,149,156,157,150
a,150,157,158,151
a,151,158,159,152
a,152,159,160,153
a,153,160,161,154
a,148,149,142,141
a,142,149,150,153
adele,262
ldele,371,372
a,142,149,150,143
a,143,150,151,144
a,144,151,152,145
a,145,152,153,146
a,146,153,154,147
a,141,142,135,134
a,135,142,143,136
a,136,143,144,137
a,137,144,145,138
a,138,145,146,139
a,139,146,147,140
a,134,135,133
a,135,136,133
```

```
a,136,137,133
a,137,138,133
a,138,139,133
a,139,140,133
l,133,60
l,134,105
l,141,112
l,148,119
l,155,126
l,135,106
l,142,113
l,149,120
l,156,127
l,136,107
l,143,114
l,150,121
l,157,128
l,137,108
l,144,115
l,151,122
l,158,129
l,144,116
ldele,388
l,145,116
l,152,123
l,159,130
l,138,109
l,139,110
l,146,117
l,153,124
l,160,131
l,140,111
l,147,118
l,154,125
l,161,132
a,126,127,156,155
a,127,128,157,156
a,128,129,158,157
a,129,130,159,158
a,130,131,160,159
a,131,132,161,160
a,119,120,149,148
a,120,121,150,149
a,121,122,151,150
a,122,123,152,151
a,123,124,153,152
a,124,125,154,153
a,112,113,142,141
a,113,114,143,142
a,114,115,144,143
a,115,116,145,144
a,116,117,146,145
a,117,118,147,146
a,105,106,135,134
a,106,107,136,135
a,107,108,137,136
```

```
a,108,109,138,137
a,109,110,139,138
a,110,111,140,139
a,126,119,148,155
a,127,120,149,156
a,128,121,150,157
a,129,122,151,158
a,130,123,152,159
a,131,124,153,160
a,132,125,154,161
a,119,112,121,128
adele,310
a,119,112,141,148
a,120,113,142,149
a,121,114,143,150
a,122,115,144,151
a,123,116,145,152
a,124,117,146,153
a,125,118,147,154
a,112,105,134,141
a,113,106,135,142
a,114,107,136,143
a,115,108,137,144
a,116,109,138,145
a,116,110,139,146
adele,322
a,117,110,139,146
a,117,111,140,147
adele,323
a,118,111,140,147
a,105,60,133,134
a,106,135,133,60
a,107,136,133,60
a,108,137,133,60
a,109,138,133,60
a,110,139,133,60
a,111,140,133,60
va,223,255,279,285,303,304
va,224,256,280,286,304,305
va,225,257,281,287,305,306
va,226,258,282,288,306,307
va,227,259,283,289,307,308
va,228,260,284,290,308,309
va,229,261,285,291,310,311
va,230,262,286,292,311,312
va,231,263,287,293,312,313
va,232,264,288,294,313,314
va,233,265,289,295,314,315
va,234,266,290,296,315,316
va,235,267,291,297,317,318
va,236,268,292,298,318,319
va,237,269,293,299,319,320
va,238,270,294,300,320,321
va,239,271,295,301,321,322
va,240,272,296,302,322,323
va,241,273,297,324,325
```

```
va,242,274,298,325,326
va,243,275,299,326,327
va,244,276,300,327,328
va,245,277,301,328,329
va,246,278,302,329,330
k,,pcd/2,,fh+wh+bhh   ! Making of the bolt head
l,133,162
circle,162,bd/2,60,6,180,6
circle,162,(bd/2)+gap,60,6,180,6
circle,162,bhd/2,60,6,180,6
l,162,163
l,162,164
l,162,165
l,162,166
l,162,167
l,162,168
l,162,169
l,163,170
l,164,171
l,165,172
l,166,173
l,167,174
l,168,175
l,169,176
l,170,177
l,171,178
l,172,179
l,173,180
l,174,181
l,175,182
l,176,183
l,155,177
ldele,444
l,177,148
l,178,149
l,179,150
l,180,151
l,181,152
l,182,153
l,183,154
l,170,141
l,171,142
l,172,143
l,173,144
l,174,145
l,175,146
l,176,147
l,163,134
l,164,135
l,165,136
l,166,137
l,167,138
l,168,139
l,169,140
a,177,170,171,178
a,171,178,179,172
```

```
a,172,179,180,173
a,173,180,181,174
a,174,181,182,175
a,175,182,183,176
a,163,170,171,164
a,164,171,172,165
a,165,172,173,166
a,166,173,174,167
a,167,174,175,168
a,168,175,176,169
a,163,162,164
a,164,162,165
a,165,162,166
a,166,162,167
a,167,162,168
a,168,162,169
a,148,149,178,177
a,149,150,179,178
a,150,151,180,179
a,151,152,181,180
a,152,153,182,181
a,153,154,183,182
a,141,142,171,170
a,142,143,172,171
a,143,144,173,172
a,144,145,174,173
a,145,146,175,174
a,146,147,176,175
a,134,135,164
adele,361
a,134,135,164,163
a,135,136,165,164
a,136,137,166,165
a,137,138,167,166
a,138,139,168,167
a,139,140,169,168
a,141,148,177,170
a,142,149,178,171
a,143,150,179,172
a,144,151,180,173
a,145,152,181,174
a,146,153,182,175
a,147,154,183,176
a,141,134,163,170
a,142,135,164,171
a,143,136,165,172
a,144,137,166,173
a,145,138,167,174
a,146,139,168,175
a,147,140,169,176
a,134,133,162,163
a,135,133,162,164
a,136,133,162,165
a,137,133,162,166
a,138,133,162,167
a,139,133,162,168
```

```
a,140,133,162,169
va,261,331,349,355,367,368
va,262,332,350,356,368,369
va,263,333,351,357,369,370
va,264,334,352,358,370,371
va,265,335,353,359,371,372
va,266,336,354,360,372,373
va,267,355,361,337,374,375
va,268,356,362,338,375,376
va,269,357,363,339,376,377
va,270,358,364,340,377,378
va,271,359,365,341,378,379
va,272,360,366,342,379,380
va,273,361,343,381,382
va,274,362,344,382,383
va,275,363,345,383,384
va,276,364,346,384,385
va,277,365,347,385,386
va,278,366,348,386,387
lsel,all
lsel,s,,,403
ldele,all
lsel,all
!* Making volume components
vsel,all
vsel,s,,,33,38
vsel,a,,,57,62
cm,gap,volu
vsel,all
vsel,s,,,39,44
vsel,a,,,63,68
vsel,a,,,87,92
vsel,a,,,93,110
cm,bolt_v,volu
vsel,s,,,69,86
cm,wash_v,volu
vsel,all
cmsel,u,bolt_v
cmsel,u,wash_v
cmsel,u,gap
cm,flange_v,volu
vsel,all
lsel,all
lsel,s,,,13,14,1
lsel,a,,,37,39,2
lsel,a,,,60,62,2
pipe=6
pipes=6
lesize,all,,,pipe,pipes
lsel,all
lsel,s,,,4,8,4
lsel,a,,,12,18,3
lsel,a,,,27,29,2
lsel,a,,,33,38,5
lsel,a,,,50,52,2
lsel,a,,,56
```

```
lsel,a,,,61,71,5
lsel,a,,,286,287,1
lsel,a,,,289,316,1
topv1=5
topvs1=(1/2)
lesize,all,,,topv1,topvs1
lesize,317,,,topv1,(1/topvs1)
lsel,all
lsel,s,,,371,399,1
washv1=2
washvs1=1
lesize,all,,,washv1,washvs1
lsel,all
lsel,s,,,444,466
bolthv1=3
bolthvs1=(1/3)
lesize,all,,,bolthv1,bolthvs1
lsel,all
lesize,406,,,bolthv1,(1/bolthvs1)
lsel,all
lsel,s,,,171,177,1
lsel,a,,,206,212,1
lsel,a,,,241,247,1
rocyl=4
rocyls=2
lesize,all,,,rocyl,rocyls
lsel,all
lsel,s,,,2,5,3
lsel,a,,,6
lsel,a,,,23,26,1
lsel,a,,,30,40,5
lsel,a,,,31,41,5
lsel,a,,,46,49,1
lsel,a,,,53,54
lsel,a,,,58,59
lsel,a,,,63,64
lsel,a,,,67,69
lsel,a,,,72,149
lsel,a,,,321,344
lsel,a,,,402,405,3
lsel,a,,,407,422
lsel,a,,,465
cylcirc=4
lesize,all,,,cylcirc,1
lsel,all
lsel,s,,,178,184,1
lsel,a,,,213,219,1
lsel,a,,,248,254,1
lsel,a,,,364,370,1
lsel,a,,,423,431,1
bcenrad=4
lesize,all,,,bcenrad,1
lsel,all
lsel,s,,,150,156,1
lsel,a,,,185,191,1
lsel,a,,,220,226,1
```

```
lsel,a,,,285
lsel,a,,,318,319
lsel,a,,,345,349,1
lsel,a,,,432,436,1
rad1cyl=2
rad1cyls=1
lesize,all,,,rad1cyl,rad1cyls
lsel,all
lsel,s,,,157,163,1
lsel,a,,,192,198,1
lsel,a,,,227,233,1
lsel,a,,,284
lsel,a,,,350,356,1
lsel,a,,,439,443,1
lsel,a,,,467
rad2cyl=3
rad2cyls=1
lesize,all,,,rad2cyl,rad2cyls
lsel,all
lsel,s,,,1,10,9
lsel,a,,,19,21,2
lsel,a,,,42,44,2
hubedge=6
hubedges=0.25
lesize,all,,,hubedge,hubedges
lsel,all
lesize,16,,,hubedge,(1/hubedges) ! on hub curve
lesize,28,,,hubedge,(1/hubedges)
lesize,51,,,hubedge,(1/hubedges)
!*
lesize,445,,,rad2cyl,rad2cyls
lesize,404,,,bolthv1,(1/bolthvs1)
lesize,317,,,topv1,(1/topvs1)
!*
csys,1                          ! adding taper angle
k,200,0,0,0.10407
k,201,(fd/2)+5,-5,0.0707
k,202,(fd/2)+5,nsegm+5,0.0707
l,201,202
csys,0
l,200,201
l,200,202
a,200,201,202
allsel
vsel,s,,,1,5,4
vsel,a,,,9,14,1
vsel,a,,,21,32,1
vcta,388,all
!*
agen,2,7,24,17,,,-5,,0,0
agen,2,57,74,1,,,-5,,0,0
!*
vdele,112,150,2,1
cmsel,s,flange_v
vsel,a,,,111,149,2
cm,flange_v,volu
```

```
!*
allsel
cmsel,s,flange_v
aslv
lsla
lsel,r,loc,z,2,fh-r-1
basev1=3
basevs1=2
lesize,all,,,basev1,basevs1
allsel
cmsel,s,bolt_v
aslv
lsla
lsel,r,loc,z,2,fh-r-1
lesize,all,,,basev1,(1/basevs1)
nummrg,kp
allsel
lsel,s,,,473,488,15
lsel,a,,,476
lesize,all,,,hubedge,(1/hubedges)
lsel,all
lsel,s,,,501,502,1
lsel,a,,,514,562,12
lesize,all,,,rocyl,(1/rocyls)
lsel,all
lsel,s,,,500,560,12
lsel,a,,,569,701,12
lesize,all,,,cylcirc,1
lsel,all
lsel,s,,,573,574,1
lsel,a,,,586,634,12
!*
lsel,a,,,713,725,2      ! on symmetry surface
lesize,all,,,rad1cyl,rad1cyls
lsel,s,,,645,646,1
lsel,a,,,658,706,12
lesize,all,,,rad2cyl,rad2cyls
lsel,all
lsel,s,,,477,557,12
lsel,a,,,478,490,12
lsel,a,,,521,557,12
lesize,all,,,cylcirc,1
lsel,all
uphub=4
uphubis=2
uphubos=3
lsel,s,,,17,32,15
lsel,a,,,55
lesize,all,,,uphub,uphubis
lsel,s,,,11,34,23
lsel,a,,,57
lesize,all,,,uphub,uphubos
lsel,all
!*
allsel
cmsel,s,flange_v   ! meshing of components
```

```
type,1
mat,1
vmesh,all
cmsel,s,bolt_v
type,1
mat,2
vmesh,all
cmsel,s,wash_v
type,1
mat,3
vmesh,all
allsel
!*
cmsel,s,flange_v    build other element and node components eslv,s
cm,flange_e,elem
nsle,s
cm,flange_n,node
cmsel,s,bolt_v
eslv,s
cm,bolt_e,elem
nsle,s
cm,bolt_n,node
cmsel,s,wash_v
eslv,s
cm,wash_e,elem
nsle,s
cm,wash_n,node
nummrg,kp
nummrg,node
nummrg,elem
!*                      ! generate other contact surface !*
allsel
!*
adele,1,8,7
a,270,267,268,269
a,269,268,271,272
csys,1
k,,(pid/2)-elmlnth,,-5          !addition at pid
k,,(pid/2)-elmlnth,nsegm1,-5    ! for contact surface
k,,(pid/2)-elmlnth,nsegm,-5
a,267,3,4,268
a,268,4,10,271
k,17,(fd/2)+elmlnth,,-5                 !addition at fd
k,18,(fd/2)+elmlnth,nsegm1,-5   ! for contact surface
k,27,(fd/2)+elmlnth,nsegm,-5
a,18,299,300,17
a,27,298,299,18
lsel,s,,,6,23,17
lsel,a,,,47
lsel,a,,,72
lesize,all,,,cylcirc,1
lsel,s,,,1,19,18
lsel,a,,,24,67,43
lsel,a,,,42,46,4
lesize,all,,,1,1
allsel
```

```
!*
nummrg,kp
!*
asel,s,loc,z,-6,-4
type,2
real,1
mat,5                   ! meshing of contact areas
ESHAPE,2,0              ! using quads only
local,12,1,(pcd/2),0,0,0,0,0,1,1
esys,12
amesh,all
csys,1
nrot,all
allsel
!*
esel,s,type,,2
enorm,4400
ensym,0,,0,all
allsel
!*
nummrg,node
nummrg,elem
!*
CMSEL,S,FLANGE_N  ! selection of contact nodes
nsel,r,loc,z,0,1    ! on flange base as 'contact'
cm,contact,node
!*
nsel,all
nsel,s,loc,z,-6,-4   ! creating component 'target'
cm,target,node
allsel
!*
type,3
real,2
mat,4
gcgen,contact,target,4  ! generating contact elements
!*
!*      Boundary Conditions - contact step
!*
allsel
cmsel,s,bolt_n
nsel,r,loc,z,0  ! bolt base
dsym,symm,z,1
allsel
CSYS,1
nsel,s,loc,y,0  ! CSA side symm
dsym,symm,y,1
nsel,all
nsel,s,loc,y,nsegm  ! opp side symm
dsym,symm,y,1
nsel,all
!*
esel,s,type,,2
nsle,r,1
d,all,uz,5.0001
esel,all
```

```
nsel,all
save
FINISH
!*
/solu
antype,static,new
autots,on                          ! autotime stepping
pred,on,,on                        ! turns on predictor for nonlinear analysis
neqit,50                           ! maximum number of iterations
lnsrch,on                          ! promotes convergence
outres,all,last
lswrite,1
lssolve,1
!*
cmsel,s,bolt_n
nsel,r,loc,z,-1,1
ddele,all
sf,all,pres,-720
allsel
lswrite,2
lssolve,2
!*
cmsel,s,bolt_n
nsel,r,loc,-1,1
sfdele,all
d,all,0
csys,1
nsel,s,loc,z,0,jh
nsel,r,loc,x,pid/2
sf,all,pres,pint                   ! internal pressure (N/mm2)
paxial=pint*pid**2/(pod**2-pid**2)
allsel
nsel,s,loc,z,jh
sf,all,pres,-paxial                ! axial effect from int press
allsel
lswrite,3
lssolve,3
!*
fini
!*
/post1
rsys,1
/inp,presstmp,inp
allsel
save
fini
exit
```